FORMULATION OF HYALURONIDASE ENZYME SENSITIVE TOPICAL NANOMICROBICIDES FOR HIV VIRUS TRANSMISSION PREVENTION

A DISSERTATION IN

Pharmaceutical Sciences

and

Chemistry

Presented to the Faculty of the University
Of Missouri-Kansas City in partial fulfillment of
The requirements for the degree

DOCTOR OF PHILOSOPHY

By

Vivek Agrahari

M. Pharm, Medicinal & Pharmaceutical Chemistry, Rajiv Gandhi Proudyogiki

Vishwavidyalaya, India, 2008

Kansas City, Missouri

2015

FORMULATION OF HYALURONIDASE ENZYME SENSITIVE TOPICAL NANOMICROBICIDES FOR HIV VIRUS TRANSMISSION PREVENTION

Vivek Agrahari

Candidate for the Doctor of Philosophy Degree

University of Missouri-Kansas City, 2015

ABSTRACT

The objective of this dissertation is to design and optimize a nanoformulations (nanoparticle and nanofiber) delivery system loaded with anti-HIV topical microbicides for HIV prevention in women.

In chapters 1 and 2, the overview of the problem, research objectives as well as the literature review of the technical and scientific background of this dissertation are introduced.

In chapter 3, a study was designed to test the hypothesis that a triggered release of a topical anti-HIV microbicide (tenofovir: TFV) from hyaluronic acid based nanoparticles (HA-NPs) can be achieved under the influence of hyaluronidase (HAase) enzyme. The Fractional Factorial Experimental Design (FFED) was employed to examine the formulation variables such as: molar concentrations of adipic acid dihydrazide (X_1) and 1-Ethyl-3-[3-dimethylaminopropyl]carbodiimide hydrochloride (X_2), volume of acetone (X_3) and reaction time (X_4), and their influence on the responses such as Y_1; particle mean diameter: PMD (nm), Y_2; polydispersity index: PDI and Y_3; zeta (ζ) potential: (mV). The cross-linking efficiency of NPs was characterized by Fourier Transform Infra-Red **(**FT-IR), and ^{13}C-nuclear magnetic

resonance (NMR) analyses. When formulated with X_1; 2.49 mM, X_2; 9.96 mM, X_3; 60 mL, X_4; 6 h, the HA-NPs exhibited a spherical shape with PMD, PDI, ζ potential, and drug loading of 70.6 ± 4.1 nm, 0.07 ± 0.02, -38.2 ± 2.8 mV, and 26.1 ± 1.2% w/w, respectively, (n = 3). Unlike for HA based gel, HAase notably triggered the drug release and HA degradation from the NPs after 24 h (~90% w/w and 65% w/w, respectively); whereas, in its absence, these values were ~39% w/w and 26% w/w, respectively. The NPs were non-cytotoxic to human vaginal VK2/E6E7 and End1/E6E7 cells and had no effect on *Lactobacillus* viability. These data suggested the possibility of using HA-NPs as a delivery system for intravaginal delivery of topical microbicides for the prevention of HIV transmission.

In chapter 4, a study was designed to test the hypothesis that a stimuli-sensitive, safe and mucoadhesive thiolated hyaluronic acid (HA) based nanofibers (NFs) loaded with a topical vaginal microbicide (TFV) can be used for the prevention of HIV virus vaginal transmission in women. To test this, a novel thiolated sulfhydryl (-SH) group modified HA (HA-SH) was synthesized to fabricate the TFV loaded HA-SH-NFs (mean diameter ~75 nm) using electrospinning method. Sulfhydryl (-SH) group modified HA (HA-SH) were characterized for their size distribution, surface morphology, surface chemistry, crystallinity, mucoadhesion property, and *in vitro* drug release profile using size exclusion chromatography, powder X-ray diffraction, FT-IR, and ^{1}H-NMR analyses. Mucin interaction and ellipsometer measurements confirmed that mucoadhesion of HA-SH-NFs was increased compared to that of native HA polymer based on an increase in the size (~4 fold), thickness (~3 fold) and adsorbed mucin amount (~2 fold) after 3 h incubation of HA-SH-NFs with mucin. A triggered drug release (~87% w/w) from NFs (drug loading ~17% w/w) occurred after 1 h in the presence of seminal hyaluronidase enzyme. It was observed that in the absence of HAase, the drug release from NFs followed the Peppas kinetic model whereas, in the presence of HAase, NFs followed Weibull model. The HA-SH-NFs were non-cytotoxic to vaginal VK2/E6E7 and End1/E6E7

cells and *L. crispatus* bacteria for 48 h. The results suggested that TFV loaded HA-SH-NFs templates developed in this study have the potential of vaginal delivery of topical microbicides for the prevention of HIV transmission.

In chapter 5, *in vivo* evaluations of the developed HA-NPs and HA-SH-NFs were performed in female C57BL/6 mice. The histological analysis on the mice genital tract and other organs did not show any signs of damage upon once-daily administration of HA-NPs or HA-SH-NFs up to 7 days. Following 24 h exposure, HA-NPs or HA-SH-NFs did not show any significant immune (CD45) cell infiltration in mice vaginal tissues. The cytokines ((IL-1α, IL-1β, IL-6, IP-10, IL-7, MKC, TNF-α) levels (pg/mL) in cervicovaginal lavage and cervicovaginal tissues were not significantly changed compared to control mice data analyzed after 24 h. The cytokine results confirmed the non-immunogenicity of developed nanoformulations. The *in vitro* anti-HIV activity of HA-NPs and HA-SH-NFs was analyzed at the MOI of 10,000, 5,000, and 1,000 using a luciferase assay. The pseudotyped HIV virus particles were generated using lipofectamine plasmid transfection method. The size distribution, mean diameter (~128 nm), and titer (~3.07×10^{10}) of pseudotyped virus particles was analyzed using nanoparticle tracking analysis measurements. The *in vitro* anti-HIV activity data showed that the TFV loaded HA-NPs and HA-SH-NFs were able to inhibit the pseudotyped HIV virus replication. Moreover, the results also confirmed that the structural integrity and anti-HIV activity of TFV was preserved after the nanofabrication processes. The *in vivo* results illustrated that these nanoformulations (HA-NPs and HA-SH-NFs) are promising delivery systems and offered a safe delivery of anti-HIV microbicide candidates.

Overall, the data presented here highlight the applicability and potential of TFV loaded HA-NPs and HA-SH-NFs templates for the topical vaginal delivery of anti-HIV/AIDS microbicide candidates.

APPROVAL PAGE

The faculty listed below, appointed by the Dean of the School of Graduate Studies, have examined the dissertation titled "Formulation of Hyaluronidase Enzyme Sensitive Topical Nanomicrobicides for HIV Virus Transmission Prevention", presented by Vivek Agrahari, candidate for the Doctor of Philosophy Degree, and certify that in their opinion it is worthy of acceptance.

Supervisory Committee

Bi-Botti C. Youan, Ph.D., Committee Chair

Division of Pharmaceutical Sciences

William G. Gutheil, Ph.D.

Division of Pharmaceutical Sciences

Nathan A. Oyler, Ph.D.

Department of Chemistry

Agostino Molteni, Ph.D.

School of Medicine

James B. Murowchick, Ph.D.

Department of Geosciences

CONTENTS

LIST OF FIGURES

LIST OF TABLES

LIST OF REACTION SCHEMES

ACKNOWLEDGMENTS

My wholehearted gratitude goes to my Ph.D. committee chair, **Dr. Bi Botti C. Youan** of the Division of Pharmaceutical Sciences, UMKC, whose mentorship and guidance has not only made this dissertation possible but has proven to be invaluable in this project. He has been the greatest source of inspiration, and encouragement of my Ph.D. career and taught me a great deal about the research, while always making it enjoyable along the way. He has been superb in commenting the drafts I handed in and giving very constructive feedback and critics. I sincerely dedicate all my scientific understanding and passion to him.

I am grateful to my **Ph.D. committee members**, for their invaluable discussions and comments over the years and for their invaluable time. Their unlimited enthusiasm and zeal to the exploration of science have been the major driving force throughout my graduate career.

I am extremely thankful to **Dr. William G. Gutheil** of the Division of Pharmaceutical Sciences, UMKC, for his constant support, guidance on mass spectrometry and analytical chemistry experiments. I earnestly thank him for dedicating time and efforts in reviewing this dissertation and for serving in my Ph.D. committee.

I am deeply thankful to **Dr. Nathan O. Oyler** of the Department of Chemistry, UMKC, for his invaluable suggestions and helps on NMR and FT-IR experiments. I cannot thank him enough for his valuable comments on this dissertation and serving in my Ph.D. supervisory committee.

I highly appreciate **Dr. James B. Murowchick** of the Department of Geosciences, UMKC, for his kind help in XRD experiments and data interpretation. I earnestly thank him for his time in serving in my Ph.D. supervisory committee and genuinely applaud his compassionate gesture.

I am grateful to **Dr. Agostino Molteni** and **Dr. Betty L. Herndon** of the School of Medicine, UMKC, for providing me a great deal of guidance on *in vivo* experiments. Without

their constant suggestions, the *in vivo* experiments were not that easy to perform. Their unlimited enthusiasm to explore the science has been extraordinary and motivational to me. I also thank both of them for serving on my Ph.D. supervisory committee.

I am thankful to **Dr. Russell B. Melchert,** and **Dr. Ashim K. Mitra**, of School of Pharmacy, UMKC, for providing me a great deal of guidance, support and encouragement throughout of my Ph.D. career. I am greatly thankful to them for their inspiring interactions and care devoted towards success of every graduate student.

I express my sincere & heartfelt gratitude to the professors of Division of Pharmaceutical Sciences, UMKC, **Dr. Thomas Johnston**, **Dr. Kun Cheng, Dr. Chi Lee, Dr. Simon Friedman,** and **Dr. Dhananjay Pal** for helping me in building up my concepts and developing the ethics of my profession. I extend my sincere thanks to staff members of School of Pharmacy, UMKC, **Joyce Johnson**, **Sharon Self**, **Nancy Bahner, Shana Eisentrager, Jane Poe, Tamica liege, Julie Willyard,** and **Ashley Ismert** for their invaluable unwavering support and timely help.

My sincere thanks to **Dr. Denis M. Medeiros,** and **Dr. Jennifer Friend** of the School of Graduate Studies, UMKC, for providing me a great deal of guidance, and suggestions. The travel supports/scholarships time-to-time provided by SGS was very helpful in my studies. I am thankful to the staff members of the **SGS and ISAO** at UMKC for their kind support, suggestions on my applications.

Over the years, I am fortunate to work with a team of brilliant scientists in my lab. My heartfelt thanks to **Dr. Youm Ibrahima**, for providing me with both a great deal of guidance and friendship. He has been a constant source of moral support, patience, and humor when things were not always easy. I would like to express my thanks to, **Dr. Miezan Ezoulin**, **Dr. Tao Zhang**, **Jianing Meng**, and other lab mates for their time, support, and friendship. Thanks to all of them for training and collaborating in different lab projects and scientific discussions.

I also owe my thanks to **Dr. Sandeep Putty**, **Dr. Chi Zhang**, and **Sudhanshu Purohit** for their kind supports in mass spectrometry, NMR and FTIR experiments.

My sincere thanks to Dr. James Addo of School of Biological Sciences, UMKC, for his kind help in computation modelling experiments of this dissertation. I am deeply thankful **to Dr. Lane K. Christenson** and **Wei-Ting Hung** of the University of Kansas Medical Center for their kind helps in nanoparticle tracking analysis measurements. My sincere thanks to **Dr. Daniel C. Dim, Dr. Nilofer Qureshi** and **Tim Quinn** of School of Medicine, UMKC, for their kind help and suggestions in histopathology, immunohistochemistry, and bioluminescence assays. I am thankful to **Dr. Michael B. Kruger** and **Joseph A. Crow** of the Department of Physics for allowing me to use the ellipsometer instrument and helping in taking measurements. I am also thankful to **Dr. James N. Hilfiker** and **Dr. Ron Synowicki** of J. A. Woollam Co., Inc., for their kind help and suggestions in ellipsometer data interpretation.

My gratitude goes to my seniors and friends **Dr. Satyakam Singh**, **Dr. Ravi Shukla**, and **Dr. Ashaben Patel**. They brought me through a time where I have been everything from enthusiastic, challenged, and stressed about my work. I feel short of words to express my thanks to them for being a great company during my Ph.D.

My very special and heartfelt thanks to **my family members** whom I owe everything I am today. My Parents, **Munna Lal Gupta** and **Meena Gupta,** who have given me unconditional faith, love and support over the years, and for that I am eternally grateful. They instilled in me the desire to do my best at whatever I have attempted, and that with hard work I was capable of anything. Their sacrifices have helped me become what I am today. I thank my other family members **Vikas Agrahari, Vishal Agrahari, Vinay Agrahari**, **Shraddha Gupta**, **Pragya Agrahari,** and **Aashvi** for their love, friendship, and encouragements in my studies. I also owe my thanks to my in-laws family members **Dr. Vishnukant Kabra**, **Sadhana Kabra**, **Swati Kabra**, **Naveen Mantri and Navaansh** for their faith, support and love.

My heartfelt thanks to my loving wife **Vibhuti Agrahari**, who has been my enduring source of strength and helped with the research and writing of this dissertation in numerous ways. Sometimes, I have even felt lonely during this time, trapped in a nano-world, but as the sentences go: she supported me better & better and stood by me in tough times.

I am thankful to the funding institutions, the **National Institutes of Health (NIH)** and **the National Institute of Allergy and Infectious Diseases (NIAID)** for providing the financial supports (R01AI087304, R21AI083092) in this project. I owe my thanks to the NIH AIDS Research and Reference Reagent Program, Division of AIDS, NIAID, for providing the plasmids and cell lines to perform the in anti-HIV activity assays.

This list is not comprehensive and there were many others who have contributed to my research experience and my enjoyment of these last several years. Thanks to all of them!

CHAPTER 1

INTRODUCTION

1.1. Overview and Statement of the Problem

Acquired immunodeficiency syndrome (AIDS) is a disease caused by Human immunodeficiency virus (HIV) infections. According to the recent report of the global AIDS epidemic, there are approximately 37 million people currently living with HIV/AIDS infections (Figure 1), corresponding to 0.8% of the total population of adults aged 15-49 years according to The Joint United Nations Programme on HIV and AIDS (UNAIDS) statistics (1). Since the epidemic began in the early 1980s, more than 75 million people have been infected and more than 30 million people have died of HIV-related infections. With 2.0 million new infections and 1.2 million deaths in 2014-2015, AIDS still remains the deadliest epidemic of our time (1).

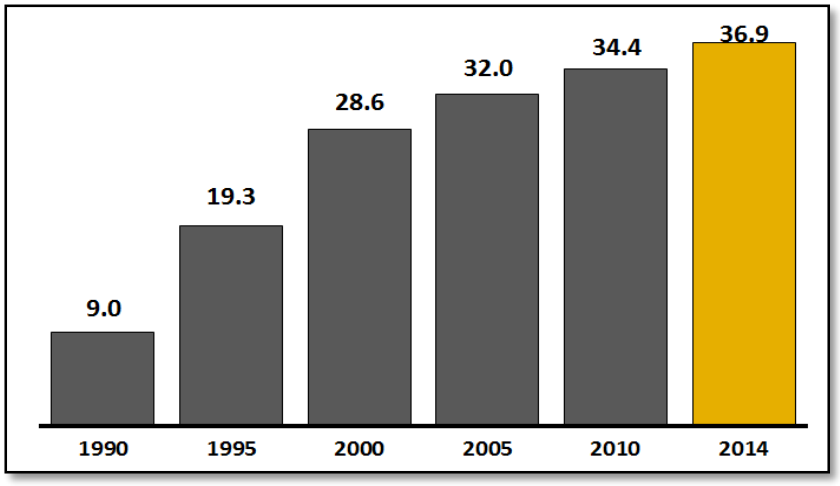

Figure 1. Global Estimates of People Living with HIV/AIDS 1990-2014.

Unprotected heterosexual vaginal intercourse has become one of the major routes of HIV/AIDS infections and in general, women are at greater risk of heterosexual transmission of HIV virus (2). Women constitute over 50% of the HIV infected population, although in African

countries this percentage rises to approximately 60% (Figure 2A & 2B) (3). Moreover, young women aged 15-24 years are more likely (twice) to be infected with HIV compared to men of the same age.

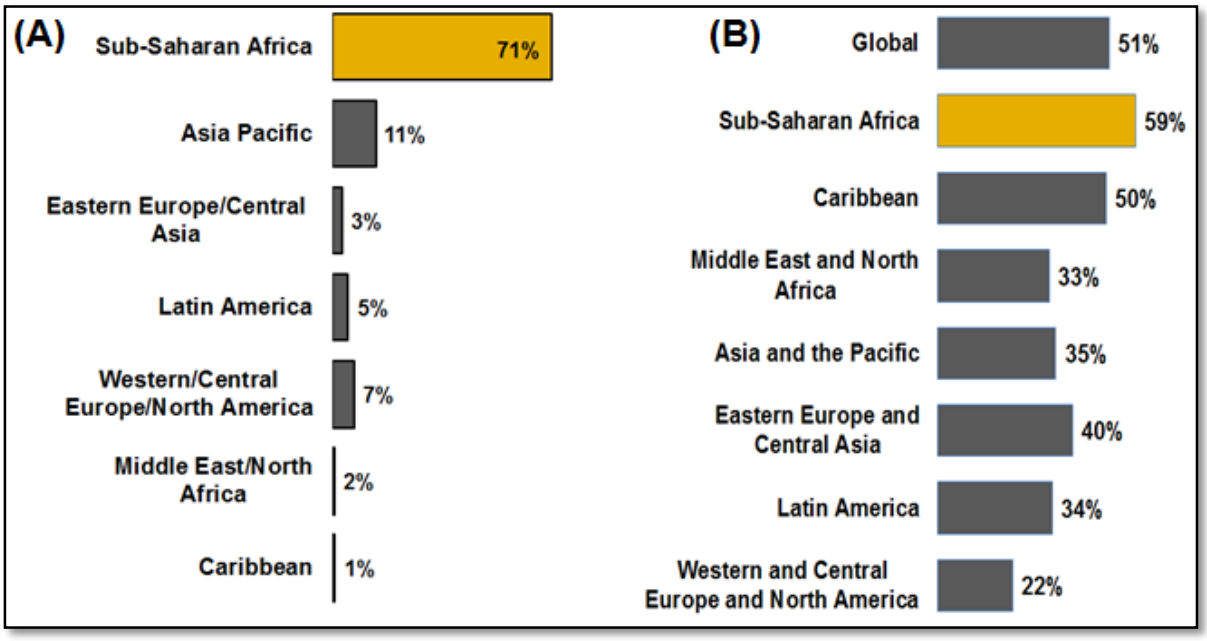

Figure 2. (A) People Living with HIV by Region as Percent of Global Total, (2014). (B) Women as Share of People Living with HIV by Region, (2014).

There are multiple factors such as biological susceptibility, presence of other sexually transmitted diseases (STDs), hormonal contraceptive use and sociocultural discrepancies those amplify women's vulnerability to HIV infection (4). Moreover, among the efficiency of heterosexual transmission from male-to-female is 2 to 3 times greater under normal conditions and 8 times more in the presence of STDs as compared to that from female-to-male. Pregnancy is also shown to cause a two-fold increase in the risk of HIV due to thinned vaginal epithelium and exposure of columnar cervical epithelium. Early efforts were focused on the use of physical barriers such as condoms. However, this approach has its own limitations such as expensive and cumbersome to use and is not a female controlled method of HIV prophylaxis (5). Moreover, condom effectiveness has been estimated to be approximately 80% against

heterosexual transmission and 70% against male-to-male sexual transmission of HIV infection, respectively, (6).

Over the years, various delivery systems have been developed for prophylaxis of HIV (7, 8). Broadly, these systems can be divided into four categories viz. vaccines, macromolecular HIV entry inhibitors, antiretroviral (ARV) drugs, and nucleic acid-based therapeutics (3, 8, 9). Development of vaccines has been the most prominent prophylactic strategy for HIV virus infections. However, developing a safe and effective vaccine against HIV is a very challenging because of the vast genetic diversity and high mutation rate of HIV virus (9, 10). Several macromolecule entry inhibitors inhibit the binding of HIV to their target CD4 cells by interacting with envelope glycoproteins. These entry inhibitors showed a great promise in preclinical models, however, the clinical trials in humans failed to show any significant protection (9, 10). To date, despite a great deal of effort, there are no effective vaccines or prevention method against HIV infection is available. Thus, it is important to develop an effective method for prevention of HIV virus vaginal transmission that can be used by women.

Currently, female-controlled prophylactic methods using microbicides are the major focus among HIV prevention strategies (3, 8, 9). These are agents applied within the vagina or rectum to prevent the transmission of sexually transmitted diseases including the HIV infections (11). A great variety of HIV microbicides candidates have been studied and tested (12-15). A lot of the emphasis has been put on the microbicide gel formulation, (16-20). however, such gel systems suffer from several disadvantages such as their limitation of encapsulating hydrophobic microbicides, the low retention time requires a high dosing frequency (21), poor acceptability and adherence. Also, to achieve a significant effect, the ideal microbicide formulation should have high vaginal retention time, higher drug loading and be able to release a high dose of microbicides in a short period of time when required *(On-demand delivery systems)*.

With the recent advances in delivery system, nanotechnology provide one possibility of microbicide delivery due to their unique characteristics, such as small size, protection of native drug against harsh environment, ability to reduce irritation at the target site, and the ability of targeted and controlled release of drugs (22). Since, human semen is a potential carrier of the HIV virus during male to female intercourse (23), designing a semen-triggered nanoformulations delivery system would have the potential to inactivate or kill the HIV virus prior to exposure and penetration of the vaginal mucosa and systemic exposure. Human semen contains various specific enzymes in its content such as, hyaluronidase, acidic and alkaline phosphatases. Therefore, to develop a delivery system capable of giving response in the presence of specific enzymes of human seminal fluid will have the potential to inactivate or kill the HIV virus prior to exposure and penetration of the vaginal mucosa.

1.2. Research Hypothesis

Based on the above mentioned facts, the research hypothesis of this work is to formulate a stimuli-sensitive and stable anti-HIV nanomicrobicides delivery system that will be safe and effective for HIV/AIDS therapeutics in women (Figure 3).

1.3. Objectives

The presented dissertation aims at exploring different nanoformulations strategies for HIV therapeutics in women. The objectives of this dissertation are:

(1) To design and optimize a stimuli-sensitive nanoparticle formulation loaded with anti-HIV topical microbicide. Design of experiments (DOE) is applied in the formulation and process variables screening and optimization. The developed formulations should

has a rapid/triggered release of microbicide drug under the influence of human seminal fluid enzyme.

(2) The knowledge gained in previous aim is then applied in the development of stimuli-sensitive mucoadhesive nanofiber formulations loaded with anti-HIV topical microbicide tenofovir.

(3) In both the aims, the physicochemical characteristics of nanoformulations such as mean diameter, drug loading, surface morphology, stability, *in vitro* drug release profile and drug release kinetics were evaluated. The developed nanoformulations should be safe and thus, the *in vitro* cytotoxicity and cellular uptake are evaluated using vaginal epithelial and endothelial cells. Finally, nanoformulations were evaluated for their preclinical safety, non-immunogenicity, and *in vitro* anti-HIV activity in mice model.

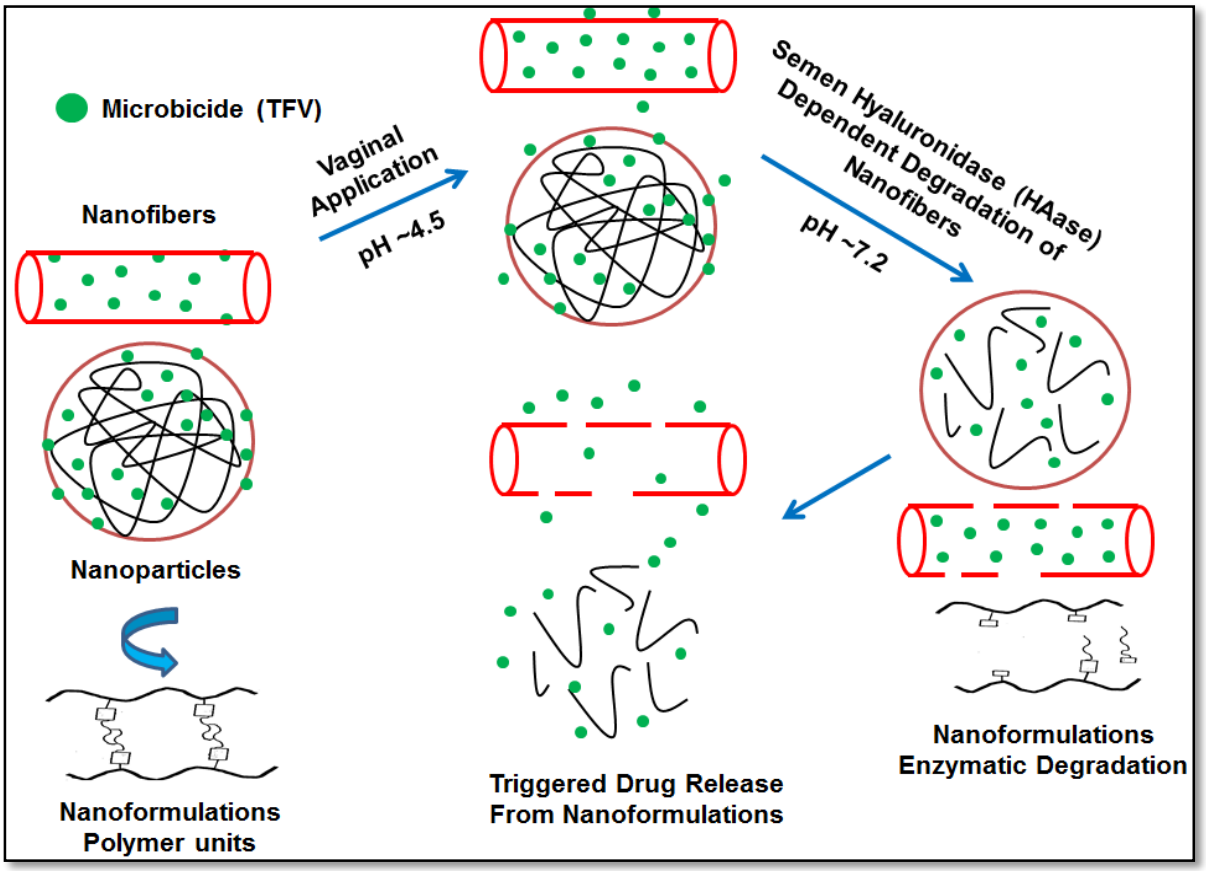

Figure 3. Microbicide Loaded Stimuli-sensitive Nanoformulations Delivery System for HIV Prevention and Treatment.

CHAPTER 2

OVERVIEW AND PANDEMIC OF HIV INFECTIONS

2.1. Steps Involved In HIV Life Cycle and Vaginal Acquisition of HIV Infection

Unprotected heterosexual vaginal intercourse has become one of the major routes of HIV infection. To develop a delivery system for prevention of vaginal transmission of HIV, an understanding about the steps involved in HIV life cycle and its cervicovaginal (CV) mucosal transmission is required (Figure 4). There are multiple steps in the life cycle of HIV (24, 25) as explained below.

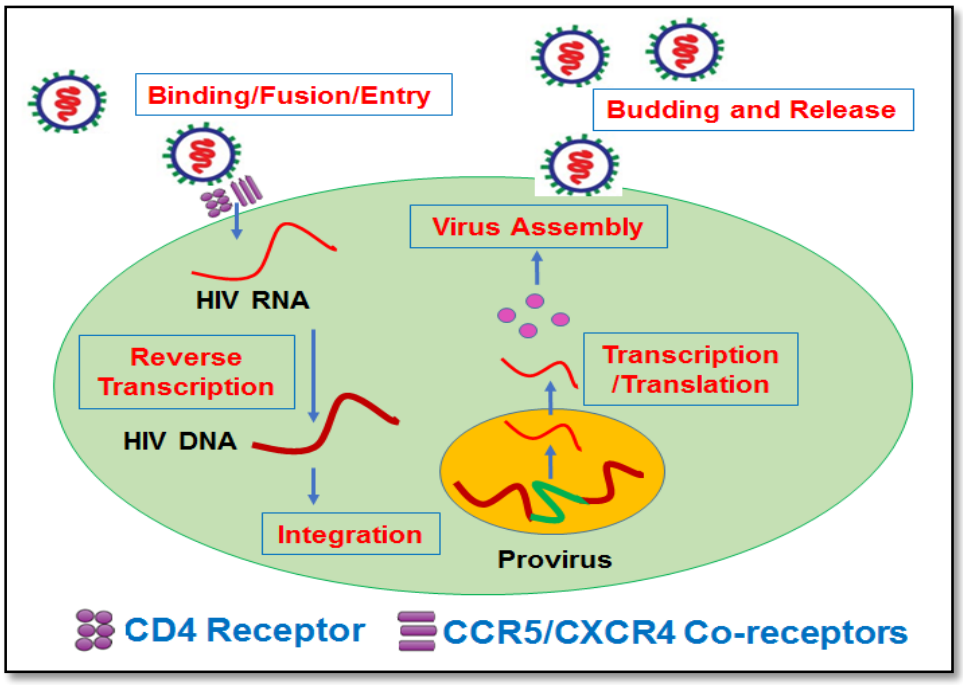

Figure 4. Life cycle of HIV Virus.

1. **Binding and Fusion**: The first step in the HIV entry process is binding of HIV gp120 to the host cell CD4 receptors, expressed on the surface of T lymphocytes, monocytes, macrophages and dendritic cells. Binding to CD4 is essential to the HIV infection process

because it induces conformational changes in the viral envelope that are necessary for membrane fusion and viral entry. The next step is the binding of gp120 to co-receptors CCR5 and CXCR4. After the first conformational change during the binding of gp120 to CD4 cell receptor, the viral gp120-gp41 glycoprotein complex undergoes further conformational changes, exposing the N-terminal domain of gp41 and allowing the fusion peptide sequence to insert into the cellular membrane of the host cell.

2. **Reverse Transcription**: The fusion stage is followed by the reverse transcription and integration stages. The reverse transcriptase (RT) enzyme converts single-stranded HIV RNA into double-stranded HIV DNA through a process called reverse transcription, so it can be integrated into the host DNA.
3. **Integration**: The new virus genetic material enters the nucleus of the CD4 cell and integrate itself into host genetic material with the help of integrase enzyme. Once the viral DNA has integrated into the host cell's DNA, the host cell is infected for the remainder of its life. The integrated viral DNA is now called as a provirus.
4. **Transcription and Translation**: The provirus DNA serves as a template for the creation of new viral RNA via a process known as transcription using the host cell enzymes**.** This results in the production of multiple copies of viral RNA. The newly formed viral RNA moves out of the infected cell's nucleus. The viral RNA carries code for the synthesis of viral proteins and enzymes through the translation process. The code is translated into long chains of amino-acids (polypeptide chains), which fold to produce structural proteins such as the viral envelope and enzymes (reverse transcriptase, integrase, and proteases).
5. **Assembly, Budding and Release**: The protease enzymes cut the longer HIV proteins into individual proteins. When these come together with the virus genetic material, a new virus bud has been assembled. Budding is the final stage of the HIV virus life cycle. In this stage, the virus pushes itself out of the host cell, taking with it part of the membrane of the cell.

This outer part covers the virus and contains all of the structures necessary to bind to a new CD4 cell and receptors and begin the process again. A single infected cell can release many new HIV particles which move on to infect other cells in various parts of the body, where the viral life cycle is repeated. The infected cells are eventually destroyed.

Vaginal Acquisition of HIV Infection

The integrity of vaginal and cervical epithelium has been highly associated as a risk factor in vaginal acquisition of HIV (26). It has been shown that the virus can penetrate through thin gaps between the squamous epithelial cells and pass several cell layers from the luminal side. The mucosal surface, when intact, serves as a natural barrier for HIV. The vaginal microbiota in healthy adult women is dominated by *Lactobacillus* species. Some features such as low pH in the environment and the hydrogen peroxide (H_2O_2) produced by vaginal *Lactobacillus* flora has a virucidal effect (27, 28). Therefore, the chance of vaginal acquisition of HIV is relatively low when the mucosal barrier is intact (29-31). If vaginal mucosal barrier is compromised, cell-free HIV virion can easily gain access to the Langerhans cells (LC), which is a type of dendritic cells (DC) having dendritic projections (dendrites) that might extend to the mucosal surface (32, 33). This allows the DCs to directly entrap HIV when there's only minor tissue damage at mucosal surface. Meanwhile, CD4+ T cells and macrophages, the primary target cells of HIV, usually reside in the lamina propria and columnar epithelium come closer to the CV mucosa. Within hours of infection, these target cells in the sub-epithelium are infected (26). The mechanism of vaginal acquisition of HIV infection was shown in Figure 5.

There are several other factors which may can significantly increase the likelihood of HIV transmission by disrupting the integrity of vaginal mucosal. These factors including the dry or traumatic sex (34-36), bacterial vaginosis (37, 38), or inflammatory diseases of the vagina (39-42). These factors enhance the HIV vaginal transmission through increasing the amount of

target cells to the vaginal mucosa, alteration of normal vaginal microbiota and vaginal pH, disruption of H_2O_2 producing *Lactobacillus* bacteria, thinning and disrupting the cellular lining, and recruiting a pool of target cells for local HIV expansion [17]. After HIV expands locally, dissemination of infection occurs and the movement of virus to lymph nodes and secondary lymphoid organs generates a systemic infection.

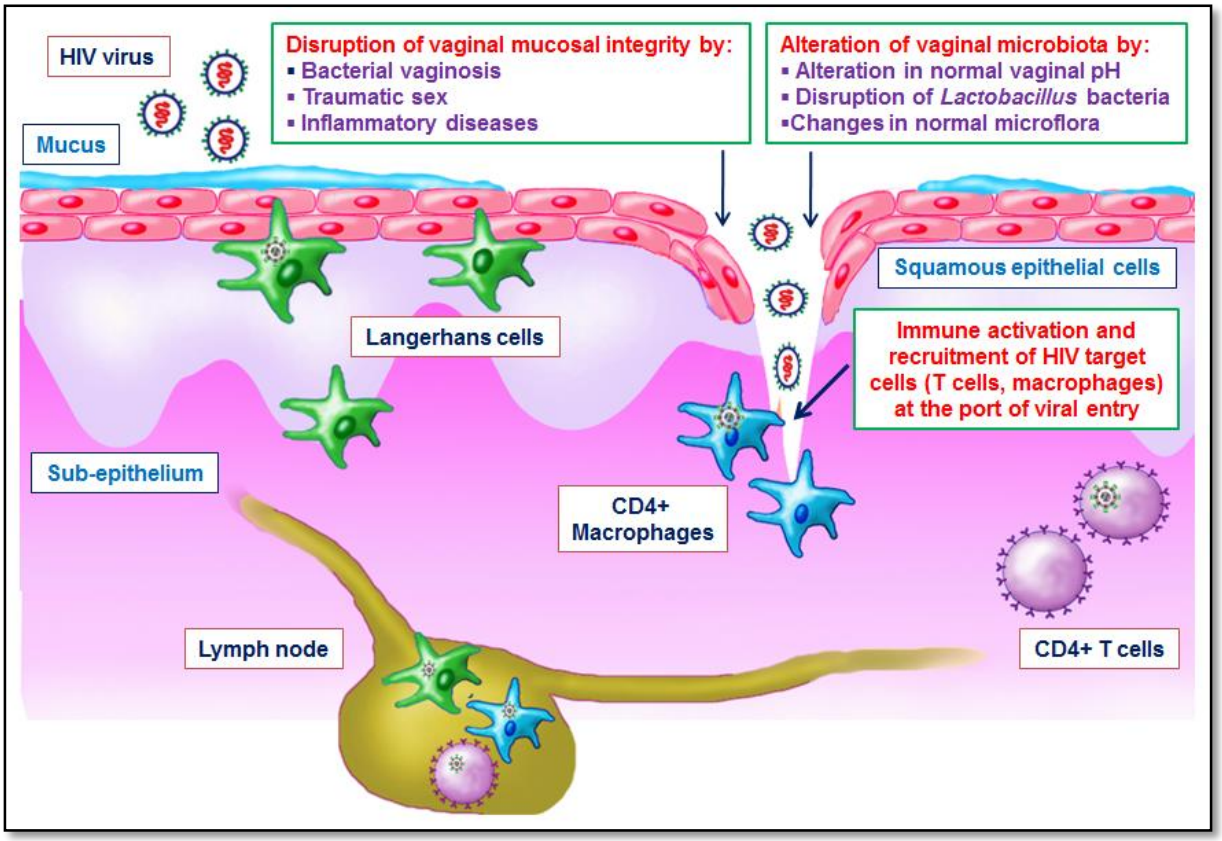

Figure 5. Factors Affecting and the Mechanism of Vaginal Acquisition of HIV Infection.

2.2. Topical Microbicides for HIV Prevention

Microbicide candidates prevent or reduce the sexual transmission of HIV or other sexually transmitted infections (STIs) when used in the vagina or rectum. Currently, the leading microbicide candidates are the antiretroviral (ARV) drugs and there are more than 25 ARVs targeting different steps of the viral cycle have been approved by the U.S. Food and Drug

Administration (FDA) (3). There are several categories of ARV drugs that have been used as potential microbicides including Reverse-transcriptase inhibitors, Protease inhibitors, Integrase inhibitors, Entry/Fusion inhibitors and, Maturation inhibitors (Table 1) (9, 43).

Table 1: Classification of Antiretroviral Drugs.

Classifications	**Ref.**
Category: Reverse Transcriptase (RT) Inhibitors **MOA:** RT Inhibitors prevent the RT enzyme from converting single-stranded HIV RNA into double-stranded HIV DNA through a process called reverse transcription. ***Subcategory-1:*** Nucleoside/nucleotide RT inhibitors **(**NRTIs**)** **MOA:** NRTIs act by blocking RT enzyme. These drugs are preferentially incorporated into HIV DNA, leading to termination of DNA synthesis. **Drugs:** Tenofovir, Lamivudine, Emtricitabine, Zidovudine, Abacavir, Adefovir, Didanosine, Zalcitabine, Entecavir, Stavudine, Tenofovir disoproxil fumarate, Tenofovir alafenamide fumarate, Festinavir, Apricitabine. ***Subcategory-2:*** Non-nucleoside RT inhibitors **(**NNRTIs**)** **MOA:** NNRTIs bind to a pocket near the active site, which causes a conformational change of the enzyme and inhibition of reverse transcription. **Drugs:** Efavirenz, Nevirapine, Etravirine, Rilpiverine, Delavirdine, Doravirine	(44-46)
Category: Integrase Inhibitors **MOA:** Block the action of HIV enzyme integrase, which the virus uses to integrate its genetic material into the DNA of the host cell. **Drugs:** Raltegravir, Elvitegravir, Dolutegravir	(47, 48)
Category: Protease Inhibitors **MOA:** Inhibits virus-specific processing of viral Gag and Gag-Pol polyproteins in HIV infected cells by inhibiting viral protease.	(49)

Drugs: Saquinavir, Lopinavir, Atazanavir, Darunavir, Ritonavir, Indinavir, Nelfinavir, Amprenavir, Fosamprenavir, Tipranavir	
Category: Entry Inhibitors **MOA:** Interfere with the virus ability to bind to gp120 receptors on the outer surface of the cell it tries to enter. **Drugs:** Maraviroc, Vicriviroc	(50)
Category: Fusion Inhibitors **MOA:** Binds to the HIV-1 membrane glycoprotein gp41 and prevents the conformational changes required for viral membrane fusion with the cells. This prevents HIV from entering a cell. **Drugs:** Enfuvirtide, Sifuvirtide	(50)
Category: Maturation Inhibitors **MOA:** Maturation inhibitors inhibit the last step in gag processing in which the viral capsid polyprotein is cleaved, thereby blocking the conversion of the polyprotein into the mature capsid protein. Because these viral particles have a defective core, the virions released consist mainly of non-infectious virus particles. **Drugs:** Alpha interferon, Bevirimat, Vivecon.	(51, 52)
Category: Capsid Inhibitors **MOA:** Inhibitors of HIV-gag polypeptide assembly. Dismantles assembled HIV-1 capsid assembly tubes. **Drugs:** under development	(53)
Newer categories under development: RNaseH inhibitors, Budding inhibitors, LEDGF-based inhibitors, Vpu/tetherin-based inhibitors, Vif/APOBEC3G-based inhibitors, CA/TRIM5α-based inhibitors.	(54)

The only topical microbicide candidate to show high efficacy to date is the Tenofovir (TFV) which belongs to the category of ARV drugs under the subcategory of NRTIs (17, 55). TFV is a BCS Class III drug with high solubility but low permeability (9). It is a small molecule (molecular weight of 287.213 g/mol), hydrophilic drug with a log P value of -1.6 and two pKa values of 2.0 and 6.7 (56). TFV formulations such as vaginal gel (57), vaginal ring (58), solid lipid NPs (59), mucoadhesive chitosan NPs (60, 61), pH responsive NPs (62) and, microspheres (63), intended for the prevention of HIV transmission, have been successfully engineered. Although, TFV has been successfully considered as a topical vaginal microbicide, the extreme hydrophilicity of the TFV poses a major problem for its encapsulation into formulations.

2.3. Formulation and Delivery Considerations of Topical Microbicide Candidates

In the case of prophylaxis using ARV drugs, oral, rectal and vaginal routes have mainly been explored (9, 64) (Table 2). Oral route is most convenient and preferred however, it presents several challenges in microbicide delivery compared to vaginal and rectal routes (Table 2). Since, the heterosexual transmission of HIV through CV mucosa is the major route of HIV infection, vaginal route has been explored vastly for anti-HIV drug delivery applications.

Table 2: Anti-HIV Delivery System Routes.

Delivery route	Advantages	Limitations	Ref.
Oral	• Convenient and preferred. • Easy and economical. • Non-invasive. • High patient acceptability.	• Therapeutic agent's instability under harsh acidic environment of stomach and various digestive enzymes.	(9, 64)

		• First-pass metabolism.	
Vaginal	• Potential for non-invasive, controlled delivery of drugs intended for both local and systemic effect. • The avoidance of hepatic first-pass metabolism. • The large surface area, permeability and rich blood supply of the mucous membrane of the vagina, provide significant potential for the delivery of a wide range of compounds, including peptides and proteins. • Large surface area and rich blood supply, provides a rapid drug absorption and quick onset of action.	• As hormone levels (especially estrogen) change over the menstrual cycle, several alterations in vaginal conditions are induced involving the thickness of the epithelial cell layer, the width of intercellular channels, pH, and secretions. These all affect the drug efficacy and distribution. • Low retention to the vaginal epithelium. • Leakage and messiness, thereby causing poor patient compliance. • Limitation of volume of drug formulations to be used in small vaginal cavity.	(64, 65)
Rectal	• Non-invasive and relatively stable conditions such as pH, temperature and rectal fluid volume. • Rich blood and lymphatic drainage may allow significant	• Erratic drug absorption. • Presence and traffic of stool. • Acceptability (cultural) issues.	(64, 66, 67)

systemic levels for different drugs. • Low enzymatic activity compared to the GI tract. • Relatively high amounts of drug can be administered. • Rapid onset of effect. • Self-administration, painless delivery.	• May cause irritation dependent on drug and drug product characteristics. • May cause discomfort, leakage. • Low patient acceptability. • Smaller surface area of the rectal mucosa limits its absorptive capacity.

Characteristics of an Ideal Vaginal Microbicide Candidate

In order to achieve a therapeutic concentrations of a microbicide drug at the target site, several factors should be taken into consideration as given below. Such factors may have an impact on the drug release from the delivery system and consequently on the drug concentration in the target cells, and thus they may influence their potential therapeutic effects (3, 8, 9).

- Drug physicochemical properties: Solubility, ionization, molecular weight, logP, permeability, and crystalline/amorphous nature.
- Formulation aspects: Compatibility, toxicity, release rate of drug, mucosal surface coverage, homogeneity of drug distribution in formulation systems.
- Anatomical site characteristics: Vaginal fluid composition and pH before and after sexual intercourse, effect of seminal fluid, etc.
- Physio-pathological conditions of vagina at the time of product administration: Menstrual cycle changes, presence of seminal fluid, bacterial vaginosis or other genital infections.

- Physio-pathological conditions applying at the time of administration such as menstrual cycle changes, presence of seminal fluid, bacterial vaginosis or other genital infections.

Several important criteria for vaginal microbicide products with regard to their efficacy and safety have been established (3, 8, 9). The required characteristics of an ideal vaginal microbicide formulation product are shown in Table 3.

Table 3: Characteristics of an Ideal Vaginal Microbicide Product (3, 8, 9).

Property	Description
Acceptability/ feasibility of manufacturing	• Products should be simple and have a convenient dosage regimen. • Products must be acceptable by high-risk populations. • Product should be non-irritating, effective, with a long-lasting action. • Formulation production must be feasible, allowing for the production in the amounts needed to meet projected needs. • Product that can be used in conjunction with sex should be developed. • Should also be compatible with the existing prevention strategy, the male condom, and have no adverse effects on reproductive health.
Efficacy	• Microbicides must be efficient in preventing HIV transmission. • Active against a range of sexually transmitted pathogens • Should provide a long-term efficacy. It is also essential that the product is not inducing any drug resistance.
Low cost	• Microbicides must be affordable by high-risk populations. The product must be economically feasible as well as easy to use without interfering with sexual pleasure.

Safety	• Products should be safe, with no localized/systemic toxicity. • Product should not have any effect on fertility and/or fetal abnormalities. • Have no-effect on the normal vaginal microbiota. • Must show inertness towards the vaginal epithelium.
Stability	• The microbicide products should be stable under diverse environmental conditions of vagina such as low pH of 3-4.5 and pH of about 7-8 during the sexual intercourse and in the presence of hydrogen peroxide released from *Lactobacill*i. • The product must have adequate shelf-life, with tropical conditions and the potential for lack of proper storage being considered.
Drug delivery	• A microbicide product should provide a significant drug level at the target site. • Product should provide a controlled, sustained or stimuli sensitive drug release as required. • Higher compatibility with different types of drugs having different physicochemical properties. • The dosage forms should allow the active drug to distribute through the vaginal epithelium for adequate time in order to be able to penetrate and reach the target cells. • Prolonged residence time on vaginal site

Safety Consideration of an Ideal Vaginal Microbicide Candidate

An ideal topical microbicide would not only be effective to prevent the vaginal transmission of HIV-1 virus but would also be safe for CV application, preserving the inherent defense system of the genital tract and causing little or no epithelial damage or inflammation

to the genital tract tissues. Based on this, it is important to evaluate the physicochemical properties, safety/cytotoxicity, cytokine secretion, epithelial damage, and tissue inflammatory reaction for any microbicide formulations (Table 4).

Table 4: Vaginal/Rectal Microbicide Product Characterization.

Physicochemical properties	**Activity/Efficacy**	**Toxicity/Safety**	**Pharmacokinetics/ Biodistribution**
Size, pH, charge, viscosity, stiffness, hardness, osmolality, spreading, retention, stability, permeation, compatibility, odor, appearance.	Cell lines *Ex vivo* *In vivo* (animal model)	Cell lines Vaginal microbiota Immune response *In vivo* (animal model), Epithelial integrity/damage	Cell lines *Ex vivo* *In vivo* (animal model)
End point	**End point**	**End point**	**End point**
Optimal physicochemical properties of microbicide products based on the specific requirements	Anti-HIV activity (EC_{50}) Cell uptake Cell-resistance *In vivo* protection	Cytotoxicity effect (CC_{50}) Pro-inflammatory potential *Lactobacillus* viability, vaginal pH changes Potential for infection enhancement	Permeability Drug distribution in tissues/plasma Drug metabolism PK/PD correlation

Cytokines play an important role in HIV infection and transmission through CV mucosa (68, 69) and must be evaluated for any microbicide formulation. A microbicide formulation may elicit a transient change in the mucosal tissues, significant production and secretion of proinflammatory cytokines. A microbicide formulation was supposed to be in contact with the CV epithelium for a variable time before sexual intercourse and thus, should not cause the onset of inflammation or cytokine secretions (31). The role of different cytokines and in HIV infection and transmission is given in Table 5.

Table 5: Cytokine Effects on HIV Disease Progression and Viral Replication.

Cytokine	**Producing cells**	**Alteration in HIV infection**	**Potential effect in HIV replication**
IL-1	Macrophage, B cells, endothelial cells and fibroblasts in response to infections and inflammation	↑	↑ Replication ↑ CD8+ T cell-mediated HIV suppression
IL-2	CD4 and CD8 T cells	↓	↑ Replication
IL-4	Activated CD4 T cells, but also by NK cells, mast cells and basophils	↑	↑ Replication ↓TNF-α and IL-1β
IL-6	T cells, B cells, monocytes, macrophages, fibroblasts and endothelial cells, in response to viral or bacterial infection	↑	↑ Replication
IL-7	• Prostate in semen. • Stromal cells in the bone marrow and thymus.	↑	↑ Replication ↑ HIV-1 transmission and dissemination

	• Keratinocytes, dendritic cells, hepatocytes, neurons, and epithelial cells.		↑ CD8+ T cell mediated effect
IL-8	Macrophages, T cells, neutrophils and endothelial cells in acute and chronic inflammatory states	↑	↑ Replication
IL-10	Activated T and B cells, monocytes, macrophages and keratinocytes	↑	↓ Replication
IL-12	Dendritic cells of macrophage lineage	↑ initially but as HIV progresses, IFN-γ ↓ and thus IL-12 level ↓	↑ Replication
IL-13	Dendritic cells and T cells	↓	↓ Replication, ↓ RT
IL-15	Monocytes, macrophages and dendritic cells	↑	↑ Replication ↑ CD8+ T cell-mediated HIV suppression
IL-16	CD4 T cells, mast cells and eosinophils in response to stimuli (mitogens, histamine and serotonin)	↓	↓ Replication
IL-17	CD4+ T helper (Th) cells, referred to as Th17 cells	↑	↑ Speed of HIV pathogenesis

IL-18	Macrophages and other cells	↑ Serum level	↑ HIV Production through NF-kB pathway
TFN-α/β	Monocytes, macrophages, T cells, B cells, NK cells, neutrophils and microglia cells	↑	↑ Replication
IFN-α/β/γ	• IFN-α is produced in leukocytes infected with virus. • IFN-β is from fibroblasts infected with virus. • IFN-γ is induced by the stimulation of sensitized lymphocytes with antigen or non-sensitized lymphocytes with mitogens.	↓	Antiviral effect

2.4. DOSAGE FORMS FOR THE VAGINAL DELIVERY OF MICROBICIDES

Microbicides have been extensively investigated in numerous dosage forms such as gels, creams, films, nanoformulations, liposomes, quick-dissolving tablets and intravaginal rings. The advantages, and limitations of the different types of microbicide dosage forms are presented in Table 6.

Table 6: Vaginal Delivery Systems, Their Advantages and Limitations (3, 8, 9).

Delivery systems	**Advantages**	**Limitations**
Gels	• Female controlled. • Provide lubrication.	• Messy and may leak out of the vaginal cavity.

	• Easy to manufacture. • Relevant for pericoital or daily use.	• Non-uniform distribution and leakage which lower the anti-HIV efficacy. • The short bio-retention requires the user to apply hours before sex, which leads to significant patient compliance issues.
Rings	• Designed to release microbicides in a controlled manner after insertion. • Enhanced product stability as a solid dosage form. • Easy to insert and remove, and no side-effects are experienced. • Can provide a long-term drug release resulting in less frequent application and thus, improved patient compliance.	• Expensive to fabricate. • The rings needs to be carefully compressed and placed in the upper third part of vagina to avoid involuntary expulsion. • May not release drug at levels equal to what is achievable with gels, films.
Films	• Compared to gels, films may be easier to apply and less messy. • Increased user acceptability. • The films rapidly dissolve once in contact with the vaginal fluids with	• Commercial application of vaginal films is limited and the optimization is still under development. • Usually, very low drug loadings (<1% w/w).

	no introduction of additional fluids, thus reducing the leakage. • Their rapid dissolving nature ensures quick release once inserted. • Increased patient acceptability, retention time, and drug stability. • The small size of the film and the lack of the need for applicators results in a less expensive product.	• Low overall mass may preclude delivery of sufficient doses of drugs. • The physical properties of films must be controlled to avoid sharp edges that could induce abrasion upon application and use.
Tablets	• Female controlled and easy to formulate. • Coitally independent: daily; every few days to once a week coitally dependent: prior to coitus; before and after coitus. • No leakage. • Cost effective formulation.	• Applicator may be required. • Disintegration of product and dissolution of drug depend on local hydration. • CV distribution is a concern. • May leave a grainy residue in the vaginal cavity after dissolution
Suppositories	• Self-Controlled and no leakage. • No applicator required. • Low potential for side-effects. • Possibility for rapid/sustained release of drugs. • Stable formulation	• Absorption in vaginal epithelia may be controlled by hydration issues. • Vaginal epithelium irritation may result from contact of solids.

Nanoparticles (NPs)	• Not only to protect the active agent but also facilitate penetration into the vaginal mucosa, allowing drug to reach HIV target cells. • Can provide sustained release of drugs, necessary for maintaining protective drug concentrations between the time of dosing and the time of intercourse. • More controlled vaginal absorption compared to gel, thereby potentially requiring reduced amounts of drug. • Encapsulation and delivery of various drugs on one nanocarrier. • Adjustable physicochemical properties (size, shape, surface functionality).	• Challenges include the biocompatibility, toxicity, safety and stability • Scale-up of nanoformulations development. • Small size and large surface area can leads to particle aggregation. • Burst release of drug. • Non-uniformity of size distribution.
Nanofibers (NFs)	• Typically soft and non-abrasive, highly flexible. • Variety of possible geometries and mechanical properties. • No leakage or messiness with delivery of fibers into the vaginal cavity.	• Expensive process compared to conventional fibers due to low production rate and high instrumentation cost. • The vapors emitting from the electrospinning solution

		used may be toxic and raise concern over health hazard. • Electrospinning process depends on several variables.
Liposomes and Solid Lipid NPs	• Can provide a sustained and controlled release of an incorporated drug. • An increase in drug stability, the ability of incorporating both lipophilic and hydrophilic drugs. • Higher biocompatibility and non-immunogenicity.	• Manufacturing cost, scale up. • Lipid instability and toxic by-products. • Low drug loading capacity. • Liquid nature of the preparation is a problem since they cannot offer the required effective-retention/contact with the vaginal epithelium. • The commercial production of sterile liposomes is expensive.
Dendrimers	• Controlled synthesis and different drugs could be conjugated to a single dendrimer. • Can be tailored by manipulating the structure/composition or number of	• Complexity of preparation methods. • Potential toxicity issues.

	surface functional groups to obtain the desired properties. • Thermodynamically stable system.

Nanotechnology-Based Approaches for HIV/AIDS Prevention

The introduction of nanotechnology in the field of drug delivery opened exciting therapeutic options for the treatment of several diseases using macromolecule or small molecule drugs (70-72). The development of nanoparticle-based vaginal drug delivery formulations has largely been focused on HIV pre-exposure prophylaxis (PrEP) (3, 8, 9). Nanocarriers offer various advantages which would be useful to overcome challenges/problems associated with current HIV prophylactic modalities (3, 8, 9). The specific advantages of nanotechnology in microbicide product development compared to conventional vaginal dosage forms are given in Table 7. Although there are benefits, but, there are several challenges that must be overcome in the future for successful translation of nano-microbicides to clinical settings. These challenges include the biocompatibility, safety, stability, as well as the scale-up of nanoformulations development. It is also important that the developed nanotechnology should offer significant cost-to-benefit ratio in order to gain wide acceptability as the majority of HIV affected individuals are from economically poor and developing countries.

Table 7: Advantages of Nanotechnology over Conventional Vaginal Dosage Forms (3, 8, 9).

Feature	Conventional dosage form	Nano-sized delivery systems
Patient compliance	• Leakage and messiness. • Short residence time and require repeated dosing. • Undesirable adverse effects.	• Enhanced patient compliance. • Potentially no leakage. • Reduced adverse effects.

Vaginal physiological conditions	• Has significant influence on drug efficacy.	• Has less effects on drug efficacy. • Vaginal physiological factors can be exploited, e.g., pH, temp., enzyme, for stimuli-responsive drug release. • Can provide improved drug distribution to target cells and tissues, improving efficacy.
Physico-chemical properties of microbicides	• Low encapsulation efficiency. • Considerable effect on drug absorption and efficacy. • Low water solubility results in decreased drug efficacy. • Low drug stability may be due to hydrolysis and or enzymatic degradation.	• Ability to encapsulate high drug content. • Feasibility of carrying both lipophilic and hydrophilic drugs. • Can facilitate the dissolution of hydrophobic drugs, while improving drug stability from hydrolysis and enzymatic degradation. • Increase the aqueous solubility of pharmaceuticals. • Deliver drugs for slow release to maintain the therapeutic dose.
Specificity and targeting ability	• Non-specific drug delivery and response.	• Specific drug delivery is possible by surface functionalization with targeting ligands. • Improve the active/passive target specificity in drug delivery.

	• Improve the bioavailability and biocompatibility of drugs, non-toxic, non-allergenic and non-irritating.

2.5. Stimuli-Sensitive Nanoformulations Delivery System in Vaginal Microbicide Research

The development of stimuli-sensitive delivery systems is an active area of pharmaceutical research (73, 74). These novel delivery systems, usually termed 'smart' are able to respond to their environment to trigger the release of macromolecules/small molecule drugs and localize the therapeutic moiety within a particular site. Stimuli responsive materials are based on the principle that a specific stimulus can change the structural confirmation of formulations which can facilitate the release of drugs encapsulated in the delivery system. Although, the concept of stimuli-responsive systems are widely used in cancer therapeutics, it is an exciting research area in the nanocarrier development for HIV therapeutics. There are a number of signals (pH, temperature, enzymes, oxidative stress, magnetic field, etc.) those can be used as a stimulus in anti-HIV drug delivery systems (74, 75).

Normal Vaginal Physiology and Change during the Sexual Intercourse

Vaginal flora plays a significant role in maintaining a healthy vaginal environment. The pH of the CV mucosa with healthy vaginal microflora is acidic (pH 3.5-4.5) due to the presence of lactic acid produced by *Lactobacillus* bacteria (76). Women with bacterial vaginosis (BV) and other genital infections have a higher mean CV pH of 5 to 6 (76, 77). The CV pH is also significantly higher (6 to 7) during the menstruation cycle (78). During the sexual intercourse, CV fluid is neutralized (pH 7.0-7.4) by the alkaline pH (7.0-8.0) of human semen (with higher buffer capacity) within couple of seconds of arrival of seminal fluid (Figure 6) (77, 79). The

neutralization of CV fluid provides a favorable condition to increase male to female HIV virus transmission. Moreover, the anatomy and physiology of the mucosal barrier changes significantly during the menstrual cycle and in sexually transmitted disease conditions such as BV which could further enhance the virus transmission process (77). This change in pH of the vaginal flora can be targeted to develop a stimuli-sensitive system for HIV therapeutics.

Human seminal fluid contains several enzymes including the Hyaluronidases (HAase) (80), which is also abundant in other body fluids and tissues (81). The amount of HAase in human semen is entirely dependent on the sperm count. The HAase content of human semen containing 100 million sperms/mL is about 0.38 U/mL with the total amount of 1.08 U considering the average volume of human ejaculate is 3 mL (82). One could therefore envision designing a smart microbicide delivery system which can trigger for burst release of microbicides from the delivery system into vagina in the presence of HAase to inactivate the potential high viral load present after ejaculation.

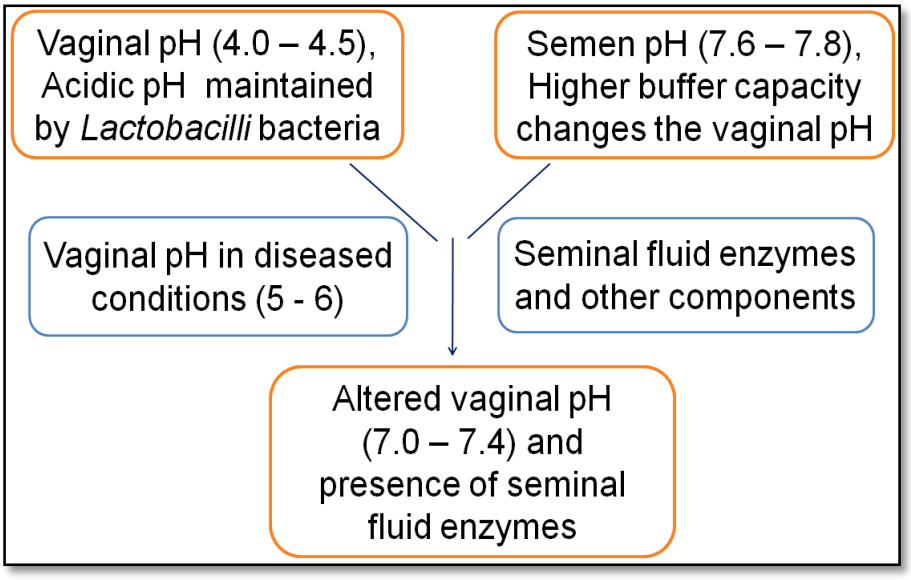

Figure 6. Changes in Vaginal Physiology during the Sexual Intercourse.

There are several delivery systems (nanoparticles, hydrogels, nanofibers, microparticles, etc.) are elaborated, those are able to release the anti-HIV therapeutic molecules

in response to specific stimuli at the target site (Table 8). However, there is no delivery system is developed that has been utilized the seminal fluid HAase enzyme as a triggering element. Considering these facts, the present study aimed at developing a microbicide delivery system capable of degradation on exposure to seminal fluid HAase enzyme that provides a triggered release of microbicide at the vaginal target site.

Table 8: Stimuli-Sensitive Delivery Systems for anti-HIV Drug Delivery Applications.

Stimulus	**Delivery system, (Active moiety)**	**Ref.**
pH	Nanoparticle, (Tenofovir)	(83)
	Nanoparticle, (Dapivirine and Etravirine)	(84)
	Lipid nanoparticles, (Atazanavir and Darunavir)	(85)
	Microparticle, (Tenofovir disoproxil fumarate)	(43)
	Osmotic pump tablet, (IQP-0528)	(86)
	Mucin-like polymer constructed with phenylboronic acid and salicylhydroxamic acid, (Dapivirine and Etravirine)	(87)
	Nanofibers, (Dapivirine and Etravirine)	(84)
	Fibers, (TMC 125, tenofovir disoproxil fumarate)	(88)
Enzyme	Nanoparticles, (Tenofovir)	(89)
	Microparticles, (Sodium poly(styrene-4-sulfonate) (pSS))	(90)
Temperature	Thermosensitive gel, (Raltegravir and Efavirenz)	(91)
	Mucoadhesive hydrogels, (MiniCD4 M48U1)	(92)

Osmotic pressure	Rings	(93)
Hydrogen peroxide	Drug transmucosal deliver, (Bovine insulin)	(94)
Magneto-electric	Nanoparticles, (Zidovudine)	(95)
pH + temperature	Liposome gel, (Arctigenin)	(96)
	Hydrogels, (Acid orange dye, FITC-Dextran)	(97)

CHAPTER 3

DEVELOPMENT OF HYALURONIDASE SENSITIVE TENOFOVIR LOADED HYALURONIC ACID BASED NANOPARTICLES

3.1. Rationale

As explained in Chapters 1 and 2, female-controlled prophylactic methods using microbicides are the major focus among HIV prevention strategies (98-100). This study aimed at developing a semen-triggered nanoparticles (NP) delivery system that provides a triggered release of microbicide on exposure to seminal hyaluronidase (HAase) enzyme. Since, human semen is the carrier of HIV virus transmission during male to female intercourse (23), this would have the potential to inactivate or kill the HIV virus prior to exposure and penetration of the vaginal mucosa.

In recent years, hyaluronic acid (HA) has been used widely, owing to its biodegradable, non-immunogenic and mucoadhesive properties (81, 101). It is a non-sulfated, hydrophilic, naturally occurring anionic mucopolysaccharide made of repeating disaccharide units of D-glucuronic acid and N-acetyl-D-glucosamine, linked through β(1-4) and β(1-3) glycoside bonds (101, 102) (Figure 7A). HA is hydrolysable under treatment with the HAase enzyme (80), which is abundant in human seminal fluid (82) as well as other body fluids and tissues (81). The mechanism of degradation of HA has already been reviewed in detail (103). Due to its excellent physicochemical properties, medical and biological functions, HA has been widely used for NP designs (101) and other drug delivery applications (104). HA has also been reported to possess antioxidant properties, preventing oxidative damages by scavenging free radicals or increasing the antioxidant enzymes activities (105). The lubricant properties of HA may represent an additional benefit for vaginal delivery of HIV/AIDS microbicides (106).

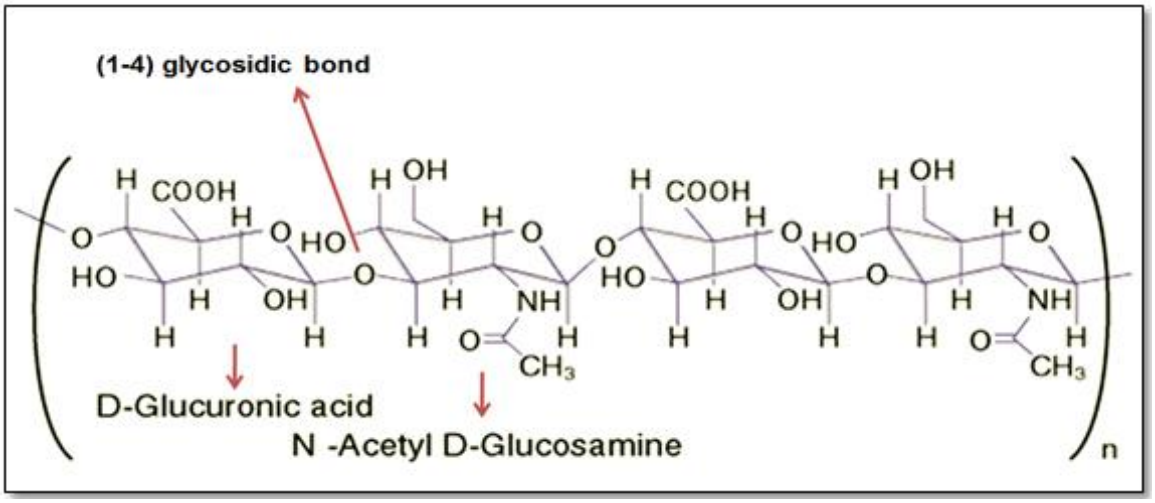

Figure 7A. Chemical Structure of Hyaluronic Acid (HA).

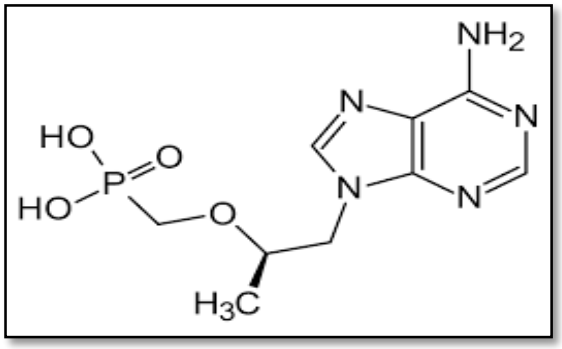

Figure 7B. Chemical Structure of Tenofovir (TFV).

Tenofovir (TFV) (Figure 7B), used as a model microbicide in this study, belongs to the category of anti-retroviral drugs under the sub-category of nucleotide reverse transcriptase inhibitors (107). The currently available vaginal dosage forms of TFV such as gels and suppository cause a somewhat uncomfortable wetness, lack of vaginal retention, and drug leakage (100). The NPs delivery systems to the vagina may be beneficial by causing much less discomfort and reducing the dosing frequency simultaneously (22). To achieve this aim, in this study, the NPs containing TFV were developed using a surfactant-free cross-linking method (108). The effects of various formulation factors over physicochemical properties of NPs were analyzed using fractional factorial experimental design (FFED) (109).

3.2. Materials and Methods

Chemicals

Tenofovir (99% purity) was purchased from Beijing Zhongshuo Pharmaceutical Technology Development Co. Ltd. (Beijing, China). Hyaluronic acid sodium salt of different molecular weight was supplied by Zhenjiang DongYuan Biotech Co., Ltd., (Jiangsu, China). Hyaluronidase (HAase) from bovine testes with a specified activity of 810 U/mg, bovine serum albumin (BSA, Fraction V), N-Hydroxysuccinimide (NHS), adipic acid dihydrazide (ADH), sodium D-glucuronate and acetone were purchased from Sigma-Aldrich (St. Louis, MO). 1-Ethyl-3-[3-dimethylaminopropyl] carbodiimide hydrochloride (EDC) was from Thermo Fisher Scientific Inc. (Rockford, IL).

The human vaginal (VK2/E6E7), endocervical (End1/E6E7) cells and *Lactobacillus crispatus* bacteria were purchased from the American Type Culture Collection (ATCC, Manassas, VA). The CellTiter 96® AQueous One Solution Proliferation assay kit with [3-(4,5-dimethylthiazol-2-yl)-5-(3-carboxymethoxyphenyl)-2-(4-sulfophenyl)-2Htetrazolium, inner salt; MTS] reagent and CytoTox- ONE™, lactate dehydrogenase (LDH) cytotoxicity assay kit was from Promega (Madison, WI). Keratinocyte serum-free medium supplements (EGF Human recombinant and bovine pituitary extract), nonyl acridine orange (NAO), rhodamine 123 and the cell-permeant 2',7'-dichlorodihydrofluorescein diacetate (H_2DCFDA) dye were obtained from Invitrogen Life Technologies (Grand Island, NY). Fluorescein isothiocyanate (FITC) was purchased from Acros Organics (Morris Plains, NJ). Trypsin inhibitor from Glycine max (soybean), 0.25% trypsin/EDTA solution, calcium-magnesium-free Dubelco's Phosphate Buffer Saline (DPBS), camptothecin, calcium chloride, H_2O_2, sodium nitroprusside (SNP), neutral red, hoechst 33342, propidium iodide (PI), resazurin, monochlorobimane were all obtained from Sigma-Aldrich (St. Louis, MO). CellTiter 96® Aqueous One and Griess

reagent system kits were purchased from Promega Corp., (Madison, WI). Deionized water was obtained from a Millipore Milli-Q water purification system (Millipore Corp., Danvers, MA). All other chemicals were of analytical grades and used as obtained from suppliers.

Design of Experiments Approach in Formulation Development

The design of experiment is now getting much attention and the US FDA and the International Conference on Harmonization (ICH) guidelines (Q8, Q9 and Q10) recommend the use of the design of experiment approaches in formulation development (110-113). Traditional approaches for formulation development involve the time consuming process of varying one factor at a time and examining its effect, which requires a large number of experimental runs. Generally, if there are *k* numbers of independent variables (factors), each at two levels (high and low), the full factorial experimental design would require 2^k runs (109). However, if there are four or more factors, it is generally too complicated and also unnecessary to run all the possible combinations of factor levels and experiments(114). In these conditions, fractional factorial experimental design (FFED) is useful as it requires only half of the runs (2^{k-1}) instead of the original 2^k runs in a full factorial design (109). The FFED design provides the possibility of obtaining maximum information from the minimal number of experiments. Thus, in this work the FFED design was employed with *k* value of four (independent variables) as shown in Table 9.

Formulation of HA-NPs, HA-Gel and Drug Encapsulation

The HA-NPs were prepared by a surfactant-free cross-linking method adopted from a previous report (108) with some modifications (Reaction Scheme 1). Chemical structures were drawn in a linear format using CS ChemDraw Ultra® version 6.0 (Cambridge Soft Corp., Cambridge, MA). Briefly, 1 mg/mL aqueous solution of HA was prepared by dissolving the HA powder in

milli Q water with continuous stirring for 1 h at room temperature. A small amount of acetone (in a total amount of 40%v/v) was added in the above solution (primary addition) and stirred for 1 h to make sure that all the components were well dispersed. Two hundred and fifty microliters of aqueous solutions of EDC, NHS, and ADH were added to the above solution and stirred for 30 min, respectively, after the addition of each solution. The carbodiimide mediated cross-linking was continued with stirring at room temperature for 15 h, leading to the formation of amide bonds between the carboxylic acid (-COOH) groups of glucuronic acid units of HA and the hydrazide groups of ADH. Finally, a secondary addition of acetone occurred to raise the volume 3-6 times with respect to the aqueous phase (X_3). After that, the solution was stirred continuously for various time points. The color of the solutions turned to light blue after the secondary acetone addition due to the Tyndall effects. The organic solvent was evaporated by using a rotatory evaporator (BUCHI Labortechnik AG, Flawil, Switzerland).

The colloidal dispersion was ultra-centrifuged, using a Beckman L8-70M ultra-centrifuge (Beckman Instruments Inc., Palo Alto, CA) at 20,000 rpm and 10˚C for 45 min to isolate the NPs. After isolation, the NPs were purified using dialysis method against one liter of milli Q water for 24 h with three water changes at every 8 h. After the dialysis, NPs were freeze-dried (Labconco Corp., Kansas City, MO) and the process yield of the recovered NPs was determined using mass balance calculation. The soaking method (115, 116) was employed for encapsulation of TFV in the HA-NPs. Briefly, 10 mg of purified and freeze-dried NPs were immersed in an aqueous solution of TFV. The NP: drug ratio in the loading solution was varied from 10:1 to 1:1 (w:w). This was left to soak for three days at room temperature. The percent encapsulation efficiency (% EE) and drug loading (% DL) was determined indirectly from the supernatant (after ultra-centrifugation, washing and appropriate dilution) using a high performance liquid chromatography (HPLC) assay (117) applying the Equations 1 and 2,

respectively. The formulation of HA-gel was based on hydration and internal cross-linking reaction of the native HA at the concentration of 2% w/v in water (118).

$$EE\,(\%) = \frac{Total\ amount\ of\ drug\ used\ in\ mg - Drug\ content\ of\ supernatant\ in\ mg}{Total\ amount\ of\ drug\ used\ in\ mg} \times 100 \qquad (1)$$

$$LC\,(\%) = \frac{Total\ amount\ of\ drug\ used\ in\ mg - Drug\ content\ of\ supernatant\ in\ mg}{Weight\ of\ nanoparticles\ and\ drug\ used\ in\ mg} \times 100 \qquad (2)$$

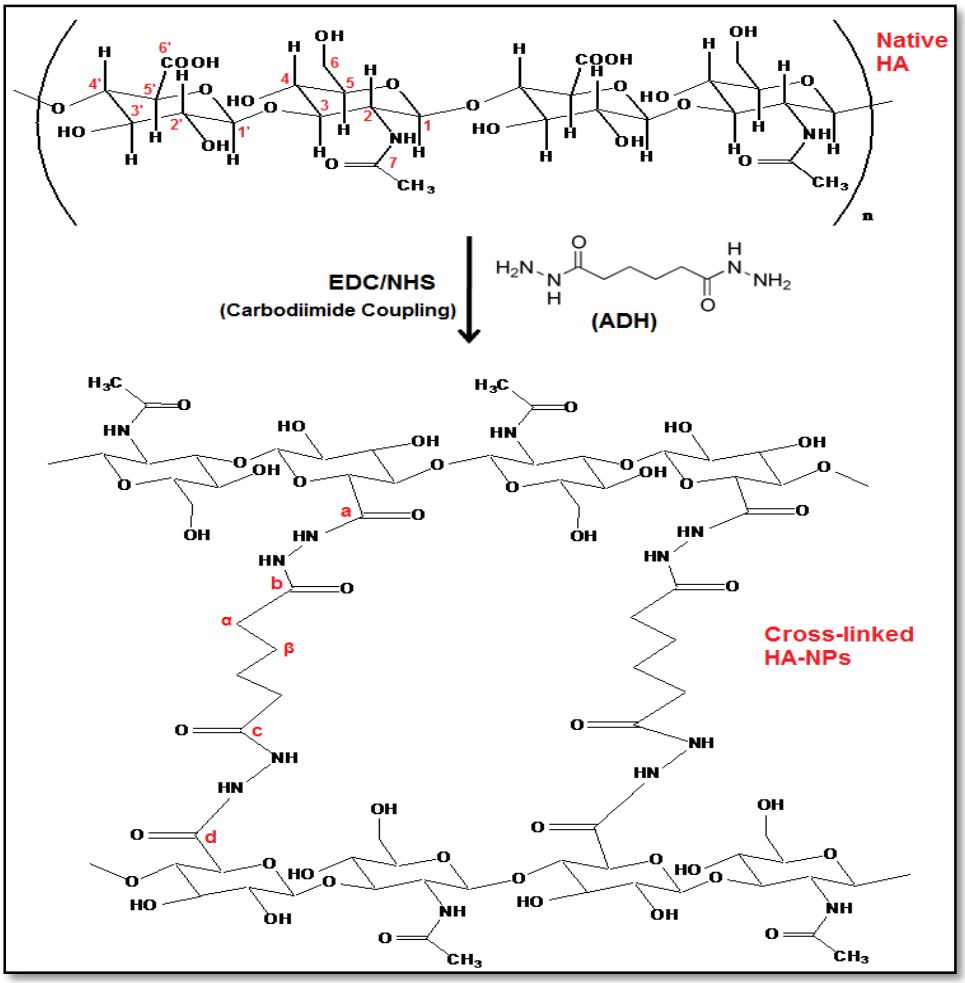

Reaction Scheme 1. Formulation of HA-ADH cross-linked NPs

Briefly, the HPLC system (Waters, Milford, MA) was consisted of a 1575 binary pump system, 717 plus auto sampler, 2487 dual wavelength absorbance detector, and a Bridge™ C_{18} column (150mm X 4.6mm, 5µm). Results were acquired and processed with Breeze™ software (version 3.3). The assay was performed isocratically at ambient temperature at the detection

wavelength of 259 nm. The mobile phase composition was water (pH 5.1): acetonitrile (35:65 v/v) delivered at a flow rate of 1 mL/min. To prepare the aqueous phase (pH 5.1), 0.1% v/v of triethylamine was added to water and the final pH was adjusted with orthophosphoric acid (85% v/v) to 5.1. The sample volume of 10 µL was injected in each run. The standard solution of TFV (100 µg/mL) was prepared by dissolving 1 mg of drug in 10 mL of milli Q water. The calibration curve at the concentration range of 0.1-10 µg/mL was prepared using the above standard solution. The method was validated according to the ICH Q2:R1 guidelines (117).

Table 9: Independent and Dependent Variables With Their Corresponding Levels in the FFED Design.

Variables	**Levels**		
	Low	**Medium**	**High**
Independent variables (factors)			
Coded values of levels of X_1, X_2, X_3 and X_4	-1	0	+1
Actual values of X_1, X_2, X_3 and X_4			
X_1; molar concentration of ADH: mM[a]	2.49	6.23	9.96
X_2; molar concentration of EDC: mM[a]	2.49	6.23	9.96
X_3; volume of acetone: mL[b]	30	45	60
X_4; reaction time: hour[c]	2	4	6
Dependent variables (responses)			
Y_1; particle mean diameter (PMD): nm			
Y_2; polydispersity index (PDI)			
Y_3; zeta (ζ) potential: mV			

[a] Molar concentration with respect to the molar concentration of HA (constant at 2.49 mM).

[b] Volume of acetone with respect to the volume of aqueous phase (kept constant at 10 mL)

[c] Reaction time after secondary acetone addition.

Physicochemical Characterization of HA-NPs

Spectral Analysis by Fourier Transform Infra-Red (FT-IR) Spectroscopy

The cross-linking between HA and ADH (Reaction Scheme-1) was assessed by FT-IR analysis using Nicolet iS10 Spectrometer (Thermo Scientific, West Palm Beach, FL). The instrument was equipped with a deuterated triglycine sulfate (DTGS) detector and was controlled by OMNIC™ Spectra™ software version 7.0. A transmission mode was selected to make observations with the sampling area of about 1 mm. Analysis was systematically performed at 650 to 4000 cm^{-1} (wavenumbers). The background data was collected at ambient conditions before analyzing freeze dried samples of the HA-NPs. Spectra were automatically corrected with a linear baseline. No specific sample preparation method was used before FT-IR analyses.

Spectral Analysis by ^{13}C-CP/MAS NMR Spectroscopy

The cross-linking between HA and ADH (Reaction Scheme-1) was further assessed by using solid state high resolution ^{13}C cross-polarization magic angle spinning (CP/MAS) nuclear magnetic resonance (NMR) analysis. The NMR spectra were acquired on a Tecmag Apollo console (Houston, TX) with a homebuilt, 2-channel, wide-bore NMR probe at ^{1}H and ^{13}C Larmor frequencies of 357.2 MHz and 89.827 MHz, respectively. The MAS spinning frequency, proton RF field decoupling strength, cross polarization contact time and 90^0 pulse length is, 13 kHz, 110 kHz, 2 ms and 5 µs, respectively. All MAS experiments were performed at ambient temperature without any corrections for sample heating. About 30 mg of NP sample was taken for each analysis. The NMR signals were represented as chemical shift (δ) values in ppm.

Size Distribution and Zeta (ζ) Potential Analyses using Dynamic Light Scattering

The NPs were analyzed for their particle mean diameter (PMD); nm, polydispersity index (PDI), and size distribution by dynamic light scattering (DLS) method using Zetasizer

Nano ZS (Malvern Instruments Ltd., Worcestershire, UK). The ζ potential was analyzed by Laser Doppler Velocimetry and Phase Analysis Light Scattering methods using the same Nano ZS instrument. After suspending 100 µL of NP dispersion in 1 mL of water, the measurement was undertaken at 25°C. The PMD of the NPs was represented as *Z*-average diameter following the cumulant model (119). It is noteworthy that estimation of the PMD and PDI was based on the intensity of the light signal processed according to the cumulant method. Cumulants were defined as the coefficients of an expansion of a MacLaurin series (120). The PDI value was given by Eq. (3):

$$PDI = K_2 / K_1 \quad (3)$$

The cumulant K_1 is an effective mean diffusion coefficient; whereas, K_2 describes the relative width of the size distribution if normalized by K_1 (120). The instrument was calibrated by using nanosphere™ of PMD (59.0 ± 2.5 nm) and ζ potential standards (-68.0 ± 6.8 mV) prior to the analysis. According to the National Institute Standard, a sample with a PDI value < 0.05 was considered mono-dispersed (121).

Size Distribution Analyses using Nanoparticle Tracking Analysis

The NPs were analyzed for their particle mean diameter (PMD); nm, using Nanoparticle Tracking Analysis (NTA) measurements. NTA analysis was performed using a NanoSight LM20 instrument (NanoSight, Amesbury, UK). The instrument was equipped with a sample chamber with a 640-nm laser and a Viton fluoro-elastomer O-ring. NTA version 2.3 Build 0017 software was used for the capture and data processing. The samples were injected in the sample chamber with syringe and measurements were performed at room temperature. The samples were measured for 90 sec with manual shutter and gain adjustments.

Surface Morphology Analysis of HA-NPs

The surface morphology of HA-NPs was analyzed by transmission electron microscopy (TEM) using a Philips TEM CM12 instrument (FEI, Hillsboro, OR). The instrument was

equipped with the large format (II Megapixel), retractable and fiber-optical coupled SC100 ORIUS© CCD camera (Gatan, Inc., Pleasanton, CA) for digital image acquisition. The TEM analysis was performed by placing a drop (10 µL) of colloid dispersion of the HA-NPs over a carbon-coated copper grid. The excess fluid was removed before samples were completely dried at room temperature and examined for TEM imaging without any further modifications. The TEM observations were performed at an accelerating voltage of 80 kV.

Enzymatic Degradation Analysis of HA-NPs

An Uronic acid-carbazole assay (122) was used to analyze the degradation of the HA-NPs under the influence of HAase enzyme. The degradation analysis was performed with the amount of HAase that is normally present in human ejaculate (82). The amount of HAase in human semen is entirely dependent on the sperm count. The HAase content of human semen containing 100 million sperms/mL is about 0.38 U/mL with the total amount of 1.08 U considering the average volume of human ejaculate is 3 mL (82). The degradation study was performed at pH 7.1, which was equivalent to the pH condition of vaginal fluid during sexual intercourse (23). The optimum pH for maximum hydrolytic activity of HAase is 4 to 5 (123, 124). However, HAase exerts its activity also at weakly acidic (pH 5 to 6) (124) and alkaline conditions (pH 7 to 8) (123, 125). The bovine testicular HAase was used as a model enzyme, since it was commercially available and, like human HAase, it catalyzes the hydrolysis of the β (1-4) glycosidic bonds in HA (126).

Briefly, the HA-NPs (10 mg) were dispersed in 3 mL of the simulant mixture (pH 7.1) of vaginal fluid simulant (VFS, pH 4.2) and seminal fluid simulant (SFS, pH 7.8), prepared according to the previous reports (127, 128). The 1:4 volume ratios of the VFS and SFS, respectively, were used for preparing the simulant mixture, considering that the volumes of normal human vaginal fluid and male ejaculate (127, 128). The pH of VFS and SFS buffers

was adjusted using hydrochloric acid (HCl) or sodium hydroxide (NaOH) solutions, prepared accordingly. The NP dispersion was transferred to a dialysis bag (Spectra/Por Float-A-Lyzer G2, MWCO, 3.5-5 kDa), supplied from Spectrum Lab., Inc. (Rancho Dominguez, CA), and placed inside a dialysis tube containing 20 mL of the simulant buffer mixture. The whole system was then placed in a thermostatic shaking water bath (BS-06, Lab Companion, Seoul, Korea) with 60 rpm at 37°C. Aliquots of 100 µL solutions were taken from the medium at different time intervals (0, 1, 3, 6, 24, 48, 72, 96, 120 h), boiled for 10 min to inactivate the enzyme and analyzed for the amount of glucuronic acid released. The fresh simulant mixture was added at the same rate to maintain the sink condition.

The Genesys 10 Bio UV-Vis Spectrophotometer (Thermo Electron Sci. Inst., LLC, Madison, WI) was used for the degradation analysis of HA-NPs at the wavelength of 530 nm. The amount of glucuronic acid released at each time point was determined by using the standard curve of sodium D-glucuronate. The curve was found linear in the concentration range of 0-200 µg/mL (Correlation coefficient: r = 0.998). The measured amount of D-glucuronic acid was represented as percent cumulative degradation (%w/w) of HA-NPs compared to the degradation of native HA incubated either in the presence or absence of HAase. The reaction mechanism of the Uronic acid-Carbazole assay was given in Reaction scheme 2.

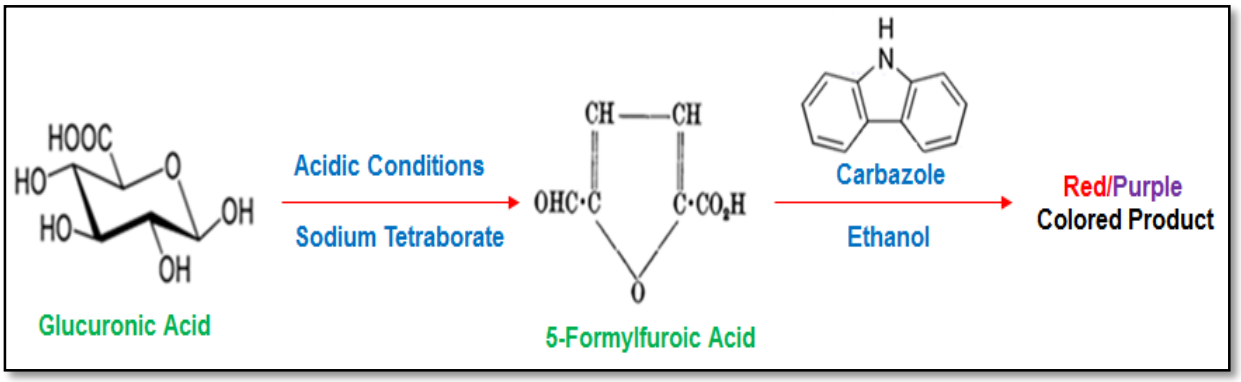

Reaction Scheme 2. Reaction Mechanism of the Uronic acid-Carbazole Assay.

In Vitro Drug Release Analysis of HA-NPs

The release study was performed with the 10 mg of drug loaded HA-NPs or HA-gel using the dialysis method as explained above for the enzymatic degradation analysis. The blank HA-NPs, HA-gel and TFV powder were taken as control samples. Aliquots of samples (1 mL) were taken at, 0, 1, 3, 6, 9, 12, 24, 48, and 72 h from the release medium. Simultaneously, an equivalent volume of fresh simulant mixture was added at the same rate to the release medium to maintain the sink condition. The amount of TFV was quantified by using HPLC assay (117).

Enzymatic Degradation and *In Vitro* Drug Release Kinetics

The drug release kinetics of HA-NPs was analyzed by using zero order, first order, Higuchi, and Korsmeyer-Peppas models as given by Equations (4), (5), (6), and (7), respectively, (129).

$$M_t = M_0 + K_0 t \tag{4}$$

$$\log M_t = \log M_0 + K_1 t/2.303 \tag{5}$$

$$M_t = K_H t^{0.5} \tag{6}$$

$$M_t/M_\infty = kt^n \tag{7}$$

In these Equations, M_t is the amount of drug released at time *t*, M_0 is initial amount of drug in solution, K_0 is zero order release constant, K_1 is first order release constant, K_H is Higuchi dissolution constant, M_t/M_∞ is the fraction of drug released at time *t*, M_∞ is the total amount of drug released, *k* is a kinetic constant and *n* is the exponent explaining the drug release mechanisms (129). The exponent *n* is classified as Fickian diffusion ($n \leq 0.5$), case-II transport ($n = 1$), anomalous transport ($0.5 < n < 1$) and super case-II transport ($n > 1$) (129).

The Eq. (7) in Peppas model was further depicted in a log-transformed Eq. (8):

$$\log M_t/M_\infty = n \log t + \log k \tag{8}$$

The model independent approach was then applied to compare the enzymatic degradation and drug release kinetics of the HA-NPs (test compounds) with HA-gel (reference compound) as per US FDA guidance to industry (129). In the case of HA degradation study, the difference (f_1) and similarity factors (f_2) were calculated, using Equations (9), and (10), respectively.

$$f_1 = \left\{\left[\sum_{t=1}^{n}\left|R_t - T_t\right|\right] \Big/ \left[\sum_{t=1}^{n} R_t\right]\right\} \times 100 \quad (9)$$

$$f_2 = 50 \times log\left\{\left[1 + (1/n)\sum_{t=1}^{n}\left(R_t - T_t\right)^2\right]^{-0.5} \times 100\right\} \quad (10)$$

Where, n is the number of time points, R_t and T_t are the cumulative degradation and drug release (% w/w) at time t for reference (HA-gel) and test compounds (HA-NPs) in the presence or absence of enzymes, respectively. Here, f_1 measured the percent errors while f_2 measured the sum-squared error between the test and reference compounds over all time points. The curves for the samples with f_1 and f_2 values close to 0 and 100, respectively, were considered similar. Generally, $f_1 < 15$ (0-15) and $f_2 > 50$ (50-100) ensured equivalence of the two curves (129). Here, the difference and similarity factors were represented as f_1 and f_2 and f_1' and f_2', for drug release kinetics and enzymatic degradation of HA-NPs, respectively.

Computational Modelling: Interaction of TFV with HA and HA-NPs and its Effect over Encapsulation and Drug Release Properties of NPs

Computational modelling (CM) and dynamics that could predict and quantify drug-NP interactions would greatly reduce the costs and time associated with formulation development (130). A better understanding of these interactions could help in explaining drug encapsulation and release process from nanocarriers (131). In this study CM was investigated to understand the effect of cross-linking of HA for the drug loading efficiency and drug release properties of HA-NPs. The chemical structure of TFV was docked into native HA (tetramer unit) and cross-

linked HA-NPs using Glide (Grid-Based Ligand Docking with Energetic) software version 5.5 from Schrodinger (LLC, New York, NY).

Glide is a docking program to predict the binding modes through a scoring function (132, 133). Grids were prepared with the size of the bounding box enclosing the whole molecule. Glide XP Mode was employed using default options in Glide for all docking calculations and 100 poses were kept per molecule of ligand. Generally, Glide utilizes standard-precision (SP) and extra-precision (XP) Glide Scoring functions to rank-order compounds. Glide Score was the sum of van der Waals (VWs), hydrogen bonds (H-bonds), electrostatic, lipophilic, and some additional interaction energy (IE) terms as given in Eq. (11) below (133, 134). The IE was considered as the difference between the total energy of the drug loaded NPs and the sum of the energies of the drug and the native polymer.

Glide Score = 0.065 VWs + 0.130 Electrostatic + Lipophilic + H-bonds + K (11)

Here, K is the sum of the metal-binding term, penalty for buried polar groups, penalty for freezing rotatable bonds, polar interactions in the active site, hydrophobic enclosure reward, reward for low molecular weight, electrostatic reward, chemscore lipophilic pair term and fraction of the total VW energy. Glide's Scoring functions were used to evaluate binding energies of the docking output comprising low energy docked poses. The docking output was clustered into conformational families and analysed in terms of lowest energy conformation and the most populated clusters.

Degradation Kinetics and Stability Evaluation of Tenofovir

The stability evaluation of TFV under various stress conditions was analyzed using a liquid chromatography (LC) and mass spectrometric (MS) assay since the drug was exposed to acidic and alkaline pH conditions of the medium to perform the release and degradation analyses of the HA-NPs. Briefly, LC analysis was carried out on a UFLC Shimadzu

prominence system (Shimadzu USA manufacturing Inc., Torrance, CA) consisting of a LC-20 AD low pressure gradient pump, SPD-M20A photodiode array (PDA) detector, SIL-20AST auto sampler, and DGU-20As degasser. A reversed phase Waters Symmetry® C_{18} column (150 mm × 4.6 mm, 5 µm) was used as a stationary phase. The LC elution conditions were as follows (all solvent percentages were volume fractions): mobile phase-A, 0.1% v/v formic acid in water; mobile phase-B, 0.1% v/v formic acid in acetonitrile; mobile phase-C, 30% A + 70% B. The time program was: 0.01 min, 100% A; 10 min, 100% C; 13 min, 100% B; 14 min, 100% A; and 18 min, 100% A. The flow rate was 0.6 mL/min and the detection was carried out at 259 nm under ambient temperature conditions using a sample injection volume of 10 µL in each analysis.

MS studies were performed on a 3200 QTrap mass spectrometer (Applied Biosystems Sciex, Framingham, MA). Spectra were recorded using Enhanced mass spectrum (EMS) scan in positive mode. Analyst® software version 1.4.2 (Applied Biosystems Sciex, Framingham, MA) was used for data acquisition. MS operational parameters were as follows: Collision activated dissociation (CAD): high; Ion source Gas1 (GS1): 50 psi; Gas2 (GS2): 50 psi; Turbo ion spray voltage (IS): 5500 V; Source temperature (TEM): 350 °C; Collision energy (CE); 5 V; Declustering potential (DP): 2 V, and Entrance potential (EP): 2 V. Nitrogen gas was used as the nebulizer, and the scan rate was 4000 amu/sec. The spectra were obtained by scanning between 100-700 amu. The validation of the LC-MS assay was performed according to the ICH, Q2:R1 guidelines.

LC-MS Sample Preparation and Forced Degradation Analysis

The drug at the concentration of 1 mg/mL was subjected to stress degradation under various stress conditions (Table 10). A stock solution of TFV (10 mM) in Milli Q water was diluted with mobile phase-A (0.1% v/v formic acid in water) to yield the solutions in the concentration range of 7.81-500 µM for the calibration curve. The stressed samples were

collected after each time period and diluted with the same mobile phase to the concentration of 250 µM and to make them suitable for LC analysis (135). For comparison, a freshly prepared TFV (250 µM) and the blank samples (without TFV, processed in the similar way as of stressed samples) were also analyzed. In all the assays, the drug was considered stable if there was < 10% degradation of the initial amount was observed (136, 137).

Table 10: Stress Conditions Employed For the Forced Degradation Analysis of TFV.

Stress conditions	Solvent	Analysis time	Experimental conditions
Hydrolysis			
Acidic	0.1 N HCl, pH 1	Up to 5 days	Reflux
Acidic	0.1 N HCl, pH 4.5	Up to 5 days	Reflux
Basic	0.1 N NaOH	Up to 5 days	Reflux
Neutral	Water	Up to 5 days	Reflux
Oxidation	3% and 30% H_2O_2	Up to 7 days	Room temperature (RT)
Long term (accelerated)			
Solid samples	-	Up to 12 months	-20°C
			5°C
			25°C/60% RH
			40°C/75% RH
Thermal stress			
Solid samples	-	Up to 12 months	40°C, 50°C, 60°C
		Up to 30 days	80°C
Liquid samples	0.1 N HCl	Up to 10 days	25°C, 40°C
	HCl, pH 4.5	Up to 10 days	25°C, 40°C

Powder X-ray Diffraction Analysis

Powder X-ray diffraction (PXRD) analysis is a well-established and the most versatile techniques for the determination of crystalline forms of bio-active molecules. The effects of temperature and % relative humidity (RH) conditions on the crystal structure of TFV (unstressed sample and samples stored at -20°C, 5°C, 25°C/60% RH, 40°C/75% RH, 50°C, and 80°C) was determined using solid state powder X-ray diffraction (PXRD) analysis. The PXRD patterns were obtained using a Rigaku MiniFlex automated X-ray diffractometer (Rigaku, The Woodland, TX). The samples were mounted on single-crystal Si zero-background plates for analysis. The analyses were performed at room temperature using Cu Kα radiation produced at 35 kV and 15 mA, with a Ni filter. The scan angle (2θ) was from 5° to 40° with a step size of 0.05° 2θ and 3 sec per step. The diffraction patterns were processed using Jade 8+ software (Materials Data, Inc., Livermore, CA).

Stability Analysis Using Arrhenius Plot

The influence of temperature on the degradation kinetics of TFV was further determined using accelerated stability testing and Arrhenius equation (138-140) (Eq. 12).

$$ln(k) = ln(A) - \frac{E_a}{RT} \quad (12)$$

Where, k is the degradation rate constant, A is the frequency factor, E_a is the activation energy, R is the gas constant and T is the absolute temperature in degrees Kelvin. The k value depends on the E_a and is characteristic of a specific compound (141).

Based on the first order reaction kinetics (138), Eq. (13) was generated into its logarithmic form.

$$log \frac{C}{C_0} = -\frac{kt}{2.303} \quad (13)$$

In this Eq. (13), k, C_0, C and C/C_0 are the first order rate constant, initial concentration and concentration of drug remaining after time t, and fraction of drug remaining after time t,

respectively. The values of *k* at each temperature was determined using Eq. (13), from the slope of the regression equation of the plot between log % drug remaining and time (*t*) in months.

To construct the Arrhenius plot, the value of 1000/*T* (in Kelvin) was calculated for each temperature and the Arrhenius plot between *ln (k)* vs. 1000/*T* was constructed. The slope and intercept values of this plot were equal to $-E_a/R$ and *ln (A)*, respectively, according to Eq. (12). The E_a was calculated by multiplying the slope value by *R* (8.314 $J.mol^{-1}.Kelvin^{-1}$). The significance of the E_a value was to determine the temperature dependency of a chemical reaction. The higher the value of E_a for a chemical reaction the greater the acceleration with increase in temperature and the more the stability of a drug is temperature dependent (141, 142) Generally, drugs with lower E_a values have significantly lower reduction and longer shelf-lives (141). The rate constant (k_{25}) that corresponds to room temperature (25°C) was calculated from the regression equation. The shelf-life ($t_{90:}$ time required for the drug to decrease its amount by 10% of its initial amount) was calculated as explained below.

The k_{25} value was used for the calculation of shelf-life (t_{90}), half-life (t_{50}), and the time required for the drug to decrease its initial amount by 90 % (t_{10}). The determination of the t_{90}, t_{50}, and t_{10} values was based on Eq. (13). The t_{50} is the time required for 50% degradation. This was calculated by replacing *C* and *t* with $C_0/2$ and t_{50}, respectively, in Eq. (13). This gives the Eq. (14) after logarithmic calculations. The t_{90} was calculated by replacing *C* and *t* with 0.9 C_0 and t_{90}; whereas, t_{10} was calculated by replacing *C* and *t* with 0.1C_0 and t_{10} in Eq. (13), which were given by Equations, 15, and 16, respectively.

$$t_{50} = \frac{0.693}{k} \tag{14}$$

$$t_{90} = \frac{0.105}{k} \tag{15}$$

$$t_{10} = \frac{2.303}{k} \tag{16}$$

Cytotoxicity Assays: Effects of the HA-NPs on the Vaginal Epithelial Cells

The safety of vaginal microbicides is an important concern in anti-HIV formulation development and is critical to understand the effect of interaction of the nanocarriers with the vaginal epithelial cells. Considering that, this study was designed to test the hypothesis that the developed HA-NPs are non-cytotoxic to the cervicovaginal (CV) keratinocyte cells. The VK2/E6E7, and End1/E6E7 cells were selected as *in vitro* models as they were the primary exposure route for HIV transmission and NPs exposure to vaginal mucosa (143). A series of cell-based assays were performed to investigate several endpoints which may upon disruption lead to cell death. These end points were; plasma membrane integrity, mitochondrial functions (metabolism/respiration, membrane potential and mass), cellular redox state (reactive oxygen species and intracellular glutathione). Moreover, the inflammatory response was studied via the release of the pro-inflammatory mediator nitric oxide (NO). As the safety of 1% TFV gel has already been determined (17, 144), in this study blank HA-NPs (without drug) at the concentration of 1-1000 µg/mL were tested for their effects on the viability and membrane integrity of VK2/E6E7, and End1/E6E7 cells.

Cells were grown and routinely maintained in monolayer culture, in 75 cm^2 culture flasks (TPP, Switzerland), at 37°C in a humidified atmosphere of 5% carbon dioxide (CO_2), 95% air. The cells were cultured in an antibiotic-free keratinocyte medium supplemented with EGF human recombinant (0.1 ng/mL), bovine pituitary extract (0.05 mg/mL), and calcium chloride $CaCl_2$ (0.4 mM). The culture medium was replaced every 2-3 days. Before confluence, cultures were washed with DPBS, and cells were subsequently detached by enzymatic treatment by using 0.25% trypsin/EDTA solution for 3-5 min at 37°C (which was inhibited by soybean trypsin inhibitor at a molar ratio of 1:1), washed, and seeded in new flasks or treatment wells. The HA-NPs were dispersed in the culture medium at the concentration range of 1-1000 µg/mL and sterilized for 30 min under UV light (145). The cells were then exposed up to 24 h

to 100 µL of HA-NPs at the concentration of 1, 10, 100 and 1000 µg/mL, corresponding to 0.3125, 3.125, 31.25 and 312.5 µg of NPs/cm^2, respectively, considering the growth surface of each well is 0.32 cm^2. Wells containing cells without HA-NPs were used as the negative controls whereas, 1% Triton-X-100, H_2O_2 (100 mM), camptothecin (100 µM) and 1 mg/mL of sodium nitroprusside (SNP) were used as positive controls in their respective assays.

Assessment of Cell Viability Using MTS and Resazurin Assays

Briefly, cells were seeded to 96-well plates in a keratinocyte-serum free medium and were allowed to grow until 80% confluence was reached. The medium was replaced with 100 µL of HA-NPs at different concentrations and kept in contact with the cell lines for 24 h. The amount of formazan product formed was determined by adding 20 µL of MTS reagent to culture wells. The wells were further incubated for 4 h at 37°C in a humidified, 5% CO_2 atmosphere and the absorbance was measured at 490 nm using a DTX 800 multimode microplate reader (Beckman Coulter, Brea, CA). The medium and 1% Triton-X-100 were used as negative and positive controls, respectively. The %cell viability was determined by Eq. (17):

$$Viability(\%) = \frac{ABS\ (test)}{ABS\ (control)} \times 100 \qquad (17)$$

Where, *ABS (test)* and *ABS (control)* represented the absorbance of the amount of formazan product formed in viable cells.

Assessment of Cell Membrane Integrity

The effects of HA-NPs on the cell membrane integrity was measured using the specific accumulation of the vital dye neutral red (NR) in the lysosomes (146). The neutral red uptake assay provided a quantitative estimation of the number of viable cells in a culture. After the NPs exposure to the cells for 24 h, cells were washed twice with DPBS and replaced with fresh medium (100 µL) containing 50 µg/mL of NR dye followed by incubation for 3 h to allow the viable cells to accumulate NR dye in the lysosomes. After the incubation time, cells were washed twice with DPBS followed by disruption with a solution of 1% acetic acid/50% ethanol

(100 µL/well). The plate was shaken for 15 min in the dark to solubilize the NR dye crystals, prior to the fluorescence intensity was measured (530-560 nm excitation, 590 nm emission) using the above microplate reader. The % cytotoxicity was determined using Eq. (18):

$$Cytotoxicity(\%) = \frac{Experimental - Background}{Positivecontrol - Background} \times 100 \quad (18)$$

Here, experimental, background and positive control represented the fluorescence of the wells with NP treatment, without NP treatment and with 1% Triton-X-100 treatment, respectively.

Assessment of Apoptosis through Chromatin Condensation

The detection of apoptosis was performed using Hoechst 33342 (HO) assay (147). After exposure to the HA-NPs for 24 h, the cells were washed twice with DPBS and replaced with 100 µL of DPBS containing HO and propidium iodide (PI) at the final concentrations of 10 µg/mL and 2 µg/mL, respectively. The PI was added to the HO solution to control necrotic cells, as PI allowed HO to stain the viable and apoptotic cells only. The assay plate was incubated in the dark for 30 min at room temperature to allow the HO dye to stain viable and apoptotic cells. The fluorescence intensity was monitored using the above microplate reader (350 nm excitation, 450 nm emission). Camptothecin (100 µM), a well-known apoptosis inducer was used as positive control. Results were displayed by calculating the index ratio (HO/NR) and compared with the untreated cells (148). This index allowed differentiating apoptosis and necrosis process by evaluating the importance of chromatin condensation in comparison with the number of cells with intact membrane: apoptosis (HO/NR > 1), proliferating cell (HO/NR=1) and necrosis (HO/NR < 1).

Assessment of Mitochondrial Functions

In an effort to identify specific cellular events that may contribute to NPs-induced cytotoxicity, the mitochondrial functions were analyzed as given below.

Mitochondrial Respiratory Function

Mitochondrial respiratory function (MRF) was examined using Resazurin assay. After exposure to HA-NPs for 24 h, the cells were washed twice with DPBS and replaced with fresh medium (100 µL). Then, 10 µL of resazurin (0.1 mg/mL in DPBS) was added to each well. The assay plate was shaken briefly for 30-60 s to ensure uniform distribution of resazurin and incubated for 3 h. The plate was further shaken for 30-60 s and fluorescence intensity (530-560 nm excitation, 590 nm emission) was determined using the above microplate reader.

Mitochondrial Membrane Potential

The mitochondrial membrane potential ($\Delta\Psi_m$) was analysed by assessing the accumulation of Rhodamine-123 dye inside the mitochondria (149). After the exposure to HA-NPs for 24 h, the cells were washed with DPBS and replaced with fresh medium containing Rhodamine-123 (10 µg/mL). The plate was incubated for 30 min to allow Rhodamine-123 uptake. The cells were washed twice with DPBS, replaced with fresh medium and incubated at 37°C for 1 h to allow cells to efflux Rhodamine-123 dye. The cells were washed again with DPBS followed by disruption with a solution of 1% acetic acid/50% ethanol (100 µL/well). The plate was shaken for 15 min in the dark at room temperature and fluorescence intensity was measured (490 nm excitation, 535 nm emission) using the above microplate reader.

Mitochondrial Mass

The mitochondrial mass was assessed by using the fluorescent dye nonyl acridine orange (NAO), which specifically binds to cardiolipin in mitochondria independently of their $\Delta\Psi_m$ (150). After exposure to HA-NPs for 24 h, the cells were washed twice with DPBS and replaced with fresh medium containing NAO (10 µM). The assay plate was incubated for 30 min to allow NAO to bind to cardiolipin. NAO loaded cells were washed twice with DPBS and replaced with fresh medium and incubated at 37°C for 1 h to allow cells to efflux NAO dye. The cells were washed twice with DPBS followed by disruption with a solution of 1% acetic

acid/50% ethanol (100 µL/well). The plate was shaken for 15 min in the dark at room temperature prior to the fluorescence intensity was measurement (490 nm excitation, 535 nm emission) using the above microplate reader.

Assessment of Intracellular Reactive Oxygen and Nitrogen Species Production

Reactive Oxygen Species Production

Reactive oxygen species (ROS) are produced by a variety of nanomaterials (151-154). Mitochondria are a major source of ROS production as by-products of cellular energy metabolism (155), and an over-production of ROS may lead to the cell death. ROS induce the cell toxicity by damaging macromolecules (DNA, lipids, proteins) and depleting intracellular glutathione (GSH), an antioxidant that helps to prevent damage to cellular components caused by ROS. A potential effect of HA-NPs in inducing ROS production was investigated using the 2',7'-dichlorodihydrofluorescein diacetate (H_2DCFDA) dye (156). Cells were pre-incubated for 30 min with a 20 µM H_2DCFDA solution before any treatment. After that, the cells were washed twice with DPBS followed by the exposure with the HA-NPs for 3 and 24 h. The fluorescence intensity was measured at the excitation and emission wavelengths of 490 nm and 535 nm, respectively, using the above microplate reader.

Nitric Oxide Production

Nitric oxide (NO) production in the culture supernatant is a measure of iNOS activity. Inducible NO Synthase (iNOS)-mediated NO production is widely used as a marker of inflammation (157). Thus, the potential of HA-NPs in inducing NO secretion within the genital keratinocyte cells was examined by measuring the nitrite accumulation (158). After exposure to HA-NPs for 24 h, supernatant was collected centrifugation at 1000 g for 10 min to remove cellular debris and particulate materials. Then, 50 µL of the supernatant was placed into a new plate and mixed with Griess reagent (Promega Corp., Madison, WI) according to the manufacturer instructions. Absorbance was measured at 540 nm and nitrite concentration was

calculated using the standard curve of sodium nitrite. Sodium nitroprusside (SNP), an external donor of NO was used as the positive control at the concentration of 1 mg/mL (159).

Cellular Antioxidant Glutathione Assessment

Intracellular antioxidant glutathione (GSH) is a key natural non-enzymatic antioxidant within the eukaryotic cells and a sensitive biomarker to determine the oxidative stress. GSH content was quantified using monochlorobimane dye (MCB) (156). After exposure to HA-NPs for 24 h, the cells were washed twice with DPBS and replaced with 100 µL of fresh solution of MCB (110 µM). Then, the assay plate was left at room temperature in the dark to incubate for 45 min to allow MCB dye to react with cellular GSH. The fluorescence intensity was measured at the excitation and emission wavelengths of 360 nm and 480 nm, respectively, using the above microplate reader.

Lactobacillus **Viability Assay of HA-NPs**

The acidic environment of vagina is maintained by *Lactobacilli*, which lowers the risk of HIV infection by its natural defense mechanism (76). Hence, any microbicide formulation will need to preserve the vagina's natural defense mechanism by not disturbing the *Lactobacilli* layer. This was assessed by using *Lactobacillus* viability assay (62). The *L. crispatus* was used as model bacteria was grown in ATCC medium 416 *Lactobacilli* MRS broth (BD, Franklin Lakes, NJ) at 37°C and the viability assay was performed using an established method (160). Briefly, the bacteria density was adjusted to an OD_{670} of 0.06, which corresponds to 0.5 McFarland Standard or 10^8 CFU/mL (161). *L. crispatus* was seeded in a 96-well plate at a volume of 100 µL and incubated with 100 µL of the NP suspension for 48 h at 37°C. The bacterial wells treated with 10 µg/mL of commercially available penicillin-streptomycin solution (positive control) from Invitrogen (Carlsbad, CA). After the incubation, 20 µL MTS

reagent was added to each well and viability was expressed using Eq. (17) and determined by measuring the absorbance at 490 nm using the above microplate reader.

Cell Uptake Assay of Fluorescently Labelled HA-NPs

Fluorescently labelled HA-NPs were prepared via a stable covalent bond between Fluorescein isothiocyanate (FITC) and HA-NPs (162). The FITC-labelled NPs were purified in the dark using dialysis method and lyophilized. After treatment with FITC labelled HA-NPs at the concentrations ranging from 1 to 1000 μg/mL for 24 h, VK2/E6E7 and End1/E6E7 cells were washed twice with DPBS and stained for DNA with Hoechst 33342 dye. The assessment and visualization of cellular uptake of HA-NPs was carried out by a laser scanning confocal microscopy (Leica TCS SP5) using a Leica TSC SP5 inverted confocal microscope with a 100x oil immersion objective (N.A. 1.44). FITC was excited using a 488 nm line of an argon ion laser, and the detection window was set from 505-575 nm. For detection of Hoechst 33342 in a separate scan, excitation was performed using a 405 nm diode laser with a detection window set from 412-497 nm. Detector gain and laser power for all channels were set to result in no detector saturation with the highest concentration of HA-NPs used. Images were processed using ImageJ software (National Institutes of Health, http://rsbweb.nih.gov/ij/).

Data Analyses

JMP® - Release 9.0.2 (SAS Institute Inc. Cary, NC) was used for the statistical analysis and experimental design. Values were expressed as mean ± standard deviation (SD) and the differences in measured variables between treated groups and corresponding control were determined by one-way analysis of variance (ANOVA) followed by Dunnett post hoc test using JMP 9.0.2 software. Difference among means was considered significant at $p < 0.05$.

3.3. Results and Discussion

Mechanism of Formation of Cross-linked HA-NPs

In the surfactant-free cross-linking method, the HA-NP formation was based on cross-linking efficiency of HA, water-HA, water-acetone and acetone-HA interactions. The rationale for the selection of four factors (independent variables) in FFED design (Table 9) was based on the fact that the molar concentrations of ADH (X_1) and EDC (X_2) were significant for efficient cross-linking between HA and ADH while the interactions among aqueous phase, organic solvent and HA were critical for NP formation (108, 163). In the aqueous phase, the HA polymer was swollen and took an expanded coil conformation due to the inter- and intra-molecular hydrogen bonding among its functional groups and water molecules (164). The repulsive force exerted by the negatively charged carboxylate (-COOH) groups of HA also contributed in its expanded coil confirmation. Moreover, the organic solvent (acetone) induced the breakage of the hydrogen bonds of HA. After this, the -COOH groups of HA became available to be cross-linked with ADH through amide bond coupling.

The adequate ratio (X_3) between the volume of acetone and the aqueous phase initiated the cross-linking reaction and NP formation. After the secondary addition of acetone, water was diffused into acetone and caused the precipitation of HA with a coil-to-globule transition. Since, HA was cross-linked with ADH, it underwent molecular transition to form the HA-NPs (165). The reaction time (X_4) after the secondary acetone addition, when the color of the solution changed from clear to light blue (Figure 8) due to the Tyndall effects and the transformation of HA from extended coil confirmation to a compact globular structure confirmed the NP formation.

There are few methods have been described for the preparation of HA-NPs; such as reversed-phase micro-emulsion (115) and surfactant-free (108) methods. The surfactant-free

method adopted in this study was advantageous in terms of avoiding the use of surfactants, which might be deleterious and difficult to remove from the final formulation and could cause significant loss of NPs in the washing steps. Moreover, the modified surfactant-free cross-linking method described in this work required lesser time (< 24 h) compared to the surfactant-free method (> 44 h) (108) previously reported to produce the NPs. The shorter time was achieved by effective screening of the factors responsible for NPs formation using the FFED design as given in Table 9.

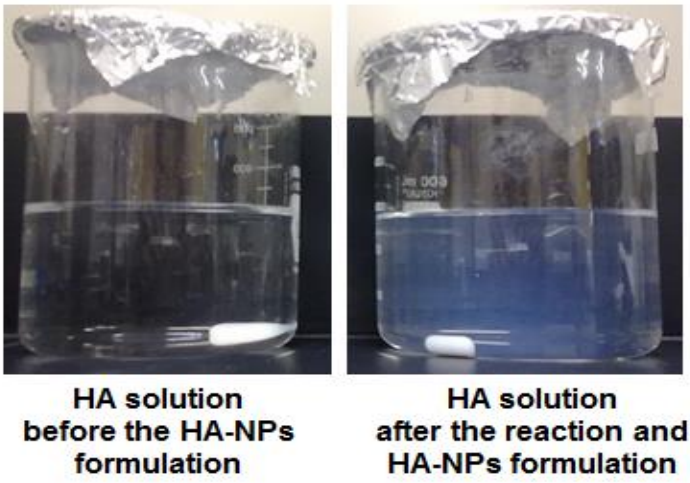

Figure 8. HA-NPs Solution Turned To Light Blue After the Secondary Acetone Addition Due To the Tyndall Effects.

Experimental Data Analysis in HA-NP Formulations Development

The measured values for responses Y_1 (PMD), Y_2 (PDI) and Y_3 (ζ) for runs F1 to F12 were summarized in Table 11. The polynomial Equations (19), (20), and (21) for the responses Y_1, Y_2, and Y_3, respectively, were developed after the data analysis in order to evaluate the best predictive model for each responses in relation to each factors.

$$Y_1 = 122.75-1.81X_1+0.47X_2-4.14X_3-12.52X_4+9.61X_1X_2+21.57X_1X_3+17.14X_1X_4 \quad (19)$$

$$Y_2 = 0.179-0.007X_1-0.067X_2-0.016X_3-0.013X_4-0.0004X_1X_2+0.033X_1X_3-0.028X_1X_4 \quad (20)$$

$$Y_3 = -38.18-0.091X_1+0.84X_2-0.99X_3-1.09X_4+0.88X_1X_2+1.21X_1X_3+0.086X_1X_4 \quad (21)$$

Table 11: FFED Design Showing Factors With Their Corresponding Measured Responses.

Run	Factors[a]				Measured responses		
	X_1	X_2	X_3	X_4	Y_1; PMD: nm	Y_2; PDI	Y_3; ζ: mV
F1	- 1	- 1	+1	+1	78.7	0.22	-42.4
F2	+1	- 1	+1	- 1	124.0	0.30	-41.4
F3	- 1	+1	- 1	+1	111.8	0.18	-38.1
F4	- 1	+1	+1	- 1	119.7	0.06	-38.6
F5	+1	+1	- 1	- 1	109.3	0.13	-38.4
F6	+1	- 1	- 1	+1	98.4	0.18	-42.3
F7	+1	+1	+1	+1	153.4	0.08	-38.4
F8	- 1	- 1	- 1	- 1	189.4	0.29	-34.1
F9	0	0	0	0	115.4	0.22	-36.9
F10	0	0	0	0	128.7	0.19	-34.1
F11	0	0	0	0	121.1	0.15	-36.3
F12	0	0	0	0	123.2	0.16	-37.1

[a] Coded values of factors, X_1; molar concentration of ADH in mM, X_2; molar concentration of EDC in mM, X_3; volume of acetone in mL, X_4; reaction time in hour.

In the above Equations, the positive coefficients before the terms demonstrated an increasing effect; whereas, the negative coefficients showed a decreasing effect on the selected responses. The interaction terms displayed how the responses changed when the two factors were varied simultaneously. To confirm the acceptability of the model, analysis of variance (ANOVA) was performed (Table 12). The acceptability criterion for a good model is a *p* value in ANOVA analysis < 0.01 and RSquare (R^2, ratio of the difference to the reduced negative log-likelihood values) should be in the range of $0.70 \leq R^2 \leq 0.90$ (59). According to the

acceptability criteria, the polynomial Equations for Y_1 and Y_2 fitted very well with the data modelling. However, the polynomial Eq. (21) for response Y_3 (ζ potential) did not fit well according to the acceptability criteria and was not considered for subsequent modeling and prediction efforts. This might be due to the fact that NPs were made of HA as a main matrix, which did not lead to a significant changes in the ζ potential (Y_3) values.

Table 12: ANOVA Analysis.

Responses	**ANOVA analysis**						
	Source	**df[a]**	**SS[b]**	**MS[c]**	R^2	**F ratio**	***p* value**
Y_1; PMD	model	7	8231.16	1175.88	0.99	50.46	0.001
	error	4	93.21	23.30			
	total	11	8324.37				
Y_2; PDI	model	7	0.055	0.01	0.94	9.65	0.022
	error	4	0.033	0.001			
	total	11	0.058				
Y_3; ζ	model	7	53.55	7.65	0.99	0.97	0.545
	error	4	31.51	7.88			
	total	11	85.06				

[a] Degree of freedom. [b] Sum of squares. [c] Mean sum of square.

To understand the factors effects and significance, Pareto charts were generated as shown in Figure 9A and 9B, for the responses Y_1, and Y_2, respectively. The values on the *x*-axis of the Pareto charts represented the standardize effects; the ratio of estimate and the standard error of the factor effect (t_{ratio} values). These *t* values were obtained on the basis of the estimate of factor effects, which were the coefficients in Equations (19), (20), and (21) and the standard error of an effect (166). The obtained *t* value was compared with a tabulated critical *t* value

($t_{critical}$ = 2.78) as shown in the vertical lines in the Pareto charts. This $t_{critical}$ value was determined at α = 0.05 for residual degrees of freedom (residual *df* = number of runs-number of terms-1) (166). In Figure 9A and 9B, the absolute *t* value of the factors whose length of the chart passed the vertical line ($t_{critical}$ at $p < 0.05$ and $df = 4$) had significant effects on responses.

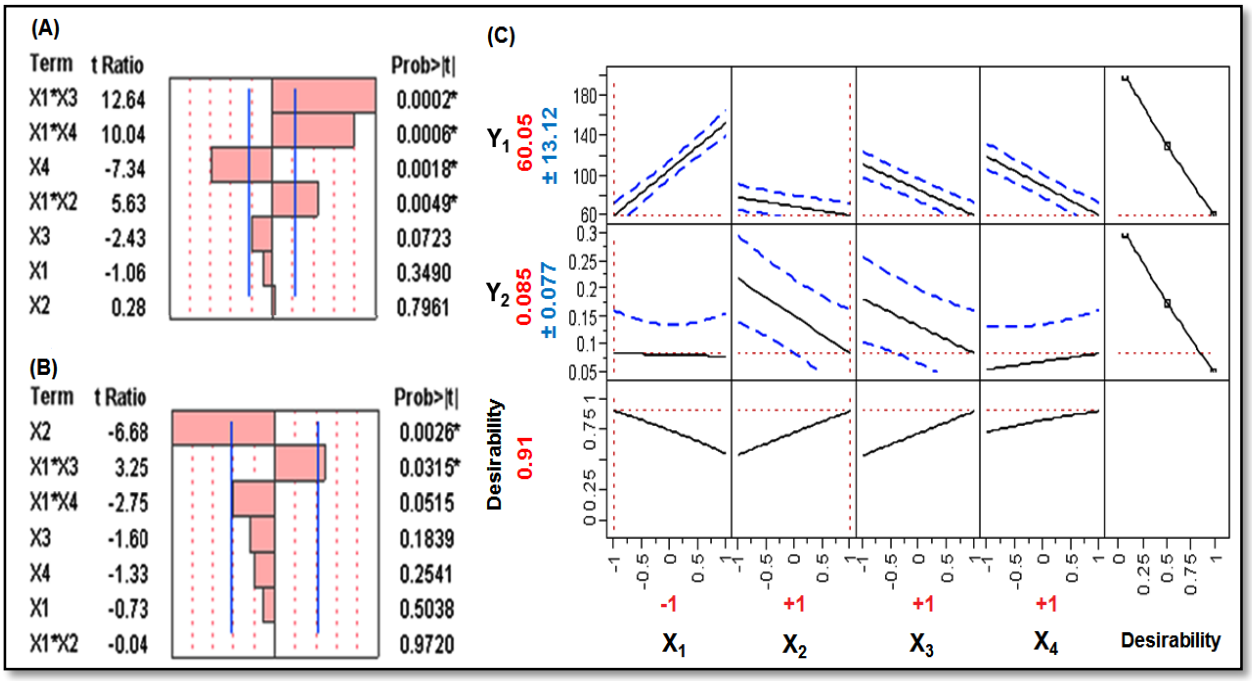

Figure 9. Pareto Charts Showing the Standardized Effect of Factors, X_1; molar concentration of ADH: mM, X_2; molar concentration of EDC: mM, X_3; volume of organic phase: mL, X_4; reaction time: h, and their interactions for responses. (A) Y_1; particle mean diameter: PMD, nm. (B) Y_2; polydispersity index: PDI. Bars extended past the vertical lines indicated the values reaching statistical significance (α = 0.05). Asterisk (*) indicated the significant effect ($p <$ 0.05) of factors over the responses. (C) Prediction profiler and desirability plot showing the effect of factors, X_1, X_2, X_3, and X_4, on the responses, Y_1 and Y_2. The desirability value of 0.91 corresponded to the optimized HA-NPs formulation (F13) with the coded values of, X_1 = -1; X_2 = +1; X_3 = +1; and X_4 = +1. The coded values listed above corresponded with the actual values of, X_1 = 2.49 mM; X_2 = 9.96 mM; X_3 = 60 mL; and X_4 = 6 h.

According to Figure 9A, Y_1 was significantly affected by interactions of X_1X_2, X_1X_3, X_1X_4 (all positively) and X_4 (negatively). The response Y_2 was significantly affected by X_1X_3 (positively) and X_2 (negatively) (Figure 9B). By considering only the significant effects, it appeared that X_1 interacted with the factors X_2, X_3 and X_4 that increased the PMD and PDI values of the NPs. The physical significance of this is explained later in the dissertation. The relationship among factors and responses was further investigated by constructing a prediction and desirability plot (Figure 9C).

According to the desirability value of 0.91, one that was very close to the ideal value (d = 1) (Figure 9C), the run *F13 (coded values: X_1 = -1; X_2 = +1; X_3 = +1; X_4 = +1; Actual values of, X_1 = 2.49 mM, X_2 = 9.96 mM, X_3 = 60 mL; and X_4 = 6 h)* was selected as the optimized NP formulation which showed the Y_1 and Y_2 values of 70.6 ± 4.1 nm and 0.07 ± 0.02, respectively, (n = 3). Meanwhile, to evaluate the effect of molar concentrations of ADH (X_1) and EDC (X_2) over the enzymatic degradation, drug release, and % DL of the NPs, the runs *F1 (Coded values: X_1 = -1; X_2 = -1; X_3 = +1; X_4 = +1; Actual values: X_1 = 2.49 mM; X_2 = 2.49 mM; X_3 = 60 mL; and X_4 = 6 h), and F7 (Coded values: X_1 = +1; X_2 = +1; X_3 = +1; X_4 = +1; Actual values: X_1 = 9.96 mM; X_2 = 9.96 mM; X_3 = 60 mL; and X_4 = 6 h)* were selected as control formulations. These control formulations F1 and F7 had the lowest and highest molar concentrations of ADH and EDC, respectively. The rationale for this selection was based on the fact that the free -COOH groups on HA were the recognition sites to initiate its degradation by HAase enzyme (167). Increasing the molar concentrations of ADH and EDC could affect the cross-linking between HA and ADH. Theoretically, this affected the degradation kinetics of the HA-NPs due to the higher cross-linking density of the -COOH groups and was not favorable for the attack of HAase on its recognition site.

Checkpoint Analysis

The resultant model was analyzed for its acceptability and validity with the theoretical optimum run, F13, which shows the maximum desirability value (Figure 9C), while minimizing both Y_1 and Y_2 values as given in Table 13. Two randomly selected runs, F14 (coded values; X_1 = -0.5; X_2 = -0.5; X_3 = +1; X_4 = +1) and F15 (coded values; X_1 = 0; X_2 = 0; X_3 = +1; X_4 = +1) were also analyzed to perform the checkpoint analysis (n = 3) to ensure reproducibility of the model. The difference between the predicted and measured values was statistically insignificant ($p > 0.05$).

Table 13: Checkpoint Analysis (n = 3).

Responses	Run	Measured value	Predicted value	% Error	*p* value
Y_1; PMD: nm	F13	70.6 ± 4.1	60.1 ± 13.1	-17.6	0.25
	F14	96.3 ± 5.3	89.8 ± 9.2	-7.22	0.35
	F15	108.4 ± 3.9	106.1 ± 7.7	-2.13	0.68
Y_2; PDI	F13	0.07 ± 0.02	0.09 ± 0.08	17.7	0.70
	F14	0.17 ± 0.01	0.18 ± 0.05	7.61	0.60
	F15	0.16 ± 0.02	0.15 ± 0.05	-7.38	0.79

Physicochemical Characterization of HA-NPs Formulations

PMD, Size Distribution, and % DL

The size distribution, PMD and PDI values for the NPs were analyzed by DLS measurements and shown in Figure 10A and Table 14. The % DL and % yield of HA-NPs calculated after purification and freeze-drying process was given in Table 14. The size distribution of NPs (F13) was also measured using NTA method and results were shown in Figure 10B. Both the analyses (DLS and NTA) confirmed the NPs formation in the nanoscale size range.

Table 14: Physicochemical Characterization of HA-NPs.

HA-NPs	Y_1; PMD: nm*	Y_2; PDI*	DL (% w/w)*	Yield (% w/w)*
F13	70.6 ± 4.1	0.07 ± 0.02	26.1 ± 1.2	93.3 ± 0.7
F1	81.5 ± 2.6	0.21 ± 0.01	22.0 ± 0.7	90.9 ± 0.8
F7	157.7 ± 4.0	0.08 ± 0.02	10.6 ± 1.8	84.2 ± 1.1

* Values were given as mean ± SD, n = 3.

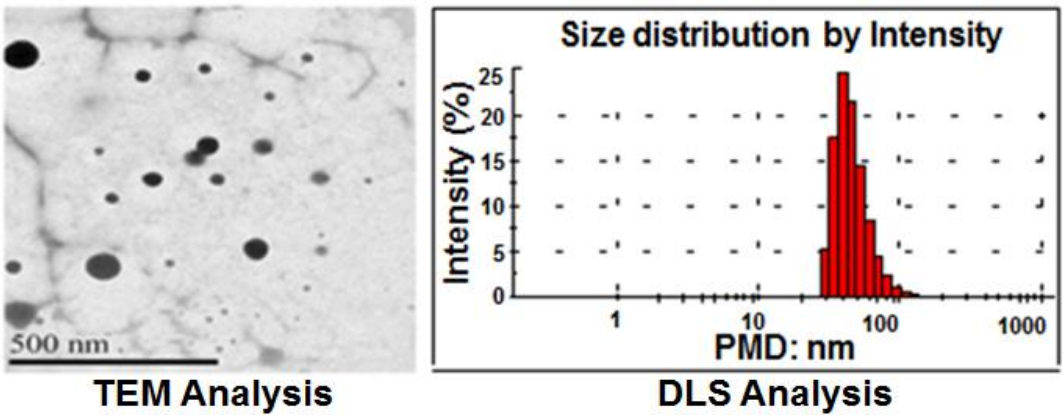

Figure 10A. Surface Morphology and Size Distribution of HA-NPs (F13) by TEM and DLS Analyses.

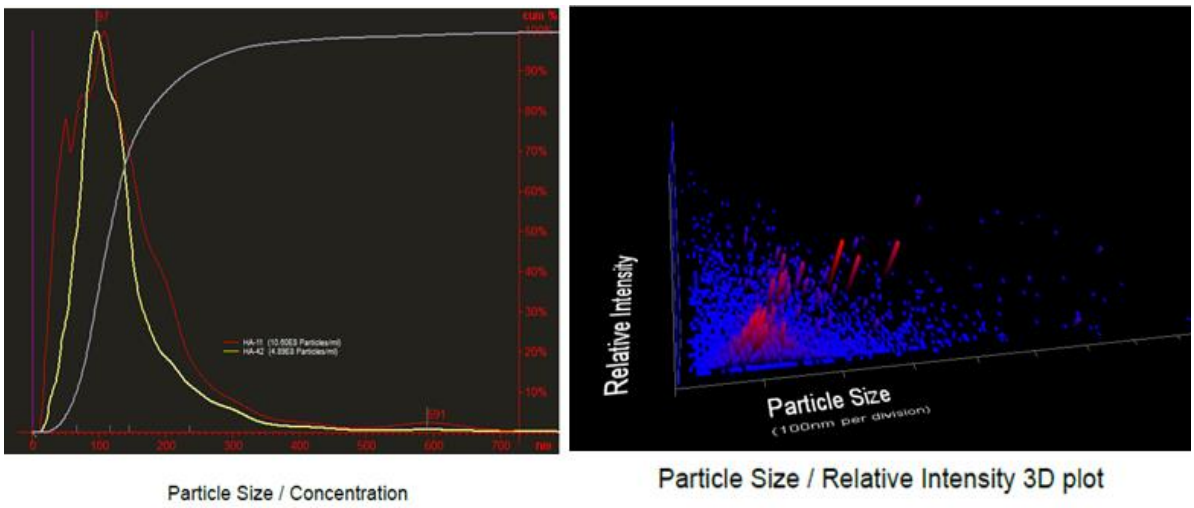

Figure 10B. Size Distribution Analysis of HA-NPs (F13) by NTA Measurements.

The NPs were found stable as the ζ potential value was -38.2 ± 2.8 mV (n = 3), which was above (absolute value) the ζ potential limits (± 30 mV) for a colloidal dispersion to be

stable (168). The % DL of the NPs was increased with increasing the drug concentration in the loading solution. The % DL was increased from about 16 to 26% for F13, 13 to 22% for F1 and 5.5 to 11% w/w for F7, when the ratio of drug to NPs was changed from 1:10 to 1:1 (w/w), respectively, in the loading solution. This was probably due to the presence of a higher concentration of drug in the loading solution as also observed by other researchers (169, 170). In addition, increasing the NP amount and thus the concentration of HA polymer in the loading solution might have exhibited greater molecular tortuosity which have interfered with the diffusion of drug into the NPs and lowered the drug loading as previously explained (170, 171).

There are other factors such as pH and temperature that could have also affected the drug loading of HA-NPs. In this study, the drug loading experiment was performed at neutral pH (greater than the pKa value of HA; 2.9) (172). It was anticipated that at this pH, due to the presence of ionized -COOH groups in the HA-NP matrix (belonging to HA), there was an electrostatic repulsion among the HA chains (115). This might have increased the inter-chain distances and degree of swelling leading to higher drug loading inside the NPs (115).

The higher % DL associated with F13, compared to F1 and F7 formulations can be explained by the effect of the lower cross-linking density of -COOH groups of HA in F13. Thus, there would be higher electrostatic interaction of the positively charged amino group of TFV and the negatively charged -COOH of HA. Also, the introduction of cross-linking into native HA produced porous surfaces, while native HA has a fibrous and irregular structure (173). This might have also promoted the diffusion of TFV inside the HA matrix and increased the % EE and DL of the HA-NPs. The porosity was further affected by high molar concentration of EDC compared to the ADH in the F13 NP formulation (174).

Spectral Analysis by FT-IR spectroscopy

To assess the cross-linking between HA and ADH (prepared according to the Reaction Scheme 1), FT-IR analysis was performed. The peaks observed in the FT-IR spectra were

summarized in Table 15 together with their peak assignments. In the FT-IR spectra of NPs (Figure 11E, F and G), instead of a single band at 1620 cm^{-1} as present in the spectrum of HA (Figure 11C) there were two intense bands at about 1650 cm^{-1} (associated with the amide bond formed between HA and ADH) and at 1550 cm^{-1} (due to the presence of secondary amide groups of ADH). The reduced intensity of the small band at 1405 cm^{-1} in the NPs spectrum compared to that of native HA was attributed to the reduction in the numbers of -COOH groups of HA due to the amide coupling.

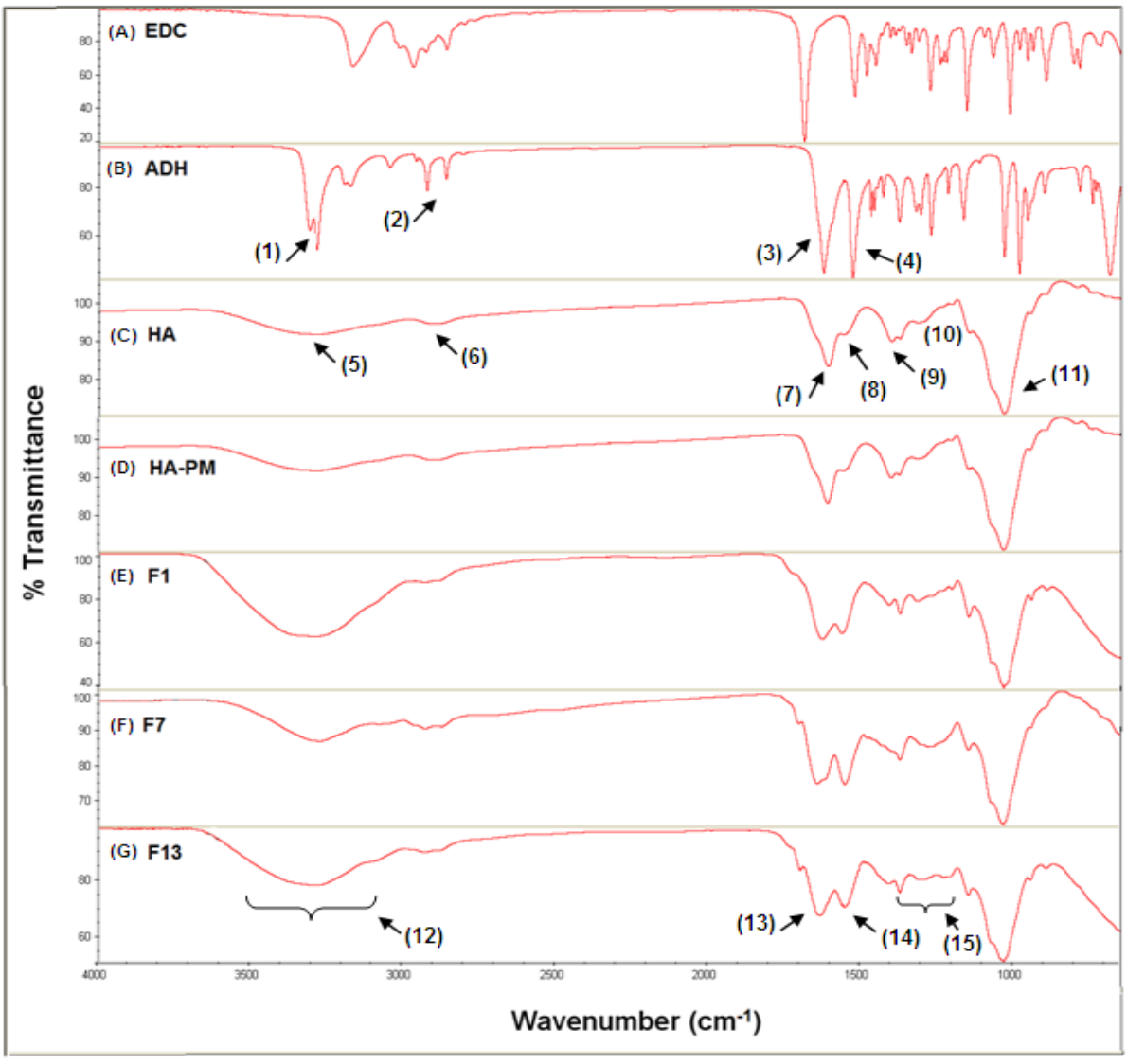

Figure 11. FT-IR Spectrum: (A) EDC. (B) ADH. (C) Native HA. (D) HA-PM. (E) HA-NP; F1. (F) HA-NP; F7. (G) HA-NP; F13.

Past studies showed similar FT-IR spectrum of native HA (175), ADH (173), and HA cross-linked with dihydrazide (175), which strongly supported the hypothesis of this work that HA and ADH were indeed cross-linked, using carbodiimide chemistry. The NP formation reaction was also performed excluding the cross-linking agents (ADH, EDC and NHS) to further assess the eventual effects of external factors on the formation of NPs. The product of this reaction (HA-PM: Figure 11D) generated the similar spectrum as of native HA (Figure 11C). This clearly indicated that the ADH and EDC were critical to formulate the cross-linked HA-NPs.

Table 15: Peaks Observed in the FT-IR Spectra with Their Peak Assignments.

Sample	**Wavenumbers (cm^{-1})**	**Peak assignments (peak designation in the spectrum)**
ADH	3200-3400	Stretching vibrations of -NH and $-NH_2$ groups (1)
	2800-2950	C-H stretching (2)
	1640	C=O stretching vibration (3)
	1530	Secondary amide group (4)
Native HA	3290	OH and -NH stretching vibrations (5)
	2850-2950	CH_2 asymmetric and symmetric stretching (6)
	1620	Asymmetric stretching of C=O of COO^- group (7)
	1550	Amidic -NH bending of acetamide group (8)
	1405	COO^- symmetric stretching (9)
	1160	C-O-C glycoside bond in saccharidic units (10)
	950-1150	C-O stretching vibrations in alcoholic groups (11)

NPs (F1, F7 and F13)	3100-3500	Stretching vibrations of -NH and -NH_2 groups of ADH also associated with the -OH and -NH stretching vibrations of HA (12)
	1650	Amide-I, due to the cross-linked HA and ADH (13)
	1550	Amide-II, amide group of ADH (14)
	1200-1400	C-N, C-O and CH_2 stretch, indicating the presence of pendant hydrazide groups of ADH (15)

Solid State ^{13}C-CP/MAS NMR Spectroscopy for Spectral Analysis

The NMR spectra were given in Figure 12 and the results were summarized in Table 16, together with their peak assignments as shown in reaction scheme 1. The NMR. The intense signal at 175 ppm was attributed to the amide group associated carbonyl carbon in the spectrum of ADH (Figure 12B); whereas, it was associated with -COOH and carbonyl acetamido carbons in the spectrum of HA (Figure 12C). In the spectrum of HA-NPs the characteristic signal at about 175 ppm was associated with the carbonyl carbons of amide groups formed due to the cross-linking between native HA and ADH. One remarkable difference among the spectrum of the NPs, native HA and ADH was that the signals in the NPs spectrum were considerably broader and extended over a larger region possibly due to the ionic interactions between the randomly cross-linked HA.

The similar spectrum of native HA and dihydrazide cross-linked HA (176) have been observed in previous studies, which also confirmed that HA and ADH were indeed cross-linked in this study. The signal at about 156 ppm was more intense in F13 (Figure 12F). This could be due to the presence of higher molar concentration of EDC in F13 compared to F1 and F7.

Thus the intermediate product of HA and EDC was formed efficiently and showed an intense signal (80, 176).

Overall, the results indicated by FT-IR (Figure 11, Table 15) and NMR (Figure 12, Table 16) analyses confirmed the cross-linking between HA and ADH.

Table 16: Chemical Shift (δ: ppm) Values Observed with Their Peak Assignments.

Sample	**Chemical shift (δ: ppm)**	**Peak assignments**
ADH	175	Amide group associated carbonyl carbons
	36 and 26	α and β carbons, respectively, corresponded with the aliphatic region
HA	175	Carboxylate and acetamido carbonyl carbon
	100	Two anomeric carbons of D-glucuronic acid moiety of HA associated with C-O-C glycoside bonds
	65-80	Ring carbons
	45-65	Methylene carbons
	25	Methyl carbon of acetamido group
NPs (F1, F7 & F13)	175	Amide group associated carbonyl carbons of HA and ADH
	36 and 26	α and β carbons of ADH, respectively

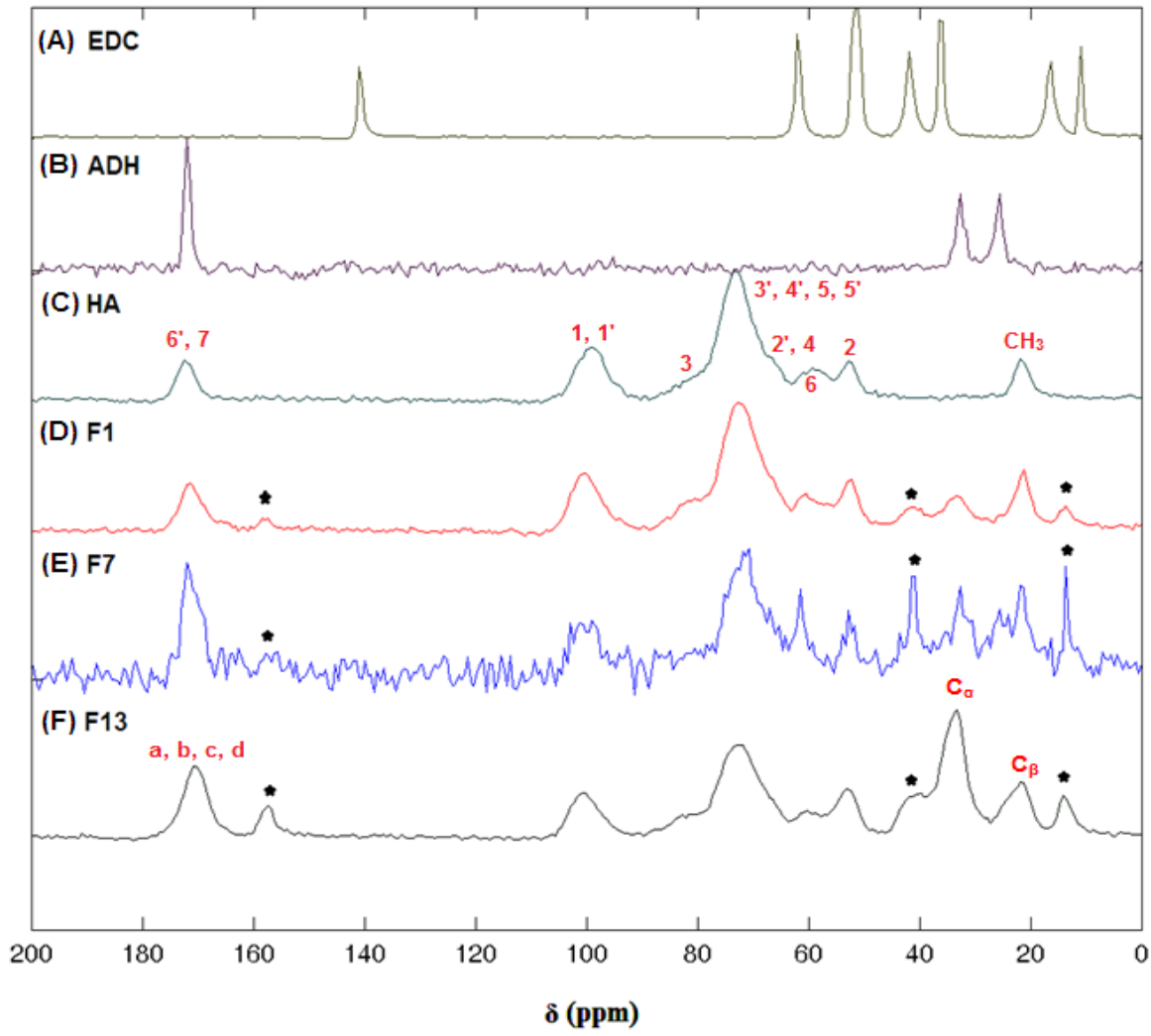

Figure 12. Solid State ^{13}C-CP/MAS NMR Spectrum: (A) EDC. (B) ADH. (C) Native HA. (D) HA-NP; F1. (E) HA-NP; F7. (F) HA-NP; F13. Asterisked (*) Signals Indicated the Formation of EDC-HA Adduct.

Enzymatic Degradation Analysis of HA-NPs

The percent cumulative degradation either in the presence or absence of HAase enzyme was analyzed using Uronic acid-Carbazole assay and represented in Figure 13A, B, C and D for native HA, F13, F1, and F7 NPs formulations, respectively. It was observed that in the presence of HAase, the degradation of native HA was higher in comparison to formulation F13,

F1 and F7. The variance in the degradation of these samples was due to the different interactions of HAase with its recognition site of HA as explained below.

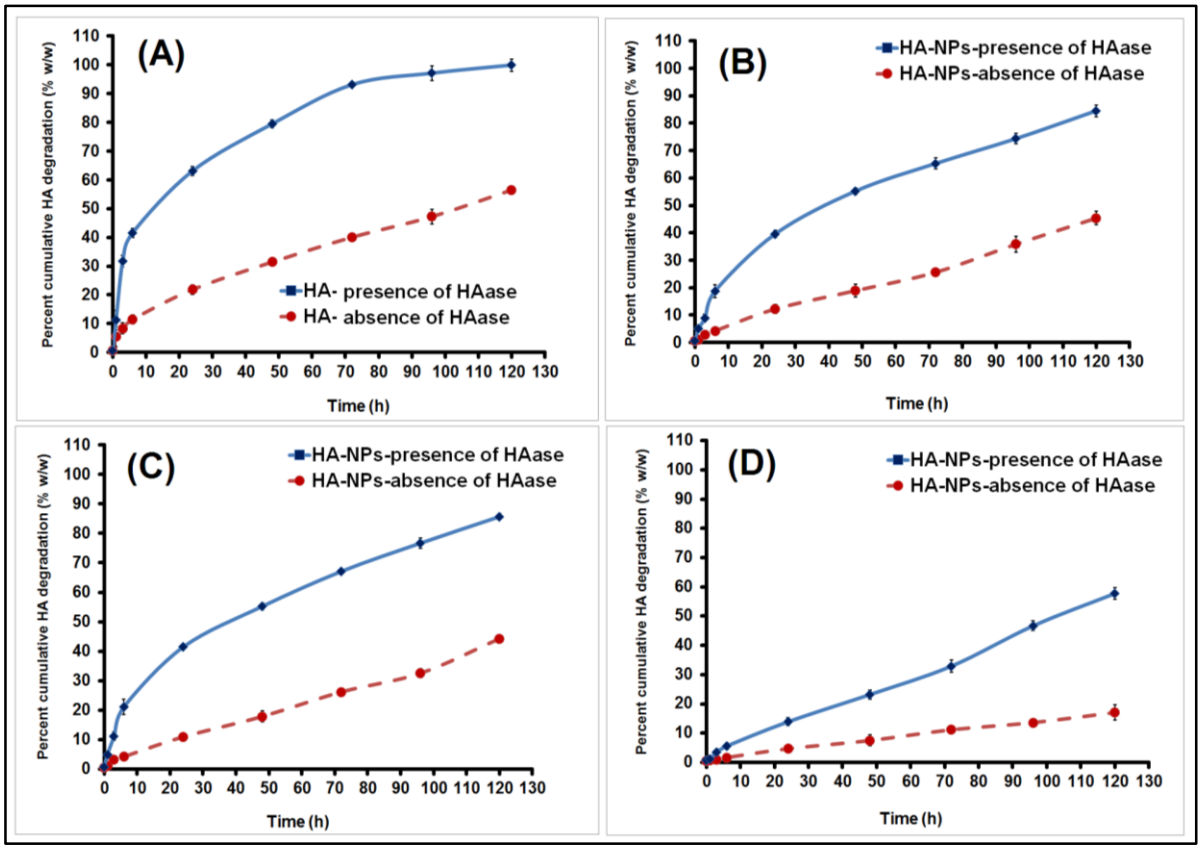

Figure 13. Percent Cumulative HA degradation (% w/w) either in Presence or Absence of HAase enzyme at pH 7.1. (A) HA-gel. (B) HA-NP; F13. (C) HA-NP; F1 and (D) HA-NP; F7. Results are given as mean ± SD, n = 3.

It is well known that HAase begins its action by effecting the free -COOH groups of HA (167). Thus, the molar concentrations of ADH (cross-linking agent) was considered as the major formulation variable in the formulation design that could have significantly affected the cross-linking density, enzymatic degradation and release kinetics of the HA-NPs. It was observed that the degradation was highest for native HA as compared to the HA-NPs since, in the native HA all the -COOH groups were free to interact with HAase enzyme. The slower degradation rate for formulation F7 can be explained by the fact that, in this, the molar

concentrations of ADH and EDC were highest in F7 with the maximum -COOH groups of HA being blocked by forming the amide bonds with ADH. The degradation of native HA and HA-NPs in the absence of HAase might be due to the hydrolytic degradation of HA as previously explained (80, 103). Overall, the degradation rate for HA-gel and HA-NPs was faster in the presence of HAase compared to its absence.

In Vitro Drug Release Analysis of HA-NPs

The *in vitro* drug release profile was depicted in Figure 14A, B, C and D for TVF containing HA-gel and native TFV control, F13, F1, and F7 NPs, respectively. A significantly triggered release of drug (~90% w/w) was observed from NPs (F13) in the presence of HAase enzyme; whereas, in its absence the value was ~39% w/w as analyzed after 24 h. It was observed that HA-gel exhibit a burst release at ~78% and ~73% w/w of the drug was released in first 6 h in the presence and absence of HAase, respectively. However, ~97% w/w of drug was released from HA-gel either in the presence of absence of HAase after 24 h (Figure 14A). These results indicated that the drug release rate was much faster from the HA gel; whereas, comparatively slow release of TFV was observed in the case of HA-NPs. This might be due to the difference in cross-linking density of the HA-NPs and HA-gel that has been significantly affected their enzymatic degradation behavior as explained before (Figure 13). In addition, the van der Waal and electrostatic interactions of TFV with HA polymeric chains inside the NPs could also be one of the reasons for the slow release of drug from NPs as explained below.

TFV has two pKa values at 2.0 and 6.7 (56), whereas HA has a pKa value at 2.9 (172). Hence, both TFV and HA were negatively charged at pH 7.1 (above their pKa values). Therefore, there was a minimal possibility of interaction between them. Due to these minimal interactions of HA with TFV a higher drug release rate was observed in case of the native HA-gel. However, after the cross-linking of native HA polymeric chains inside NPs, the cross-

linker (ADH) increased the interactions of HA with TFV through its nonpolar carbon atoms and its amino groups (positively charged at the working pH of 7.1). These interactions might have caused a slower drug release rate from the NPs.

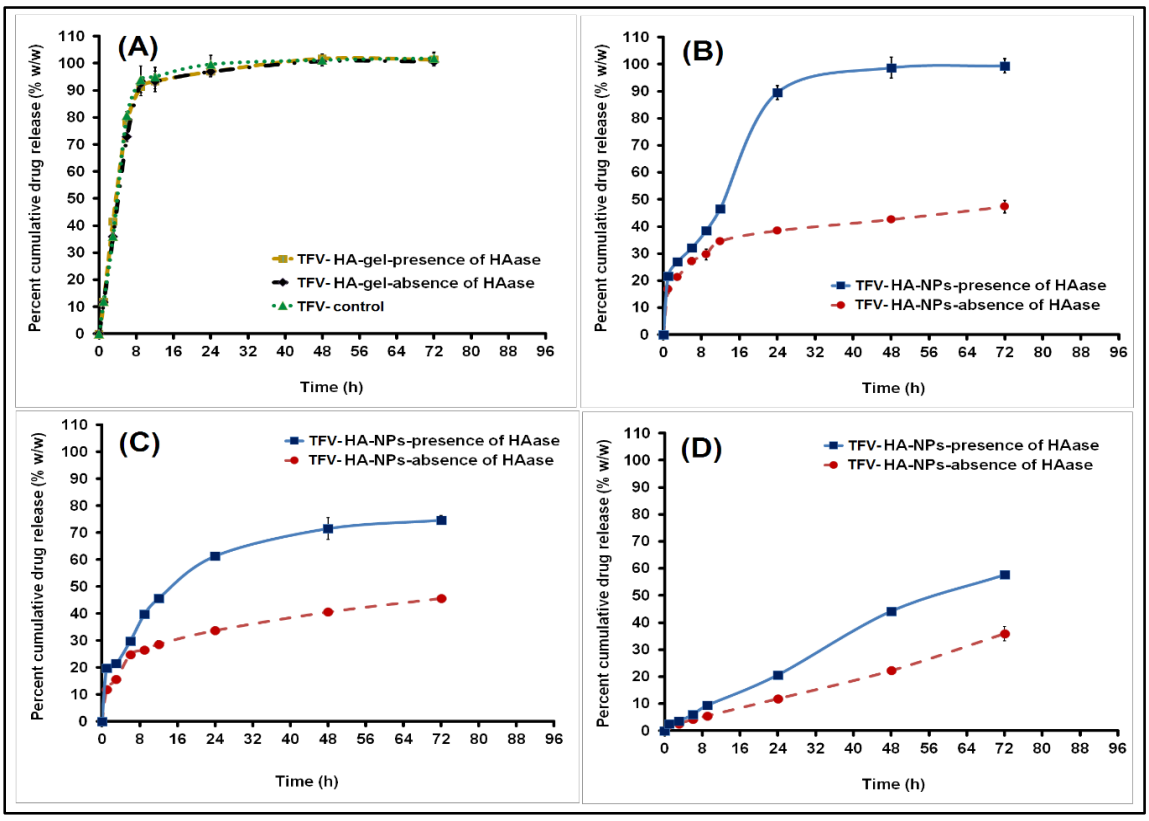

Figure 14. Percent Cumulative Drug Release (% w/w) profile either in Presence or Absence of HAase at pH 7.1. (A) HA-gel and TFV control. (B) HA-NPs; F13. (C) HA-NPs; F1. (D) HA-NPs; F7. Results are given as mean ± SD, n = 3.

The effective molar concentration (EC_{50}) of TFV required for *in vitro* anti-HIV activity varies between 5-7.4 µM (177). The HIV virus can cross the CV mucosa barrier in 2 to 6 h and interacts with the macrophages, and dendritic cells (178). Ideally, the effective concentration (EC_{50}) of TFV required to exhibit its activity should be released from the NPs before the HIV virus crosses the vaginal mucosa between 2-6 h. Based on the drug loading of HA-NPs (~26 %w/w), the actual amount of TFV was ~91 µM per 100 mg of NPs. Considering the 20 mg of HA-NPs will be used in each treatment dose, this would be equivalent to ~18 µM of TFV drug dose. It is noteworthy that although, only ~32% w/w of the drug was released in 3-6 h from the

optimized formulation (F13), the EC_{50} value of TFV was achieved in that critical timeframe in the presence of HAase; whereas, more than 9 h was required in the absence of HAase based on the release data (Figure 13).

Kinetics of Enzymatic Degradation and *In Vitro* Drug Release Profile of HA-NPs

The drug release was analyzed using various *in vitro* kinetic models as given by Equations (4), (5), (6), and (8), respectively. The parameters obtained were given in Table 17. It was observed that in the absence of HAase the drug release from F13 and F1 followed the Peppas model. However, in the presence of HAase enzyme, F13 and F1 followed first order and Peppas models, respectively. The drug release kinetics from HA-gel followed first order model (r^2: 0.97), whereas drug release from F7 was governed by the combination of zero and first order kinetic models (Table 17), either in the presence or absence of HAase.

To further determine the drug release mechanism from NPs and gel formulation the Korsmeyer-Peppas model was applied. The decision to use the Korsmeyer-Peppas model was based on its simplicity and efficiency in analyzing the drug release mechanism when more than one form of mechanisms were involved. It was observed that the drug release from F13 and F1 occurred by Fickian diffusion *($n < 0.5$),* whereas F7 followed anomalous transport (diffusion and erosion controlled release) mechanism since $0.5 < n < 1$. The drug release from the HA-gel followed Super Case-II transport (erosion of and degradation of HA) since $n > 1$.

The f_1 and f_2 values were calculated using Equations (9), and (10), respectively (129), and shown in Table 17. Results indicated that there was a significant difference between the HA degradation and drug release kinetics from HA-gel and HA-NPs either in the presence and absence of HAase enzyme.

Table 17: Estimated Parameters: *In Vitro* Drug Release and Degradation Kinetics Models.

HA-NPs	Zero order	First order	Higuchi model	Korsmeyer-Peppas model	Model independent analysis	
	r^2 [a]	r^2 [a]	r^2 [a]	r^2 [a], (exponent *n*)	Enzymatic degradation f_1, (f_2)	*In Vitro* drug release f_1', (f_2')
F13[b*]	0.785	0.969	0.926	0.928, (0.29)	32.0, (12.9)	26.4, (13.3)
F13[c*]	0.626	0.718	0.855	0.982, (0.25)	35.4, (28.6)	57.3, (-3.1)
F1[b]**	0.754	0.882	0.938	0.952, (0.34)	29.7, (14.5)	40.9, (3.8)
F1[c]**	0.716	0.798	0.916	0.971, (0.32)	36.8, (28.2)	62.3, (-4.9)
F7[b*]**	0.993	0.995	0.946	0.973, (0.78)	64.3, (-2.3)	61.4, (-1.5)
F7[c*]**	0.996	0.988	0.926	0.950, (0.68)	74.5, (12.5)	83.4, (-7.6)

[a] Correlation coefficient. [b] Presence of HAase enzyme. [c] Absence of HAase enzyme.

Surface Morphology and Size Distribution Analysis of HA-NPs during the Enzymatic Degradation Process

The HA-NPs demonstrated a spherical shape and small PMD, as analyzed by TEM and DLS analyses (Figure 15A). The surface morphology of the NPs during the enzymatic degradation process was analyzed for up to 3 days (Figure 15B) showed that the surface morphology in the absence of HAase was not changed significantly; whereas, in its presence there was a significant change (Figure 15C) compared to that of native HA-NPs (Figure 15A). This was potentially due to the degradation of HA at the surface of the NPs, which generated the fragments of HA and caused its transition from globular to coil confirmation (164).

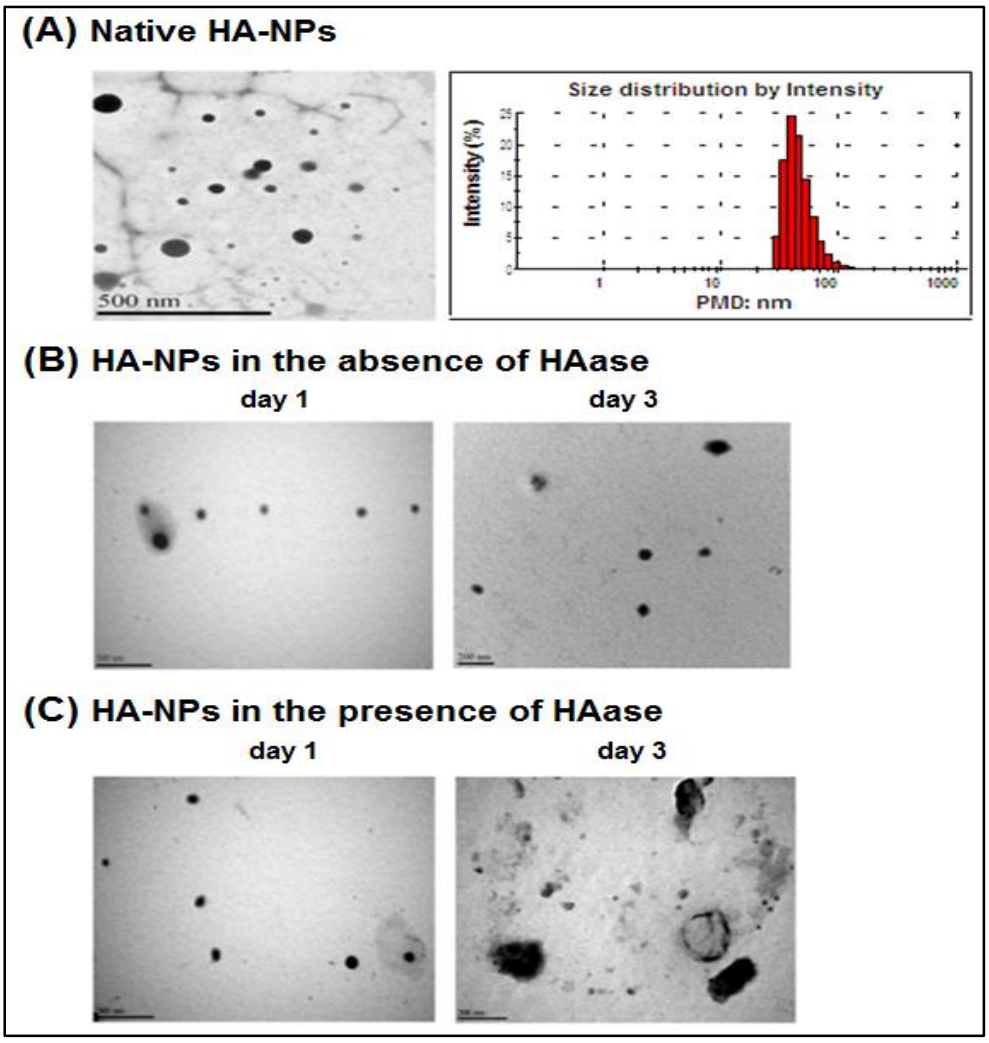

Figure 15. (A) Surface morphology: scale bar, 500 nm, and size distribution analysis of native HA-NPs (F13) by TEM and DLS analyses. Surface morphology of formulation F13: (B) in the absence of HAase, after day one: scale bar, 500 nm, and day three: scale bar, 200 nm. (C) in the presence of HAase, after day one: scale bar, 500 nm and day three: scale bar, 200 nm.

The PMD of the degradation medium (taken as control) at day zero was 7.03 ± 0.49 nm (n = 3), (Figure 16A). The PMD observed was mainly due to the presence of bovine serum albumin (BSA;~7 nm) (179) at high concentration (~40 mg/mL) (127) in the degradation medium. A slight increase (~2 fold) observed in the NPs diameter when incubated in medium in the absence of enzyme (Figure 16A) could be due to the interaction of BSA with HA (180) and self-aggregation (179, 181) of BSA. This was further confirmed by UV-Vis spectroscopy

and ζ potential measurements as explained below. The PDI value of all the samples was very high (> 0.5) which could be due to the presence of particles of variable diameters.

Self-aggregation of BSA and its Interaction with HA: Effect over PMD and Enzymatic Degradation of HA-NPs

BSA is a globular protein that has been stabilized by electrostatic repulsions in its native form (179). The diameter of the BSA has been affected greatly by various factors such as time, temperature, concentration, and its self-aggregation (179). The interaction between BSA and HA is a pH dependent process and maximum at pH 4 to 5 (172). In this study the enzymatic degradation analysis was conducted at pH 7.1, which was substantially higher than the isoelectric points of BSA (5.2) and HA (2.9) (172). But, due to the heterogeneity of the charge of the BSA molecule, the binding sites can be localized even at pH 7.1 (182). Thus, the existence of positive charge patches at the BSA surface, allowed the electrostatic interaction of HA at this pH. This was confirmed by an increase in the UV absorbance value of the solution containing BSA and HA at 400 nm (Figure 16B). The interaction between BSA and HA was further analyzed by ζ potential measurements as shown in Figure 16C. The self-aggregation and size distribution analysis of native HA-NPs (F13) in the presence of BSA (release medium) was analyzed by DLS analysis (Figure 17).

The slow enzymatic degradation rates of the HA-NPs could also be explained on the basis of interaction between BSA and HA, since BSA compete with HAase to form electrostatic complex with HA (172, 183). Also, at high concentration, BSA formed a dense complex with HA and covered it completely (adsorption layer), hindering the hydrolysable sites on HA (172, 183). This ultimately inhibited or slowed down the degradation of HA by HAase. Indeed, the study of complex formation between BSA and HA and several other components (enzymes, amine bases) present in the vaginal and seminal fluids was complicated and needs further

analysis techniques such as, X-ray photoelectron spectroscopy (XPS) and Auger electron spectroscopy in the future work.

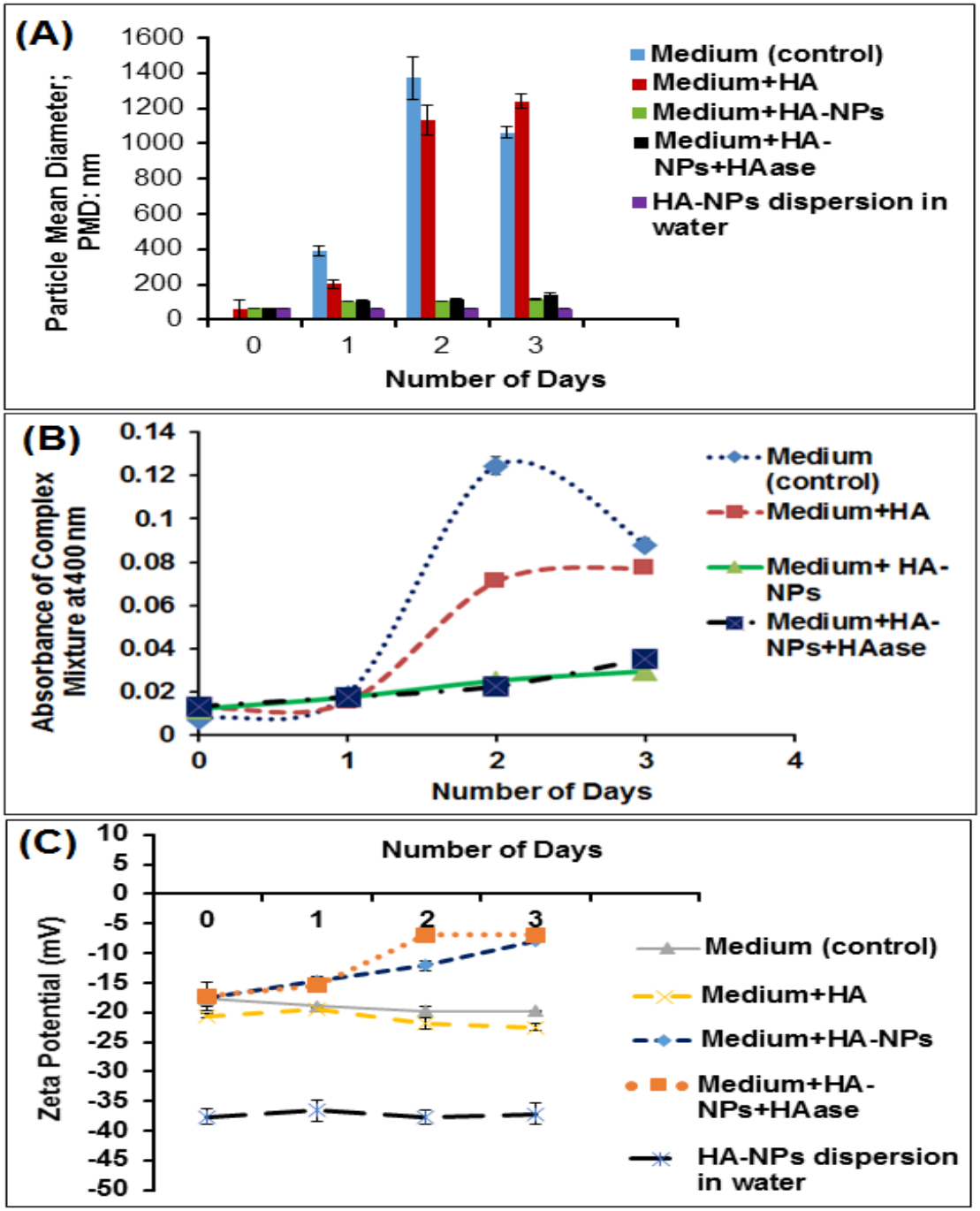

Figure 16. (A) Particle mean diameter; PMD; nm. (B) Absorbance of complex mixture of BSA and HA at 400 nm. (C) Zeta potential analysis. Results are analyzed up to three days of incubation at 37°C and given as mean ± SD, n = 3.

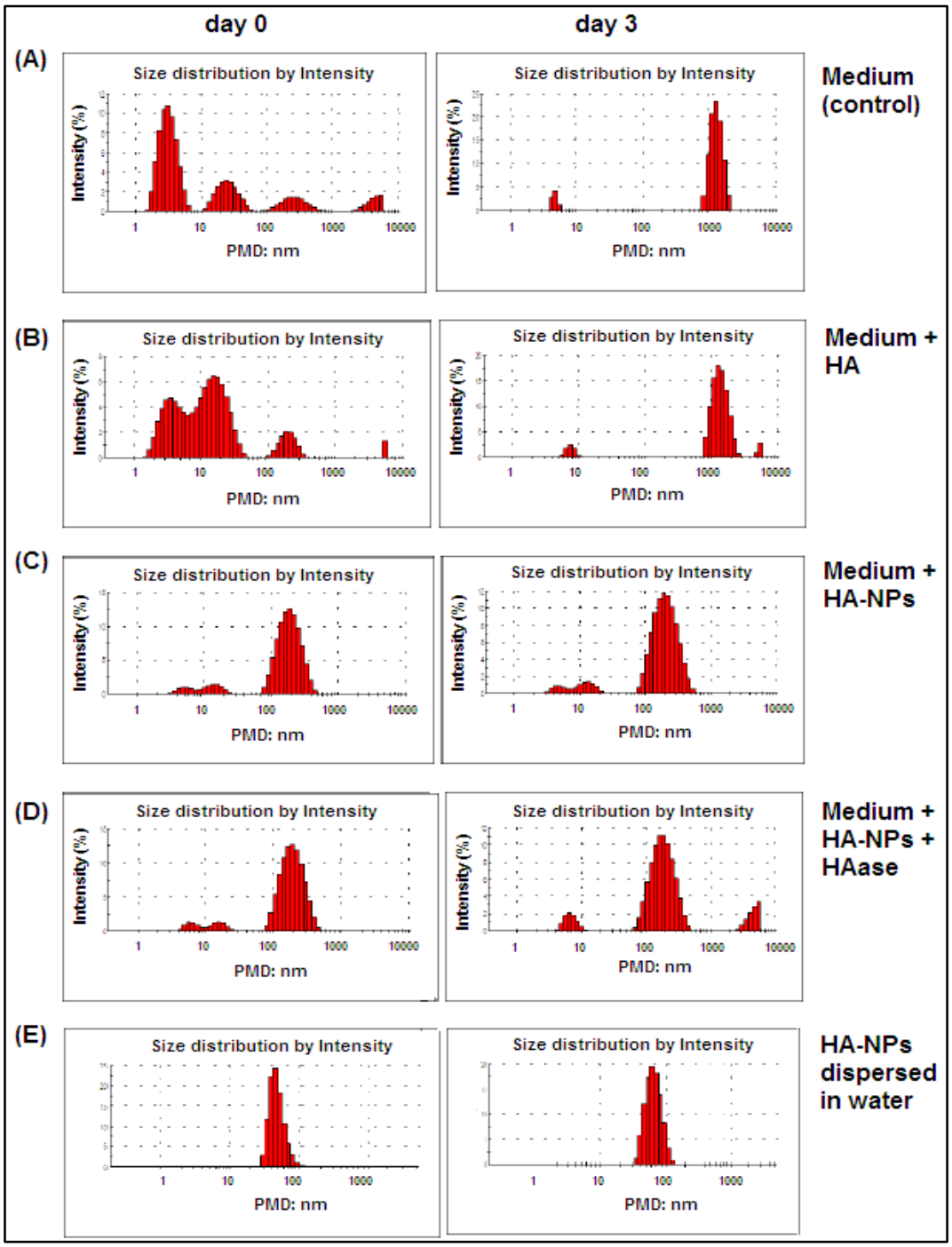

Figure 17. Self-aggregation of BSA and its Interaction with HA-NPs.

Modelling the Interaction of TFV with HA and HA-NPs and its Effect over Drug Loading and Drug Release Profile of NPs

The lowest energy conformation of TFV within core assembly of native HA and HA-NPs after the docking calculations was shown by Figure 18A and 18D, respectively. In this

case, the lowest energy conformation also belongs to the most populated cluster and was selected for the analysis. Amide cross-linking of HA placed its units at a distance that facilitated the formation of H-bonds of each unit to an appropriately positioned heteroatom's (N and O) of TFV at an appropriate distance by forming three H-bonds with hydroxyl groups of HA. This facilitated the encapsulation of drug inside NPs. This phenomenon was further analysed by interaction energy (IE) calculation.

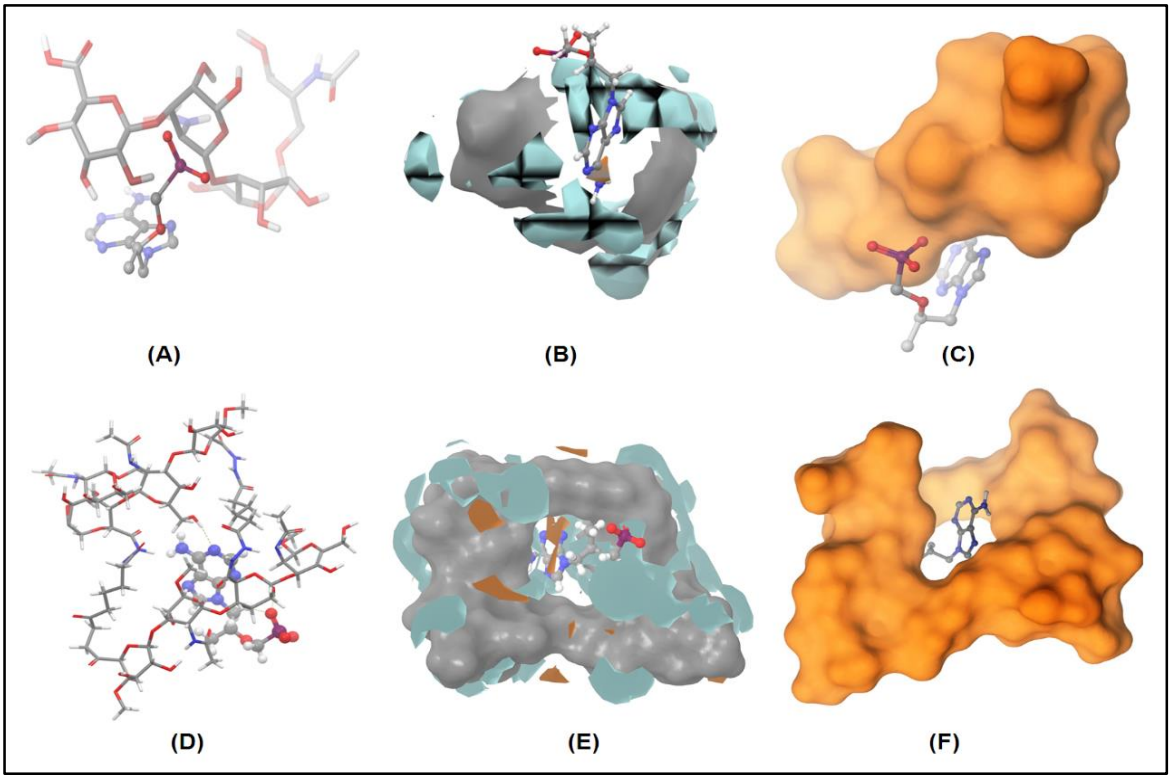

Figure 18. Structural Representation of Computational Modelling Interaction of TFV with: (A) Native HA. (D) HA-NPs. Surface representation with hydrophilicity/hydrophobicity projected onto a molecular surface of TFV with: (B) Native HA. (E) HA-NPs. Surface representation with hydrophilicity/hydrophobicity projected onto a molecular surface of TFV for better visualization with: (C) Native HA. (F) HA-NPs, showing cavity formation which is beneficial for drug entrapment. The colour code was based on the atom type: in Grey were the carbons, in Blue were the nitrogen's, in Red were the oxygen's, and in purple was the phosphorus atom. Hydrophilic surface (turquoise) and hydrophobic surface (blue).

The VW interaction appeared to be a predominant determinant of the IE between drug and HA-NPs affecting the encapsulation and release properties of NPs (Table 18). The increased VW interactions energy between TFV and the HA-NPs components compared to that of TFV and native HA resulted in the higher drug encapsulation by the NPs. This was expected because the cross-linking of HA introduces more nonpolar carbon atoms, which interacted with the polar parts of TFV, and increased the polar VW (induced dipole-dipole) interactions. There was also a polar-polar interaction between the polar parts of the HA-NPs and TFV (N and O atoms), contributed to the total VW interactions. The lipophilic component of the VW interactions was very small (not many nonpolar VW interactions e.g. carbon-carbon interactions resulted from temporarily polarization). The surface representation of the interaction between TFV with native HA (Figure 18B and 18C) and with HA-NPs (Figure 18E and 18F), respectively, clearly showed the cavity formation in the NPs structure which was beneficial for the encapsulation of TFV inside NPs. The surfaces were found to be highly hydrophilic (hydrophilic: 448.57A^0; hydrophobic: 6.93A^0). The purine moiety of the TFV was partially buried with its phosphonic acid group and extended out of the cavity to interact with hydrophilic solvents through the formation of H-bonds.

Table 18: Molecular Docking Simulation for Interaction Energy (IE) Calculations.

Types of interactions	**IE (kcal/mol) (between TFV and native HA)**	**IE (kcal/mol) (between TFV and NPs)**
Hydrogen bond (H-bond)	-1.63	-1.52
Van der Waal (VW)	-6.03	-16.3
Lipophilic	-0.56	-0.94
Electrostatic	-10.9	-9.72
Glide Score*	-4.71	-5.28

*Glide Score is the predicted binding energy, calculated by using Eq. (11) in the text.

The theoretical observation from CM was correlated with the experimentally determined *in vitro* drug release profile of HA-NPs. As most of the drug was solvent exposed, which resulted in relatively faster release rate of TFV when a hydrophilic solvent (ex. water) replaced the H-bonds between drug and HA-NPs, which was also seen in this study as NPs showed a burst release in first couple of hours (Figure 14). However, due to the higher VW interaction of TFV with NPs (Table 18), a slow release was observed later. Overall, the modelling prediction was informative and explanatory in terms of getting theoretical information's about drug encapsulation and release from HA-NPs in the rational design of delivery systems in the future work.

Stability Evaluation of Tenofovir

Solid State PXRD Analyses

PXRD analyses confirmed that the drug was stable and maintained its original crystalline pattern under the variable stress conditions of temperature and % RH. The characteristic peaks of native TFV were observed at the diffraction angle of 2θ = 7.44°, 14.89°, 18.11°, 18.59°, 22.41°, 23.45°, 24.75°, 28.90°, and 29.80° (Figure 19). The PXRD pattern of the unstressed sample of TFV were similar to that observed in a previous study (43).

Degradation Kinetics of TFV under Hydrolytic Conditions

The degradation mechanism of TFV under hydrolytic, oxidation, thermal and accelerated stress conditions was analyzed using a validated LC-MS assay. The drug showed degradation in acidic (0.1 M HCl) and alkaline (0.1 M NaOH) hydrolytic conditions, and followed first order degradation kinetics behavior (Figure 20A). The drug was found stable at pH 4.5 (< 10% degradation) (vaginal pH environment) under refluxing conditions for 5 days. No significant degradation (< 5%) and degradation products were observed at pH 4.5 whether the temperature was 25°C or 40°C as analyzed for up to 10 days. TFV was also found stable under oxidative

stress conditions in 3% and 30% v/v H_2O_2 solutions as incubated up to 7 days at room temperature. On exposure to acidic (0.1 and 0.01 M HCl) and alkaline (0.1 and 0.01 M NaOH) conditions at 25°C and 40°C, the drug was found stable (< 5% degradation). The drug was also found stable in thermal, and accelerated stress conditions (data not shown).

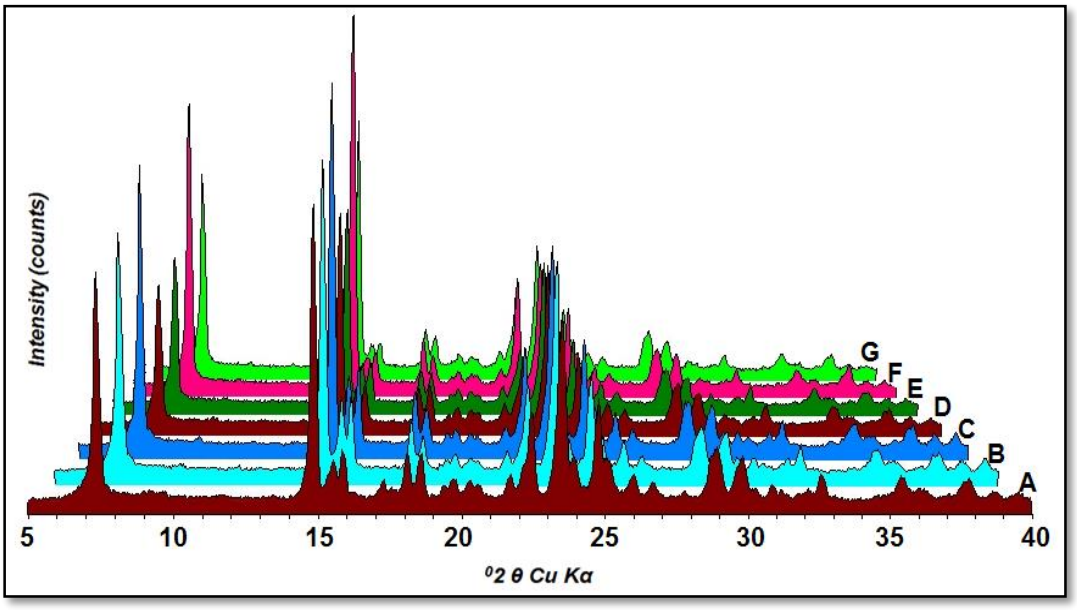

Figure 19. Solid State PXRD Pattern of TFV (unstressed) and TFV Stressed Samples. From bottom to top, (A) TFV-unstressed sample, (B) TFV at -20°C, (C) TFV at 5°C (D) TFV at 25°C/60% RH, (E) TFV at 40°C/75% RH, (F) TFV at 50°C and, (G) TFV at 80°C. Each sample was analyzed after 12 months of stressed conditions applied except the sample at 80°C which was analyzed after one month of exposure.

Arrhenius Equation Plot

The degradation kinetic plot of TFV between *ln* (% drug remaining) and time (*t*) in months at 40, 50, and 60°C was shown by Figure 20B. The *k* values determined from the slope of the regression equation were observed as 0.60 (± 0.04), 0.70 (± 0.06), and 0.84 (± 0.06) × 10^{-2} $months^{-1}$ at 40, 50, and 60°C, respectively, after triplicate analysis (n = 3). A linear relationship between *ln* (*k*) in $months^{-1}$ and 1000/*T* (in Kelvin) at 40°C (313.15 Kelvin), 50°C

(323.15 Kelvin), and 60°C (333.15 Kelvin) was observed in the Arrhenius plot (Figure 20B). The slope and r^2 values were found to be -1.75 ± 0.29 and 0.974 ± 0.032, respectively, (n = 3). The k_{25} value was 0.45 × 10^{-2} (± 0.03) $months^{-1}$ (n = 3).

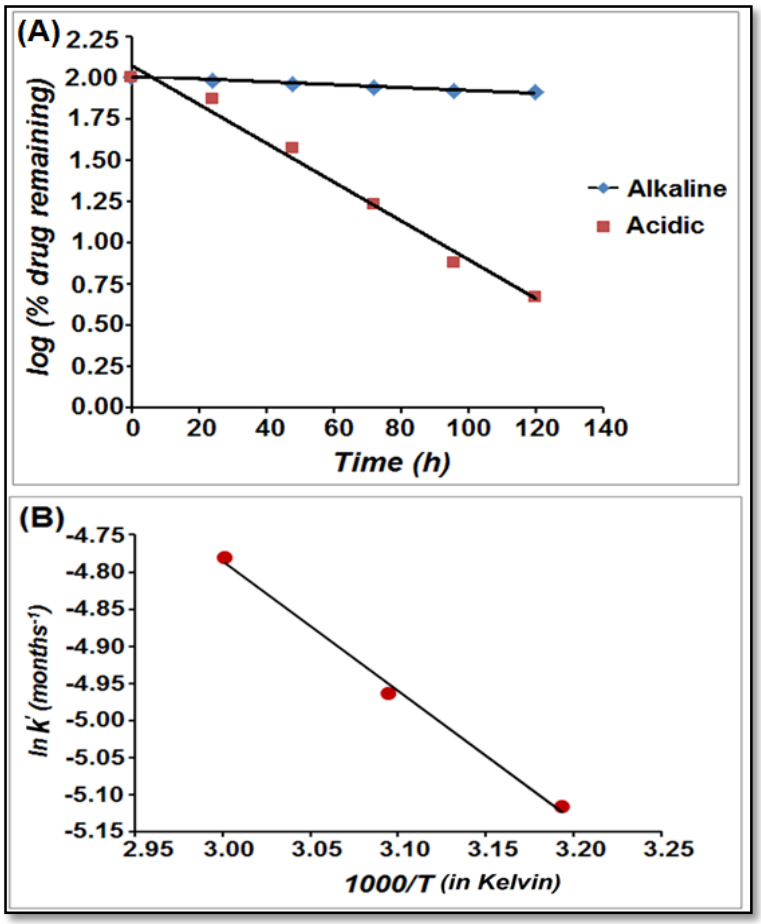

Figure 20. (A) First order Degradation Kinetic Plots of TFV between *log* (% drug remaining) and Time in Hours under Acidic (0.1 M HCl;■) and Alkaline (0.1 M NaOH;◆) Hydrolytic Conditions. (B) Arrhenius Plot of TFV between *ln* (*k*) in $Month^{-1}$ and $1000/T^{-1}$ (in $Kelvin^{-1}$) at 40°C, 50°C, and 60°C.

The E_a value derived from the slope of Arrhenius plot (Figure 20B) was calculated as 14.54 ± 2.45 kJ/mol (n = 3). The lower E_a value obtained here reflected that the stability of TFV under an accelerated condition was temperature independent. The shelf-life (t_{90}) of TFV calculated using the obtained k_{25} value and Eq. (15) was found to be 23.40 ± 1.56 months (1.95

± 0.13 years), (n = 3). This was close to the shelf-life of TFV (24 months: two years) found in the literature under the recommended storage conditions (184). Overall, stability analyses revealed that formulation strategies should be implemented to protect the TFV from strong acidic and alkaline conditions. However, stability of TFV at pH 4.5 (normal vaginal pH), oxidative, accelerated, and thermal stress conditions makes TFV a suitable topical microbicide candidate for long-term storage and controlled vaginal delivery applications.

Cytotoxicity Evaluations of HA-NPs

Nanoparticles Characterization in Cell Culture (Keratinocyte) Medium

The size distribution of HA-NPs (optimized formulation F13) was characterized in the supplemented keratinocyte medium after 24 h incubation at 37°C before the *in vitro* cytotoxicity evaluations. The ζ potential of blank medium after 24 h of incubation at 37°C was ~ -12 mV, the PMD was 929.23 ± 549.86 nm with a high PDI values (0.734 ± 0.247), (n = 3) indicated a broad size distribution (Figure 21B**)**. The TEM image of blank (no NPs) keratinocyte medium was shown in Figure 21B. The higher PDI values of size distribution of keratinocyte medium could be due to the presence of various proteins, nutrients and electrolytes (185, 186). These proteins tend to form electrostatic interaction and agglomeration with other components in the culture medium during the incubation process. This led to an increased PMD of HA-NPs in keratinocyte medium (PMD: 238.87 ± 4.21 nm; PDI: 0.322 ± 0.002; -12.33 ± 0.68 mV, n = 3) (Figure 21C**)** compared to the PMD of HA-NPs dispersion in water (PMD: 100.20 ± 20.00 nm; PDI: 0.07 ± 0.01; ζ potential: -42.30 ± 1.70 mV, n = 3) (Figure 21A**)**. An increase in the ζ potential of HA-NPs in keratinocyte medium was due to the presence of various positively charges proteins adsorbed on NPs surface. The TEM image showed that the proteins in the culture medium were adsorbed onto the HA-NPs surface to form a protein-NPs

corona (Figure 21D**)**. The presence of the corona corroborated well with the decrease in ζ potential of HA-NPs in the culture medium.

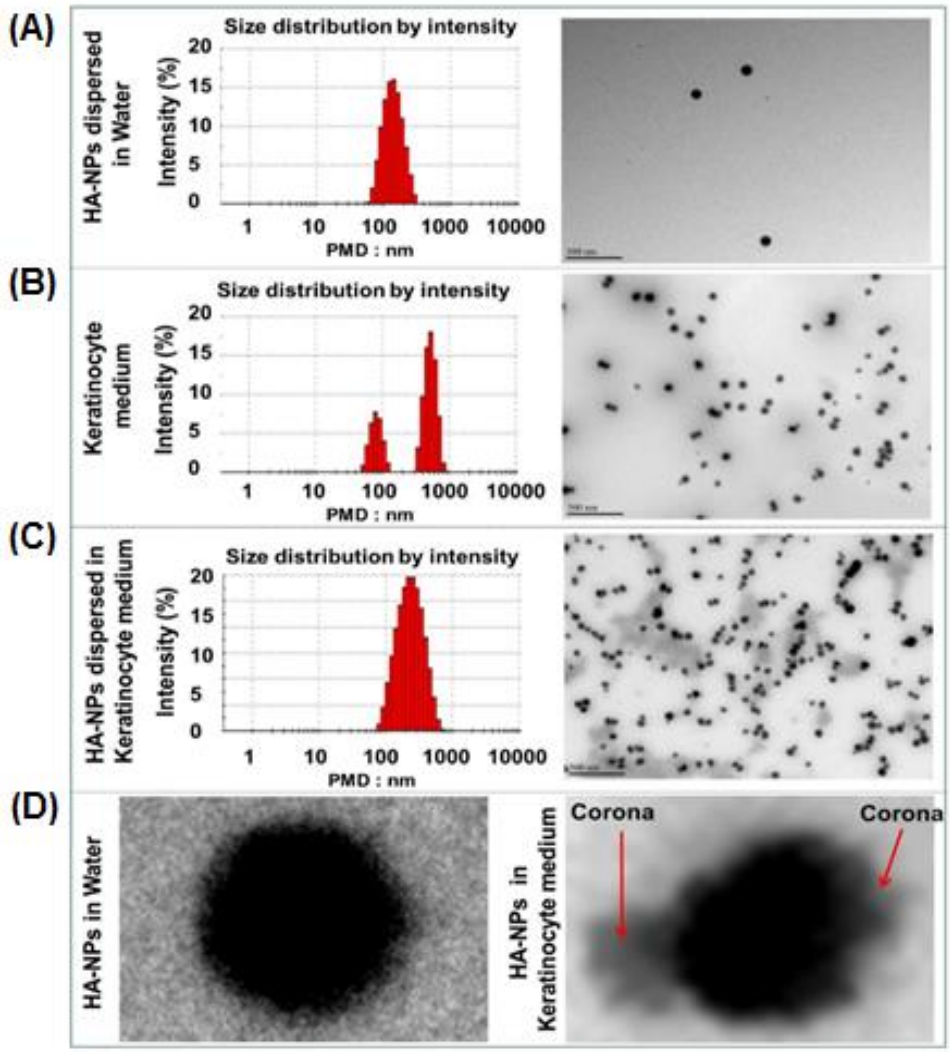

Figure 21. Size Distribution Analysis of HA-NPs in Keratinocyte Medium and Water by DLS and TEM Measurements.

The discrepancy between DLS and TEM results regarding the size of HA-NPs in cell culture medium could be explained as following (187, 188) (189). The DLS analysis provided the hydrodynamic diameter of the NPs. When NPs were dispersed in a liquid medium, a thin hydration layer of the solvent attached to their surface, which influenced their Brownian motion in the medium. Thus, the hydrodynamic diameter provided the information about the NPs core

size in addition to the coating layer and the solvent layer interacted with the NPs. Whereas, TEM analysis estimated the projected area diameter of the NPs. In this case, only the information about the core size of the NPs was provided. This led to a greater hydrodynamic diameter of the NPs in DLS compared to the size estimated by TEM. Although, the TEM measurements gave accurate core size of the NPs, the size assessment of the coating layer can sometimes be underestimated or missed in the event of a poor contrast of TEM. Contrary to TEM measurements, the hydrodynamic diameter of the NPs provided a better understanding of the NPs migration in the liquid media.

Cell Viability Assay of HA-NPs

Resazurin and MTS assays demonstrated that HA-NPs did not have any significant effects ($p > 0.05$) on the viability of VK2/E6E7 and End1/E6E7 cells, compared to the cell culture medium (negative control) (Figure 22).

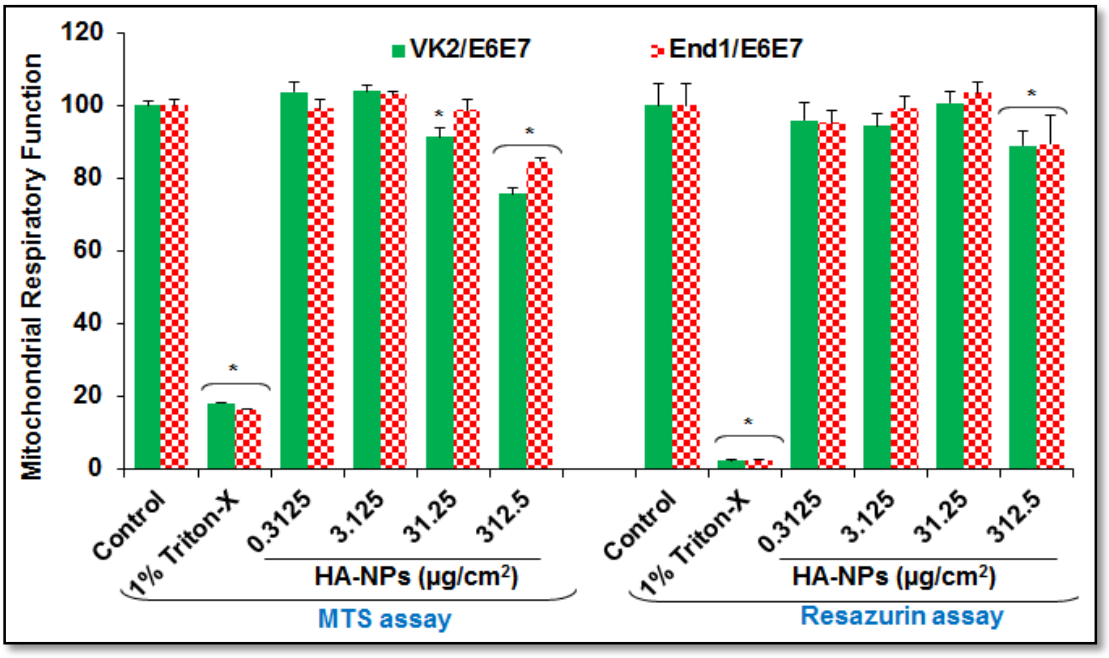

Figure 22. Effects of HA-NPs on Cell Viability in VK2/E6E7 and End1/E6E7 Cells. The results are represented as mean ± SD of three independent experiments carried out in five replicates. Statistically significant differences relative to control were indicated at $p < 0.05$.

Assessment of Cell Membrane Integrity

The HA-NPs were investigated for their effect on plasma membrane integrity. As suggested in Figure 23, HA-NPs did not significantly compromise the cell membrane integrity in vaginal epithelial cells. However, on exposure to the positive control (1% Triton-X-100), the epithelial cells showed a significant loss of cell membrane integrity to < 10% ($p<0.01$) compared to the negative control (medium).

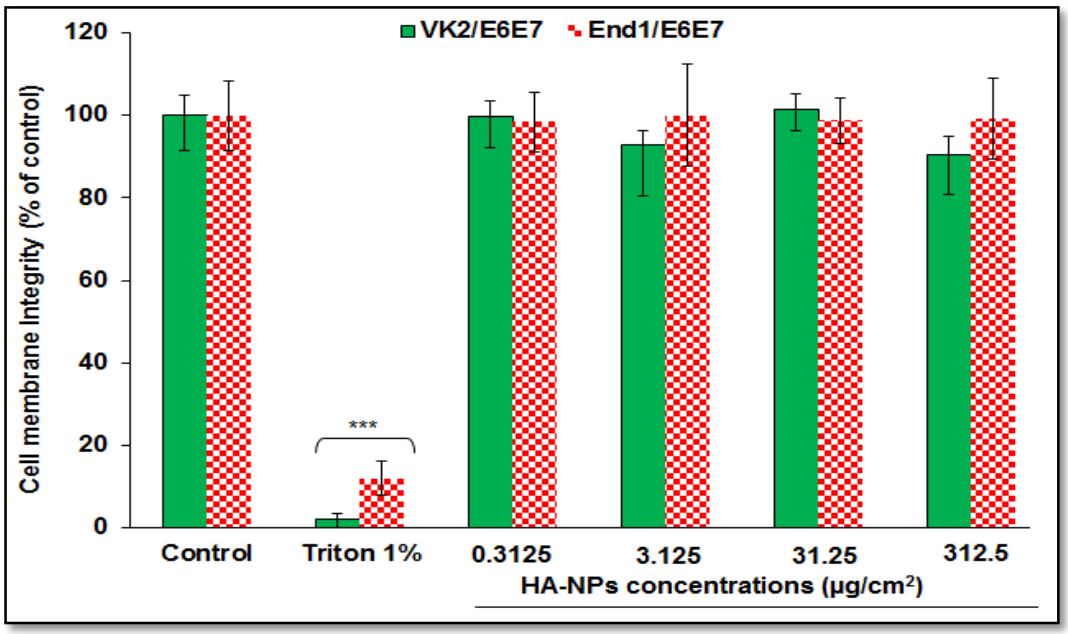

Figure 23. Effects of HA-NPs on Cell Membrane Integrity in VK2/E6E7 and End1/E6E7 Cells. The results are represented as mean ± SD of three independent experiments carried out in five replicates. Statistically significant differences relative to control were indicated at $p < 0.05$.

Assessment of Apoptosis through Chromatin Condensation

Apoptotic cells can be erroneously classified as viable cells since the plasma membrane integrity of cells undergoing apoptosis is preserved (190). Cells were examined for evidence of chromatin condensation, one of the characteristic features of apoptosis. The ratio of fluorescence intensity from HO/NR ratio was determined as previously described (148). As shown in Figure 24, no significant variation of HO/NR ratio was noted in the presence of HA-

NP compared to untreated cells, indicated the absence of apoptosis in both the cell lines. For comparison, camptothecin (100 µM), a well-known inducer of apoptosis (191), markedly increased the HO/NR ratio to 1.8-3.4 ($p<0.01$), reflected the presence of apoptosis.

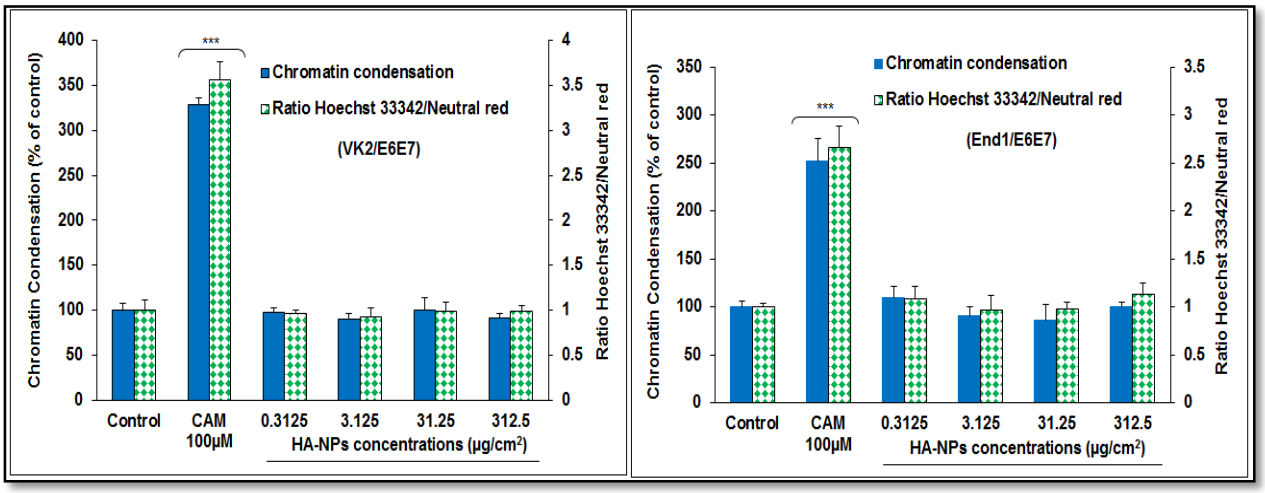

Figure 24. Effects of HA-NPs on Chromatin Condensation in VK2/E6E7 and End1/E6E7 Cells. The results are represented as mean ± SD of three independent experiments carried out in five replicates. Statistically significant differences relative to control were indicated at $p < 0.05$.

Assessment of Mitochondrial Function

Assessment of Mitochondrial Respiratory Function

Resazurin assay was used to evaluate the activity of mitochondrial respiratory enzymes. The genital epithelial cells showed a high tolerance to HA-NPs exposure at the time point examined however, MRF was significantly decreased ($p<0.01$) in both cell lines in the presence of positive control ($p<0.01$) (Figure 25).

Assessment of Mitochondrial Membrane Potential (ΔΨm)

Results (Figure 26) showed that the ΔΨm was maintained by proton and pH gradients across mitochondrial inner membrane after the NPs treatment. Contrary to End1/E6E7 cells, HA-NPs significantly decreased the ΔΨm in VK2/E6E7 cells ($p<0.05$) at higher concentration

(1000 µg/mL). However, the lower concentrations (1-100 µg/mL) of NPs did not show any significant ($p>0.05$) effect. The positive control (100 mM H_2O_2) significantly decreased the $\Delta\Psi m$ ($p<0.01$) compared to the negative control.

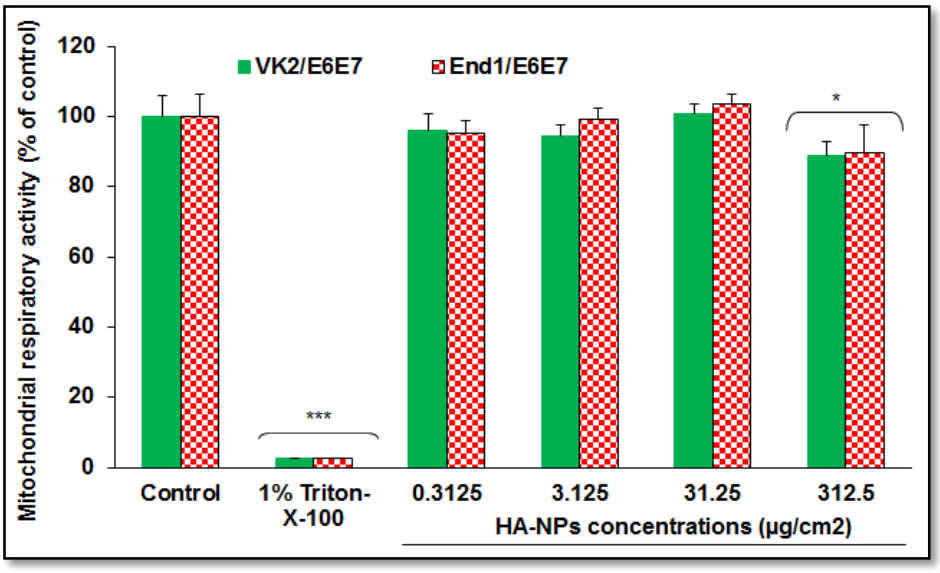

Figure 25. Effects of HA-NPs on Mitochondrial Respiratory Function in VK2/E6E7 and End1/E6E7 Cells. The results are represented as mean ± SD of three independent experiments carried out in five replicates. Statistically significant differences relative to control were indicated at $p < 0.05$.

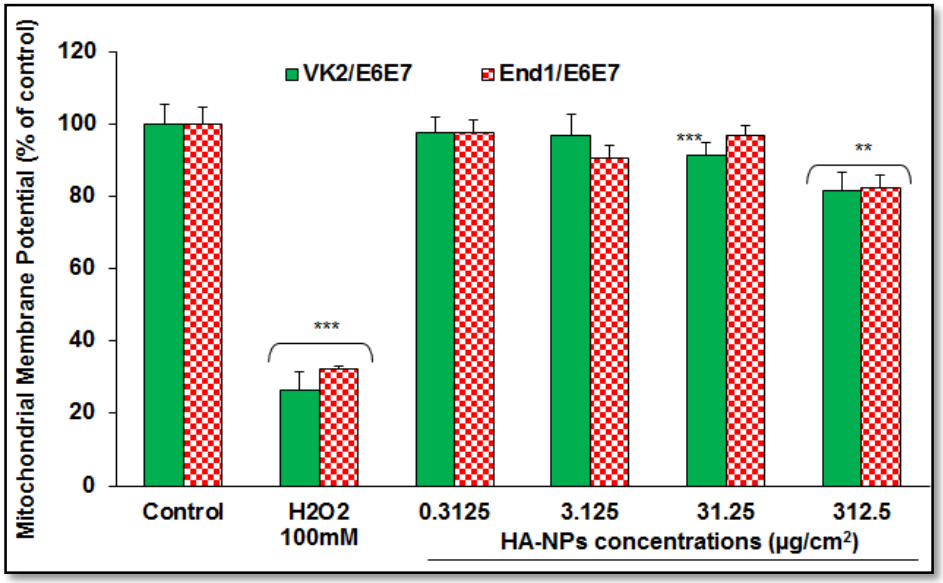

Figure 26. Effects of HA-NPs on Mitochondrial Membrane Potential (*ΔΨm)* in VK2/E6E7 and End1/E6E7 Cells. The results are represented as mean ± SD of three independent experiments carried out in five replicates. Statistically significant differences relative to control were indicated at $p < 0.05$.

Assessment of Mitochondria Mass

Results indicated that up to 100 µg/mL of HA-NPs, there was no significant ($p>0.05$) variation in NAO fluorescence intensity in both the genital epithelial cell lines (Figure 27). However, exposure of cells to the positive control (100 mM H_2O_2) caused a significant decrease of NAO fluorescence intensity ($P<0.01$).

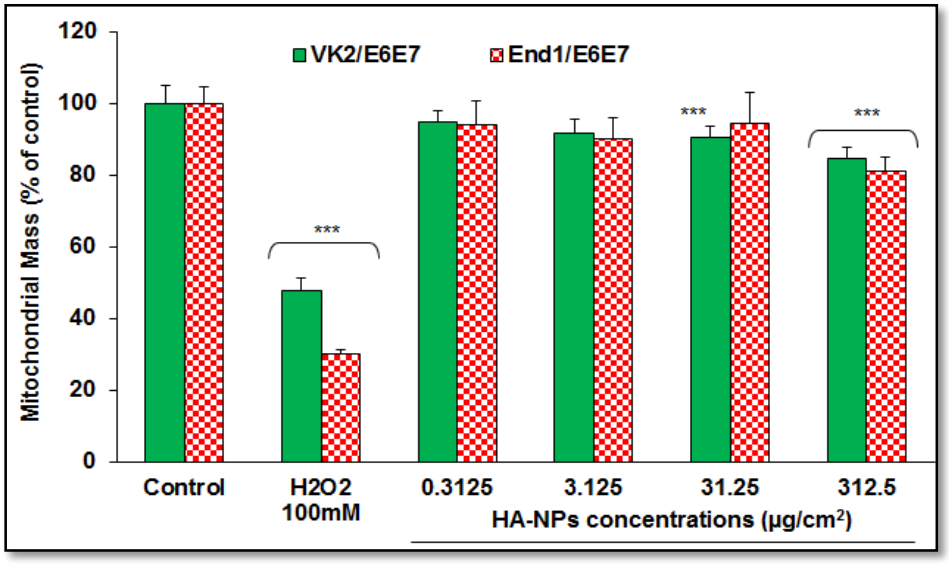

Figure 27. Effects of HA-NPs on Mitochondrial Mass in VK2/E6E7 and End1/E6E7 Cells. The results are represented as mean ± SD of three independent experiments carried out in five replicates. Statistically significant differences relative to control were indicated at $p < 0.05$.

Intracellular ROS Production

HA-NPs did not increase the ROS level at all concentrations tested compared with the positive control (100 mM H_2O_2) (Figure 28). Instead, a significant decrease in the endogenous ROS production ($p<0.05$) below the basal level was observed at the concentrations of 10-1000

µg/mL. Results suggested an important role for HA-NPs in ROS scavenging, which was consistent with the antioxidant properties of the HA (105).

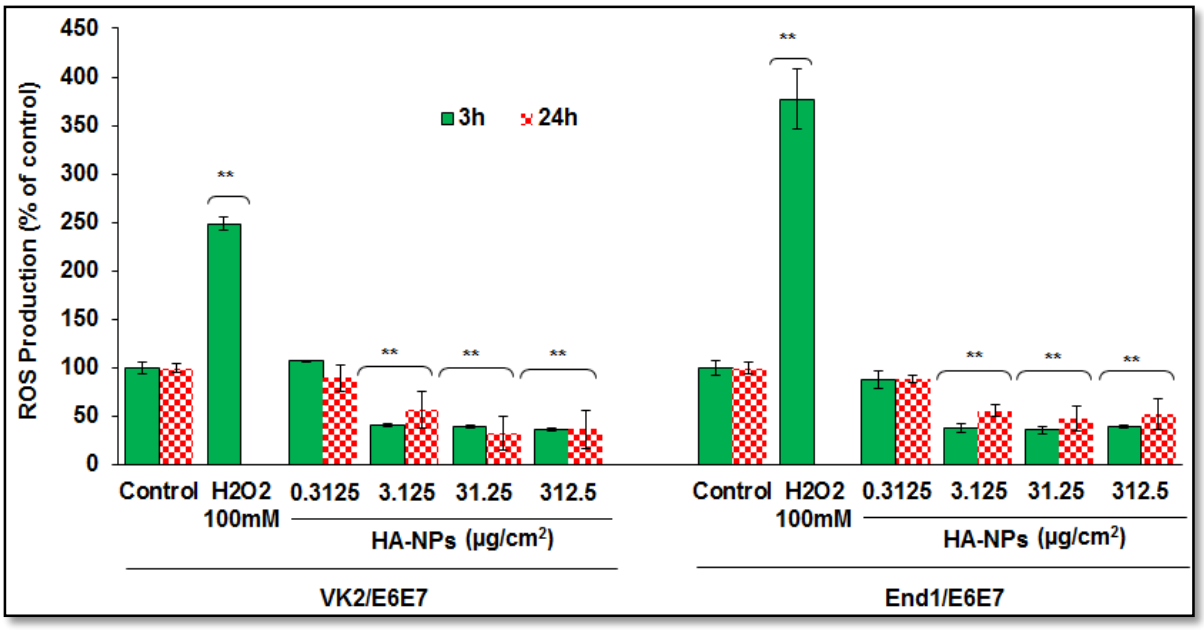

Figure 28. Generation of Reactive Oxygen (ROS) Species Induced by HA-NPs in VK2/E6E7 and End1/E6E7 Cells. The results are represented as mean ± SD of three independent experiments carried out in five replicates. Statistically significant differences relative to control were indicated at $p < 0.05$.

Intracellular NO Production

In the presence of positive control (SNP), a significant higher amount of nitrites (> 30 µM) was released in the culture medium (Figure 29). However, in the presence of HA-NPs, the NO profile was not altered and all determinations were similar to those of the endogenous NO (5-10 µM) regardless the concentrations of NPs tested. These data indicated that HA-NPs did not induce the iNOS-mediated inflammation.

Intracellular Antioxidant GSH Assay

The intracellular GSH has been examined to evaluate the cellular redox state that consists in equilibrium between the pro-oxidant and antioxidant systems. It was observed that

upon HA-NPs exposure, the intracellular GSH content was not significantly affected ($p>0.05$) (Figure 30). Whereas, positive control significantly reduced the intracellular GSH level in both the cell lines ($p<0.01$) compared to the negative control.

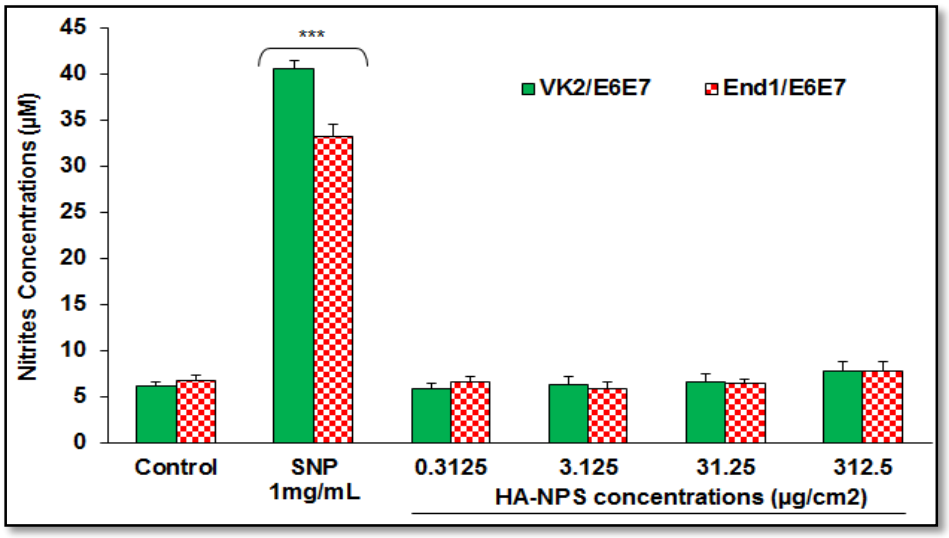

Figure 29. Generation of NO Induced by HA-NPs in VK2/E6E7 and End1/E6E7 Cells. The results are represented as mean ± SD of three independent experiments carried out in five replicates. Statistically significant differences relative to control were indicated at $p < 0.05$.

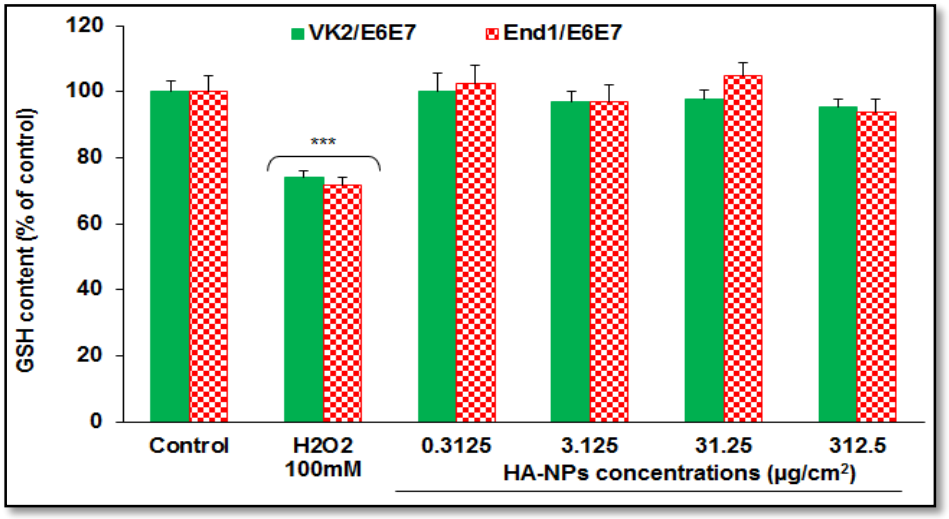

Figure 30. Effects of HA-NPs on Antioxidant Glutathione (GSH) Content in VK2/E6E7 and End1/E6E7 Cells. The results are represented as mean ± SD of three independent experiments carried out in five replicates. Statistically significant differences relative to control were indicated at $p < 0.05$.

Effects of HA-NPs on the Viability of *Lactobacillus Crispatus* Bacteria

A microbicide formulation should not disturb the normal *Lactobacillus* vaginal microflora since it is a key component of the innate immune environment which can reduce the risk of HIV transmission through vaginal mucosa. As shown in Figure 31, the HA-NPs had no statistically significant effect ($p > 0.05$) over the viability of *L. crispatus* bacteria compared to the cell culture medium.

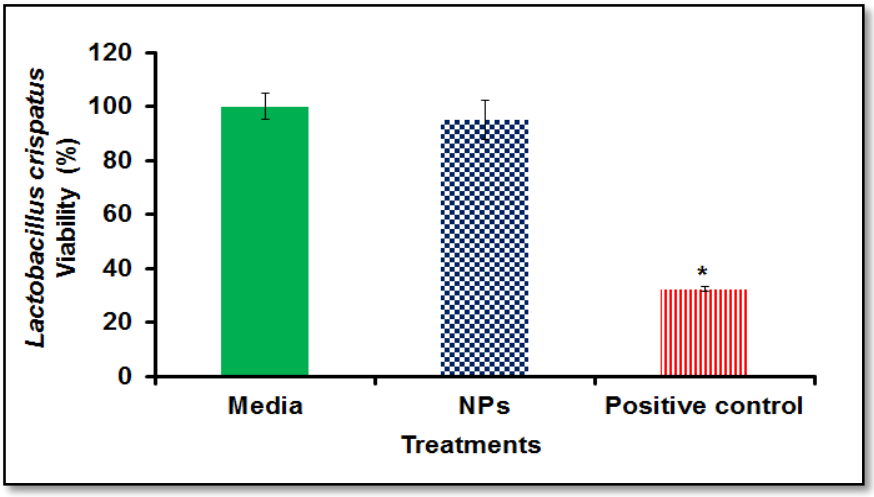

Figure 31. Effect of HA-NPs over the viability of *L. crispatus* Bacteria. Results are given after 48 h of incubation as mean ± SD, n = 3. Statistically significant differences relative to control were indicated at $p < 0.05$.

Intracellular Uptake Assay of HA-NPs

Fluorescence and confocal microscopy were employed to study the uptake and localization of HA-NPs in the VK2/E6E7 (Figure 32) and End1/E6E7 (Figure 33) epithelial cells at the concentration of 1-1000 µg/mL. Results showed that the uptake of NPs was concentration dependent as almost a negligible cellular uptake was observed below the concentration of 100 µg/mL. The data proved the internalization and distribution of HA-NPs across the treated cells which were localized mostly in the cytoplasm and around the nucleus. The uptake in VK2/E6E7 (Figure 32) and End1/E6E7 (Figure 33) cell lines appeared to be

comparable, which could be indicative of a similar cellular uptake mechanism. At the NPs concentration of 1000 µg/mL, a higher uptake was observed which was due to the presence of clusters or agglomerates of NPs at the cell membrane. At lower concentrations, the uptake was almost negligible, suggesting that the uptake might be governed by an endocytic mechanism rather than a direct translocation or penetration. A very few bright spots were visible inside the cells even at the NPs concentration of 100 µg/mL. Thus, for a very small size NPs, a critical threshold density on the cell membrane has to be exceeded to trigger the internalization process.

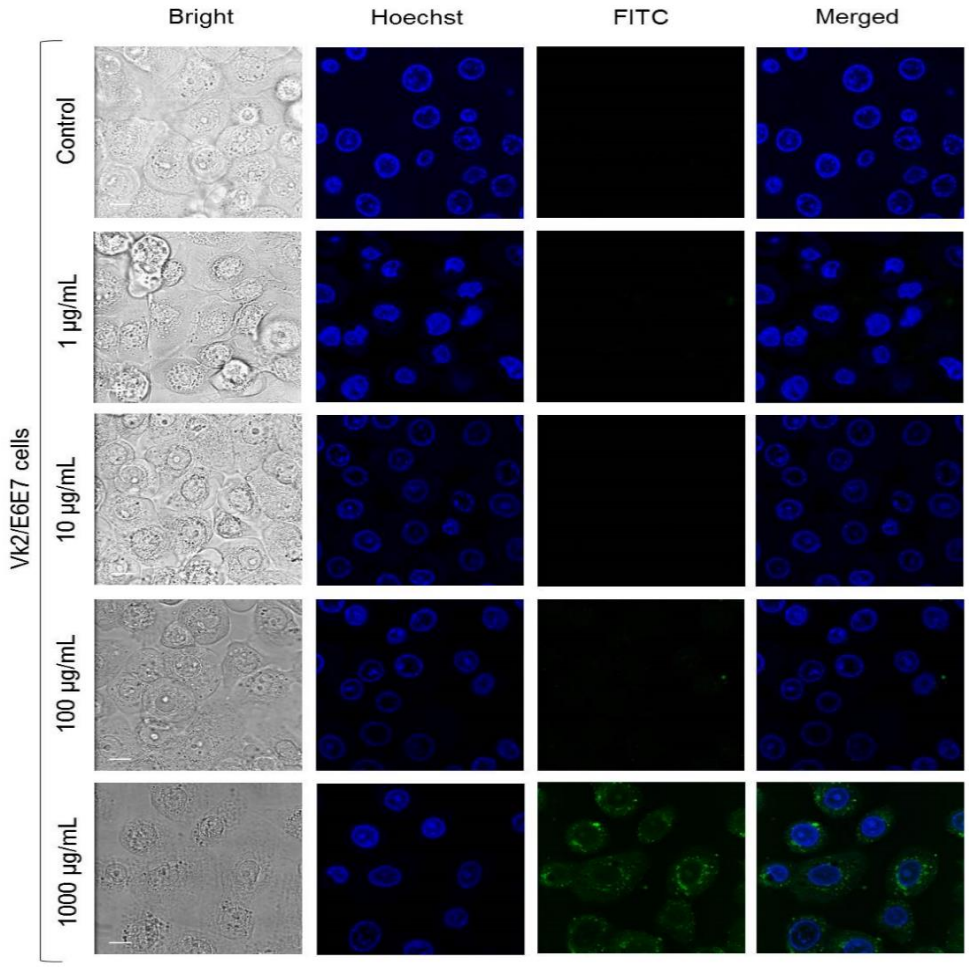

Figure 32. Cellular Uptake in VK2/E6E7 Cells Exposed for 24 h to FITC-labelled HA-NPs (1 - 1000 µg/mL). FITC and Hoechst 33342 (for nuclei) appeared as green and blue fluorescence, respectively. The merged image represented overlay of green and blue fluorescence channels. Scale bar: 10 µm.

Further studies were needed to fully clarify the time and concentration-dependent uptake mechanisms of HA-NPs. It is noteworthy that the HA-NPs surface chemistry was changed when suspended in culture medium, as shown by the TEM analysis which revealed the presence of a protein layer on the HA-NPs surface (Figure 21). At this time, it was unclear how this corona might have modulated the actual biological response of the epithelial cells to HA-NPs exposure, since NPs were expected to interact with cell membrane (101). However, it was suspected that, the protein corona around NPs may act as a protective layer, shielding the NP surface from direct interactions with receptors on the cell membrane that remain to be elucidated further.

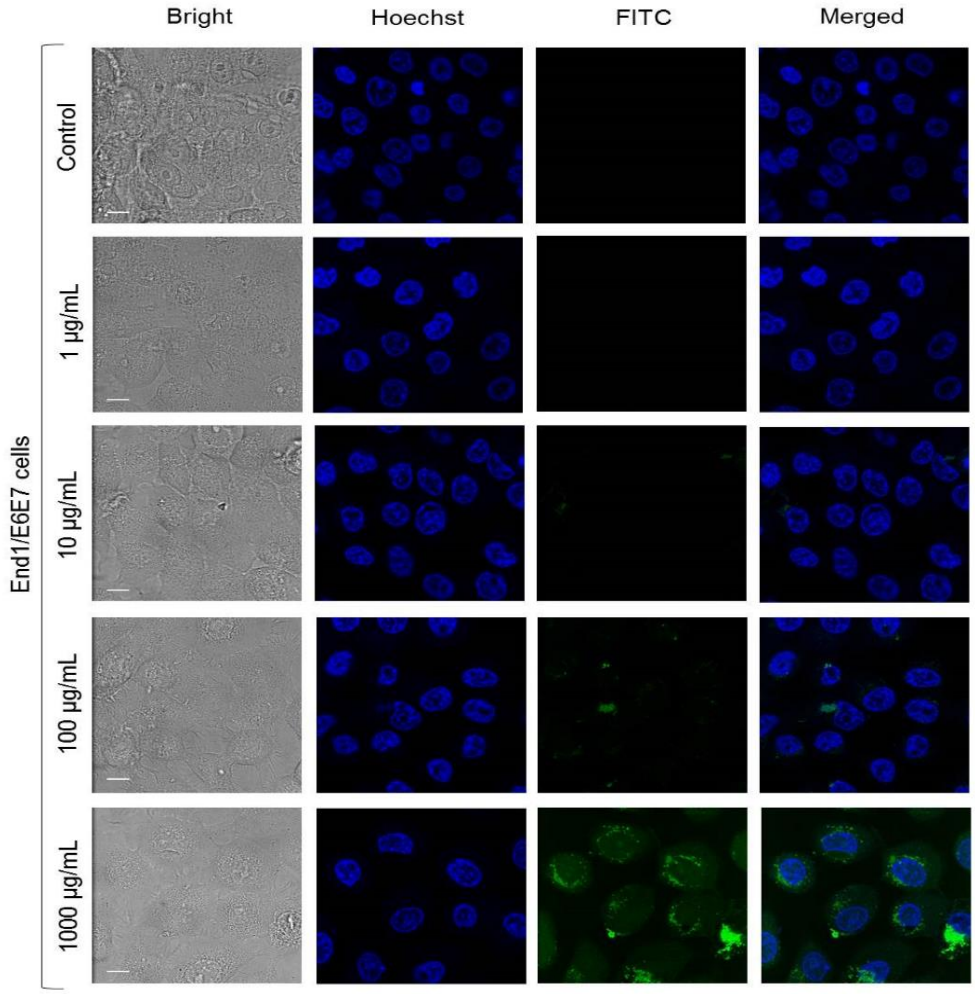

Figure 33. Cellular Uptake in End1/E6E7 Cells Exposed for 24 h to FITC-labelled HA-NPs (1 - 1000 µg/mL). FITC and Hoechst 33342 (for nuclei) appeared as green and blue fluorescence,

respectively. The merged image represented overlay of green and blue fluorescence channels. Scale bar: 10 μm.

3.4. Conclusion

The HAase sensitive HA-NPs loaded with TFV were formulated using surfactant free cross-linking method. The modified surfactant-free method used in this study required less time (< 24 h) compared to native surfactant-free method (> 44 h) to produce the NPs. The shorter time was achieved by effective screening of the factors responsible for NPs formation using experimental design applications. The NPs were found stable, small PMD (~75 nm) and exhibited a spherical shape as confirmed by TEM analysis. It was observed that HAase enzyme significantly triggered the degradation and drug release of the HA-NPs. The cytotoxicity data demonstrated that the HA-NPs were well tolerated by both cervical (End1/E6E7) and vaginal (VK2/E6E7) epithelial cells and had no effect on *Lactobacillus* bacteria viability. Collectively, these results suggested that TFV loaded HAase sensitive HA-NP templates developed in this study have the potential of topical vaginal delivery of microbicides for the prevention of HIV transmission after successful completion of safety and efficacy studies.

Although, several positive results have been observed, there were certain limitations in the current NPs design. One of the major concern was that the HAase triggered drug release from the NPs took about 24 h to reach ~90% w/w. The limitations, their possible reasons and prospective solutions were summarized below in Scheme 1. These limitations led to the development of stimuli-sensitive tenofovir loaded mucoadhesive nanofibers as explained in the following Chapter 4.

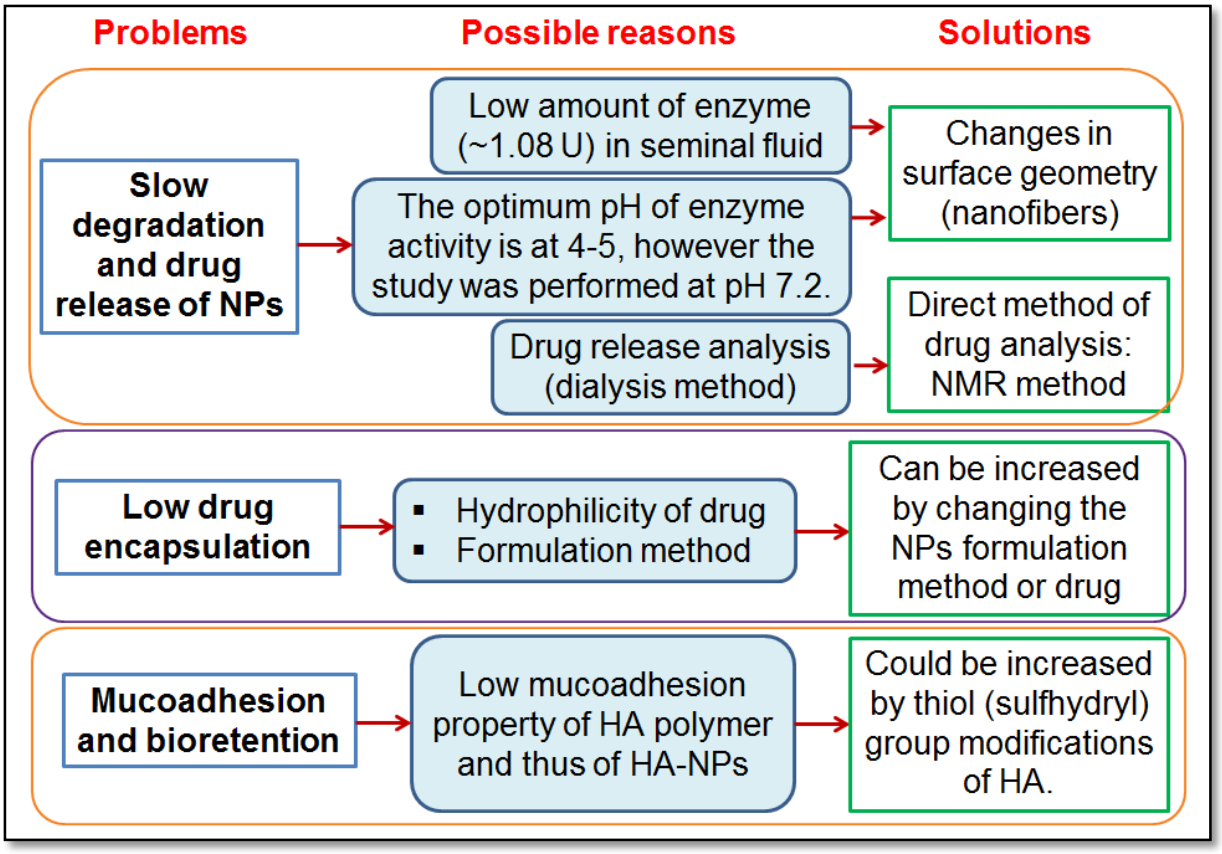

Scheme 1. Limitations of the HA-NPs Systems and Possible Solutions.

Acknowledgments

The project was supported by Award Number R01AI087304 from the National Institute of Allergy and Infectious Diseases (Bethesda, MD).

CHAPTER 4

FABRICATION OF HYALURONIDASE SENSITIVE TENOFOVIR LOADED HYALURONIC ACID BASED MUCOADHESIVE NANOFIBERS

4.1. Rationale

The success of vaginal delivery systems depends on the locally prolonged residence time of drug-containing formulations (192). Mucoadhesive polymers are widely used in vaginal delivery due to their prolonged contact with the adsorption site (193). These polymers interact with mucus by Vander Waals, hydrophobic, electrostatic, and hydrogen bond interactions. Consequently, through the mucoadhesion process the therapeutic efficacy of drug can be efficiently improved (193). As explained in Chapter 3, hyaluronic acid (HA) has been widely used in drug delivery applications (81, 101, 102). The hyaluronic acid based nanoparticle (HA-NPs) delivery system has been successfully developed and explained in chapter 3. Although, HA is characterized by its weak mucoadhesive properties due to the presence of carboxylate (-COOH) groups on its glucuronic acid units which promotes the weak hydrogen bonding with mucin (194). In contrast, functionalized polymers bearing sulfhydryl (-SH) groups on their backbone are capable of forming strong interactions with cysteine subunits of mucin (195).

Nowadays, electrospun nanofibers (NFs) are extensively studied in drug delivery applications (112, 196). The NFs formulations may offer various potential advantages in vaginal delivery such as flexibility to be formulated in various shapes, higer bio-retention, and no leakage or messiness (110, 111, 197). The added advantages of electrospun fibers include high surface-to-volume ratio and high porosity. These benefits make the NFs a particularly attractive candidate for vaginal formulations of therapeutic molecules. Furthermore, the

encapsulation of labile molecules in polymeric delivery systems such as NFs can enhance their stability against a harsh acidic vaginal environment and presence of enzymes such as proteases, hydrolases, and phosphatases.

Considering these facts, in this study, a stimuli-sensitive and mucoadhesive delivery system that is capable of degradation on exposure to seminal HAase enzyme to provide a triggered release of microbicide (TFV) was designed, as illustrated in Reaction scheme 3. To test this hypothesis, sulfhydryl (-SH) group modified thiolated HA (HA-SH) derivatives were synthesized. Thiolated HA-SH derivatives were then used to fabricate the NFs (having different geometry compared to the HA-NPs) and physicochemically characterized as described below.

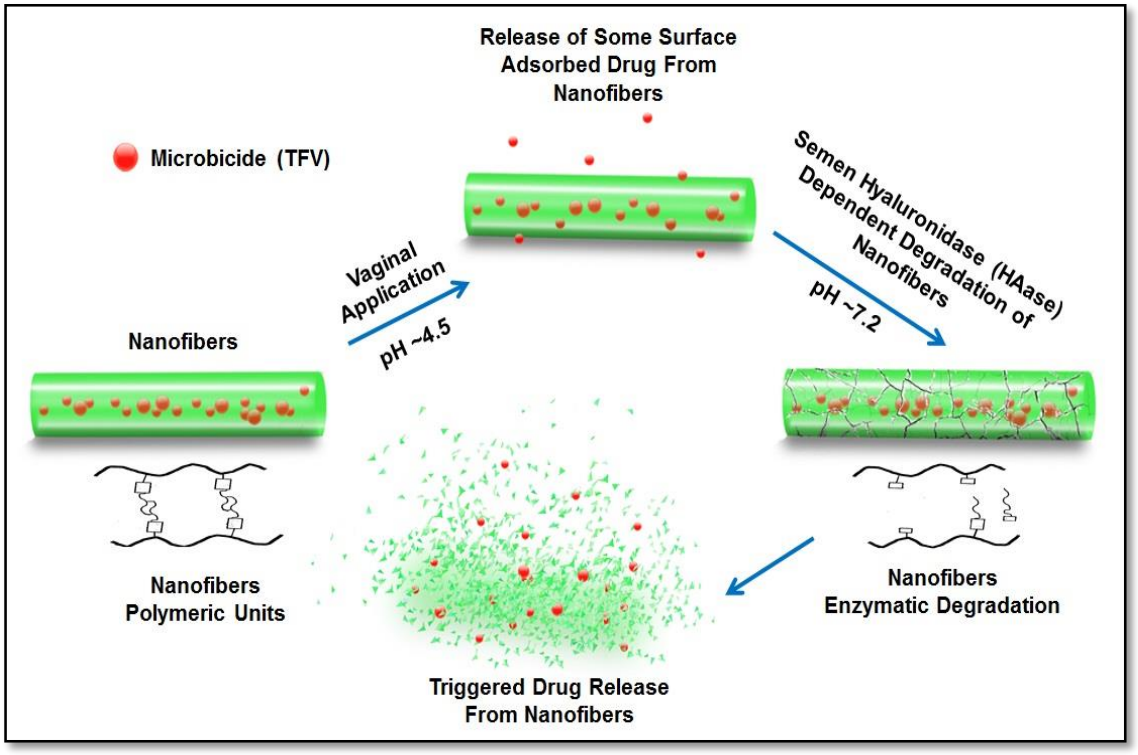

Reaction Scheme 3. Mechanism of Microbicide Loaded Stimuli-sensitive Nanofibers.

4.2. MATERIALS AND METHODS

Chemicals

Tenofovir was purchased from Beijing Zhongshuo Pharmaceutical Technology Development Co. Ltd. (Beijing, China). Hyaluronic acid sodium salt was kindly provided by Mr. Jack Liu (Zhenjiang DongYuan Biotech Co., Ltd., Jiangsu, China). Hyaluronidase (HAase) from bovine testes with a specified activity of 810 U/mg, purified type II mucin from porcine stomach, 5, 5'-Dithio-bis-(2-nitrobenzoic acid) (DTNB), poly (ethylene oxide) (PEO: MW of 400 kDa), cysteine hydrochloride, ethylene sulfide (ES), Dithiothreitol (DTT), and deuterium oxide (D_2O) were from Sigma-Aldrich (St. Louis, MO).

The human vaginal epithelial cell lines (VK2/E6E7), endocervical epithelial cell lines (End1/E6E7) and *Lactobacillus crispatus* bacteria were from the American Type Culture Collection (ATCC, Manassas, VA). The CellTiter 96® AQueous One Solution Proliferation assay kit with [3-(4,5-dimethylthiazol-2-yl)-5-(3-carboxymethoxyphenyl)-2-(4-sulfophenyl)-2Htetrazolium, inner salt; MTS] reagent and CytoTox- ONE™, lactate dehydrogenase (LDH) cytotoxicity assay kit were from Promega (Madison, WI). Deionized water for all the experiments was obtained through a Millipore Milli Q water purification system (Millipore Corp., Danvers, MA). All other chemicals were of analytical grades and used as obtained from the suppliers. The pH adjustment of all the solutions was measured using a SevenEasy pH meter (Mettler Toledo, Schwerzenbach, Switzerland) under ambient temperature (22-24°C).

Synthesis of Thiolated Hyaluronic Acid (HA-SH) Derivatives

The sulfhydryl (-SH) group modified thiolated HA derivatives (HA-SH) were synthesized using the nucleophilic opening reaction of ethylene sulfide (198) as shown by the Reaction scheme 4. Briefly, aqueous solution of HA (0.5% w/v) was prepared in the Milli Q water and stirred for 2 h to make a homogeneous solution. The pH of the solution was raised to 9.5 using NaOH solution. A five-fold molar excess of the ethylene sulfide was added drop-wise to the above solution and the reaction mixture was stirred for 24 h at room temperature.

To separate the precipitate observed due to the oligomerization of ethylene sulfide (ES), the solution was vacuum filtered. To the clear filtrate, a five-fold molar excess of DTT was added to reduce the disulfide (S-S) bonds. The pH of the solution was raised to 8.5 using NaOH solution and mixture was further stirred for 24 h at room temperature. The pH of the reaction mixture was then lowered to 3.5 using the HCl solution. To purify the final HA-SH product , the acidified solution was dialyzed against diluted HCl solution (pH 3.5) for 24 h using the dialysis membrane (Spectra/Por Float-A-Lyzer G2, MWCO: 8-10 kDa) supplied from Spectrum Laboratories Inc. (Rancho Dominguez, CA) with three media changes at every 8 h. The final product was then lyophilized (Labconco Corp., Kansas City, MO) and stored at 4°C until further analyses.

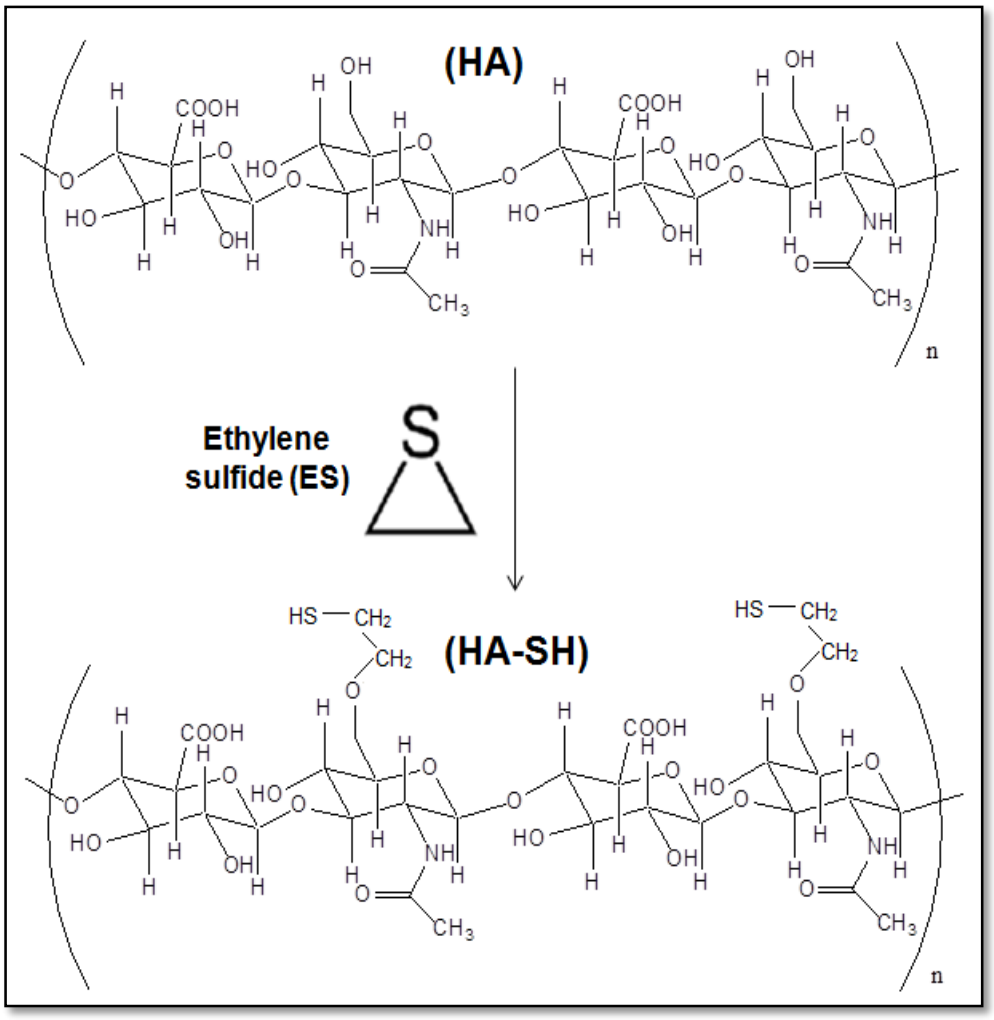

Reaction Scheme 4. Synthesis of Thiolated Derivatives (HA-SH) of Hyaluronic Acid.

Characterization of the Synthesized HA-SH Derivative

Spectral Analyses Using Proton Nuclear Magnetic Resonance (^{1}H-NMR) Spectroscopy

The ^{1}H-NMR spectra of HA-SH derivatives were acquired on a 400 MHz NMR instrument (Varian Inc., Palo Alto, CA). The data were analyzed by Mnova Lite software and spectra were acquired with a 90° pulse length of 14.2 μs and recorded with 64 scans with a recycle time of 1 sec at 25°C. Tetramethylsilane (TMS) was used as internal reference compound. Chemical shifts were reported as δ in parts per million (ppm). The NMR samples were prepared by dissolving each sample in 500 μL of D_2O as solvent in a 5-mm outer diameter NMR tubes (Wilmad-LabGlass, Vineland, NJ).

Spectral Analyses Using Fourier Transform Infrared (FT-IR) Spectroscopy

The FT-IR analysis of HA-SH derivatives was performed using Nicolet iS10 Spectrometer (Thermo Scientific, West Palm Beach, FL). The instrument was equipped with a deuterated triglycine sulfate (DTGS) detector and was controlled by OMNIC™ Spectra™ software. A transmission mode was selected to make observations with the sampling area of about 1 mm. The analysis was performed at 500 to 4000 cm^{-1} wavenumbers. The background data was collected at ambient temperature conditions before analyzing the samples. The spectra was automatically corrected with a linear baseline. No specific sample preparation method was used before the FT-IR analyses.

Sulfhydryl Group Quantitation using Ellman's Method

The amount of SH groups on HA-SH derivatives was determined using Ellman's method (199). Cysteine hydrochloride (MW: 157.62 Da) in the concentration range of 0.19-1.50 mM was used as the standard for making the calibration curve. Briefly, 50 μL of Ellman's reagent solution (4 mg/mL of DTNB in reaction buffer (pH 8.0) contacting 0.1 M sodium phosphate and 1 mM EDTA was added to a test tube contacting 2.5 mL of the same reaction buffer. Two hundred and fifty microliters of cysteine standard was added, mixed and incubate

at room temperature for 15 min. The absorbance of the yellow color developed was measured at 412 nm using Genesys 10 Bio UV-Vis Spectrophotometer (Thermo Electron Sci. Inst., LLC, Madison, WI).

Size Exclusion Chromatography (SEC)

The molecular weight (MW) and eventual degradation of HA during the -SH group modification was determined using size exclusion chromatography (SEC). Briefly, the SEC system (Waters, Milford, MA) consisted of a 1575 binary pump, 717 plus auto sampler, 410-differential refractive index (RI) detector, and Ultrahydrogel 500 and 250 columns (7.8 X 300 mm) connected in series. The mobile phase was composed of 0.1 M sodium nitrate ($NaNO_3$) at the flow rate of 1 mL/min. The mobile phase solvent was filtered with 0.2 μm cellulose acetate membrane filter (Sterlitech™, Kent, WA) and degassed using Ultrasonic bath sonicator (Model 150 D; VWR International., West Chester, PA) for 10 min before its use. The internal and external temperatures of the SEC column was maintained at 35°C using Waters column heater module controlled by 410 RI detector. The data were acquired and processed with Waters Millenium[32] software (version 3.2). A calibration curve was prepared by using Dextran SEC standards (Polymer Standards Service-USA, Amherst, MA) in the MW range of 5.2 to 410 kDa. A volume of 200 μL was injected into the SEC system in each analysis.

Powder X-ray Diffraction (PXRD) Analysis

To determine any changes in the amorphous nature of the native HA during the –SH group modification reaction process, the PXRD patterns were analyzed using Rigaku MiniFlex automated X-ray diffractometer (Rigaku, The Woodland, TX). The samples were mounted on single-crystal Si zero-background plates and the analysis were performed at room temperature using Cu K_α radiation produced at 35 kV and 15 mA, with a Ni filter. The scan angle (2θ) was from 5° to 40° with a step size of 0.05° 2θ and 3 sec per step. The diffraction patterns were processed using Jade 8+ software (Materials Data, Inc., Livermore, CA).

Fabrication of HA-SH Based Nanofibers using Electrospinning Method

Native HA or HA-SH solutions alone were difficult to processed by electrospinning into NFs due to their high viscosity and enormous water affinity (200). To improve the electrospinnability of HA, poly (ethylene oxide) (PEO: MW 400 kDa), a well-known fiber forming polymer (201, 202) was used as a core material. The potential use of PEO as a fiber forming polymer and for other biomedical applications has attracted a great attention due to its water-soluble, biodegradable, and biocompatible characteristics (203). Preliminary experiments were performed to get the optimal conditions for the electrospinning process. The electrospinning process parameters such as feeding rate, applied voltage, and needle tip-to-collector distance were optimized. However, the formulation variables were the concentration, MW, and solubility of the polymers (110, 111).

During the electrospinning process, a polymer solution was injected through a needle by electrostatic repulsive forces on a grounded collector (Figure 34) (204). The charged fluid jet underwent a highly stretching and whipping process through the air and the solvent evaporated quickly, and as a result, NFs were formulated and deposited on the collector. To prepare the HA-SH-NFs, the aqueous solutions of HA-SH (20 mg/mL) and PEO (30 mg/mL) were prepared at room temperature by stirring for 2 h, and 24 h, respectively. An electrospun system with a coaxial nozzle (NaBond Technologies Co., Ltd., Hong Kong, China) was used for HA-SH-NFs production. The inner core (PEO) and outer shell (HA-SH) solutions were placed separately in two glass syringes (Becton, Dickinson and Company, NJ). To prepare the drug (TFV) loaded HA-SH-NFs, free TFV (10 mg/mL) was mixed with the PEO solution and used as core material. Two syringe pumps (Cole-Parmer Instrument Company, IL) were used to provide a constant feeding rate (0.02 mL/h) of each solutions. A voltage of 15 kV was applied in the electrospinning process using a high voltage power supply (Gamma High Voltage Research, Inc., FL). The distance from electrospinning syringe needle tip-to-collector

was kept constant at 10 cm. The NFs were collected onto an aluminum foil connected to the ground. The HA-SH-NFs were vacuum dried at room temperature for 48 h and stored in a vacuum desiccator until further uses.

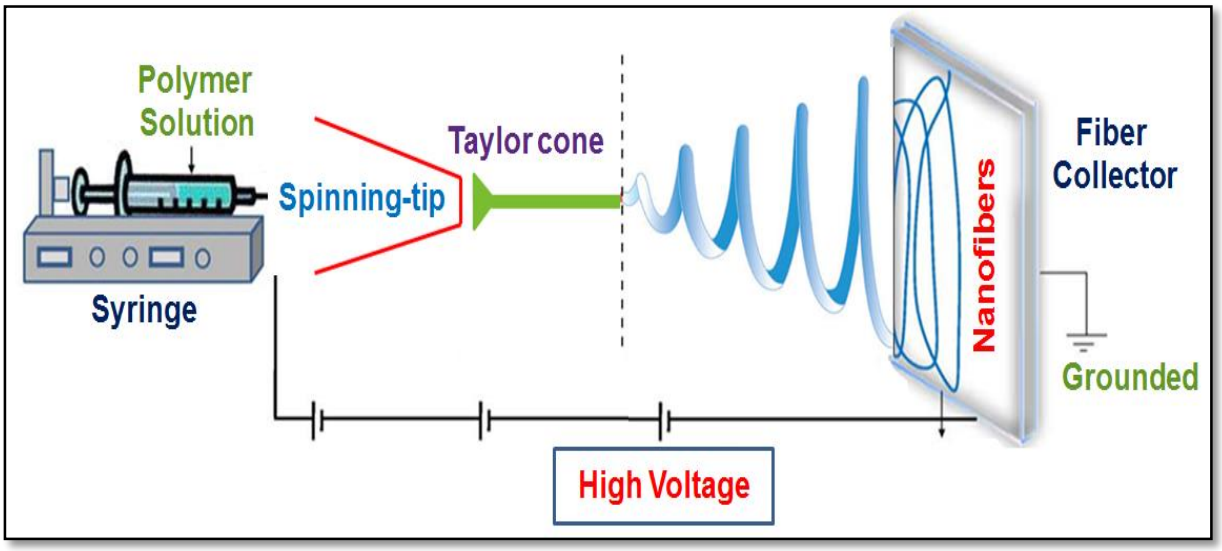

Figure 34. Nanofibers Fabrication using Electrospinning Method.

Physicochemical Characterization of HA-SH-NFs

The developed HA-SH-NFs were characterized for their physicochemical properties such as surface morphology, size distribution, mucoadhesive property and *in vitro* drug release profile.

Surface Morphology, Size Distribution Analyses and Drug Loading Determination

The surface morphology of NFs was analyzed by scanning electron microscopy (SEM) method. A small amount of the NFs was put onto a grid. The membrane was mounted on a 1/200 SEM stubs with double-sticky carbon tape. The NFs samples were then sputter coated with 20 nm thickness of gold and visualized under a Philips SEM 515 microscope (Eindhoven, The Netherlands) and observations were performed at an accelerating voltage of 5 kV. The diameter of individual NFs was analyzed using Image Pro® Plus software (Image-Pro®Plus 6.0, Media Cybernetics, Silver Spring, MD). At least 100 NFs were counted per group. The

histogram and distribution curve were generated by IBM® SPSS® Statistics software Version 23 (IBM Corp., Armonk, NY).

To determine the drug loading, NFs at the concentration of 1 mg/mL were kept in water under constant shaking at 100 rpm for 48 h to allow complete dissolution of the PEO core and vortexed for 5 min. The sample was centrifuged at 19,500 g for 30 min and the supernatant was analyzed by liquid chromatography-mass spectroscopy (LC-MS) assay of TFV (205) explained later in this chapter. The drug loading was calculated using Eq. (22).

$$Drug\ Loading\ (\%) = \frac{Total\ amount\ of\ TFV\ in\ mg}{Total\ amount\ of\ NFs\ in\ mg} \times 100 \quad (22)$$

In Vitro Mucoadhesion Analyses

The in vitro mucoadhesion analysis of HA-SH-NFs was performed using mucin interaction (206, 207) and ellipsometer measurements (208-210). Mucin interaction method was used to study the mucin-NFs interactions in solution form and ellipsometer was used to study the interactions between the HA-SH-NFs and mucin-coated silica surfaces.

Mucoadhesion Assessment by Mucin Interaction Method

The mucin interaction analysis was performed using native HA, and HA-SH-NFs at the concentration of 10 mg/mL in PBS (pH 7.4), VFS (pH 4.2), and in water (with 10 mM NaCl), prepared accordingly (127, 128). The mucin at the concentration of 1.5% w/v (207) was used in the analysis. The polymer samples were incubated for 0, 3, 6, and 24 h at 37°C and 60 rpm with or without mucin. The size and zeta (ζ) potential values were analyzed by Laser Doppler Velocimetry and Phase Analysis Light Scattering methods using Zetasizer Nano ZS (Malvern Instruments Ltd., Worcestershire, UK) at 25°C. The instrument was calibrated by using nanosphere™ of PMD (59.0 ± 2.5 nm) and ζ potential standards (−68.0 ± 6.8 mV).

Mucoadhesion Assessment by Ellipsometer Measurements

Ellipsometer is the study of adsorbed mass on a polymer surface (210). The adsorption of mucin and polymers on methylated silicon wafer surface was studied using an alpha-SE®

ellipsometer (J.A. Woollam Co. Inc., Lincoln, NE) at a single angle of incidence. The acquisition and analysis of ellipsometer data were performed using CompleteEASE® software version 5.03 (J.A. Woollam Co. Inc., Lincoln, NE). The 2-inch-diameter silicon wafers (WRS Materials, San Jose, CA) were hydrophobized (methylated) to enhance the interaction with proteins (211, 212) as previously described (213). Briefly, silicon wafers with thermal oxide layer of 30 ± 3 nm (n = 3) were dipped into a solution of trimethylchlorosilane (TMCS) in ethanol (1:5 v/v ratios) for 2 h. Afterwards, the wafers were rinsed with water followed by ethanol (3 times each) and stored in ethanol prior to use. Immediately before use, wafers were rinsed with water, blown dry using nitrogen gas, dipped in a mucin solution (1 mg/mL) and incubated for 15 h at 37°C followed by washing with ethanol and water. The native HA and HA-SH-NFs solutions at the concentration of 10 mg/mL in PBS (pH 7.4) were added on methylated wafers and analyzed by ellipsometer after 30, 60, and 120 min.

A change in polarization was measured after light was reflected from the wafer surfaces. The data were represented as two values: Psi (Ψ, amplitude ratio) and Delta (Δ, phase difference) (214). Interference occurs as light recombined after traveling different paths through the thin film. The thickness (d) measured was used to calculate the adsorbed mass (m in µg/cm^2) using Eq. (23).

$$Adsorbed\ mass\ (m) = \frac{d\ (n - n_0)}{dn/dc} \qquad (23)$$

Where, n and n_0 are the refractive index of the sample and the ambient environment, respectively, dn/dc is the refractive index increment as a function of bulk concentration (0.165 mL/g) of mucin (215).

In Vitro Drug Release Analysis

The *in vitro* drug release analysis of HA-SH-NFs in the presence or absence of HAase enzyme was performed using the dialysis method. An amount of HAase (~1.08 U) similar to

that is normally present in human ejaculate containing 100 million sperms/mL was used in the drug release analysis considering the average volume of human ejaculate of 3 mL (82). Briefly, the drug loaded HA-SH-NFs were transferred to a dialysis bag (MWCO, 3.5-5 kDa) containing the simulant mixture (pH 7.2) of the VFS (pH 4.2) and seminal fluid simulant (SFS, pH 7.8) in 1:4 volume ratio, respectively, and placed inside a dialysis tube containing the release medium (PBS, pH 7.2). These VFS and SFS buffers were prepared according to the previous reports (127, 128). The whole system was then placed in a thermostatic shaking water bath (BS-06, Lab Companion, Seoul, Korea) at 37°C with constant agitation at 60 rpm. Aliquots of samples (100 µL) were taken at, 0, 1, 3, 6, 12, 24 h from the release medium. Simultaneously, an equivalent volume of the fresh release medium was added at the same rate to maintain the sink conditions. The amount of drug released from NFs was quantified using a LC-MS assay (205).

Briefly, LC analysis is carried out on a UFLC Shimadzu prominence system (Shimadzu USA manufacturing Inc., Torrance, CA). A reversed phase Waters Symmetry® C_{18} column (150 mm × 4.6 mm, 5 µm) is used as a stationary phase under ambient temperature conditions. The detection is carried out at 259 nm using the flow rate of 0.6 mL/min and a sample injection volume of 10 µL in each analysis. The LC elution conditions of (all solvent percentages were volume fractions): mobile phase-A, 0.1% v/v formic acid in water; mobile phase-B, 0.1% v/v formic acid in acetonitrile; mobile phase-C, 30% A /70% B is applied. The time program was: 0.01 min, 100% A; 10 min, 100% C; 13 min, 100% B; 14 min, 100% A; and 18 min, 100% A. The samples are injected in to the LC system after appropriate dilution with mobile phase-A. MS study is performed on a 3200 QTrap mass spectrometer (Applied Biosystems Sciex, Framingham, MA). Spectra are recorded by scanning between 100-700 amu using Enhanced mass spectrum (EMS) scan in positive mode. Analyst® software version 1.4.2 (Applied Biosystems Sciex, Framingham, MA) is used for data acquisition. MS operational parameters were as follows: Collision activated dissociation (CAD): high; Ion source Gas1 (GS1): 50 psi;

Gas2 (GS2): 50 psi; Turbo ion spray voltage (IS): 5500 V; Source temperature (TEM): 350 °C; Collision energy (CE); 5 V; Declustering potential (DP): 2 V, and Entrance potential (EP): 2 V. Nitrogen gas is used as the nebulizer, and the scan rate was 4000 amu/sec.

In vitro Drug Release Kinetics

The drug release kinetics of TFV loaded HA-SH-NFs was analyzed by using various kinetic models (89, 129) using the previously described add-in DDSolver program (216). The kinetic models used were zero-order (Eq. 24), first-order (Eq. 25), Higuchi (Eq. 26), Korsmeyer-Peppas (Eq. 27), Hixson-Crowell (Eq. 28), and Weibull (Eq. 29) and, Quadratic (Eq. 30) models (216). The criteria for selecting the most appropriate model were based on the correlation coefficient (*R*), the coefficient of determination (R^2), and the Akaike information criterion (*AIC*) (216). The *AIC* criteria has its wide applicability and simplicity. The model with a higher *R* or R^2 values and lower AIC value was considered to be the better model.

$$M_t = M_0 + K_0 t \quad (24)$$

$$\log M_t = \log M_0 + K_1 t/2.303 \quad (25)$$

$$M_t = K_H t^{0.5} \quad (26)$$

$$M_t/M_\infty = kt^n \quad (27)$$

$$M_0^{1/3} - M_t^{1/3} = K_{HC} t \quad (28)$$

$$M = M_0 \left[1 - e^{\frac{(t-T)^b}{a}}\right] \quad (29)$$

$$M_t = 100\ (K_1 t^2 + K_2 t\ ) \quad (30)$$

In these Equations, M_t is the amount of drug released at time *t*, M_0 is initial amount of drug in solution, K_0 is zero order release constant, K_1 is first order release constant, K_H is Higuchi dissolution constant, K_{HC} is Hixson-Crowell release constant, M_t/M_∞ is the fraction of drug released at time *t*, *T* is the lag time measured as a result of the dissolution process, M_∞ is

the total amount of drug released, *k* is a kinetic constant, K_1 and K_2 are release constants, and *n* is the exponent explaining the drug release mechanisms (129). Parameter *a,* denotes a scale parameter that describes the time dependence, while *b* describes the shape of the dissolution curve progression. The exponent *n* is classified as Fickian diffusion ($n \leq 0.5$), case-II transport ($n = 1$), anomalous transport ($0.5 < n < 1$) and super case-II transport ($n > 1$) (129).

The Eq. (27) in Peppas model was further depicted in a log-transformed Eq. (31):

$$log\ M_t/M_\infty = n\,log\ t + log\ k \quad (31)$$

One important area in release data analysis is assessment of the similarity between dissolution profiles of drug formulations. To perform this, the model independent approach was applied to compare the drug release kinetics of the HA-SH-NFs as per US FDA guidance to industry (129). The release profiles of NFs in the absence of HAase enzyme was taken as reference whereas, the release of NFs in the presence of HAase enzyme was considered as the test compound. The difference (f_1) and similarity factors (f_2) were calculated using the Eq. (32), and (33), respectively.

$$f_1 = \left\{\left[\sum_{t=1}^{n}\left|R_t - T_t\right|\right] \Big/ \left[\sum_{t=1}^{n} R_t\right]\right\} \times 100 \quad (32)$$

$$f_2 = 50 \times log\left\{\left[1 + (1/n)\sum_{t=1}^{n}\left(R_t - T_t\right)^2\right]^{-0.5} \times 100\right\} \quad (33)$$

Here, *n* is the number of time points, R_t and T_t are the cumulative drug release (% w/w) at time *t* for the reference and test samples, respectively. Generally, $f_1 < 15$ and $f_2 > 50$ ensure sameness or equivalence of the two curves (129).

In Vitro Cytotoxicity Assays of HA-SH-NFs

The cytotoxic effects of HA-SH-NFs in the concentration range of 1-1000 µg/mL were tested on the viability (MTS assay) and membrane integrity (LDH assay) of VK2/E6E7 and End1/E6E7 cells using published protocols (89).

Cell Viability Assays

To perform the cell viability (MTS) assay, cells were seeded to 96-well plates in a keratinocyte-serum free medium and were allowed to grow until 80% confluence was reached. The medium was replaced with 100 µL of native HA or HA-SH-NF samples in the concentration range of 1-1000 µg/mL. The samples were kept in contact with the cells for 48 h. The amount of formazan product formed was determined by adding 20 µL of MTS reagent to the culture wells. The wells were incubated for 4 h at 37°C in a humidified, 5% CO_2 atmosphere and the absorbance was measured at 490 nm using a DTX 800 multimode microplate reader (Beckman Coulter, Brea, CA). The medium and 1% Triton-X-100 was used as negative and positive controls, respectively. The percent (%) cell viability was determined using Eq. (34).

$$Viability\ (\%) = \frac{ABS\ (test)}{ABS\ (control)} \times 100 \tag{34}$$

Where, *ABS (test)* and *ABS (control)* represented the absorbance of the amount of formazan product generated in viable cells.

Cell Cytotoxicity (Membrane Integrity) Assays

To perform the cell cytotoxicity (LDH) assay, the cells were incubated with 100 µL medium containing the samples of native HA and HA-SH-NFs in the concentration range of 1-1000 µg/mL. The plates were incubated at 37°C for 48 h and equilibrated to room temperature for 30 min. One hundred microliters of CytoTox-One™ reagent was added in each well and vortexed for 30 sec. The plates were incubated at room temperature for 10 min. Fifty microliters of stop solution from Promega (Madison, WI) was added in each well and the plates were shaken for 10 sec. The fluorescence intensity was measured at the excitation/emission wavelengths of 560 nm/590 nm, respectively, using the above microplate reader. The percent (%) cytotoxicity was determined using Eq. (35):

$$Cytotoxicity(\%) = \frac{Experimental - Background}{Positive\ control - Background} \times 100 \quad (35)$$

Where, experimental, background and positive control represented the fluorescence intensity of the wells with and without sample, and with 1% Triton-X treatment, respectively.

Lactobacillus Crispatus Viability Assay

A microbicide formulation should not disturb the normal *Lactobacillus* vaginal microflora since this can enhance the risk of HIV transmission through CV mucosa (217). In this study, *L. crispatus* bacteria was used as representative species since it was one of the most common vaginal *Lactobacillus* (218). The *L. crispatus* was grown in ATCC medium 416 *Lactobacilli* MRS broths (BD, Franklin Lakes, NJ) at 37°C. The viability assay was performed using *Lactobacillus* viability assay (61). Briefly, the bacteria density was adjusted to an OD_{670} of 0.06, which corresponded to 0.5 McFarland Standard or 10^8 CFU/mL. The *L. crispatus* bacteria was seeded in a 96-well plate at a volume of 100 µL and incubated with 100 µL of the sample suspension for 48 h at 37°C. The wells were treated with 10 µg/mL of commercially available penicillin-streptomycin solution (positive control) from Invitrogen (Carlsbad, CA). After the incubation, 20 µL MTS reagent was added to each well and the absorbance was measured at 490 nm to express the viability using Eq. (34).

Statistical Data Analysis

The experimental values were generally presented as mean ± standard deviation (SD) of triplicate determinations (n = 3). Statistical data analysis was evaluated using Students t-test with 95% confidence interval (CI). A $p\ value < 0.05$ was considered statistically significant.

4.3. Results and Discussion

Characterization of Thiolated HA-SH Derivative

Thiol group's derivatives were generated at the primary hydroxyl group of the GlcNAc units of HA using the nucleophilic opening reaction of ethylene sulfide (Reaction scheme 4). The HA-SH derivatives exhibited to have 0.763 ± 0.016 mM (n = 3) of -SH groups determined by Ellman's method (199).

^{1}H-NMR and FT-IR Analyses

Compared to the HA spectrum, a peak corresponding to the methylene group attached to the former hydroxyl oxygen (-CH_2-CH_2-SH), appeared at 3.8 ppm in the spectrum of HA-SH. The second methylene group, closer to the -SH functionality was overlapped with GlcA and GlcNAc protons of HA at 3.0-3.8 ppm and appears at about 3.65 ppm (219) (Figure 35A).

In the FT-IR spectrum of HA-SH (Figure 35B), a small -SH group peak was observed at about 2550 cm^{-1}. The HA-SH1 and HA-SH2 were the HA-SH samples prepared on two different days. The –SH group signal was very weak and broad due to its hydrogen bonding as also observed by others (220, 221). Overall, the FT-IR and NMR analyses confirmed the effective thiol modification of HA polymer.

SEC and PXRD Analyses

The SEC analysis showed that the average MW of HA-SH was ~58 kDa which was close to the average MW of native HA (~60 kDa) (Figure 35C). This means that the native HA was quiet stable under the basic and acidic conditions used in the reaction process.

The PXRD results revealed that the amorphous nature of native HA has been maintained during the reaction process (Figure 35D). The PXRD spectrum of HA-SH showed one additional peak at 2θ of 32° which was the typical PXRD peak of sodium chloride (NaCl)

(222). This could be due to the crystallization of the NaCl resulting from the sodium ions (Na^+) of HA and the chloride ions (Cl^-) of HCl used in the pH adjustment media.

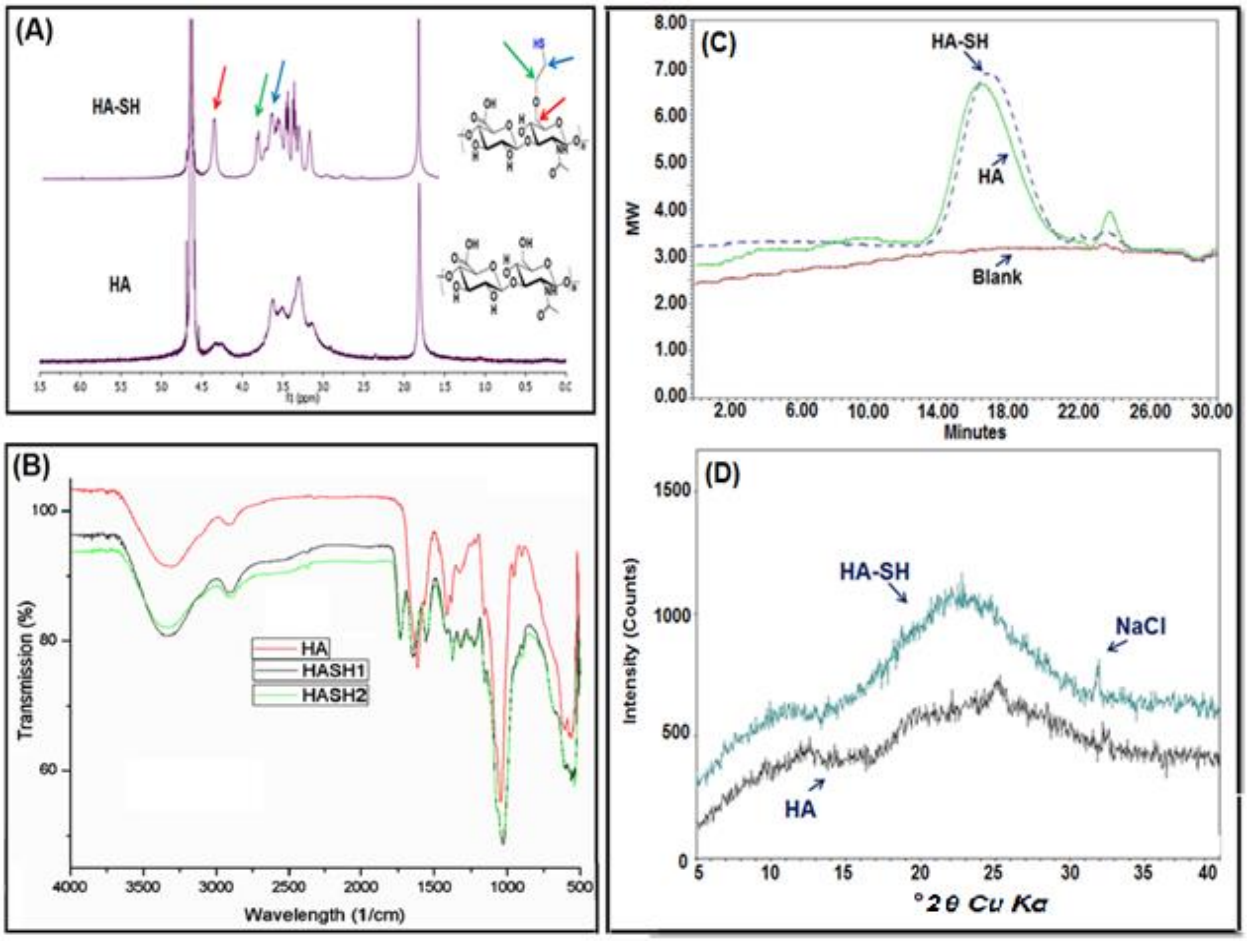

Figure 35. HA and Thiolated HA-SH Derivatives: (A) ^{1}H-NMR Spectrum. (B) FT-IR Spectrum. (C) SEC Chromatogram. (D) PXRD Pattern.

Physicochemical Characterization of HA-SH-NFs

Surface Morphology and Size Distribution

Initially, the HA-SH solution was electrospun alone and no fibers were formed (Figure 36A) due to the higher viscosity and enormous water affinity of the polymer (200). Scanning electron microscopy (SEM) images revealed that the blended HA-SH and poly (ethylene oxide) (PEO) solutions produced the HA-SH-NFs (Figure 36A) since PEO facilitated the fiber formation process during the electrospinning. Some beaded fibers were also observed (Figure

36B) which could be due to the presence of ionizable groups and concentrations of the HA-SH polymer, and feed rate of electrospinning solutions (204). During the electrospinning process, the repulsive force between the ionizable groups within the polymer backbone limit its electrospinnability and inhibits the formation of continuous fiber under the high electric field (223). To reduce the beads formation, feed ratio was optimized and positive results were obtained (Figure 36C). However, some beads were still observed (Inset Figure D) The mean diameter of HA-SH-NFs was found to be 74.96 ± 46.31 nm (n = 100) (Figure 36D).

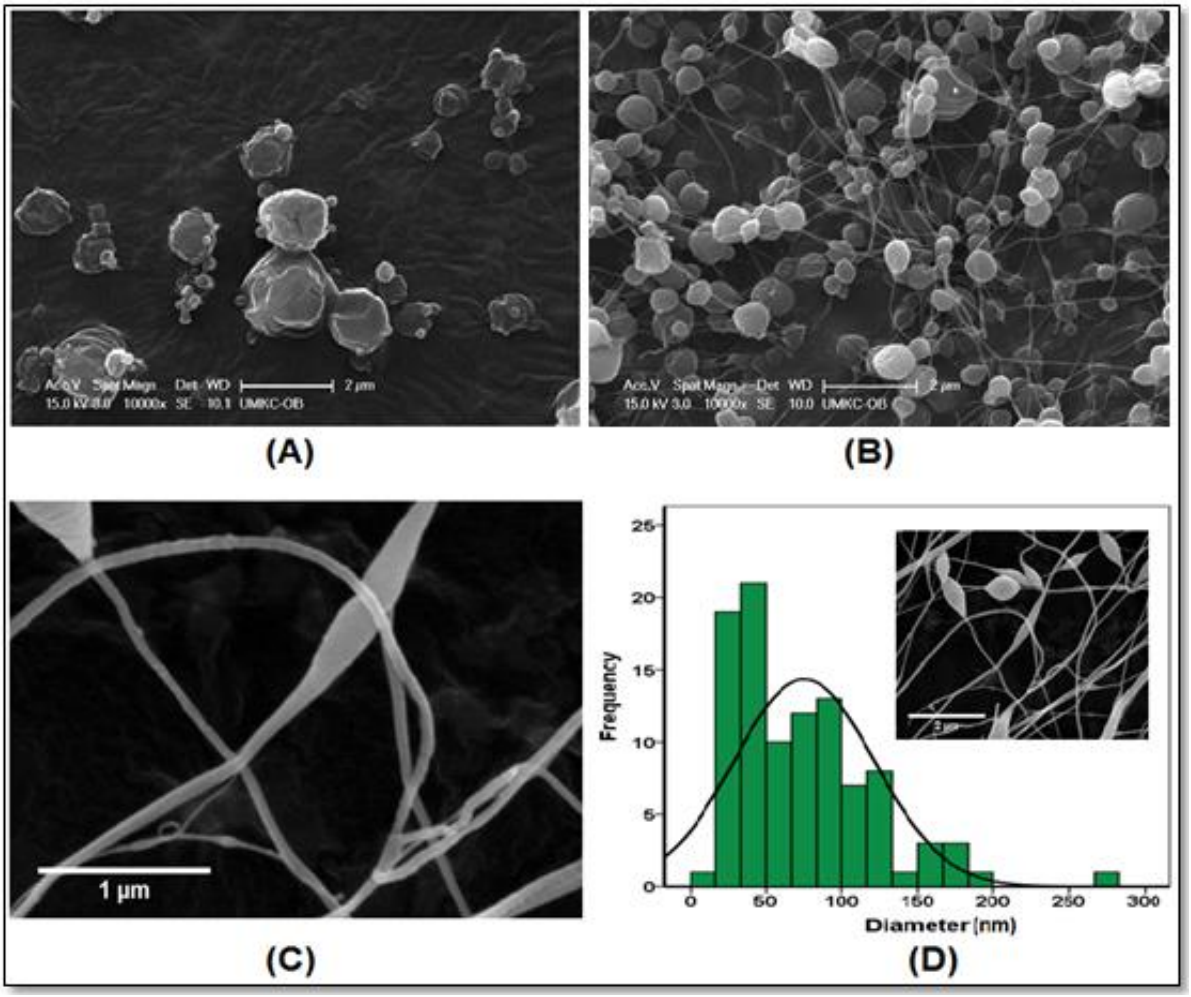

Figure 36. Surface Morphology of Nanofibers: (A) HS-SH alone; scale bar, 2 µm. (B) Beaded HA-SH-NFs; scale bar, 2 µm. (C) Optimized HA-SH-NFs; scale bar, 1 µm. (D) Size Distribution of HA-SH-NFs, averaged Using at least 100 Measurements/Group. (D) Inset figure: still some beads were observed in optimized NFs.

In Vitro Mucoadhesion Analysis

Mucin Interaction Assay

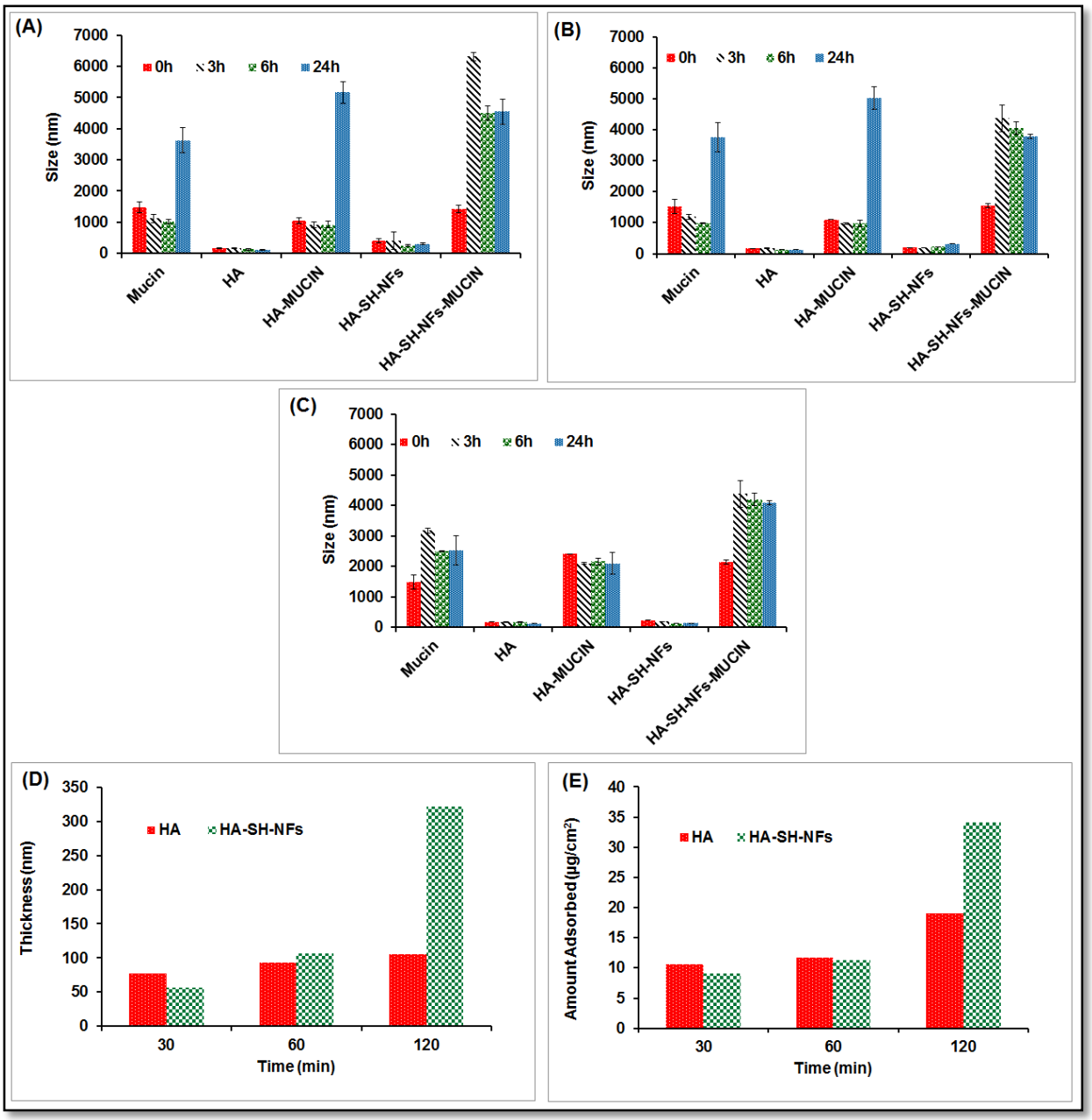

Figure 37. *In vitro* Mucoadhesion Analysis of Nanofibers using: Mucin Interaction Method; (A) PBS (pH 7.4). (B) VFS (pH 4.2). (C) Water (with 10 mM NaCl). Ellipsometer Measurements: (D) Thickness (*d*) in nm. (E) Amount adsorbed (*m*) in µg/cm^2.

In this study, the relationship between the size of mucin and polymer aggregate was correlated to the mucoadhesive property of HA-SH-NFs to native HA. The mucin interaction analysis showed that the size of HA-SH-NFs was significantly increased to ~4-7 µm compared to the native HA (~1-3 µm) in the presence of mucin as analyzed after 3h incubation in PBS (Figure 37A), VFS (pH 4.2) (Figure 37B), and water (Figure 37C). This was due to the higher thiol-thiol (S-S) group interactions between mucin and thiolated HA-SH-NFs in addition to the hydrophobic and electrostatic interactions. However, the study of mucin-HA interaction was limited due to the very large and broad size distribution of these two molecules. The interaction between mucin and HA-SH-NFs needs to be further analyzed using more sophisticated microscopy methods such as atomic force microscopy in the future.

Ellipsometer Measurements

In the ellipsometer measurements, an increased mucoadhesion of HA-SH-NFs was confirmed by an increase in thickness (~3 fold) (Figure 37D) and adsorbed mucin amount (~2 fold) (Figure 37E) of HA-SH-NFs (~321 nm, ~34 µg/cm^2, respectively) compared to the native HA (~105 nm, ~19 µg/cm^2, respectively) as calculated by Eq. (23). Overall, the mucin interaction and ellipsometer measurements confirmed the higher mucoadhesion of thiolated HA-SH-NFs compared to native HA polymer.

In Vitro Drug Release Analysis of HA-SH-NFs

The *in vitro* drug release profile for TFV loaded HA-SH-NFs (loading ~16-17 % w/w) in the presence and absence of HAase enzyme was depicted in Figure 38. A significantly triggered drug release (~87 %w/w) was observed from the HA-SH-NFs in the presence of HAase enzyme, whereas, in its absence the value was about ~54 %w/w after 1 h. However, the drug release was almost ~99% and ~62% w/w after a 6 h analysis in the presence and absence of HAase enzyme, respectively.

The observed drug release from HA-SH-NFs in the absence and presence of HAase enzyme might be due to two facts; firstly, it was anticipated that the interaction between -COOH groups of the HA and amino groups of TFV could have affected the drug release profile of the HA-SH-NFs. Since, TFV has two pKa values (2.0 and 6.7) (56), whereas HA has a pKa value at 2.9 (172), both (native TFV and HA) will have a negative charge at the working pH (7.2) of the release medium. Therefore, there would be a minimal possibility of interaction between TFV and HA. Due to these minimal interactions of HA with TFV, a higher % cumulative drug release was also observed from the HA-SH-NFs in the absence of HAase in the first couple of hours however, this drug release was significantly lower than that observed in the presence of HAase. Secondly, the large surface areas to volume ratios of HA-SH-NFs provided a larger area for drug interaction with the surrounding medium. This facilitated the mass transfer and thus, a fast release of therapeutic molecules.

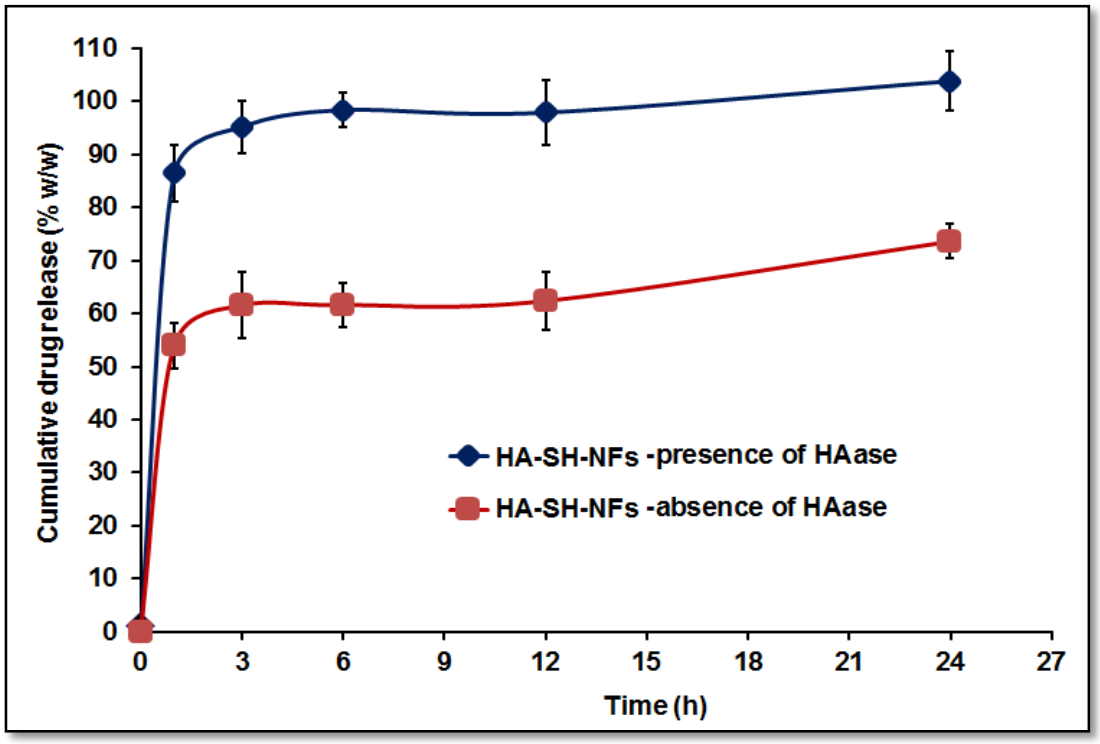

Figure 38. Percent Cumulative Drug Release (% w/w) Profile of TFV Loaded HA-SH-NFs either in the Presence or Absence of HAase. Results are given as mean ± SD, n = 3.

Ideally, the effective molar concentration (EC_{50}) of TFV (5-7.6 μM) (177) required to exhibit its anti-HIV activity should be locally released from the HA-SH-NFs before HIV virus crosses the vaginal mucosa in the time frame of 2-6 h and interacts with the macrophages, and dendritic cells (178). Based on the drug loading of HA-SH-NFs (~16-17 %w/w), the actual amount of TFV was ~59 μM per 100 mg of NFs. Considering the 10 mg of HA-SH-NFs will be used in each treatment dose, this would be equivalent to ~6 μM of TFV drug dose. It can be reasonably speculated that a microbicide released from the enzyme-sensitive HA-SH-NFs would potentially exhibit an anti-HIV effect in less than 6 h as most of the drug from HA-SH-NFs was released out (~99% w/w) in this time frame. It is noteworthy that the EC_{50} value of TFV from the HA-SH-NFs was achieved within that critical timeframe of 2-6 h in the presence of HAase. However, the *in vivo* drug release profile of these HA-SH-NFs in the presence and absence of enzyme remain to be confirmed in the future studies.

In Vitro Drug Release Kinetics of HA-SH-NFs

The drug release from the HA-SH-NFs was analyzed using various *in vitro* kinetic models (129, 216). The model with a higher R or R^2 values and lower AIC value was considered to be the better model. It was observed that in the absence of HAase the drug release from NFs followed the Peppas model (*R: 0.995; R^2: 0.990; AIC: 25.030*) however, in the presence of HAase, NFs followed the Weibull model (*R: 0.999; R^2: 0.999; AIC: 9.396*) (Table 19).

The model independent approach was then applied to compare the drug release kinetics of the HA-SH-NFs in the absence and presence of HAase enzyme. The f_1 (35.00) and f_2 (12.51) values(129) were calculated using Eq. (32), and (33), respectively. The results indicated that there was a significant difference between the drug release profiles from HA-SH-NFs in the presence and absence of HAase since the f_1 and f_2 values were >15 and <50, respectively.

Table 19: Estimated Parameters: *In Vitro* Drug Release Kinetics Models.

Kinetic model	Absence of HAase enzyme			Presence of HAase enzyme		
	R^{*}	R^{2**}	AIC^{***}	R^{*}	R^{2**}	AIC^{***}
Zero-order	0.604	-1.042	55.187	0.489	-1.448	61.088
First-order	0.805	0.109	50.207	0.999	0.996	21.993
Korsmeyer-Peppas	0.995	0.990	25.030	0.999	0.997	21.921
Higuchi	0.784	0.232	49.319	0.702	-0.015	55.803
Hixon-Crowell	0.750	-0.106	51.509	0.717	0.016	55.622
Weibull	0.995	0.990	27.497	0.999	0.999	9.396
Quadratic	0.718	0.026	52.747	0.694	-0.060	45.259

* Correlation coefficient. ** Coefficient of determination. *** Akaike Information Criterion.

In Vitro Cytotoxicity Analysis of HA-SH-NFs

According to ISO standard, if the cell viability of control samples is 100%, viability >80% is attributed to absence of cytotoxicity, 60-80% to mild cytotoxicity, 40-60% to moderate cytotoxicity and if the viability is <40%, the cytotoxicity is severe (224). Based on the results obtained, the HA-SH-NFs did not show any significant effect ($p > 0.05$) on the viability of VK2/E6E7 and End1/E6E7 cells, compared to medium (negative control) (Figure 39A). A statistically insignificant ($p > 0.05$) A lower LDH release and percent cytotoxicity was observed from the cells incubated with the HA-SH-NFs for 48 h in comparison to the negative control (medium) (Figure 39B).

Effects on the Viability of *L. Crispatus* Bacteria

A microbicide formulation should not disturb the normal *Lactobacillus* vaginal microflora since it is a key component of the innate immune environment which can reduce the

risk of HIV transmission through vaginal mucosa (217). It was observed that the HA-SH-NFs have no significant ($p > 0.05$) deleterious effect over the viability of *L. crispatus* bacteria compared to the medium as shown in Figure 39C.

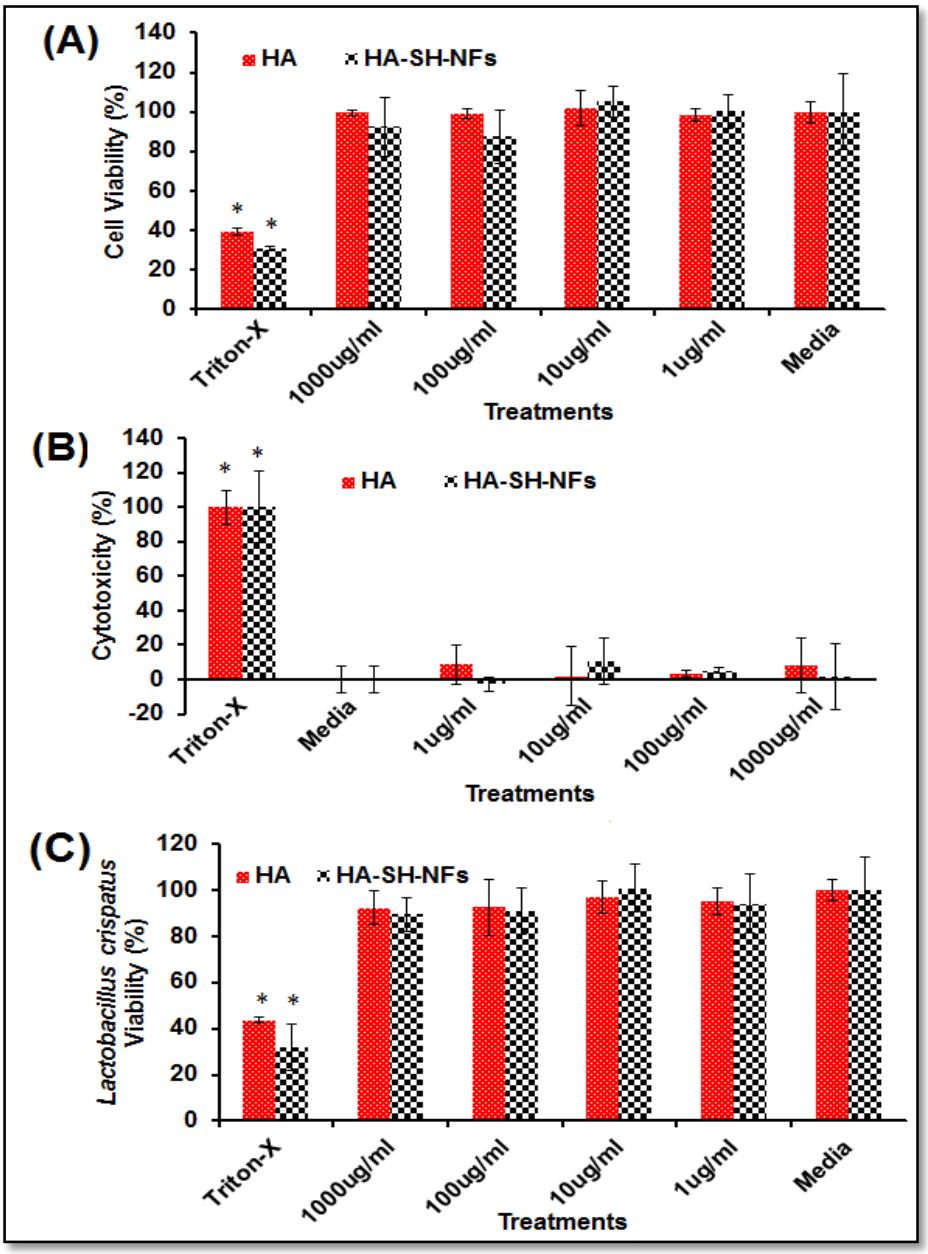

Figure 39. Cytotoxicity Assays of TFV loaded HA-SH-NFs and Native HA on VK2/E6E7 and End1/E6E7 cells. (A) Effects on the viability (MTS assay). (B) Effects on lactate dehydrogenase release (LDH assay). (C) Effects on *L. crispatus* bacteria viability. Results are given as mean ± SD, n = 3 after 48 h incubation. Asterisk (*) indicated the significant difference ($p < 0.05$), compared with the control (media).

4.4. Conclusion

In this study, a novel stimuli-sensitive and mucoadhesive thiolated HA based NF loaded with a vaginal anti-HIV microbicide tenofovir was developed using the electrospinning method. It was observed that HAase enzyme triggered a significant drug release (~87 %w/w) from the HA-SH-NFs within an hour of the enzyme incubation. The HA-SH-NFs were found to have a much better response in the presence of HAase enzyme in terms of triggered drug release compared to the NPs in the presence of HAase enzyme. In addition, NFs have a higher mucoadhesion property due to the presence of thiol groups on their surface compared to the native HA polymer thus to the HA-NPs. The triggered drug release might be due to the porous surface, large surface areas to volume ratios, and absence of any cross-linking chemistry at the HAase enzyme target size (carboxylic acid groups) of HA in HA-NFs compared to the HA-NPs. The large surface areas to volume ratios of HA-SH-NFs provided a larger area for drug interaction with the surrounding medium. This facilitated the mass transfer and thus, a fast release of therapeutic molecules was observed. The HA-SH-NFs were non-cytotoxic to human vaginal VK2/E6E7, and End1/E6E7 cells and had no deleterious effect on the viability of *Lactobacillus* bacteria. Collectively, the results suggested that TFV loaded HAase sensitive HA-SH-NFs templates developed in this study have the potential of topical vaginal delivery of microbicides for the prevention of HIV virus transmission.

Acknowledgments

The project was supported by Award Number R01AI087304 from the National Institute of Allergy and Infectious Diseases (Bethesda, MD).

CHAPTER 5

PRECLINICAL SAFETY AND *IN VITRO* HIV EFFICACY EVALUATIONS OF HYALURONIDASE SENSITIVE TENOFOVIR LOADED HYALURONIC ACID BASED NANOFORMULATIONS

5.1. Rationale

The safety of vaginal microbicides is an important concern in anti-HIV formulation development as they must preserve the integrity of the genital mucosa and demonstrate no localized toxicity, irritation and inflammation (225). Such adverse effects create a direct portal of entry for HIV virus and mucosal inflammation may activate and recruit a high level of HIV target cells (macrophages and T lymphocytes) at the port of viral entry (Figure 40) (160). This increases the susceptibility to sexually transmitted infections. Thus, it is essential that a microbicide product undergoes a rigorous safety evaluation using *in vitro* cell culture and preclinical animal models before evaluating their effects in humans.

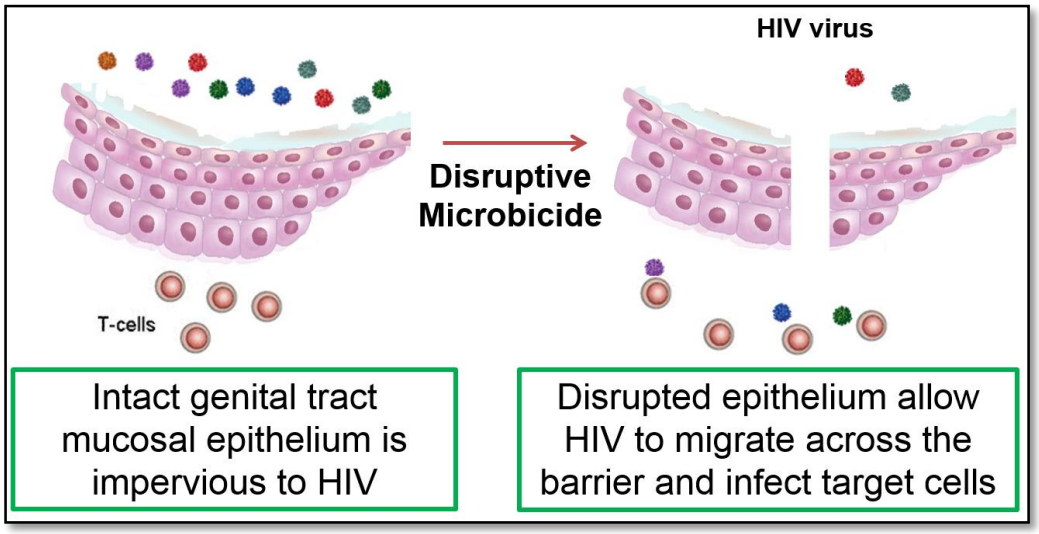

Figure 40. Assessment of Vaginal Epithelial Damage Following the Application of a Topical Microbicide Formulation.

The *in vitro* cytotoxicity assays of HA-NPs and HA-SH-NFs in cervicovaginal cell culture models (ex. VK2/E6E7, and End1/E6E7 cells) has already been explained in Chapters 3 and 4, respectively. However, they do not allow a prolonged or repeated exposure to a microbicide candidate and do not assess inflammatory responses that can only be seen in intact mucosal tissues. Hence, this study is designed to evaluate the preclinical safety, cytokine secretion, epithelial damage and tissue inflammatory responses of HA-NPs and HA-SH-NFs in an animal (mice) model. The optimized formulations of HA-NPs and HA-SH-NFs developed in Chapters 3 and 4, respectively, were used in this study. The *in vitro* anti-HIV activity of the developed HA-NPs and HA-SH-NFs was also evaluated on the pseudotyped HIV virus particles generated using a lipofectamine plasmid transfection method.

5.2. Materials and Methods

Chemicals

Tenofovir was purchased from Beijing Zhongshuo Pharmaceutical Technology Development Co. Ltd. (Beijing, China). Hyaluronic acid sodium salt was kindly provided by Mr. Jack Liu (Zhenjiang DongYuan Biotech Co., Ltd., Jiangsu, China). Medroxyprogesterone acetate (Depo-Provera®) was from Greenstone, Peapack, NJ). Nonoxynol-9 (Conceptrol®) was from Revive Personal, (Madison, NJ). Benzalkonium chloride (BZK, 2 %v/v) was from Sigma-Aldrich (St. Louis, MO). The following reagents are obtained through the NIH AIDS Research and Reference Reagent Program, Division of AIDS, NIAID, NIH: MT-4 cells from Dr. Douglas Richman; the plasmid pNL4-3.Luc.R^-.E^- from Dr. Nathaniel Landau and; pHEF-VSVG from Dr. Lung-Ji Chang. All other chemicals were of analytical grades and used as obtained from the suppliers.

In Vivo* Evaluation of Hyaluronic Acid Based Nanoformulations in *Animal (Mice) Model

Female C57BL/6 mice with an average body weight of 20 g at 8-12 weeks old from Jackson Laboratories (Harbor, ME) were used for the *in vivo* evaluations due to their easy breeding, and robustness. All mice were housed (no more than 5 per cage) under a 12 h light: dark regime in the UMKC Laboratory Animal Resource Center (LARC) facility which is a fully AAALAC (the Association for Assessment and Accreditation of Laboratory Animal Care) accredited with HEPA-filtered, temperature, humidity, and lighting control systems.

Vaginal Cytology: Mice Estrus Cycle Stages Identification

In humans, the reproductive cycle, called the menstrual cycle, lasts approximately for 28 days however, in mice, this cycle, called the estrous cycle, and lasts approximately for 4-5 days (226). Several changes occurred in the mouse estrous cycle can be detected by using a variety of methods including the vaginal cytology, measuring electrical impedance, biochemical analysis of urine, and visual observation of the external genitalia to determine the estrous cycle stages (226, 227). Out of these methods, vaginal cytology is most accurate for identifying all the stages of the estrous cycle.

The full estrus cycle in mice can be divided into four stages (227) (Figure 41):

(a) Proestrus: in this stage, there is a predominance of nucleated epithelial cells appear in clusters or individually. Occasionally, some cornified cells may also appear.

(b) Estrus: this stage is distinctively characterized by clusters of cornified squamous epithelial cells. There is no visible nucleus.

(c) Metestrus: in this stage, there is a mix of cell types with a predominance of leucocytes and a few nucleated epithelial and/or cornified squamous epithelial cells.

(d) Diestrus: this stage consists predominantly of leukocytes.

In this study, to determine the estrous stages, mice were treated with 2 mg of subcutaneous medroxyprogesterone acetate (Depo-Provera®) diluted in Lactated Ringer's

solution at 4-5 days prior to the *in vivo* experiments. This treatment induced a diestrus-like state that is characterized by thinning of the vaginal epithelial layer and reduced inter-individual variability of vaginal histology (228). Vaginal cytology analysis was then performed to identify the mice estrous cycle stages by visualizing the nucleated and cornified squamous epithelial cells and polymorph nuclear leukocytes (227).

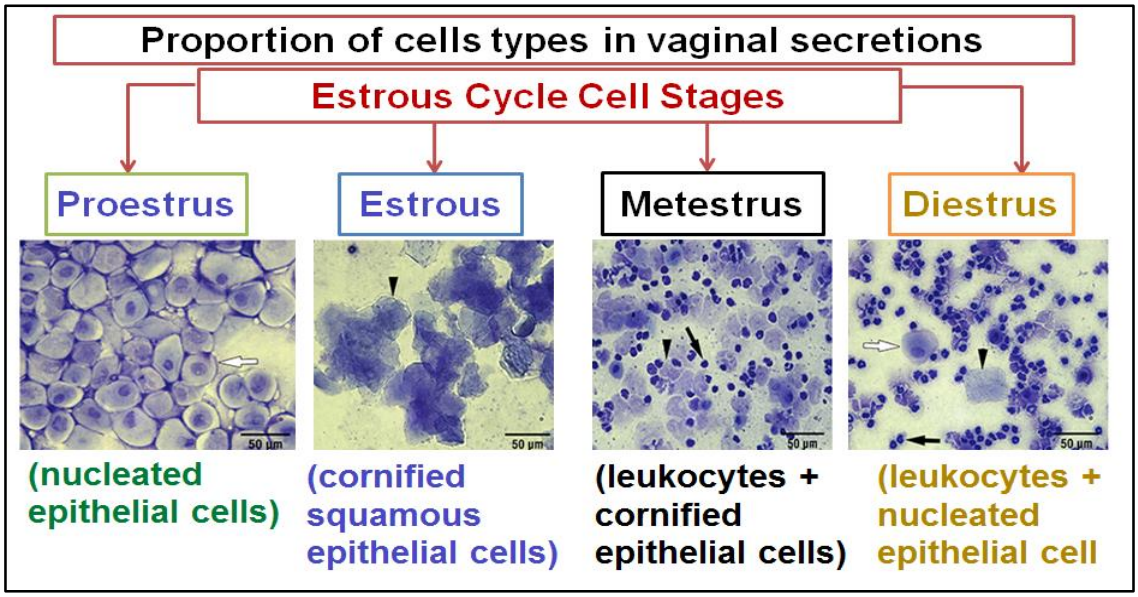

Figure 41. Vaginal Cytology: Mouse Estrus Cycle Stage Identification.

Preclinical Safety and Toxicity Evaluation

In vivo safety of HA-NPs and HA-SH-NFs at the dose of 25 mg/kg (equivalent to the drug dose of ~6.5 mg/kg), and 275 mg/kg (equivalent to the drug dose of ~46 mg/kg), respectively, upon once-daily vaginal administration up to 7 days was assessed by histological analysis of mice genital tract (vagina, cervix, uterus, and ovary), and other organs (rectum, spleen, lung, liver, kidney, heart, brain). The vagina was washed 2 times by flushing repeatedly with 50 µL of PBS with a micropipette before any treatment. To instill the samples, mice were held upwards by the base of the tail and samples were administered intra-vaginally using a micropipette with a soft tip. Care was taken in order to minimize tissue injury or disturbance of vaginal mucus. Animals were maintained in an upward position for 1 min in order to reduce

any immediate vaginal leakage. Mice treated with nonoxynol-9 (Conceptrol®, N-9, and 4% w/v) and benzalkonium chloride (BZK, 2% v/v) were used as positive control groups due to their well-recognized toxic effects on genital tract (229, 230). The mice treated with PBS were used as negative control groups. The animal experimental set-up was shown in Figure 42.

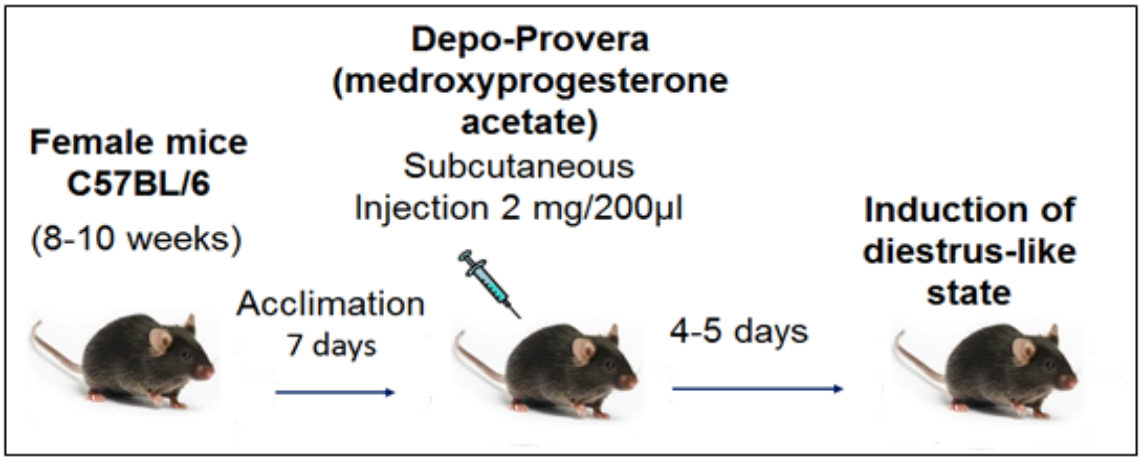

Figure 42. Animal (Mice) Experimental Set-Up.

At predetermined time points, mice were euthanized by CO_2 asphyxiation at 70% (v/v) CO_2 (30% v/v oxygen). The collected tissues were formalin fixed and embedded in paraffin following standard tissue processing procedure. Histopathologic review was performed on tissues stained with hematoxylin and eosin (H&E). Images were viewed and captured using a Nikon Labophot-2 microscope (Nikon Instruments, Inc., Melville, NY) equipped with a PAXCam digital microscope camera and analyzed using PAX-it image management and analysis software (Midwest Information Systems, Inc., Villa Park, IL).

Osmolality Determination of the Tested Samples

Ideally, the osmolality of a microbicide formulation should not exceed 400 mOsm/Kg to minimize any risk of vaginal epithelial damage (231, 232). Thus, before any treatment, the osmolality of each sample was analyzed (n = 3) using a Vapor Pressure 5520 Osmometer (Wescor, Inc., Logan, UT) calibrated with Opti-mole 100, 290 and 1000 mOsm/kg osmolality

standards. To analyze the osmolality, metal forceps were used to place a single 1/8" solute-free Whatman No.1 filter paper disc (Wescor, Inc., Logan, UT) in the central depression of the holder. Ten microliters of each sample was expelled onto the disc so that the area of the disc was fully covered by the sample. The sample holder was then inserted into the instrument and osmolality measurement was performed. The osmolality of the each samples was recorded in mOsm/kg.

Immunoassay of Cytokines Secretion in Mice Cervicovaginal Lavage (CVL) and Cervicovaginal Tissue Samples

Cytokines play an important role in HIV infection and transmission through CV mucosa and must be evaluated for any microbicide formulation (Table 5 in Chapter 2) (69). A microbicide formulation was supposed to be in contact with the CV epithelium for a variable time before sexual intercourse and thus, should not cause the onset of inflammation or cytokine secretions (31). At predetermined time points after the sample treatments, the mouse vagina was washed 2-times by flushing repeatedly with 50 μL of PBS and CVL was collected. The CVL sample was centrifuged (1000 g, 10 min, 4°C) and supernatant was collected. Mice were then euthanized by CO_2 asphyxiation and the CV tissues were collected. The CVL supernatant and the CV tissue samples were kept frozen at -20°C until further processing. The levels (pg/mL) of several cytokines including interleukins (ILs) IL-1α, IL-1β, IL-6, Interferon gamma-induced protein 10 (IP-10), IL-7, tumor necrosis factor-alpha (TNF-α), and mice keratinocyte-derived chemokine (MKC) were measured according to the manufacturer's protocol (Milliplex MAP Mouse Cytokine/Chemokine Magnetic Bead Panel, EMD Millipore Corp., Billerica, MA) as explained below.

To process the above samples for the cytokines assay, the homogenization buffer was freshly prepared by mixing the protease inhibitors cocktail (Sigma, St. Louis, MO) to the Tissue Extraction Reagent I (Invitrogen, Carlsbad, CA) following the manufacturer’s protocol. The

tissue samples were prepared in the homogenization buffer (Invitrogen, Carlsbad, CA) at the concentration of 100 mg/mL. The tissue samples were homogenized using the Omni Homogenizer (Omni International, Kennesaw, GA) at full speed, each cycle of 30 sec and a 30 sec dwell time. The tissue homogenates were kept on ice for 60 min to allow the maximum protein extraction from the samples. The tissue debris and other particulate matter from the homogenate were removed by centrifugation at 14,000 g for 15 min at 4°C. The supernatant was then removed and placed on ice. The protocol provided with the cytokine assay kit (Millipore Corp., Billerica, MA) was then followed using the Luminex MAGPIX instrument with xPONENT® version 4.2 software (Luminex Corp., Austin, TX). The extraction medium was used as the matrix solution in the blank, standards and control samples.

Briefly, premixed magnetic beads conjugated to antibodies for all 7 cytokines were mixed with equal volumes of supernatants (25 μL) in 96-well plates. Plates were protected from light and incubated on a microplate shaker overnight at 4°C. Then, magnetic beads were washed twice with 200 μL of wash buffer, and detection antibodies were added to each well. The mixtures were incubated at room temperature for 1 h. Streptavidin-phycoerythrin conjugate was added to each well, and the mixtures were incubated for 30 min at room temperature. The magnetic beads were washed twice and re-suspended in wash buffer for 5 min, the plates were assayed on the MAGPIX system. The median fluorescence intensity was analyzed using a 5-parameter logistic method from a standard curve of each respective cytokine to determine their concentration in supernatants in duplicate (n = 2). Basically, the red classification laser (635 nm) probed the internal dyes to identify bead regions. The green reporter laser (532 nm) interrogated the fluorescent reporter to measure analyte concentrations.

Immunohistochemical Analysis to Identify the Inflammatory Cells in CV Tissues

An increased lymphocytes infiltration within the vagina epithelium is indicative of vaginal inflammation (228). Thus, to identify the inflammatory cells (CD45) infiltration in

mice genital tract, the immunohistochemistry assay was performed. The CD45-associated protein is a lymphocyte-specific membrane protein. To visualize the lymphocytes, CV tissues were harvested from the treated mice following the immunohistochemistry protocol (ImmunoCruz^{TM} mouse ABC Staining System, Santa Cruz Biotechnology, Dallas, TX) as explained below.

Paraffin-embedded tissue sections were deparaffinized and rehydrated using xylene, ethanol gradient, and deionized water. Antigen retrieval was performed using steam heat method in citrate buffer/0.05%Tween-20 for 20 min. Following this incubation, tissue sections were rinsed with Tris-buffered saline/0.05%Tween-20 for 5 min each (three times). The tissue sections were then treated with 3% v/v H_2O_2 in PBS for 10 min and blocked with 10% normal goat serum for 2 h (Vector Laboratories, Burlingame, CA). Anti-CD45 from Santa Cruz Biotechnology, Inc. (Dallas, TX) was diluted in 1.5% normal goat serum to 5 µg/mL (1:50) and applied to the tissue sections overnight at 4°C in a humidified chamber. Following the incubation with primary antibody, tissue sections were rinsed three times. The appropriate biotinylated secondary antibody (Santa Cruz Biotechnology, Inc., Dallas, TX) was then diluted to 5 µg/mL (1:50) and applied to tissue sections at room temperature for 1 h. After the incubation with the secondary antibody, visualization of the cells was performed using the DAB: Peroxidase Substrate Kit (Sigma, Saint Louis, MO) under the above microscope. The tissue was then counter-stained using hematoxylin (Sigma, Saint Louis, MO) and processed through an alcohol gradient and xylene before application of a coverslip mounted using cytoseal 60 mounting media (Richard Allan Scientific, Kalamazoo, MI).

In Vitro Anti-HIV Activity of HA Nanoformulations (HA-NPs and HA-SH-NFs)

Generation and Characterization of Pseudotyped HIV Virus Particles

The pseudotyped virus particles were generated from two plasmids, one coding for the envelope, and the other for the backbone. The glycoprotein G from Vesicular Stomatitis Virus G Protein (VSV-G) was selected as the envelope protein because it allowed the infection for a very wide range of cell types from a variety of organisms and known to provide high titers (233). The proviral vector pNL4.3.Luc.R$^-$E$^-$, with envelop deleted and with the firefly luciferase gene was selected as the reporter plasmid (233).

The virus particles were produced by co-transfection of HEK293T producer cells using lipofectamine 2000 (Invitrogen) assay (Figure 43) (234, 235). The plasmids encoding VSV-G were co-transfected with luciferase expressing pNL4.3.Luc.R$^-$E$^-$ plasmid to generate VSV-G pseudotyped virus (234, 235). The viral supernatant was then harvested at 72 h post-transfection, centrifuged for 15 min at low speed (500 g) to remove the cellular debris. The supernatant was filtered through a 0.45 µm pore size filter and stored in aliquots at -80°C until used for the single-cycle infection assay.

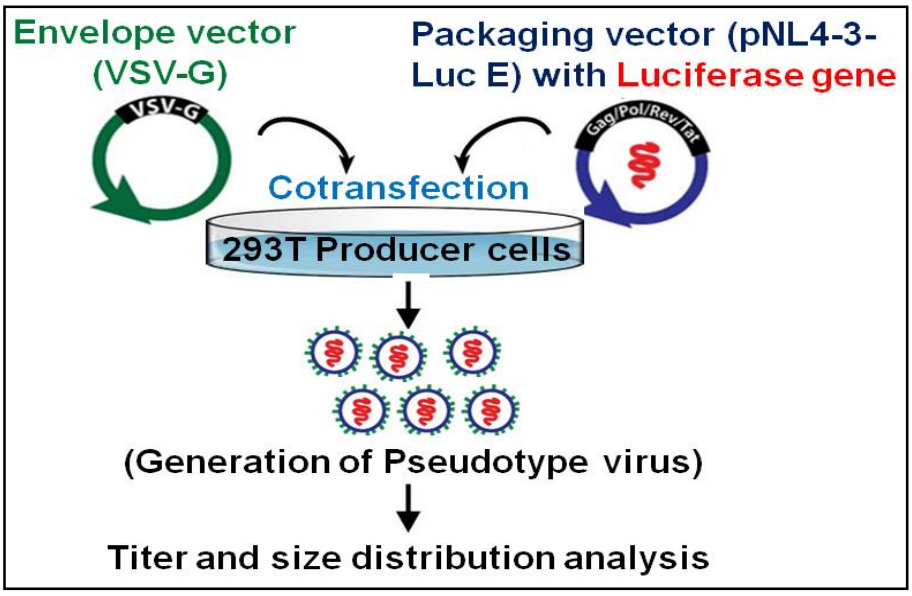

Figure 43. Generation of Pseudotyped HIV Virus Particles using Plasmid Transfection Method.

To determine the titer (number of particles/mL) and size distribution of virus particles, nanoparticle-tracking analysis (NTA) was performed using a Nanosight LM10 instrument (Nanosight, Salisbury, UK) outfitted with a LM14C laser. The samples were diluted first in PBS to meet the optimal concentration between 10^5-10^8 particles/mL. At least 300 µL of diluted sample was needed for each analysis and was mixed by vortexing before injection into the chamber. Each video of moving particles was 60 s in duration, with a shutter speed of 30 ms and camera gain of 680. Software settings for analysis were: Detection threshold: 6, Blur: auto, Minimum expected particle size: 50 nm. A minimum of 200 completed particle tracks were completed for each video and the data was analyzed using the NTA 2.3 analytical software (Malvern Inc.). Briefly, the NTA analysis determines the particle diffusion coefficient (D_t) by measuring the movement of the particle (Brownian motion) and then this employs the Stokes-Einstein equation (Eq. 36) to determine the size distribution and virus titer in each sample (236, 237).

$$D_t = \frac{TK_B}{3\pi\eta d} \tag{36}$$

Here, T = sample temperature, K_B = Boltzmann's constant, and η = solvent viscosity. Using D_t, the sphere-equivalent hydrodynamic diameter (d) of the virus particles was determined.

In Vitro Anti-HIV Activity

The anti-HIV activity assay of HA-NPs and HA-SH-NFs was performed using MT-4 cells since, they are highly permissive to viruses (238). Briefly, MT-4 cells at the density of $5x10^3$ cells/ mL were incubated with 25 µL of free TFV or TFV loaded HA-NPs or HA-SH-NFs suspended in cell culture medium. The nanoformulations were used in a concentration that is equivalent to the TFV dose of 0.035-35 µM for 24 h prior to the virus treatment (Figure 44). The cells were then exposed to 25 µL of the pseudotyped virus particles at the multiplicity of infection (MOI) of 10,000, 5000 and 1,000 and incubated for 48 h. Here, MOI was the ratio of

the number of pseudotyped virus particles to the number of cells being exposed. The inhibition of the pseudotyped HIV virus replication was analyzed using luciferase assay (Figure 44) due to its high sensitivity, and robustness toward a variety of drugs and complex biological samples (239). Briefly, after the 48 h of virus particles treatment, an equal volume of luciferase buffer and substrate (Promega, Madison, WI) was added and the plates were incubated for 10 min at 37°C under 5% CO2. The bioluminescence was then immediately measured using a Luminometer (Promega, Madison, WI), according to the manufacturer's directions. The wells with no cells were used as positive control whereas, cells suspended in medium without free TFV and HA-NPs or HA-SH-NFs were used as negative control samples, respectively. The inhibition of pseudotyped HIV virus replication was presented in terms of percentage (%) of viral load.

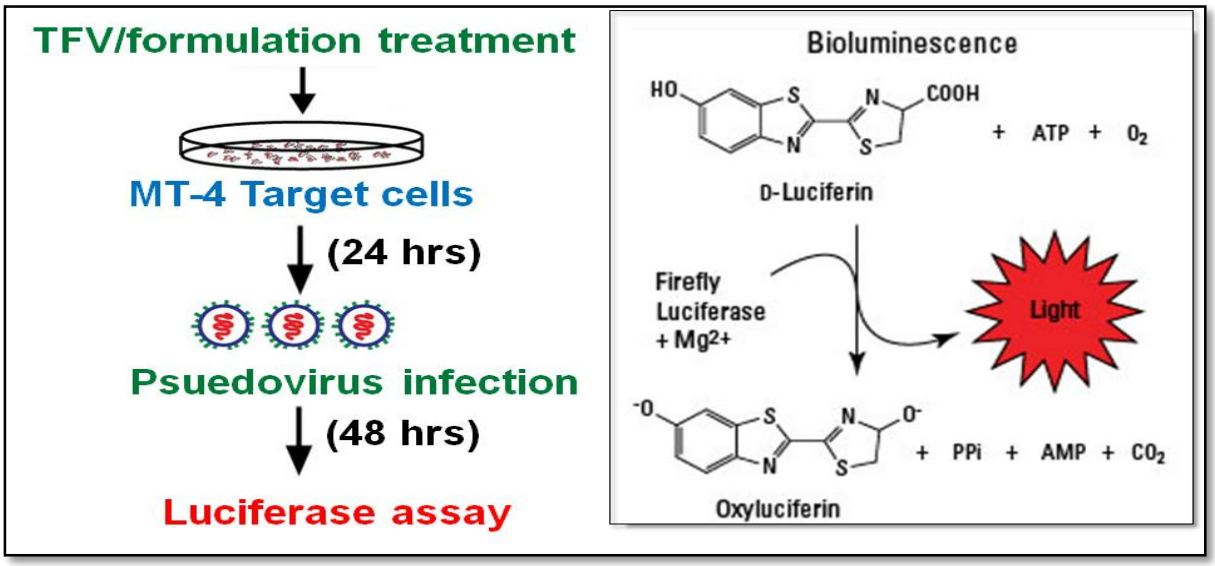

Figure 44. Luciferase Assay Protocol.

In Vitro Cytotoxicity Assay of HA-NPs on MT-4 Cells

The *in vitro* cytotoxicity assay was performed up to 48 h incubation using the MTS cell viability assay. Briefly, MT-4 cells were seeded to 96-well plates in RPMI 1640 medium (Invitrogen, Carlsbad, CA) supplemented with 10% fetal bovine serum (FBS) and were

allowed to grow until 80% confluence was reached. The medium was replaced with 100 µL of samples suspended in culture medium at different concentrations of HA-NPs or HA-SH-NFs (equivalent to the TFV dose of 0.035-35 µM) and pseudotyped virus particles with MOIs of 10,000, 5,000, and 1,000. The samples were kept in contact with the cells for 24 h at 37°C. After the incubation, 20 µL of CellTiter 96® Aqueous One Solution Reagent (Promega, Madison, WI) was added to each well and the absorbance was measured at 490 nm after 3 h incubation at 37°C. The absorbance was directly proportional to the number of viable cells as analyzed by using Eq. (37). Cells with no treatment and those treated with 1% Triton-X-100 were considered as negative and positive controls, respectively.

$$Viability(\%) = \frac{ABS\ (test)}{ABS\ (control)} \times 100 \quad (37)$$

Where, *ABS (test)* and *ABS (control)* represented the absorbance of the amount of formazan product formed in viable cells.

Statistical data analysis

The experimental values were generally presented as mean ± standard deviation (SD) of triplicate determinations (n = 3). All animal experimental conditions (treatments and time points) were tested in a group of at least four mice unless otherwise mentioned. Statistical data analysis was evaluated using Students t-test with 95% confidence interval (CI). A *p value* < 0.05 was considered statistically significant.

5.3. Results and Discussion

Preclinical Safety and Toxicity Analysis in Mice Model

The osmolality of a vaginal microbicide formulation could have profound effects on the vaginal environment and epithelium which could enhance HIV vaginal transmission and

infection (240, 241). The normal osmolality of female vaginal secretions and human seminal fluid was reported in the range of 260-290 mOsm/kg and 250-380 mOsm/kg, respectively, (128, 242). In this study, the osmolality values determined for each tested samples were well below the recommended osmolality for intra-vaginal application (<400 mOsm/kg) (231, 232) except for the N-9 (>1200 mOsm/kg). During the samples treatments, mice were inspected daily and no alterations in behavior, body weight, or temperature was noted between the treatment and control mice groups (data not shown). It was observed that Depo-Provera treatment maintained the diestrus conditions in the mice vagina as analyzed up to 9 days whereas, control mice (no Depo-Provera treatment) showed changes in the estrous cycle stages (appearance of the different types of cells) at different days (Figure 45).

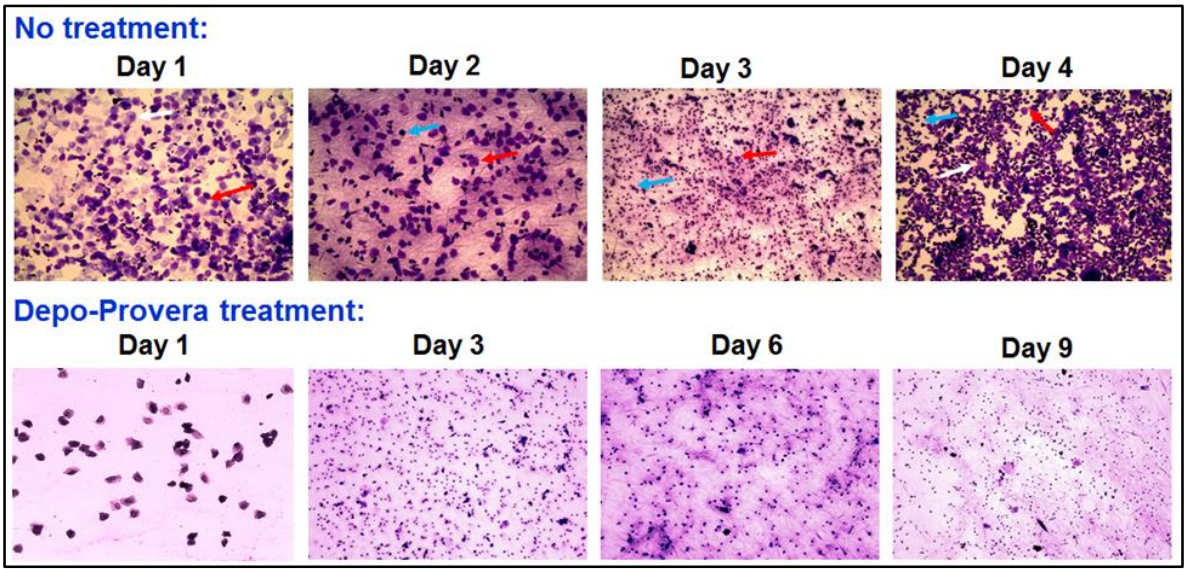

Figure 45. Cytological Assessment of Mouse CVL to Identify the Estrous Cycle Stages. Three Main Cell Types Detected in Mice CVL were: Nucleated Epithelial Cells (White Arrow); Cornified Squamous Epithelial Cells (Red Arrow); and Leukocytes (Blue Arrow).

The histological analysis of the mice genital tract (vagina, cervix, uterus, and ovary), rectum, and other organs (spleen, lung, liver, kidney, heart, brain) did not show any signs of

toxicity and damage upon once-daily administration of TFV loaded HA-NPs or HA-SH-NFs up to 24 h (Figure 46A & 46B), and 7 days (Figure 47A & 47B), respectively.

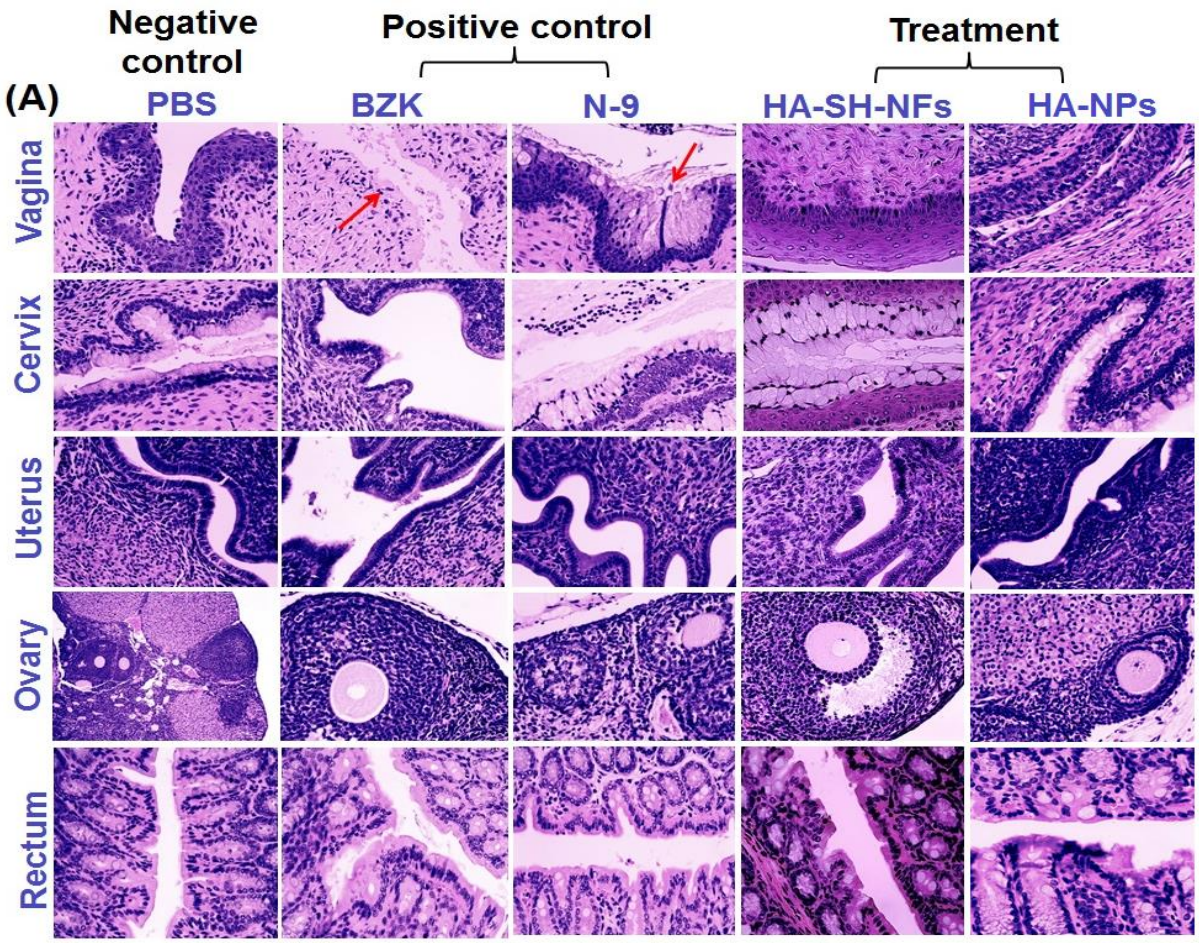

Figure 46A. Preclinical Safety Evaluation of HA-NPs and HA-SH-NFs Analyzed After 24 h Exposure to Mice Genital Tract Tissues (Vagina, Cervix, Uterus, Ovary) and Rectum.

In case of the vagina, no changes to the typical histological architecture were observed in mice treated with nanoformulations and PBS (negative control groups). However, a clear thinning of the vaginal epithelium and stripping (damage) of the epithelium was observed (indicated by red arrows) following 24 h treatment in the N-9 and BZK treated mice (positive control groups) (Figure 46A) and a layer of dead cells was shown after 7 days treatment (Figure 47A).

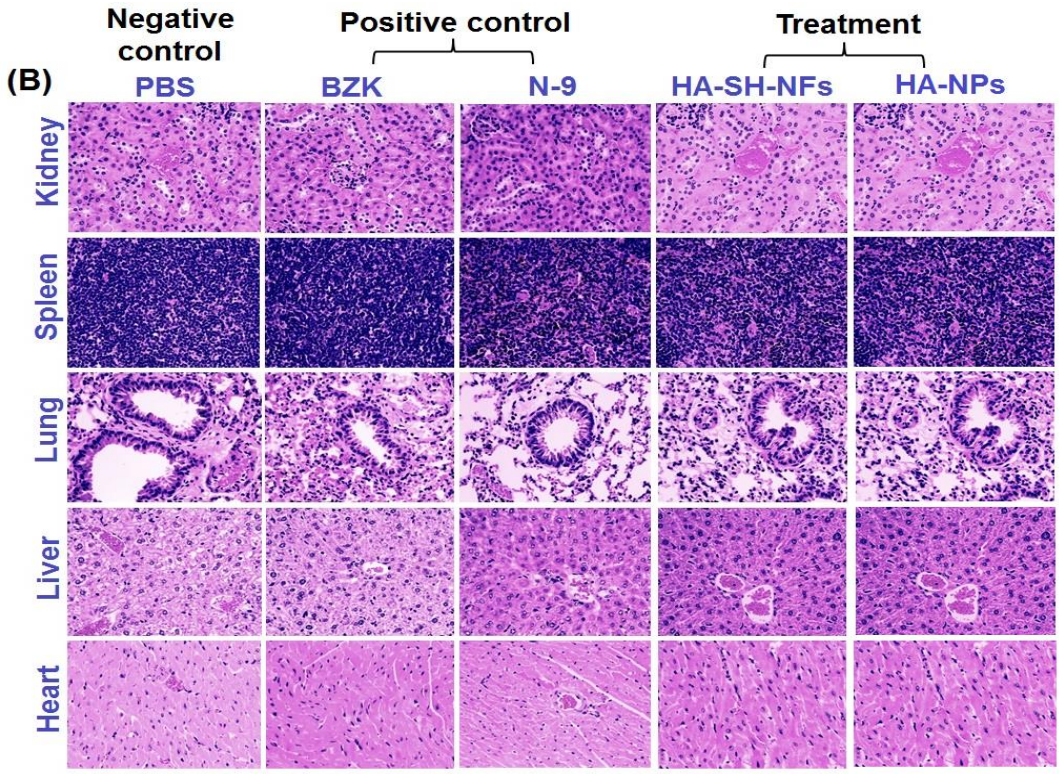

Figure 46B. Preclinical Safety Evaluation of HA-NPs and HA-SH-NFs Analyzed After 24 h Exposure to Mice Body Tissues (Kidney, Spleen, Lung, Liver, Heart).

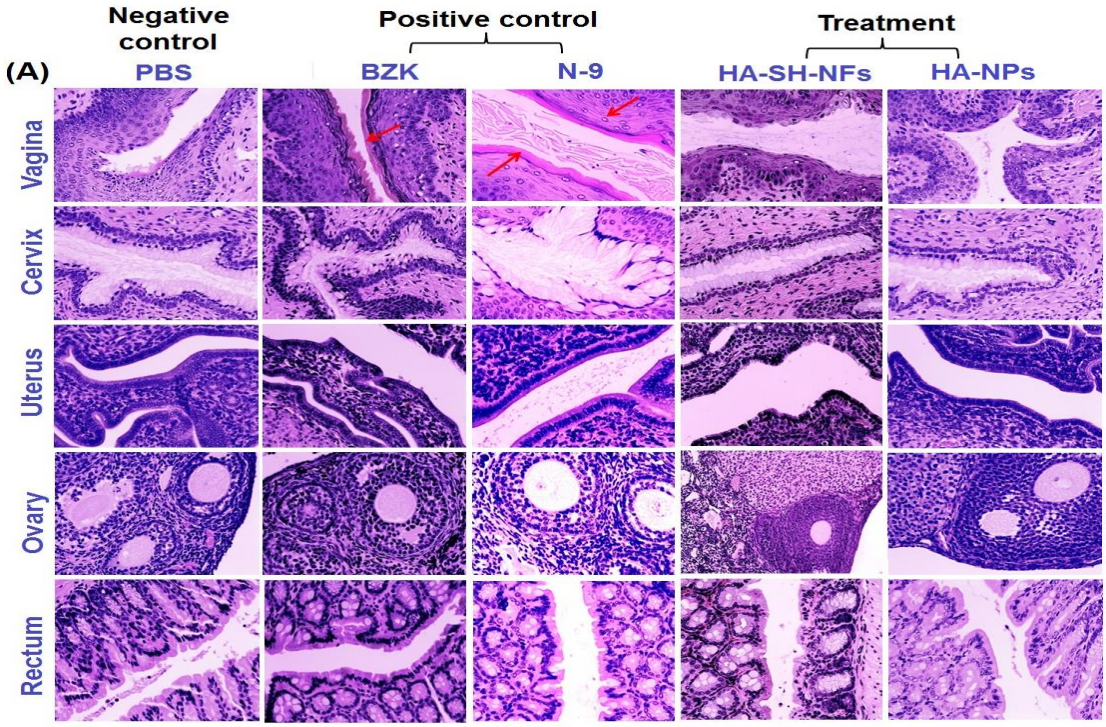

Figure 47A. Preclinical Safety Evaluation of HA-NPs and HA-SH-NFs Analyzed After 7 Days Exposure to Mice Genital Tract Tissues (Vagina, Cervix, Uterus, Ovary) and Rectum.

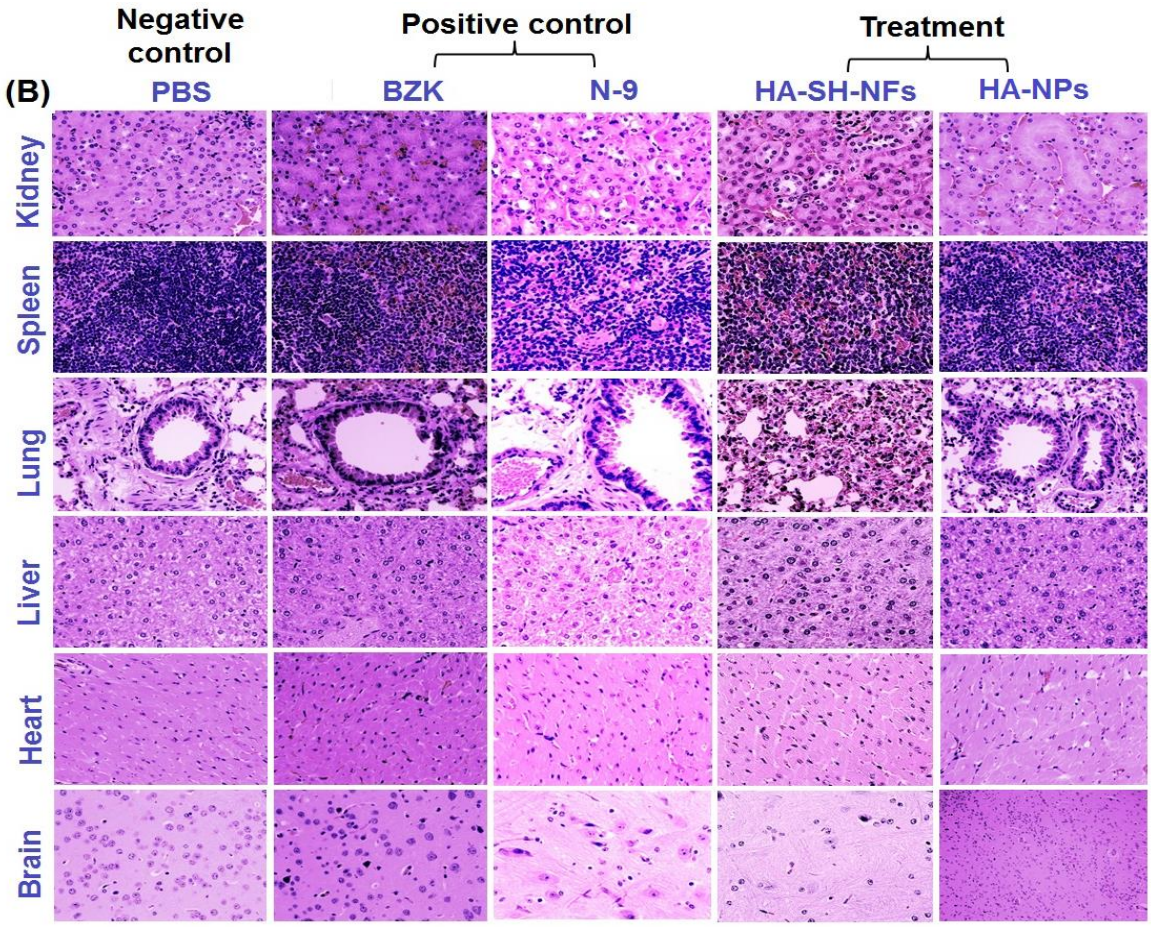

Figure 47B. Preclinical Safety Evaluation of HA-NPs and HA-SH-NFs Analyzed After 7 Days Exposure to Mice Tissues (Kidney, Spleen, Lung, Liver, Heart, Brain).

These observations further supported the toxicity of N-9 and BZK to the vaginal mucosa. For the uterus and ovary, no signs of alterations were observed in the presence of any of the tested samples including the positive controls. This suggested that N-9 and BZK were not able to reach the upper genital tract in sufficient quantities to produce any toxicity or damage. Overall, the preclinical safety data showed that the developed HA-NPs and HA-SH-NFs were safe *in vivo* at the concentrations tested.

Immunoassay of Cytokines Secretion in CVL

The levels (pg/mL) of 7 different cytokines including IL-1α, IL-1β, IL-6, IP-10, IL-7, MKC, and TNF-α, in mice CVL and CV tissues were analyzed after 24 h exposure with PBS

(negative control), N-9 and BZK (positive controls), and HA-NPs/HA-SH-NFs (treatments). The role of these cytokines in HIV virus vaginal transmission and infection is summarized below.

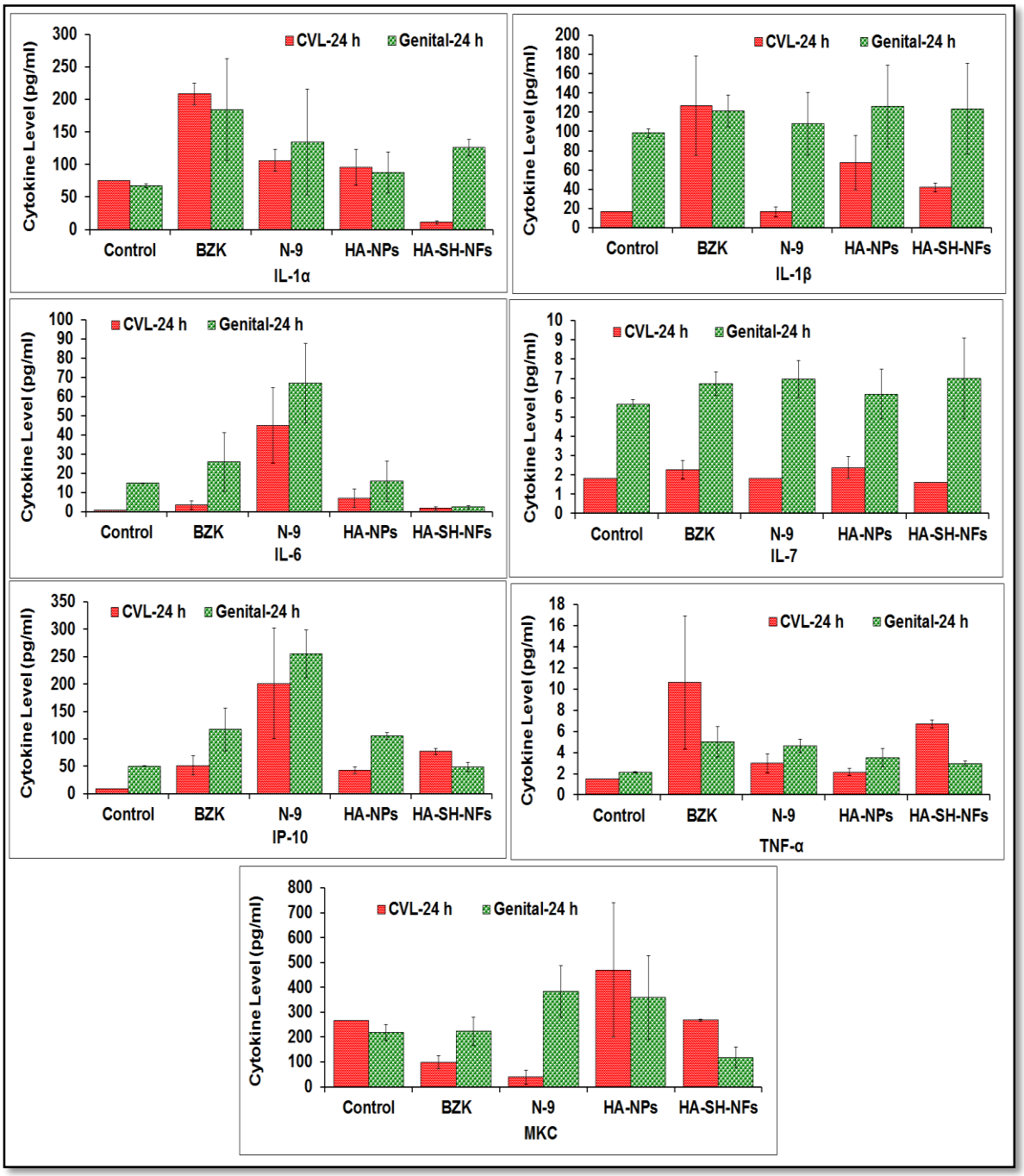

Figure 48. Cytokines (IL-1α, IL-1β, IL-6, IP-10, IL-7, MKC, TNF-α) Levels (pg/mL) after 24 h Exposure with TFV Loaded HA-NPs and HA-SH-NFs in Female C57BL/6 mice CVL and CV Tissues. Results are given as mean ± SD, n = 3.

The IL-1α and IL-1β are efficient inducers of the pro-inflammatory signals, released by injured epithelial tissues and enhance the HIV replication process (217). IL-6 enhance the HIV replication process and act as a growth factor for HIV virus. It has been recently shown that IL-7 facilitates HIV transmission to CV tissues (243). In addition, IL-7 also promotes HIV persistence during antiretroviral treatment by enhancing residual levels of viral production and inducing the proliferation of latently infected $CD4^+$ T cells (244). Thus, it is important to check the levels of IL-7 after a microbicide formulation application. IP-10 is significantly associated with high vaginal viral load and its higher level decreases the T-cell functions in HIV infected individuals on retroviral therapy (39). MKC is equivalent to human IL-8 cytokine which stimulates the HIV replication process (245). TNF-α is one of the most important pro-inflammatory cytokines that induces the levels of IL-6 and IL-8 and helps in upregulation of HIV replication (217).

It was observed that the levels of most of the cytokines was not significantly induced after HA-NPs or HA-SH-NFs treatments for 24 h compared to the control CVL and genital tissue samples (Figure 48). The levels of few cytokines was found to be higher than the control, samples however, the values were well below than their standard values. The cytokine release data supported that HA-NPs and HA-SH-NFs were potentially non-immunogenic for vaginal application.

Identification of Inflammatory Cells in CV Tissues

Following 24 h exposure, negative control (Figure 49A), HA-NPs (Figure 49D) and HA-SH-NFs (Figure 49E) treated mice tissues did not show any significant immune cell infiltration in the genital tract which suggested the lack of vaginal inflammation but, few surface and luminal lymphocytes were observed. However, a significant number of immune cells infiltrate were noted in BZK (Figure 49B) and N-9 (Figure 49C) treated mice (indicated by red arrows). Very few, but not significant CD45 cells were observed after 7 days treatment

with HA-SH-NFs compared to BZK or N-9 treated groups. Overall, the cytokine and immunohistochemistry data supported that HA-NPs and HA-SH-NFs were potentially safe for vaginal application.

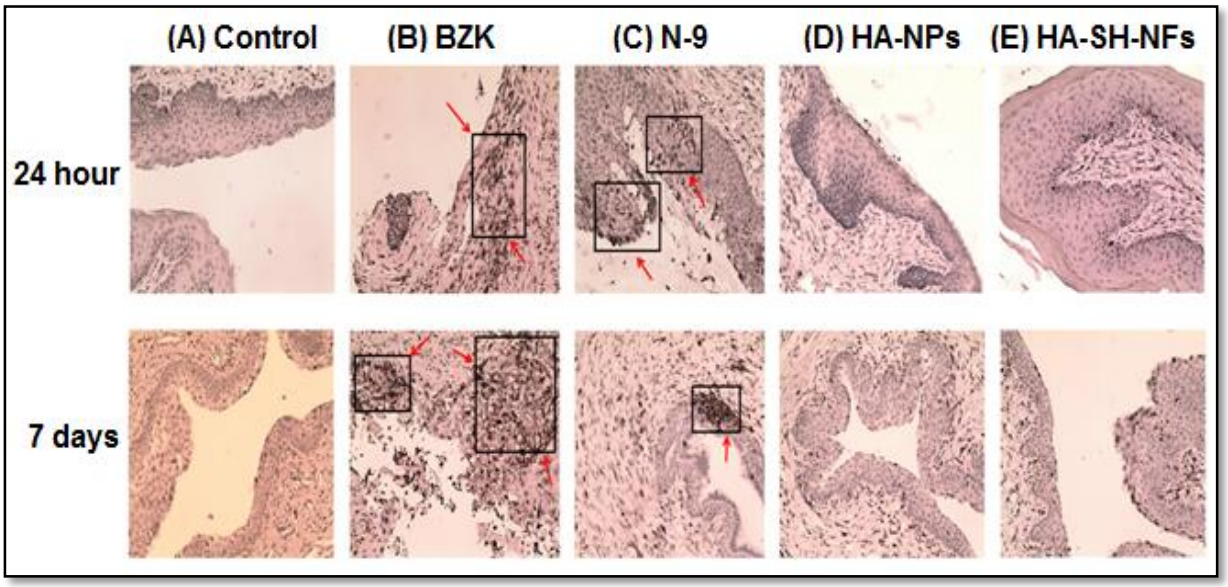

Figure 49. Immune Cells (CD45) Infiltration on Female C57BL/6 Mice Vaginal Tissues after 24 h and 7 Days Exposure. (A) Control. (B) BZK. (C) N-9. (D) TFV Loaded HA-NPs at the Dose of 25 mg/kg (equivalent to the drug dose of ~6.5 mg/kg). (E) TFV Loaded HA-SH-NFs at the Dose of 275 mg/kg (equivalent to the drug dose of ~46 mg/kg). Red Arrows Showed the CD45 Cells Infiltration in C57BL/6 mice CV Tissues.

In Vitro Anti-HIV Activity of Nanoformulations (HA-NPs and HA-SH-NFs)

Pseudotyped Virus Particle Generation and Characterization

The pseudotyped HIV virus particles were generated using plasmid transfection method (Figure 43) and analyzed using nanoparticle tracking analysis (NTA) measurements (Figure 50). The mean diameter of the virus particles was found to be 128.00 ± 15.53 nm (n = 6). The virus titer (number of particles/mL) was determined to be $3.07 \times 10^{10} \pm 0.30$/mL (n = 6) in cell culture media. A clear difference between the background and the sample containing

pseudotyped virus particles was observed (Figure 50) which also confirmed the presence of pseudotyped HIV virus particles and they are successfully generated.

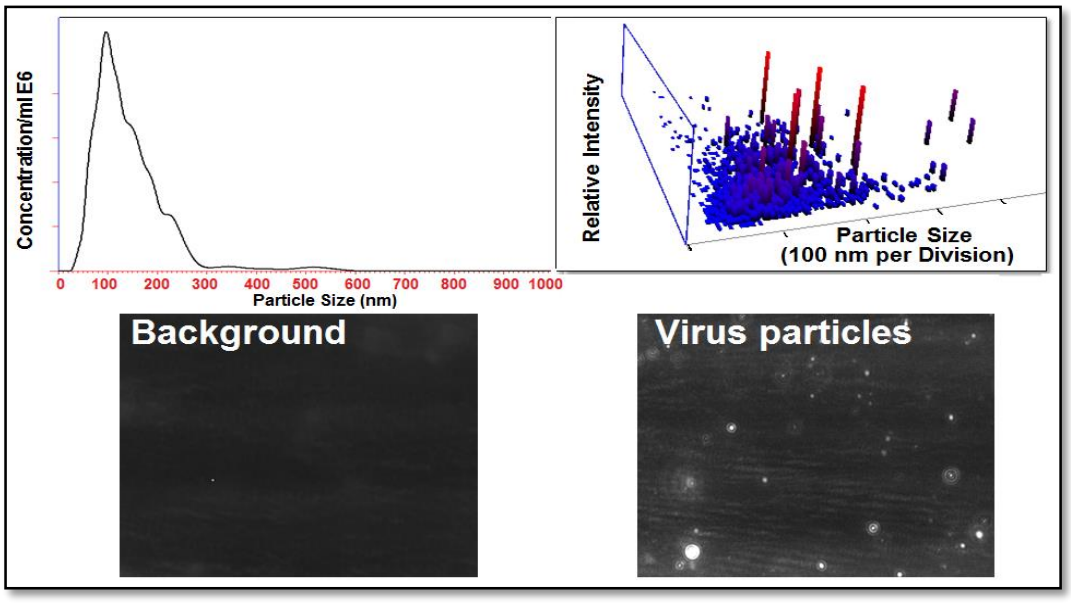

Figure 50. Characterization of Pseudotyped HIV Virus Particles Generated by Plasmid Transfection Method Using Nanoparticle Tracking Analysis (NTA) Measurements.

In Vitro Anti-HIV Activity of HA-NPs

The HIV virus replication inhibition efficacy of HA-NPs was analyzed at the concentration that is equivalent to the TFV dose of 0.035-35 µM and at the MOI of 10,000 (Figure 51A), 5,000 (Figure 51B) and 1,000 (Figure 51C).

Results showed that the HA-NPs have significantly higher anti-HIV activity against the pseudotyped virus replication compared to the free TFV (n = 3) at the MOI of 5,000 and 1,000 in all concentrations except the 35 µM. However, the efficacy of NPs was not significantly different compared to the free TFV at the MOI of 10,000. This could be due to the presence of very high number of virus particles compared to the number of cells at the MOI of 10,000. The HA-NPs were found to be non-cytotoxic to MT-4 cells and there was no statistically significant

effect ($p > 0.05$) on the viability of MT-4 cells, compared to the cell culture medium is observed (n = 3) (Figure 52).

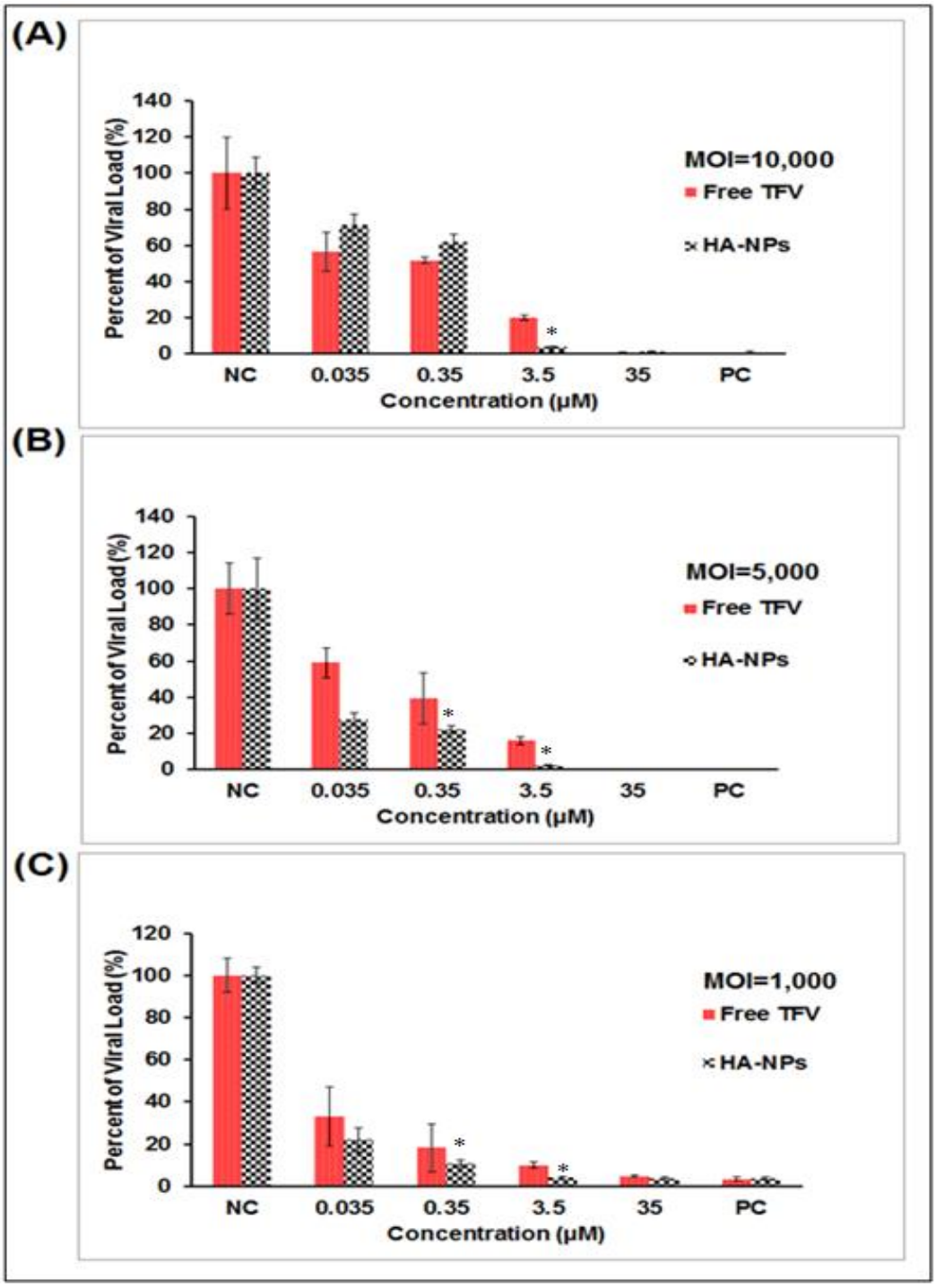

Figure 51. *In vitro* Anti-HIV Activity of TFV Loaded HA-NPs: (A) At the MOI of 10,000 (B) At the MOI of 5,000. (C) At the MOI of 1,000. Results are given as mean ± SD, n = 3. Asterisk (*) indicated the significant effect ($p < 0.05$) of NPs compared to free TFV at the same dose.

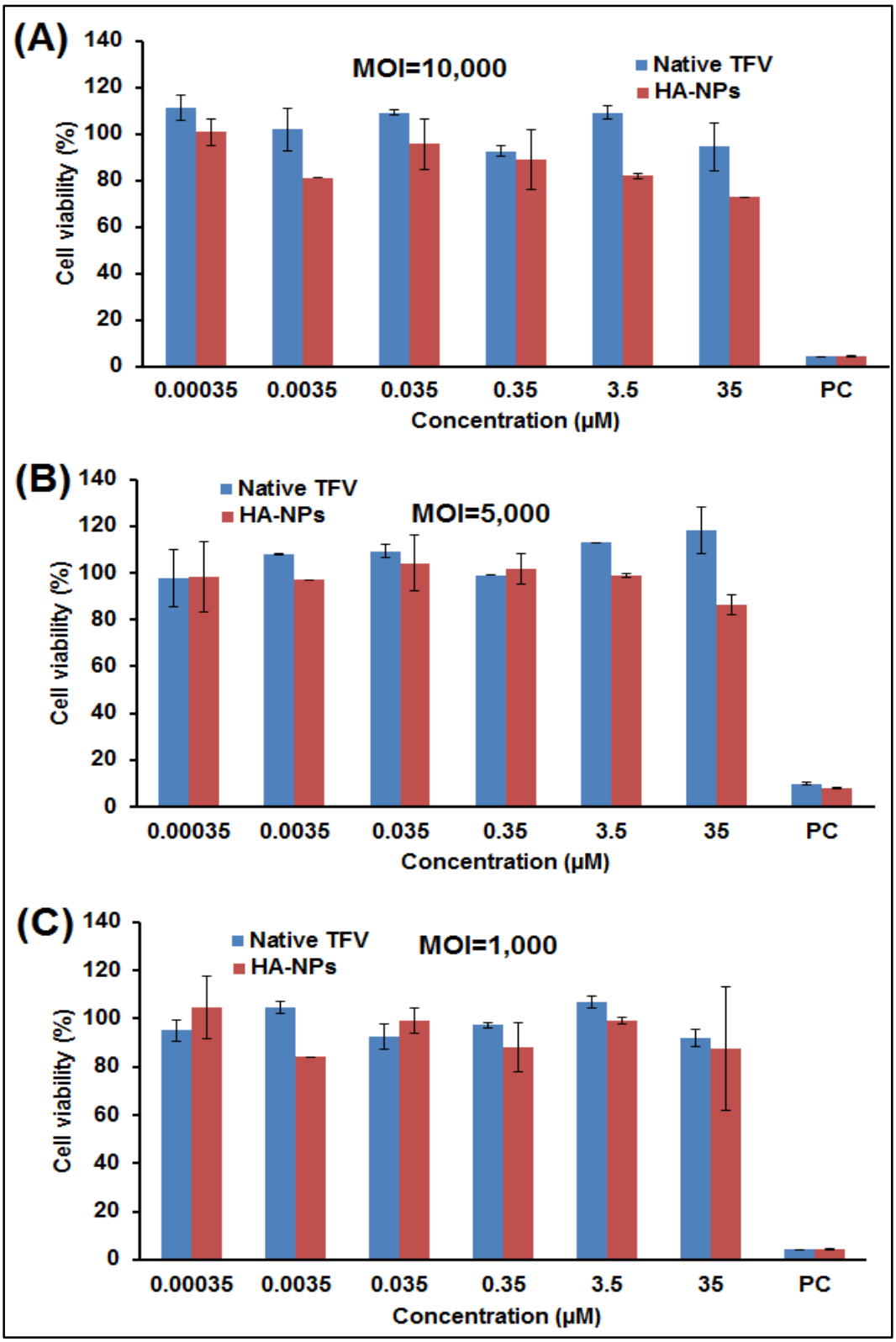

Figure 52. Cytotoxicity assay and effect of HA-NPs on the viability of MT-4 cell line analyzed by MTS assay. Results are given after 48 h of incubation as mean ± SD, n = 3.

In Vitro Anti-HIV Activity of HA-SH-NFs

The *in vitro* anti-HIV activity data (n = 3) of HA-SH-NFs at the MOI of 10,000 (Figure 53A), 5,000 (Figure 53B) and 1,000 (Figure 53C) showed that the NFs effectively inhibited the virus replication process. The *in vitro* anti-HIV activity of free TFV and TFV loaded HA-SH-NFs was significantly increased as the MOI was lowered from 10,000 to 1,000. This could be due to the presence of fewer virus particles exposed to the native TFV or TFV loaded HA-SH-NFs as MOI was lowered. However, the anti-HIV effect was not significantly different compared to that of the free TFV at all MOIs. This could be due to the facts that the cell treatment with the pseudotyped HIV virus was performed after the 24 h treatment with HA-SH-NFs and by that time, most of the encapsulated drug was released out of the NFs as shown in their release profile graphs (Figure 38). This probably led to have an equal amount of free TFV in the HA-SH-NFs treated cells as in free TFV treated cells and thus, produced almost the similar anti-HIV activity. These observations were consistent with recent studies by other researchers where they also observed that the anti-HIV activity of TFV encapsulated in nanofibers was similar to that of unformulated or free TFV (246).

Although, the anti-HIV activity of free TFV and TFV in HA-SH-NFs was not significantly different, the results suggested that the drug maintained its structural integrity, and the activity of TFV was unaffected by composite geometry of HA-SH-NFs. In addition, drug formulations such as NFs have several advantages compared to the free drug, including sustained and controlled release system, leading to better drug delivery than free drugs in solution, with a potential reduction in the side effects, and drug instability issues. In this respect, anti-HIV activity assay needs to be perform at different time points after HA-SH-NFs treatment in the presence and absence of HAase enzyme to determine the enzyme responsiveness of these nanoformulations (NPs and NFs). Comparing the anti-HIV activity of TFV loaded HA-NPs

and HA-SH-NFs, HA-NPs seemed to have higher efficacy. This was due to the several facts as explained below.

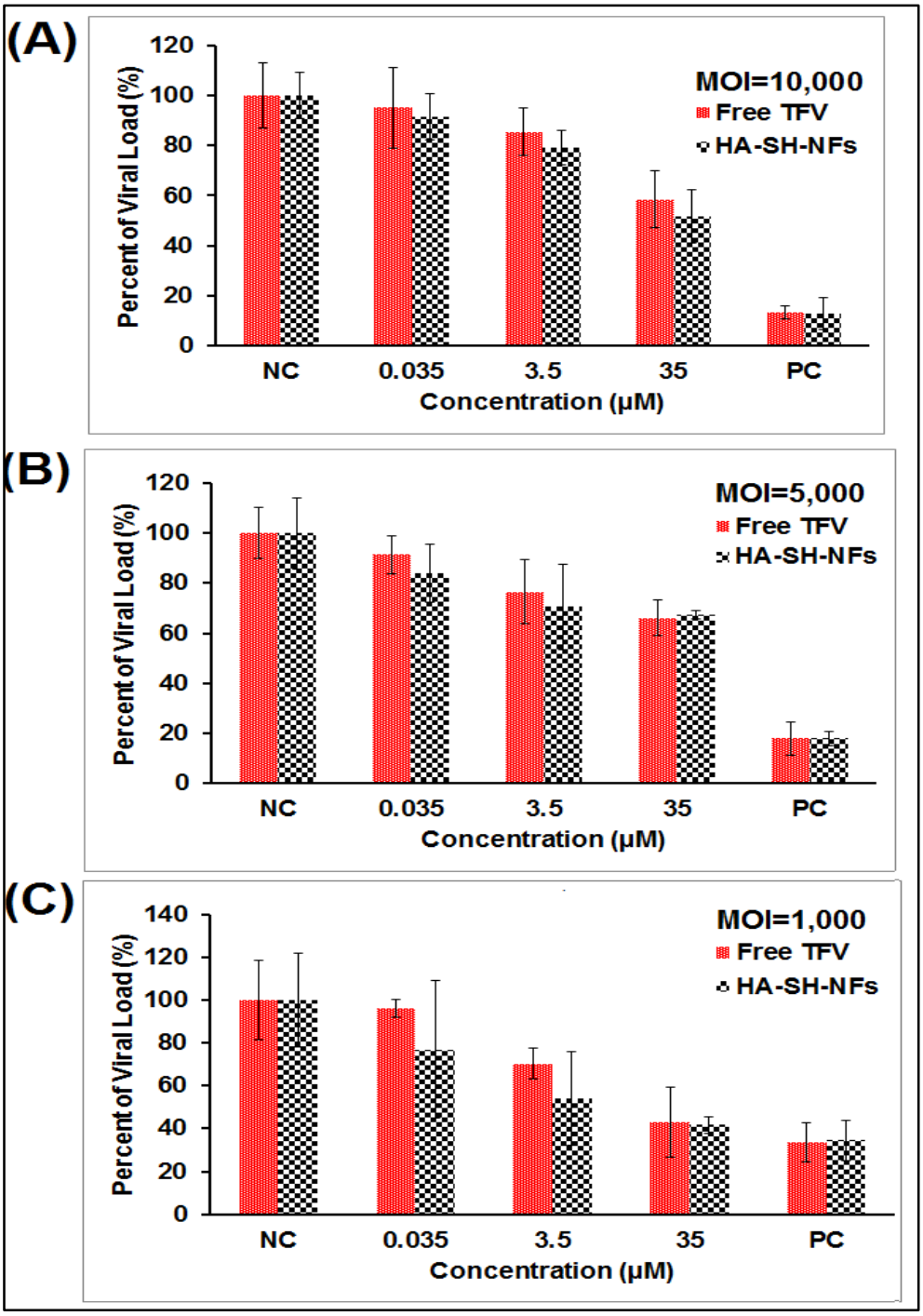

Figure 53. *In Vitro* Anti-HIV Activity of TFV loaded HA-SH-NFs: (A) At the MOI of 10,000. (B) At the MOI of 5,000. (C) At the MOI of 1,000. Results are given as mean ± SD, n = 3. Asterisk (*) indicated the significant effect ($p < 0.05$) of TFV loaded HA-NPs compared to free TFV at the same dose concentration.

Tenofovir used as a model microbicide in this study, belongs to the category of anti-retroviral drugs under the sub-category of nucleotide RT inhibitors. The nucleotide analogues must undergo a series of phosphorylation steps by intracellular kinases to transform into their active triphosphate metabolites. Thus, they need to get inside the cells either through passive diffusion or carrier-mediated transport to produce their antiviral effects. Usually, the nucleotide analogues such as tenofovir are highly hydrophilic in nature and have limited cell membrane permeability. The NPs has been proven to have a higher cellular uptake by several pathways because of their small diameter, targeting efficiency, and surface chemistry (247). It has been previously reported that the particle size contributes to the cellular internalization pathways and particles with a diameter < 200 nm enter cells preferentially via clathrin-mediated endocytosis (248). The HA-NPs formulated (chapter 3) with a mean diameter of ~70-80 nm supposed to have a higher cellular uptake compared to the NFs formulation due to the longer structure, non-spherical geometry, and mucoadhesive properties. These all helped NFs to stay longer at the cell surfaces rather than being up taken by the cells. All of these factors caused the low amount of TFV that has been up taken by cells and thus hindered the antiviral effect of TFV in case of NFs compared to the NPs.

In this dissertation, stimuli-sensitive nanoformulations have been developed those supposed to be stayed at the vaginal surface until the arrival of seminal fluid including the hyaluronidase enzyme. In this respect, the NFs is an appropriate model since, it will have higher bio-retention and less cellular uptake due to the facts as explained above compared to the NPs design. However, this remains to be elucidated in the future *in vivo* time-responsiveness and bio-retention of these nanoformulations in the presence of seminal fluid and hyaluronidases.

Bio-retention and Distribution of FITC labelled HA-NPs in the Mouse Vagina

The bio-retention and distribution of the HA-NPs in the vaginal tract was investigated after intravaginal application of FITC-labelled HA-NPs (25 mg/kg) using a female C57Bl6 mice. The mice were sacrificed at 15min, 30min, 8h, and 24 h post-treatment immediately before dissecting out the vagina. After dissection, the entire vagina was slit open lengthwise and flat-mounted on microscope slides. Images of the flat-mounted vagina was viewed and captured using a Nikon Labophot-2 microscope (Nikon Instruments, Inc., Melville, NY) equipped with a PAXCam digital microscope camera and analyzed using PAX-it image management and analysis software (Midwest Information Systems, Inc., Villa Park, IL).

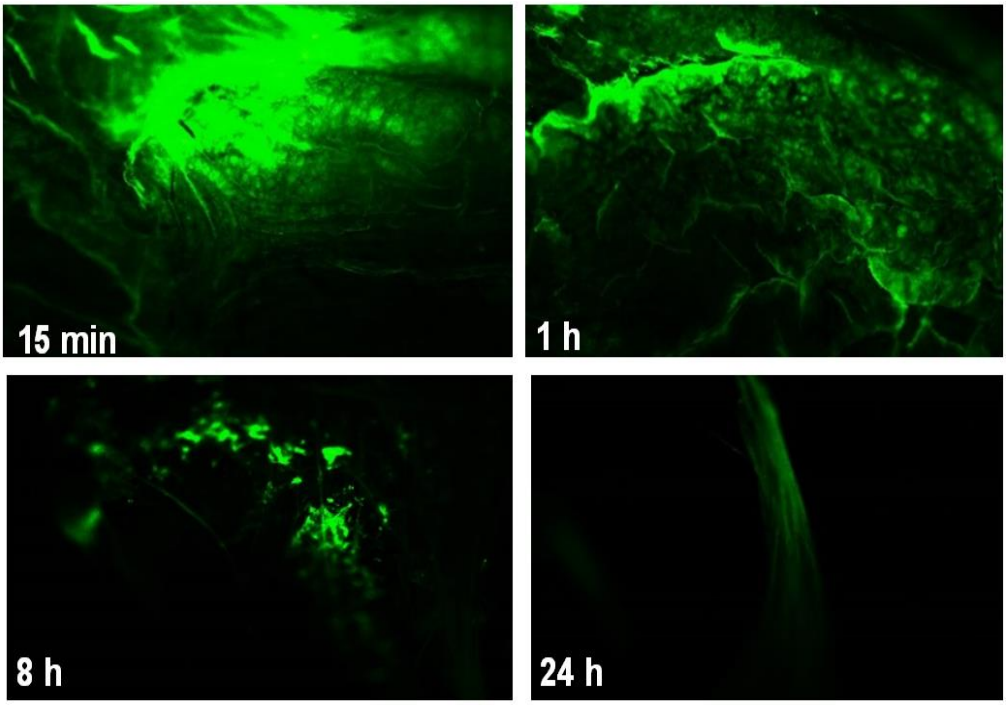

Figure 54. Vaginal Distribution of FITC-labelled HA-NPs (25mg/kg) in Female C57BL/6 Mice.

The results demonstrated the HA-NPs were distributed throughout the vaginal lumen. However, the bio-retention was very low as after 24 h, very few HA-NPs were observed in the vaginal tract (Figure 54). The results showed that the HA-NPs did not have a long residence time in mice vagina and leaked-out quickly due to their low or negligible mucoadhesion

properties and small diameter. In this respect, mucoadhesive HA-SH-NFs developed in Chapter 4, would have a better bio-retention in mice vagina due to their thiolated surface chemistry and non-spherical geometry to fulfill the goal of stimuli-sensitive formulation development in this dissertation. However, this remain to be analyzed in the future studies.

5.4. Conclusion

In this study, preclinical evaluation of HA based nanoformulations (HA-NPs and HA-SH-NFs) was performed in C57BL/6 mice model. Histological analyses confirmed the safety of NPs and NFs in mice genital tract tissues and other organs. The HA-NPs or HA-SH-NFs did not induce any CD45 immune cell infiltration in genital tract tissues. The cytokine release levels were not significantly changed for most of the tested cytokines in CVL and CV tissues. The *in vitro* anti-HIV activity data showed that the drug loaded HA-NPs and HA-SH-NFs were able to inhibit the pseudotyped HIV virus replication and the anti-HIV activity of TFV was preserved after the nanofabrication processes. Results showed that the HA-NPs have significantly higher anti-HIV activity against the pseudotyped virus replication compared to the free TFV at the MOI of 5,000 and 1,000 for most of the concentrations tested. However, the efficacy of NPs was not significantly different compared to the free TFV at the MOI of 10,000. The *in vitro* anti-HIV activity data of HA-SH-NFs showed that the NFs effectively inhibited the virus replication process. Although, there was no significant difference was observed compared to the free TFV. Overall, the data presented here highlight the potential of developed NPs and NFs templates for the vaginal delivery of anti-HIV/AIDS microbicides.

Acknowledgments

The project was supported by Award Number R01AI087304 from the National Institute of Allergy and Infectious Diseases (Bethesda, MD).

CHAPTER 6

SUMMARY, CONCLUSION AND FUTURE DIRECTIONS

6.1. Summary and Conclusion

In this dissertation, two different kinds of nanoformulations templates (nanoparticle and mucoadhesive nanofiber) have been developed. These formulations were loaded with an anti-HIV topical microbicide (tenofovir) and designed to have a stimuli-sensitive effect in the presence of semen hyaluronidase enzyme for HIV virus vaginal transmission prevention in women. The physicochemical properties such as mean diameter, drug loading, surface morphology, stability, *in vitro* drug release profile and drug release kinetics were evaluated. The *in vitro* cytotoxicity, preclinical safety, and anti-HIV activity of these formulations were also performed.

In chapter 3, hyaluronic acid based nanoparticles (HA-NPs) were designed and formulated using surfactant free cross-linking method to test the hypothesis that a triggered release of a microbicide (tenofovir) from HA-NPs can be achieved under the influence of seminal hyaluronidase enzyme. The Fractional Factorial Experimental Design was employed to examine the effect of various formulation and process variables on NPs. The HA-NPs were characterized for their particle mean diameter, size distribution, surface morphology, cross-linking chemistry, *in vitro* enzymatic degradation, stability, and *in vitro* drug release profile. HA-NPs exhibited a spherical shape with mean diameter of ~75 nm. The HAase enzyme notably triggered the drug release and HA degradation from the NPs after 24 h (~90% w/w and 65% w/w, respectively); whereas, in its absence, these values were ~39% w/w and 26% w/w, respectively. The HAase triggered drug release from the HA-NPs took about 24 h to reach ~90% w/w and was the major limitation of this design. Moreover, these HA-NPs systems found

to have a short vaginal retention time *in vivo* as analyzed using C57BL/6 mice model and explained in chapter 5. The NPs were found to be non-cytotoxic to human vaginal VK2/E6E7 and End1/E6E7 cells and had no effect on *Lactobacillus* bacteria viability. These data suggested the possibility of using HA-NPs as a delivery system for intravaginal delivery of topical microbicides for the prevention of HIV transmission after successful improvement of the HAase enzyme effectiveness and bio-retention time. Overall, the NPs provided a better control over drug release compared to the HA-gel. The study suggested that ultimately suspending the TFV loaded NPs in TFV loaded HA-gel formulation might be an alternative formulation for effective prevention of the HIV virus transmission. In this case, the gel would provide a bolus dose for immediate drug release before the HIV virus crosses the CV mucosa (in about 2-6 h) followed by a semen-triggered drug release from NPs for at least 72 h after the sexual intercourse.

Based on the knowledge gained in chapter 3, stimuli-sensitive and mucoadhesive thiolated nanofibers loaded with a vaginal microbicide (tenofovir) were formulated in chapter 4 for the prevention of HIV virus vaginal transmission in women. A novel thiolated sulfhydryl (-SH) group modified HA (HA-SH) was first synthesized and characterized to fabricate the TFV loaded HA-SH-NFs (mean diameter ~75 nm) using coaxial electrospinning method. The synthesized HA-SH-NFs were characterized for their physicochemical properties including size distribution, surface morphology, surface chemistry, crystallinity, mucoadhesion property, and *in vitro* drug release profile. Mucin interaction and ellipsometer measurements confirmed the higher mucoadhesion of HA-SH-NFs compared to native HA. A triggered drug release (~87 %w/w) from HA-SH-NFs compared to the HA-NPs was observed after 1 h of incubation in the presence of seminal HAase enzyme. This could be due to the porous surface geometry and absence of any cross-linking chemistry at the HAase enzyme target size (carboxylic acid groups) compared to the HA-NPs. Moreover, the large surface areas to volume ratios of NFs

provided a larger area for drug interaction with the surrounding medium which facilitated the mass transfer and thus, a fast release of therapeutic molecules was observed. The HA-SH-NFs were non-cytotoxic to vaginal VK2/E6E7 and End1/E6E7 cells and *L. crispatus* bacteria analyzed up to for 48 h. In addition, NFs confirmed to have a higher mucoadhesion due to the presence of thiol groups on their surface. Collectively, the results suggested that TFV loaded HAase sensitive HA-SH-NFs templates developed in this study have the potential of vaginal delivery of microbicides for the prevention of HIV transmission.

In chapter 5, the developed HA-NPs and HA-SH-NFs formulations were evaluated *in vivo* for their preclinical safety, immunogenicity in female C57BL/6 mice. The histological analysis on the female C57BL/6 mice genital tract and other organs did not show any signs of damage upon once-daily administration of these nanoformulations up to 7 days. Following 24 h of exposure, HA-NPs or HA-SH-NFs did not show any significant CD45 cell infiltration in mice vaginal tissues. The cytokines levels in CVL and CV tissues were not significantly changed compared to control (treated with PBS) mice groups analyzed after 24 h. The *in vitro* anti-HIV activity data showed that the TFV loaded HA-NPs and HA-SH-NFs were able to inhibit the pseudotyped HIV virus replication and the anti-HIV activity of TFV was preserved after the nanofabrication processes. Results showed that the HA-NPs have significantly higher anti-HIV activity against the pseudotyped virus replication compared to the free TFV at the MOI of 5,000 and 1,000 for most of the concentrations tested except at 35 µM equivalent of drug dose. However, the efficacy of NPs was not significantly different compared to the free TFV at the MOI of 10,000. The *in vitro* anti-HIV activity data of HA-SH-NFs showed that the NFs effectively inhibited the virus replication process, although there was no significant difference was observed compared to the free TFV. This could be due to the facts that the cell treatment with the pseudotyped HIV virus was performed after the 24 h treatment with HA-SH-NFs and by that time, most of the encapsulated drug was released out of the NFs as shown

in their release profile graphs. This probably led to have an equal amount of free TFV in the HA-SH-NFs treated cells as in free TFV treated cells and thus, produced the similar anti-HIV activity. These observations were consistent with recent studies by other researchers where they also observed that the anti-HIV activity of TFV encapsulated in nanofibers was similar to that of unformulated TFV. The anti-HIV activity results suggested that the drug TFV has maintained its structural integrity during the nanofabrication processes either in NPs or NFs.

The developed HA-NPs and HA-SH-NFs formulations are compared here;

Parameters	**HA-NPs**	**HA-SH-NFs**
Manufacturing feasibility	√	√ √
Scalability	√	√
Cost-effectiveness	√	√
Drug compatibility/loading	√	√ √
Stability	√ √	√
Enzyme sensitiveness	√	√ √
Bioretention	√	√ √*****
Preclinical safety	√	√
In vitro anti-HIV activity	√ √*****	√

√: High; √√: Very High; *: remains to be elucidated.

Overall, the dissertation work presented here demonstrated the applicability of two different kinds of stimuli-sensitive nanoformulations for the topical vaginal delivery of anti-HIV/AIDS microbicide candidates. These formulations are promising delivery systems and offered a safe delivery of anti-HIV microbicide candidates.

6.2. Future Directions

- Expand the application of nanoformulations templates to other topical microbicides (fusion/entry inhibitors) alone or in combination with reverse transcriptase inhibitors.
- Optimize the scalability and cost-effectiveness of developed nanoformulations to eventually meet the actual needs of third world countries.
- Address the potential *in vivo* time-responsiveness and drug release in the presence of seminal fluid and hyaluronidase enzyme.
- Analyze the *in vivo* anti-HIV efficacy of developed nanoformulations in an appropriate animal model.
- Biodistribution and pharmacokinetic profiling of nanoformulations in animal model.
- *In vivo* retention and mucoadhesion studies in animal model.

APPENDIX

SPRINGER LICENSE

TERMS AND CONDITIONS

May 19, 2016

This Agreement between Vivek Agrahari ("You") and Springer ("Springer") consists of your license details and the terms and conditions provided by Springer and Copyright Clearance Center.

License Number	3872730356645
License date	May 19, 2016
Licensed Content Publisher	Springer
Licensed Content Publication	The AAPS Journal
Licensed Content Title	Hyaluronidase-Sensitive Nanoparticle Templates for Triggered Release of HIV/AIDS Microbicide In Vitro
Licensed Content Author	Vivek Agrahari
Licensed Content Date	Jan 1, 2013
Licensed Content Volume Number	16
Licensed Content Issue Number	2
Type of Use	Thesis/Dissertation
Portion	Full text
Number of copies	1

Author of this Springer article	Yes and you are a contributor of the new work
Order reference number	None
Title of your thesis / dissertation	FORMULATION OF HYALURONIDASE ENZYME SENSITIVE TOPICAL NANOMICROBICIDES FOR HIV VIRUS TRANSMISSION PREVENTION
Expected completion date	May 2016
Estimated size(pages)	200
Total	0.00 USD

SPRINGER LICENSE

TERMS AND CONDITIONS

May 19, 2016

This Agreement between Vivek Agrahari ("You") and Springer ("Springer") consists of your license details and the terms and conditions provided by Springer and Copyright Clearance Center.

License Number	3872730514348
License date	May 19, 2016
Licensed Content Publisher	Springer
Licensed Content Publication	AAPS PharmSciTech
Licensed Content Title	Sensitive and Rapid HPLC Quantification of Tenofovir from Hyaluronic Acid-Based Nanomedicine
Licensed Content Author	Vivek Agrahari

Licensed Content Date	Jan 1, 2011
Licensed Content Volume Number	13
Licensed Content Issue Number	1
Type of Use	Thesis/Dissertation
Portion	Full text
Number of copies	1
Author of this Springer article	Yes and you are a contributor of the new work
Order reference number	None
Title of your thesis / dissertation	FORMULATION OF HYALURONIDASE ENZYME SENSITIVE TOPICAL NANOMICROBICIDES FOR HIV VIRUS TRANSMISSION PREVENTION
Expected completion date	May 2016
Estimated size(pages)	200
Total	0.00 USD

JOHN WILEY AND SONS LICENSE

TERMS AND CONDITIONS

May 19, 2016

This Agreement between Vivek Agrahari ("You") and John Wiley and Sons ("John Wiley and Sons") consists of your license details and the terms and conditions provided by John Wiley and Sons and Copyright Clearance Center.

License Number	3872721453740
License date	May 19, 2016
Licensed Content Publisher	John Wiley and Sons
Licensed Content Publication	Drug Testing and Analysis
Licensed Content Title	Evaluation of degradation kinetics and physicochemical stability of tenofovir
Licensed Content Author	Vivek Agrahari, Sandeep Putty, Christiane Mathes, James B. Murowchick, Bi-Botti C. Youan
Licensed Content Date	May 12, 2014
Pages	7
Type of use	Dissertation/Thesis
Requestor type	Author of this Wiley article
Format	Print and electronic
Portion	Full article
Will you be translating?	No
Title of your thesis / dissertation	FORMULATION OF HYALURONIDASE ENZYME SENSITIVE TOPICAL NANOMICROBICIDES FOR HIV VIRUS TRANSMISSION PREVENTION
Expected completion date	May 2016
Expected size (number of pages)	200
Total	0.00 USD

REFERENCES:

1. Li H, Lei N, Zhang M, Li Y, Xiao H, Hao X. Pharmacokinetics of a long-lasting anti-VEGF fusion protein in rabbit. Experimental eye research. 2012;97(1):154-159.
2. UNAIDS/WHO. Report on gobal AIDS epidemic. In. Geneva: UNAIDS; 2009. p. 362.
3. Sanchez-Rodriguez J, Vacas-Cordoba E, Gomez R, De La Mata FJ, Munoz-Fernandez MA. Nanotech-derived topical microbicides for HIV prevention: the road to clinical development. Antiviral research. 2015;113:33-48.
4. Dellar RC, Dlamini S, Karim QA. Adolescent girls and young women: key populations for HIV epidemic control. Journal of the International AIDS Society. 2015;18(2 Suppl 1):19408.
5. Omar RF, Bergeron MG. The future of microbicides. International journal of infectious diseases : IJID : official publication of the International Society for Infectious Diseases. 2011;15(10):e656-660.
6. Smith DK, Herbst JH, Zhang X, Rose CE. Condom effectiveness for HIV prevention by consistency of use among men who have sex with men in the United States. Journal of acquired immune deficiency syndromes. 2015;68(3):337-344.
7. Nelson AG, Zhang X, Ganapathi U, Szekely Z, Flexner CW, Owen A, Sinko PJ. Drug delivery strategies and systems for HIV/AIDS pre-exposure prophylaxis and treatment. Journal of controlled release : official journal of the Controlled Release Society. 2015.
8. Antimisiaris SG, Mourtas S. Recent advances on anti-HIV vaginal delivery systems development. Advanced drug delivery reviews. 2015.
9. Date AA, Destache CJ. A review of nanotechnological approaches for the prophylaxis of HIV/AIDS. Biomaterials. 2013;34(26):6202-6228.

10. Koff WC. HIV vaccine development: challenges and opportunities towards solving the HIV vaccine-neutralizing antibody problem. Vaccine. 2012;30(29):4310-4315.

11. Grammen C, Augustijns P, Brouwers J. In vitro profiling of the vaginal permeation potential of anti-HIV microbicides and the influence of formulation excipients. Antiviral Res. 2012;96(2):226-233.

12. das Neves J, Michiels J, Arien KK, Vanham G, Amiji M, Bahia MF, Sarmento B. Polymeric Nanoparticles Affect the Intracellular Delivery, Antiretroviral Activity and Cytotoxicity of the Microbicide Drug Candidate Dapivirine. Pharm Res. 2011.

13. Wan L, Pooyan S, Hu P, Leibowitz MJ, Stein S, Sinko PJ. Peritoneal macrophage uptake, pharmacokinetics and biodistribution of macrophage-targeted PEG-fMLF (N-formyl-methionyl-leucyl-phenylalanine) nanocarriers for improving HIV drug delivery. Pharm Res. 2007;24(11):2110-2119.

14. Mbopi-Keou FX, Trottier S, Omar RF, Nkele NN, Fokoua S, Mbu ER, Domingo MC, Giguere JF, Piret J, Mwatha A, Masse B, Bergeron MG. A randomized, double-blind, placebo-controlled Phase II extended safety study of two Invisible Condom formulations in Cameroonian women. Contraception. 2010;81(1):79-85.

15. McCormack S, Ramjee G, Kamali A, Rees H, Crook AM, Gafos M, Jentsch U, Pool R, Chisembele M, Kapiga S, Mutemwa R, Vallely A, Palanee T, Sookrajh Y, Lacey CJ, Darbyshire J, Grosskurth H, Profy A, Nunn A, Hayes R, Weber J. PRO2000 vaginal gel for prevention of HIV-1 infection (Microbicides Development Programme 301): a phase 3, randomised, double-blind, parallel-group trial. Lancet. 2010;376(9749):1329-1337.

16. Garg S, Goldman D, Krumme M, Rohan LC, Smoot S, Friend DR. Advances in development, scale-up and manufacturing of microbicide gels, films, and tablets. Antiviral Res. 2010;88 Suppl 1:S19-29.

17. Abdool Karim Q, Abdool Karim SS, Frohlich JA, Grobler AC, Baxter C, Mansoor LE, Kharsany AB, Sibeko S, Mlisana KP, Omar Z, Gengiah TN, Maarschalk S, Arulappan N, Mlotshwa M, Morris L, Taylor D, Group CT. Effectiveness and safety of tenofovir gel, an antiretroviral microbicide, for the prevention of HIV infection in women. Science. 2010;329(5996):1168-1174.

18. Joglekar N, Joshi S, Kakde M, Fang G, Cianciola M, Reynolds S, Mehendale S. Acceptability of PRO2000 vaginal gel among HIV un-infected women in Pune, India. AIDS Care. 2007;19(6):817-821.

19. Mayer KH, Maslankowski LA, Gai F, El-Sadr WM, Justman J, Kwiecien A, Masse B, Eshleman SH, Hendrix C, Morrow K, Rooney JF, Soto-Torres L. Safety and tolerability of tenofovir vaginal gel in abstinent and sexually active HIV-infected and uninfected women. AIDS. 2006;20(4):543-551.

20. Rosen RK, Morrow KM, Carballo-Dieguez A, Mantell JE, Hoffman S, Gai F, Maslankowski L, El-Sadr WM, Mayer KH. Acceptability of tenofovir gel as a vaginal microbicide among women in a phase I trial: a mixed-methods study. J Womens Health (Larchmt). 2008;17(3):383-392.

21. Karim QA, Karim SS, Frohlich JA, Grobler AC, Baxter C, Mansoor LE, Kharsany AB, Sibeko S, Mlisana KP, Omar Z, Gengiah TN, Maarschalk S, Arulappan N, Mlotshwa M, Morris L, Taylor D. Effectiveness and Safety of Tenofovir Gel, an Antiretroviral Microbicide, for the Prevention of HIV Infection in Women. Science. 2010.

22. Ma X, Wang D, Wu Y, Ho RJ, Jia L, Guo P, Hu L, Xing G, Zeng Y, Liang XJ. AIDS treatment with novel anti-HIV compounds improved by nanotechnology. Aaps J. 2010;12(3):272-278.

23. Gupta KM, Barnes SR, Tangaro RA, Roberts MC, Owen DH, Katz DF, Kiser PF. Temperature and pH sensitive hydrogels: an approach towards smart semen-triggered vaginal microbicidal vehicles. J Pharm Sci. 2007;96(3):670-681.

24. Laskey SB, Siliciano RF. A mechanistic theory to explain the efficacy of antiretroviral therapy. Nature reviews Microbiology. 2014;12(11):772-780.

25. Engelman A, Cherepanov P. The structural biology of HIV-1: mechanistic and therapeutic insights. Nature reviews Microbiology. 2012;10(4):279-290.

26. Lederman MM, Offord RE, Hartley O. Microbicides and other topical strategies to prevent vaginal transmission of HIV. Nature reviews Immunology. 2006;6(5):371-382.

27. Quayle AJ. The innate and early immune response to pathogen challenge in the female genital tract and the pivotal role of epithelial cells. J Reprod Immunol. 2002;57(1-2):61-79.

28. Klebanoff SJ, Coombs RW. Viricidal effect of Lactobacillus acidophilus on human immunodeficiency virus type 1: possible role in heterosexual transmission. J Exp Med. 1991;174(1):289-292.

29. Dezzutti CS, Guenthner PC, Cummins JE, Jr., Cabrera T, Marshall JH, Dillberger A, Lal RB. Cervical and prostate primary epithelial cells are not productively infected but sequester human immunodeficiency virus type 1. J Infect Dis. 2001;183(8):1204-1213.

30. Miller CJ, Shattock RJ. Target cells in vaginal HIV transmission. Microbes Infect. 2003;5(1):59-67.

31. Shattock RJ, Moore JP. Inhibiting sexual transmission of HIV-1 infection. Nature reviews Microbiology. 2003;1(1):25-34.

32. Wilkinson J, Cunningham AL. Mucosal transmission of HIV-1: first stop dendritic cells. Curr Drug Targets. 2006;7(12):1563-1569.

33. Wu L, KewalRamani VN. Dendritic-cell interactions with HIV: infection and viral dissemination. Nature reviews Immunology. 2006;6(11):859-868.

34. Baleta A. Concern voiced over "dry sex" practices in South Africa. Lancet. 1998;352(9136):1292.

35. Padian NS, Shiboski SC, Jewell NP. The effect of number of exposures on the risk of heterosexual HIV transmission. J Infect Dis. 1990;161(5):883-887.

36. Guimaraes MD, Vlahov D, Castilho EA. Postcoital vaginal bleeding as a risk factor for transmission of the human immunodeficiency virus in a heterosexual partner study in Brazil. Rio de Janeiro Heterosexual Study Group. Arch Intern Med. 1997;157(12):1362-1368.

37. Cohen CR, Lingappa JR, Baeten JM, Ngayo MO, Spiegel CA, Hong T, Donnell D, Celum C, Kapiga S, Delany S, Bukusi EA. Bacterial vaginosis associated with increased risk of female-to-male HIV-1 transmission: a prospective cohort analysis among African couples. PLoS Med. 2012;9(6):e1001251.

38. Low N, Chersich MF, Schmidlin K, Egger M, Francis SC, van de Wijgert JH, Hayes RJ, Baeten JM, Brown J, Delany-Moretlwe S, Kaul R, McGrath N, Morrison C, Myer L, Temmerman M, van der Straten A, Watson-Jones D, Zwahlen M, Hilber AM. Intravaginal practices, bacterial vaginosis, and HIV infection in women: individual participant data meta-analysis. PLoS Med. 2011;8(2):e1000416.

39. Blish CA, McClelland RS, Richardson BA, Jaoko W, Mandaliya K, Baeten JM, Overbaugh J. Genital Inflammation Predicts HIV-1 Shedding Independent of Plasma Viral Load and Systemic Inflammation. J Acquir Immune Defic Syndr. 2012;61(4):436-440.

40. Mayer KH, Venkatesh KK. Interactions of HIV, other sexually transmitted diseases, and genital tract inflammation facilitating local pathogen transmission and acquisition. Am J Reprod Immunol. 2011;65(3):308-316.

41. Morgan D, Mahe C, Okongo JM, Mayanja B, Whitworth JA. Genital ulceration in rural Uganda: sexual activity, treatment-seeking behavior, and the implications for HIV control. Sex Transm Dis. 2001;28(8):431-436.

42. O'Farrell N. Transmission of HIV: genital ulceration, sexual behaviour, and circumcision. Lancet. 1989;2(8672):1157.

43. Zhang T, Zhang C, Agrahari V, Murowchick JB, Oyler NA, Youan BB. Spray drying tenofovir loaded mucoadhesive and pH-sensitive microspheres intended for HIV prevention. Antiviral research. 2013;97(3):334-346.

44. Akanbi MO, Scarsi KK, Taiwo B, Murphy RL. Combination nucleoside/nucleotide reverse transcriptase inhibitors for treatment of HIV infection. Expert opinion on pharmacotherapy. 2012;13(1):65-79.

45. Cihlar T, Ray AS. Nucleoside and nucleotide HIV reverse transcriptase inhibitors: 25 years after zidovudine. Antiviral research. 2010;85(1):39-58.

46. De Clercq E. Anti-HIV drugs: 25 compounds approved within 25 years after the discovery of HIV. International journal of antimicrobial agents. 2009;33(4):307-320.

47. Messiaen P, Wensing AM, Fun A, Nijhuis M, Brusselaers N, Vandekerckhove L. Clinical use of HIV integrase inhibitors: a systematic review and meta-analysis. PloS one. 2013;8(1):e52562.

48. Pommier Y, Johnson AA, Marchand C. Integrase inhibitors to treat HIV/AIDS. Nature reviews Drug discovery. 2005;4(3):236-248.

49. Lv Z, Chu Y, Wang Y. HIV protease inhibitors: a review of molecular selectivity and toxicity. Hiv/Aids. 2015;7:95-104.

50. Kuritzkes DR. HIV-1 entry inhibitors: an overview. Current opinion in HIV and AIDS. 2009;4(2):82-87.

51. Waheed AA, Freed EO. HIV type 1 Gag as a target for antiviral therapy. AIDS research and human retroviruses. 2012;28(1):54-75.

52. Spearman P. HIV-1 Gag as an Antiviral Target: Development of Assembly and Maturation Inhibitors. Current topics in medicinal chemistry. 2015.

53. Braun K, Frank M, Pipkorn R, Reed J, Spring H, Debus J, Didinger B, von der Lieth CW, Wiessler M, Waldeck W. HIV-1 capsid assembly inhibitor (CAI) peptide: structural preferences and delivery into human embryonic lung cells and lymphocytes. International journal of medical sciences. 2008;5(5):230-239.

54. Adamson CS, Freed EO. Anti-HIV-1 therapeutics: from FDA-approved drugs to hypothetical future targets. Molecular interventions. 2009;9(2):70-74.

55. Gengiah TN, Baxter C, Mansoor LE, Kharsany AB, Abdool Karim SS. A drug evaluation of 1% tenofovir gel and tenofovir disoproxil fumarate tablets for the prevention of HIV infection. Expert opinion on investigational drugs. 2012;21(5):695-715.

56. Choi SU, Bui T, Ho RJ. pH-dependent interactions of indinavir and lipids in nanoparticles and their ability to entrap a solute. J Pharm Sci. 2008;97(2):931-943.

57. Dezzutti CS, Shetler C, Mahalingam A, Ugaonkar SR, Gwozdz G, Buckheit KW, Buckheit RW, Jr. Safety and efficacy of tenofovir/IQP-0528 combination gels - a dual compartment microbicide for HIV-1 prevention. Antiviral Res. 2012;96(2):221-225.

58. Saxena BB, Han YA, Fu D, Rathnam P, Singh M, Laurence J, Lerner S. Sustained release of microbicides by newly engineered vaginal rings. Aids. 2009;23(8):917-922.

59. Alukda D, Sturgis T, Youan BB. Formulation of tenofovir-loaded functionalized solid lipid nanoparticles intended for HIV prevention. J Pharm Sci. 2011;100(8):3345-3356.

60. Meng J, Sturgis TF, Youan BB. Engineering tenofovir loaded chitosan nanoparticles to maximize microbicide mucoadhesion. Eur J Pharm Sci. 2011;44(1-2):57-67.

61. Meng J, Zhang T, Agrahari V, Ezoulin MJ, Youan BB. Comparative biophysical properties of tenofovir-loaded, thiolated and nonthiolated chitosan nanoparticles intended for HIV prevention. Nanomedicine. 2014;9(11):1595-1612.

62. Zhang T, Sturgis TF, Youan BB. pH-responsive nanoparticles releasing tenofovir intended for the prevention of HIV transmission. Eur J Pharm Biopharm. 2011;79(3):526-536.

63. Zhang T, Zhang C, Agrahari V, Murowchick JB, Oyler NA, Youan BB. Spray drying tenofovir loaded mucoadhesive and pH-sensitive microspheres intended for HIV prevention. Antiviral Res. 2012.

64. Yu M, Vajdy M. Mucosal HIV transmission and vaccination strategies through oral compared with vaginal and rectal routes. Expert opinion on biological therapy. 2010;10(8):1181-1195.

65. Ferguson LM, Rohan LC. The importance of the vaginal delivery route for antiretrovirals in HIV prevention. Therapeutic delivery. 2011;2(12):1535-1550.

66. McGowan I. Rectal microbicide development. Current opinion in HIV and AIDS. 2012;7(6):526-533.

67. Nunes R, Sarmento B, das Neves J. Formulation and delivery of anti-HIV rectal microbicides: advances and challenges. Journal of controlled release : official journal of the Controlled Release Society. 2014;194:278-294.

68. Kedzierska K, Crowe SM. Cytokines and HIV-1: interactions and clinical implications. Antiviral chemistry & chemotherapy. 2001;12(3):133-150.

69. Connolly NC, Riddler SA, Rinaldo CR. Proinflammatory cytokines in HIV disease-a review and rationale for new therapeutic approaches. AIDS Rev. 2005;7(3):168-180.

70. Agrahari V, Agrahari V, Mitra AK. Nanocarrier fabrication and macromolecule drug delivery: challenges and opportunities. Ther Deliv. 2016;7(4):257-278.

71. Agrahari V, Agrahari V, Hung WT, Christenson LK, Mitra AK. Composite Nanoformulation Therapeutics for Long-Term Ocular Delivery of Macromolecules. Mol Pharm. 2016.

72. Mitra AK, Agrahari V, Mandal A, Cholkar K, Natarajan C, Shah S, Joseph M, Trinh HM, Vaishya R, Yang X, Hao Y, Khurana V, Pal D. Novel delivery approaches for cancer therapeutics. J Control Release. 2015;219:248-268.

73. Torchilin VP. Multifunctional, stimuli-sensitive nanoparticulate systems for drug delivery. Nature reviews Drug discovery. 2014;13(11):813-827.

74. Mura S, Nicolas J, Couvreur P. Stimuli-responsive nanocarriers for drug delivery. Nature materials. 2013;12(11):991-1003.

75. Cheng R, Meng F, Deng C, Klok HA, Zhong Z. Dual and multi-stimuli responsive polymeric nanoparticles for programmed site-specific drug delivery. Biomaterials. 2013;34(14):3647-3657.

76. Lai SK, Hida K, Shukair S, Wang YY, Figueiredo A, Cone R, Hope TJ, Hanes J. Human immunodeficiency virus type 1 is trapped by acidic but not by neutralized human cervicovaginal mucus. J Virol. 2009;83(21):11196-11200.

77. Tevi-Benissan C, Belec L, Levy M, Schneider-Fauveau V, Si Mohamed A, Hallouin MC, Matta M, Gresenguet G. In vivo semen-associated pH neutralization of cervicovaginal secretions. Clinical and diagnostic laboratory immunology. 1997;4(3):367-374.

78. Wagner G, Ottesen B. Vaginal physiology during menstruation. Annals of internal medicine. 1982;96(6 Pt 2):921-923.

79. Fox CA, Meldrum SJ, Watson BW. Continuous measurement by radio-telemetry of vaginal pH during human coitus. Journal of reproduction and fertility. 1973;33(1):69-75.

80. Schanté CE, Zubera G, Herlin C, Vandamme TF. Chemical modifications of hyaluronic acid for the synthesis of derivatives for a broad range of biomedical applications. Carbohydr Polym. 2011;85:469-489.

81. Oh EJ, Park K, Kim KS, Kim J, Yang JA, Kong JH, Lee MY, Hoffman AS, Hahn SK. Target specific and long-acting delivery of protein, peptide, and nucleotide therapeutics using hyaluronic acid derivatives. J Control Release. 2010;141(1):2-12.

82. Swyer GI. The hyaluronidase content of semen. Biochem J. 1947;41(3):409-413.

83. Zhang T, Sturgis TF, Youan BB. pH-responsive nanoparticles releasing tenofovir intended for the prevention of HIV transmission. European journal of pharmaceutics and biopharmaceutics : official journal of Arbeitsgemeinschaft fur Pharmazeutische Verfahrenstechnik eV. 2011;79(3):526-536.

84. Woodrow HNaK. pH-Responsive Nanocarriers for Delivery of HIV Antiviral Drugs. In.Society for Biomaterials; 2014.

85. Duan J, Freeling JP, Koehn J, Shu C, Ho RJ. Evaluation of atazanavir and darunavir interactions with lipids for developing pH-responsive anti-HIV drug combination nanoparticles. Journal of pharmaceutical sciences. 2014;103(8):2520-2529.

86. Rastogi R, Teller RS, Mesquita PM, Herold BC, Kiser PF. Osmotic pump tablets for delivery of antiretrovirals to the vaginal mucosa. Antiviral research. 2013;100(1):255-258.

87. Mahalingam A, Jay JI, Langheinrich K, Shukair S, McRaven MD, Rohan LC, Herold BC, Hope TJ, Kiser PF. Inhibition of the transport of HIV in vitro using a pH-

responsive synthetic mucin-like polymer system. Biomaterials. 2011;32(33):8343-8355.

88. Huang C, Soenen SJ, van Gulck E, Vanham G, Rejman J, Van Calenbergh S, Vervaet C, Coenye T, Verstraelen H, Temmerman M, Demeester J, De Smedt SC. Electrospun cellulose acetate phthalate fibers for semen induced anti-HIV vaginal drug delivery. Biomaterials. 2012;33(3):962-969.

89. Agrahari V, Zhang C, Zhang T, Li W, Gounev TK, Oyler NA, Youan BB. Hyaluronidase-sensitive nanoparticle templates for triggered release of HIV/AIDS microbicide in vitro. The AAPS journal. 2014;16(2):181-193.

90. Clark MR, Aliyar HA, Lee CW, Jay JI, Gupta KM, Watson KM, Stewart RJ, Buckheit RW, Kiser PF. Enzymatic triggered release of an HIV-1 entry inhibitor from prostate specific antigen degradable microparticles. International journal of pharmaceutics. 2011;413(1-2):10-18.

91. Date AA, Shibata A, Goede M, Sanford B, La Bruzzo K, Belshan M, Destache CJ. Development and evaluation of a thermosensitive vaginal gel containing raltegravir+efavirenz loaded nanoparticles for HIV prophylaxis. Antiviral research. 2012;96(3):430-436.

92. Bouchemal K, Frelichowska J, Martin L, Lievin-Le Moal V, Le Grand R, Dereuddre-Bosquet N, Djabourov M, Aka-Any-Grah A, Koffi A, Ponchel G. Note on the formulation of thermosensitive and mucoadhesive vaginal hydrogels containing the miniCD4 M48U1 as anti-HIV-1 microbicide. International journal of pharmaceutics. 2013;454(2):649-652.

93. Stefan Bracht MA, Harri Jukarainen, Pirjo Kortesuo, Heikki Lyytikäinen, Mikael Stolt. Osmotically active vaginal delivery system In.; 2013.

94. Fatakdawala H, Uhland SA. Hydrogen peroxide mediated transvaginal drug delivery. International journal of pharmaceutics. 2011;409(1-2):121-127.

95. Nair M, Guduru R, Liang P, Hong J, Sagar V, Khizroev S. Externally controlled on-demand release of anti-HIV drug using magneto-electric nanoparticles as carriers. Nature communications. 2013;4:1707.

96. Chen D, Sun K, Mu H, Tang M, Liang R, Wang A, Zhou S, Sun H, Zhao F, Yao J, Liu W. pH and temperature dual-sensitive liposome gel based on novel cleavable mPEG-Hz-CHEMS polymeric vaginal delivery system. International journal of nanomedicine. 2012;7:2621-2630.

97. Gupta KM, Barnes SR, Tangaro RA, Roberts MC, Owen DH, Katz DF, Kiser PF. Temperature and pH sensitive hydrogels: an approach towards smart semen-triggered vaginal microbicidal vehicles. Journal of pharmaceutical sciences. 2007;96(3):670-681.

98. Omar RF, Bergeron MG. The future of microbicides. Int J Infect Dis. 2011;15(10):e656-660.

99. D'Cruz OJ, Uckun FM. Clinical development of microbicides for the prevention of HIV infection. Curr Pharm Des. 2004;10(3):315-336.

100. Rohan LC, Sassi AB. Vaginal drug delivery systems for HIV prevention. Aaps J. 2009;11(1):78-87.

101. Mizrahy S, Raz SR, Hasgaard M, Liu H, Soffer-Tsur N, Cohen K, Dvash R, Landsman-Milo D, Bremer MG, Moghimi SM, Peer D. Hyaluronan-coated nanoparticles: the influence of the molecular weight on CD44-hyaluronan interactions and on the immune response. J Control Release. 2011;156(2):231-238.

102. Prestwich GD. Hyaluronic acid-based clinical biomaterials derived for cell and molecule delivery in regenerative medicine. J Control Release. 2011;155(2):193-199.

103. Stern R, Kogan G, Jedrzejas MJ, Soltes L. The many ways to cleave hyaluronan. Biotechnol Adv. 2007;25(6):537-557.

104. Bajaj G, Kim MR, Mohammed SI, Yeo Y. Hyaluronic acid-based hydrogel for regional delivery of paclitaxel to intraperitoneal tumors. J Control Release. 2012;158(3):386-392.

105. Ke C, Sun L, Qiao D, Wang D, Zeng X. Antioxidant acitivity of low molecular weight hyaluronic acid. Food Chem Toxicol. 2011;49(10):2670-2675.

106. Palmieri B, Rottigni V, Iannitti T. Preliminary study of highly cross-linked hyaluronic acid-based combination therapy for management of knee osteoarthritis-related pain. Drug Des Devel Ther. 2013;7:7-12.

107. Zidan AS, Spinks C, Fortunak J, Habib M, Khan MA. Near-infrared investigations of novel anti-HIV tenofovir liposomes. Aaps J. 2010;12(2):202-214.

108. Hu Z, Xia, Xiaohu, Tang, Liping. Process for synthesizing oil and surfactant-free hyaluronic acid nanoparticles and microparticles. In. USA: University of North Texas; 2009.

109. Montgomery DC. Design and analysis of experiments. New York: John Wiley and sons; 2005.

110. Hu X, Liu S, Zhou G, Huang Y, Xie Z, Jing X. Electrospinning of polymeric nanofibers for drug delivery applications. Journal of controlled release : official journal of the Controlled Release Society. 2014;185:12-21.

111. Zamani M, Prabhakaran MP, Ramakrishna S. Advances in drug delivery via electrospun and electrosprayed nanomaterials. International journal of nanomedicine. 2013;8:2997-3017.

112. Nista SV, Bettini J, Mei LH. Coaxial nanofibers of chitosan-alginate-PEO polycomplex obtained by electrospinning. Carbohydrate polymers. 2015;127:222-228.

113. Pakravan M, Heuzey MC, Ajji A. Core-shell structured PEO-chitosan nanofibers by coaxial electrospinning. Biomacromolecules. 2012;13(2):412-421.

114. Agrahari V, Meng J, Zhang T, Youan BB. Application of Design of Experiment and Simulation Methods to Liquid Chromatography Analysis of Topical HIV Microbicides Stampidine and HI443. J Anal Bioanal Tech. 2014;5(1).

115. Pitarresi G, Craparo EF, Palumbo FS, Carlisi B, Giammona G. Composite nanoparticles based on hyaluronic acid chemically cross-linked with alpha,beta-polyaspartylhydrazide. Biomacromolecules. 2007;8(6):1890-1898.

116. Zhang Y, Jiang T, Zhang Q, Wang S. Inclusion of telmisartan in mesocellular foam nanoparticles: drug loading and release property. Eur J Pharm Biopharm. 2010;76(1):17-23.

117. Agrahari V, Youan BB. Sensitive and rapid HPLC quantification of tenofovir from hyaluronic acid-based nanomedicine. AAPS PharmSciTech. 2012;13(1):202-210.

118. De Iaco PA, Muzzupapa G, Bigon E, Pressato D, Dona M, Pavesio A, Bovicelli L. Efficacy of a hyaluronan derivative gel in postsurgical adhesion prevention in the presence of inadequate hemostasis. Surgery. 2001;130(1):60-64.

119. Koppel DE. Analysis of macromolecular polydispersity in intensity correlation spectroscopy: The method of cumulants. J Chem Phys 1972;57:4814-4822.

120. Katzel U, Vorbau M, Stintz M, Gottschalk-Gaudig T, Barthel H. Dynamic light scattering for the characterization of polydisperse fractal systems: II. Relation between structure and DLS results. Part Part Syst Charact. 2008;25:19-30.

121. Hackley VA, Ferraris CF. The use of nomenclature in dispersion science and technology. NIST recommended practice guide. In: Government U, editor. Washington: US Government Printing Office; 2001.

122. Bitter T, Muir HM. A modified uronic acid carbazole reaction. Anal Biochem. 1962;4:330-334.

123. De Salegui M, Plonska H, Pigman W. A comparison of serum and testicular hyaluronidase. Archives of biochemistry and biophysics. 1967;121(3):548-554.

124. Highsmith S, Garvin JH, Jr., Chipman DM. Mechanism of action of bovine testicular hyaluronidase. Mapping of the active site. The Journal of biological chemistry. 1975;250(18):7473-7480.

125. Tomoko Honda TK, Shuji Mizumoto, Kazuyuki Sugahara, Yamada aS. Hyaluronidases Have Strong Hydrolytic Activity toward Chondroitin 4-Sulfate Comparable to that for Hyaluronan. Biomolecules. 2012;2:549-563.

126. Csoka AB, Frost GI, Stern R. The six hyaluronidase-like genes in the human and mouse genomes. Matrix Biol. 2001;20(8):499-508.

127. Owen DH, Katz DF. A review of the physical and chemical properties of human semen and the formulation of a semen simulant. J Androl. 2005;26(4):459-469.

128. Owen DH, Katz DF. A vaginal fluid simulant. Contraception. 1999;59(2):91-95.

129. Costa P, Sousa Lobo JM. Modeling and comparison of dissolution profiles. Eur J Pharm Sci. 2001;13(2):123-133.

130. Costache AD, Sheihet L, Zaveri K, Knight DD, Kohn J. Polymer-drug interactions in tyrosine-derived triblock copolymer nanospheres: a computational modeling approach. Mol Pharm. 2009;6(5):1620-1627.

131. Subashini M, Devarajan PV, Sonavane GS, Doble M. Molecular dynamics simulation of drug uptake by polymer. J Mol Model. 2011;17(5):1141-1147.

132. Halgren TA, Murphy RB, Friesner RA, Beard HS, Frye LL, Pollard WT, Banks JL. Glide: a new approach for rapid, accurate docking and scoring. 2. Enrichment factors in database screening. J Med Chem. 2004;47(7):1750-1759.

133. Friesner RA, Banks JL, Murphy RB, Halgren TA, Klicic JJ, Mainz DT, Repasky MP, Knoll EH, Shelley M, Perry JK, Shaw DE, Francis P, Shenkin PS. Glide: a new approach for rapid, accurate docking and scoring. 1. Method and assessment of docking accuracy. J Med Chem. 2004;47(7):1739-1749.

134. Li XY, Zhao Y, Sun MG, Shi JF, Ju RJ, Zhang CX, Li XT, Zhao WY, Mu LM, Zeng F, Lou JN, Lu WL. Multifunctional liposomes loaded with paclitaxel and artemether for treatment of invasive brain glioma. Biomaterials. 2014;35(21):5591-5604.

135. Singh S, Bakshi M. Guidance on Conduct of Stress Tests to Determine Inherent Stability of Drugs. Pharm Technol. 2000;4:1-14.

136. Reynolds DW, Facchine KL, Mullaney JF, Alsante KM, Hatajik TD, M.G. M. Available guidance and best practices for conducting forced degradation studies. Pharm Technol. 2002;2:48-56.

137. Maggio RM, Vignaduzzo SE, S. KT. Trends in Analytical Chemistry. 2013.

138. J. SP. Martin's Physical pharmacy and pharmaceutical sciences. Philadelphia: Lippincott Williams and Wilkins; 2011.

139. Waterman KC, Adami RC. Accelerated aging: prediction of chemical stability of pharmaceuticals. Int J Pharm. 2005;293(1-2):101-125.

140. Connors KA, Amidon GL, Stella VJ. Chemical stability of pharmaceuticals: A handbook for pharmacists. New York: Wiley-Interscience Publication; 1986.

141. Socarras S, Magari RT. Modeling the effects of storage temperature excursions on shelf life. J Pharm Biomed Anal. 2009;49(2):221-226.

142. Guo Z, Ma M, Wang T, Chang D, Jiang T, Wang S. A kinetic study of the polymorphic transformation of nimodipine and indomethacin during high shear granulation. AAPS PharmSciTech. 2011;12(2):610-619.

143. Fichorova RN, Cronin AO, Lien E, Anderson DJ, Ingalls RR. Response to Neisseria gonorrhoeae by cervicovaginal epithelial cells occurs in the absence of toll-like receptor 4-mediated signaling. J Immunol. 2002;168(5):2424-2432.

144. Rohan LC, Moncla BJ, Kunjara Na Ayudhya RP, Cost M, Huang Y, Gai F, Billitto N, Lynam JD, Pryke K, Graebing P, Hopkins N, Rooney JF, Friend D, Dezzutti CS. In vitro and ex vivo testing of tenofovir shows it is effective as an HIV-1 microbicide. PLoS One. 2010;5(2):e9310.

145. Wadajkar AS, Kadapure T, Zhang Y, Cui W, Nguyen KT, Yang J. Dual-imaging enabled cancer-targeting nanoparticles. Adv Healthc Mater. 2012;1(4):450-456.

146. Lanone S, Rogerieux F, Geys J, Dupont A, Maillot-Marechal E, Boczkowski J, Lacroix G, Hoet P. Comparative toxicity of 24 manufactured nanoparticles in human alveolar epithelial and macrophage cell lines. Part Fibre Toxicol. 2009;6:14.

147. Belloc F, Dumain P, Boisseau MR, Jalloustre C, Reiffers J, Bernard P, Lacombe F. A flow cytometric method using Hoechst 33342 and propidium iodide for simultaneous cell cycle analysis and apoptosis determination in unfixed cells. Cytometry. 1994;17(1):59-65.

148. Nakamura S, Shibuya M, Saito Y, Nakashima H, Saito F, Higuchi A, Tsubota K. Protective effect of D-beta-hydroxybutyrate on corneal epithelia in dry eye conditions through suppression of apoptosis. Invest Ophthalmol Vis Sci. 2003;44(11):4682-4688.

149. Debbasch C, Pisella PJ, De Saint Jean M, Rat P, Warnet JM, Baudouin C. Mitochondrial activity and glutathione injury in apoptosis induced by unpreserved and preserved beta-blockers on Chang conjunctival cells. Invest Ophthalmol Vis Sci. 2001;42(11):2525-2533.

150. Kirkland RA, Adibhatla RM, Hatcher JF, Franklin JL. Loss of cardiolipin and mitochondria during programmed neuronal death: evidence of a role for lipid peroxidation and autophagy. Neuroscience. 2002;115(2):587-602.

151. Thomassen LC, Napierska D, Dinsdale D, Lievens N, Jammaer J, Lison D, Kirschhock CE, Hoet PH, Martens JA. Investigation of the cytotoxicity of nanozeolites A and Y. Nanotoxicology. 2012;6(5):472-485.

152. Haase A, Rott S, Mantion A, Graf P, Plendl J, Thunemann AF, Meier WP, Taubert A, Luch A, Reiser G. Effects of silver nanoparticles on primary mixed neural cell cultures: uptake, oxidative stress and acute calcium responses. Toxicol Sci. 2012;126(2):457-468.

153. Ronzani C, Safar R, Diab R, Chevrier J, Paoli J, Abdel-Wahhab MA, Le Faou A, Rihn BH, Joubert O. Viability and gene expression responses to polymeric nanoparticles in human and rat cells. Cell biology and toxicology. 2014;30(3):137-146.

154. Sun J, Wang S, Zhao D, Hun FH, Weng L, Liu H. Cytotoxicity, permeability, and inflammation of metal oxide nanoparticles in human cardiac microvascular endothelial cells: cytotoxicity, permeability, and inflammation of metal oxide nanoparticles. Cell biology and toxicology. 2011;27(5):333-342.

155. Rigoulet M, Yoboue ED, Devin A. Mitochondrial ROS generation and its regulation: mechanisms involved in H(2)O(2) signaling. Antioxid Redox Signal. 2011;14(3):459-468.

156. Osseni RA, Debbasch C, Christen MO, Rat P, Warnet JM. Tacrine-induced Reactive Oxygen Species in a Human Liver Cell Line: The Role of Anethole Dithiolethione as a Scavenger. Toxicol In Vitro. 1999;13(4-5):683-688.

157. Blank C, Bogdan C, Bauer C, Erb K, Moll H. Murine epidermal Langerhans cells do not express inducible nitric oxide synthase. Eur J Immunol. 1996;26(4):792-796.

158. Kacimi R, Giffard RG, Yenari MA. Endotoxin-activated microglia injure brain derived endothelial cells via NF-kappaB, JAK-STAT and JNK stress kinase pathways. J Inflamm (Lond). 2011;8:7.

159. Heigold S, Sers C, Bechtel W, Ivanovas B, Schafer R, Bauer G. Nitric oxide mediates apoptosis induction selectively in transformed fibroblasts compared to nontransformed fibroblasts. Carcinogenesis. 2002;23(6):929-941.

160. Lackman-Smith C, Osterling C, Luckenbaugh K, Mankowski M, Snyder B, Lewis G, Paull J, Profy A, Ptak RG, Buckheit RW, Jr., Watson KM, Cummins JE, Jr., Sanders-Beer BE. Development of a comprehensive human immunodeficiency virus type 1 screening algorithm for discovery and preclinical testing of topical microbicides. Antimicrob Agents Chemother. 2008;52(5):1768-1781.

161. Klebanoff SJ, Coombs RW. Viricidal effect of Lactobacillus acidophilus on human immunodeficiency virus type 1: possible role in heterosexual transmission. J Exp Med. 1991;174(1):289-292.

162. Amit Boaz WA, Yayon Avner Hydrazido derivatives of hyaluronic acid In. USA: Prochon Biotech LTD, Bio-tecnology General (Israel); 2009.

163. Galindo-Rodriguez S, Allemann E, Fessi H, Doelker E. Physicochemical parameters associated with nanoparticle formation in the salting-out, emulsification-diffusion, and nanoprecipitation methods. Pharm Res. 2004;21(8):1428-1439.

164. Scott JE, Heatley F. Hyaluronan forms specific stable tertiary structures in aqueous solution: a 13C NMR study. Proc Natl Acad Sci U S A. 1999;96(9):4850-4855.

165. Zhang G, Niu A, Peng S, Jiang M, Tu Y, Li M, Wu C. Formation of novel polymeric nanoparticles. Acc Chem Res. 2001;34(3):249-256.

166. Zhang T, Murowchick J, Youan BB. Optimization of formulation variables affecting spray-dried oily core nanocapsules by response surface methodology. J Pharm Sci. 2011;100(3):1031-1044.

167. Zhong SP, Campoccia D, Doherty PJ, Williams RL, Benedetti L, Williams DF. Biodegradation of hyaluronic acid derivatives by hyaluronidase. Biomaterials. 1994;15(5):359-365.

168. Sugrue S. Predicting and controlling colloid suspension stability using electrophoretic mobility and particle size measurements. Am Lab. 1992;24:64-71.

169. Moebus K, Siepmann J, Bodmeier R. Alginate-poloxamer microparticles for controlled drug delivery to mucosal tissue. Eur J Pharm Biopharm. 2009;72(1):42-53.

170. Pornsak Sriamornsak, Kennedy RA. Effect of a small molecule on diffusion and swelling properties of selected polysaccharide gel beads. Carbohydrate Polymers. 2010;79(1):219-223.

171. Sriamornsak P, Nunthanid J, Cheewatanakornkool K, Manchun S. Effect of drug loading method on drug content and drug release from calcium pectinate gel beads. AAPS PharmSciTech. 2010;11(3):1315-1319.

172. Lenormand H, Vincent JC. pH effects on the hyaluronan hydrolysis catalysed by hyaluronidase in the presence of proteins: Part II. The electrostatic hyaluronan – Protein complexes. Carbohydr Polym. 2011;85:303-311.

173. Su WY, Chen YC, Lin FH. Injectable oxidized hyaluronic acid/adipic acid dihydrazide hydrogel for nucleus pulposus regeneration. Acta Biomater. 2010;6(8):3044-3055.

174. Deng Y, Liu D, Du G, Li X, Chen J. Preparation and characterization of hyaluronan/chitosan scaffold crosslinked by 1-ethyl-3-(3-dimethylaminopropyl) carbodiimide. Polym Int. 2007;56:738-745.

175. Kumar A, Sahoo B, Montpetit A, Behera S, Lockey RF, Mohapatra SS. Development of hyaluronic acid-Fe2O3 hybrid magnetic nanoparticles for targeted delivery of peptides. Nanomedicine. 2007;3(2):132-137.

176. Pouyani T, Harbison GS, Prestwich GD. Novel Hydrogels of Hyaluronic Acid: Synthesis, Surface Morphology, and Solid-State NMR. J Am Chem Soc. 1994;116:7515-7522.

177. Ferir G, Vermeire K, Huskens D, Balzarini J, Van Damme EJ, Kehr JC, Dittmann E, Swanson MD, Markovitz DM, Schols D. Synergistic in vitro anti-HIV type 1 activity of tenofovir with carbohydrate-binding agents (CBAs). Antiviral Res. 2011;90(3):200-204.

178. Haynes BF, Shattock RJ. Critical issues in mucosal immunity for HIV-1 vaccine development. The Journal of allergy and clinical immunology. 2008;122(1):3-9; quiz 10-11.

179. Yohannes G, Wiedmer SK, Elomaa M, Jussila M, Aseyev V, Riekkola ML. Thermal aggregation of bovine serum albumin studied by asymmetrical flow field-flow fractionation. Anal Chim Acta. 2010;675(2):191-198.

180. Xu S, Yamanaka J, Sato S, Miyama I, Yonese M. Characteristics of complexes composed of sodium hyaluronate and bovine serum albumin. Chem Pharm Bull (Tokyo). 2000;48(6):779-783.

181. Vetri V, Librizzi F, Leone M, Militello V. Thermal aggregation of bovine serum albumin at different pH: comparison with human serum albumin. Eur Biophys J. 2007;36(7):717-725.

182. Filippov A, Artamonova M, Rudakova M, Gimatdinov R, Skirda V. Self-diffusion in a hyaluronic acid-albumin-water system as studied by NMR. Magn Reson Chem. 2012.

183. Vincent JC, Lenormand H. How hyaluronan-protein complexes modulate the hyaluronidase activity: the model. Biophys Chem. 2009;145(2-3):126-134.

184. Van Rompay KK, Brignolo LL, Meyer DJ, Jerome C, Tarara R, Spinner A, Hamilton M, Hirst LL, Bennett DR, Canfield DR, Dearman TG, Von Morgenland W, Allen PC, Valverde C, Castillo AB, Martin RB, Samii VF, Bendele R, Desjardins J, Marthas ML, Pedersen NC, Bischofberger N. Biological effects of short-term or prolonged administration of 9-[2-(phosphonomethoxy)propyl]adenine (tenofovir) to newborn and infant rhesus macaques. Antimicrob Agents Chemother. 2004;48(5):1469-1487.

185. Sabuncu AC, Grubbs J, Qian S, Abdel-Fattah TM, Stacey MW, Beskok A. Probing nanoparticle interactions in cell culture media. Colloids Surf B Biointerfaces. 2012;95:96-102.

186. Maiorano G, Sabella S, Sorce B, Brunetti V, Malvindi MA, Cingolani R, Pompa PP. Effects of cell culture media on the dynamic formation of protein-nanoparticle complexes and influence on the cellular response. ACS Nano. 2010;4(12):7481-7491.

187. Alkilany AM, Murphy CJ. Toxicity and cellular uptake of gold nanoparticles: what we have learned so far? J Nanopart Res. 2010;12(7):2313-2333.

188. Dobrovolskaia MAA, P. Hall, J. B. McNeil, S. E. Preclinical studies to understand nanoparticle interaction with the immune system and its potential effects on nanoparticle biodistribution. Mol Pharm. 2008;5(4):487-495.

189. Levy ED, Pereira-Leal JB. Evolution and dynamics of protein interactions and networks. Curr Opin Struct Biol. 2008;18(3):349-357.

190. Wlodkowic D, Telford W, Skommer J, Darzynkiewicz Z. Apoptosis and beyond: cytometry in studies of programmed cell death. Methods Cell Biol. 2011;103:55-98.

191. Sanchez-Alcazar JA, Bradbury DA, Brea-Calvo G, Navas P, Knox AJ. Camptothecin-induced apoptosis in non-small cell lung cancer is independent of cyclooxygenase expression. Apoptosis. 2003;8(6):639-647.

192. Vanic Z, Skalko-Basnet N. Nanopharmaceuticals for improved topical vaginal therapy: can they deliver? Eur J Pharm Sci. 2013;50(1):29-41.

193. Valenta C. The use of mucoadhesive polymers in vaginal delivery. Adv Drug Deliv Rev. 2005;57(11):1692-1712.

194. Sandri G, Rossi S, Ferrari F, Bonferoni MC, Zerrouk N, Caramella C. Mucoadhesive and penetration enhancement properties of three grades of hyaluronic acid using porcine buccal and vaginal tissue, Caco-2 cell lines, and rat jejunum. J Pharm Pharmacol. 2004;56(9):1083-1090.

195. Leitner VM, Walker GF, Bernkop-Schnurch A. Thiolated polymers: evidence for the formation of disulphide bonds with mucus glycoproteins. Eur J Pharm Biopharm. 2003;56(2):207-214.

196. Sill TJ, von Recum HA. Electrospinning: applications in drug delivery and tissue engineering. Biomaterials. 2008;29(13):1989-2006.

197. Blakney AK, Ball C, Krogstad EA, Woodrow KA. Electrospun fibers for vaginal anti-HIV drug delivery. Antiviral Res. 2013;100 Suppl:S9-16.

198. Serban MA, Yang G, Prestwich GD. Synthesis, characterization and chondroprotective properties of a hyaluronan thioethyl ether derivative. Biomaterials. 2008;29(10):1388-1399.

199. Ellman GL. Tissue sulfhydryl groups. Arch Biochem Biophys. 1959;82(1):70-77.

200. Liang D, Hsiao BS, Chu B. Functional electrospun nanofibrous scaffolds for biomedical applications. Adv Drug Deliv Rev. 2007;59(14):1392-1412.

201. Ji Y, Ghosh K, Shu XZ, Li B, Sokolov JC, Prestwich GD, Clark RA, Rafailovich MH. Electrospun three-dimensional hyaluronic acid nanofibrous scaffolds. Biomaterials. 2006;27(20):3782-3792.

202. Ji Y, Ghosh K, Li B, Sokolov JC, Clark RA, Rafailovich MH. Dual-syringe reactive electrospinning of cross-linked hyaluronic acid hydrogel nanofibers for tissue engineering applications. Macromol Biosci. 2006;6(10):811-817.

203. Bhattarai N, Edmondson D, Veiseh O, Matsen FA, Zhang M. Electrospun chitosan-based nanofibers and their cellular compatibility. Biomaterials. 2005;26(31):6176-6184.

204. Bhardwaj N, Kundu SC. Electrospinning: a fascinating fiber fabrication technique. Biotechnol Adv. 2010;28(3):325-347.

205. Agrahari V, Putty S, Mathes C, Murowchick JB, Youan BB. Evaluation of degradation kinetics and physicochemical stability of tenofovir. Drug testing and analysis. 2015;7(3):207-213.

206. Takeuchi H, Thongborisute J, Matsui Y, Sugihara H, Yamamoto H, Kawashima Y. Novel mucoadhesion tests for polymers and polymer-coated particles to design optimal mucoadhesive drug delivery systems. Advanced drug delivery reviews. 2005;57(11):1583-1594.

207. das Neves J, Rocha CM, Goncalves MP, Carrier RL, Amiji M, Bahia MF, Sarmento B. Interactions of microbicide nanoparticles with a simulated vaginal fluid. Molecular pharmaceutics. 2012;9(11):3347-3356.

208. Svensson O, Thuresson K, Arnebrant T. Interactions between drug delivery particles and mucin in solution and at interfaces. Langmuir : the ACS journal of surfaces and colloids. 2008;24(6):2573-2579.

209. Svensson O, Thuresson K, Arnebrant T. Interactions between chitosan-modified particles and mucin-coated surfaces. Journal of colloid and interface science. 2008;325(2):346-350.

210. Ivarsson D, Wahlgren M. Comparison of in vitro methods of measuring mucoadhesion: ellipsometry, tensile strength and rheological measurements. Colloids Surf B Biointerfaces. 2012;92:353-359.

211. Svensson. O. Interactions of mucins with biopolymers and drug delivery particles. . In.: Malmö University, Malmö.; 2008.

212. Liselott Lindh P-OG, Ingemar Carlstedt, Claes Wickstro¨m,, Arnebrant T. Adsorption of MUC5B and the role of mucins in early salivary film formation. Colloids and Surfaces B: Biointerfaces. 2002;25:139-146.

213. Schmohl A, Khan A, Hess P. Functionalization of oxidized silicon surfaces with methyl groups and their characterization. Superlattices and Microstructures. 2004;36:113-121.

214. George JP, Smet PF, Botterman J, Bliznuk V, Woestenborghs W, Van Thourhout D, Neyts K, Beeckman J. Lanthanide-Assisted Deposition of Strongly Electro-optic PZT Thin Films on Silicon: Toward Integrated Active Nanophotonic Devices. ACS applied materials & interfaces. 2015;7(24):13350-13359.

215. Theisen AJ, C.; Deacon, M.P.; Harding, S.E. Refractive Increment Data-Book for Polymer and Biomolecular Scientists. Nottingham UK: Nottingham University Press; 2000.

216. Zhang Y, Huo M, Zhou J, Zou A, Li W, Yao C, Xie S. DDSolver: an add-in program for modeling and comparison of drug dissolution profiles. The AAPS journal. 2010;12(3):263-271.

217. Petrova MI, van den Broek M, Balzarini J, Vanderleyden J, Lebeer S. Vaginal microbiota and its role in HIV transmission and infection. FEMS Microbiol Rev. 2013;37(5):762-792.

218. Moncla BJ, Pryke K, Rohan LC, Yang H. Testing of viscous anti-HIV microbicides using Lactobacillus. J Microbiol Methods. 2012;88(2):292-296.

219. Choi KY, Min KH, Yoon HY, Kim K, Park JH, Kwon IC, Choi K, Jeong SY. PEGylation of hyaluronic acid nanoparticles improves tumor targetability in vivo. Biomaterials. 2011;32(7):1880-1889.

220. Li X, Yu G, Jin K, Yin Z. Hyaluronic acid L-cysteine conjugate exhibits controlled-release potential for mucoadhesive drug delivery. Pharmazie. 2012;67(3):224-228.

221. Yadav S, Ahuja M, Kumar A, Kaur H. Gellan-thioglycolic acid conjugate: synthesis, characterization and evaluation as mucoadhesive polymer. Carbohydr Polym. 2014;99:601-607.

222. Tu Luan, Lijiao Wu, Hongbin Zhang, Wang Y. A study on the nature of intermolecular links in the cryotropic weak gels of hyaluronan. Carbohydrate Polymers. 2012;87:2076-2085.

223. McKee MG, Wilkes GL, Colby RH, Long TE. Correlations of solution rheology with electrospun fiber formation of linear and branched polyesters. Macromolecules. 2004;37(5):1760-1767.

224. Rat P, Korwin-Zmijowska C, Warnet JM, Adolphe M. New in vitro fluorimetric microtitration assays for toxicological screening of drugs. Cell biology and toxicology. 1994;10(5-6):329-337.

225. Veazey RS, Shattock RJ, Klasse PJ, Moore JP. Animal models for microbicide studies. Current HIV research. 2012;10(1):79-87.

226. Caligioni CS. Assessing reproductive status/stages in mice. Current protocols in neuroscience / editorial board, Jacqueline N Crawley [et al]. 2009;Appendix 4:Appendix 4I.

227. McLean AC, Valenzuela N, Fai S, Bennett SA. Performing vaginal lavage, crystal violet staining, and vaginal cytological evaluation for mouse estrous cycle staging identification. J Vis Exp. 2012(67):e4389.

228. Catalone BJ, Kish-Catalone TM, Budgeon LR, Neely EB, Ferguson M, Krebs FC, Howett MK, Labib M, Rando R, Wigdahl B. Mouse model of cervicovaginal toxicity and inflammation for preclinical evaluation of topical vaginal microbicides. Antimicrobial agents and chemotherapy. 2004;48(5):1837-1847.

229. Schreiber CA, Meyn LA, Creinin MD, Barnhart KT, Hillier SL. Effects of long-term use of nonoxynol-9 on vaginal flora. Obstetrics and gynecology. 2006;107(1):136-143.

230. Patton DL, Kidder GG, Sweeney YC, Rabe LK, Hillier SL. Effects of multiple applications of benzalkonium chloride and nonoxynol 9 on the vaginal epithelium in the pigtailed macaque (Macaca nemestrina). American journal of obstetrics and gynecology. 1999;180(5):1080-1087.

231. Ham AS, Nugent ST, Peters JJ, Katz DF, Shelter CM, Dezzutti CS, Boczar AD, Buckheit KW, Buckheit RW, Jr. The rational design and development of a dual chamber vaginal/rectal microbicide gel formulation for HIV prevention. Antiviral Res. 2015;120:153-164.

232. Cunha AR, Machado RM, Palmeira-de-Oliveira A, Martinez-de-Oliveira J, das Neves J, Palmeira-de-Oliveira R. Characterization of commercially available vaginal lubricants: a safety perspective. Pharmaceutics. 2014;6(3):530-542.

233. Garcia JM, Gao A, He PL, Choi J, Tang W, Bruzzone R, Schwartz O, Naya H, Nan FJ, Li J, Altmeyer R, Zuo JP. High-throughput screening using pseudotyped lentiviral

particles: a strategy for the identification of HIV-1 inhibitors in a cell-based assay. Antiviral research. 2009;81(3):239-247.

234. Naldini L, Blomer U, Gallay P, Ory D, Mulligan R, Gage FH, Verma IM, Trono D. In vivo gene delivery and stable transduction of nondividing cells by a lentiviral vector. Science. 1996;272(5259):263-267.

235. Young J, Tang Z, Yu Q, Yu D, Wu Y. Selective killing of HIV-1-positive macrophages and T cells by the Rev-dependent lentivirus carrying anthrolysin O from Bacillus anthracis. Retrovirology. 2008;5:36.

236. Filipe V, Hawe A, Jiskoot W. Critical evaluation of Nanoparticle Tracking Analysis (NTA) by NanoSight for the measurement of nanoparticles and protein aggregates. Pharmaceutical research. 2010;27(5):796-810.

237. Kramberger P, Ciringer M, Strancar A, Peterka M. Evaluation of nanoparticle tracking analysis for total virus particle determination. Virology journal. 2012;9:265.

238. Zhong P, Agosto LM, Ilinskaya A, Dorjbal B, Truong R, Derse D, Uchil PD, Heidecker G, Mothes W. Cell-to-cell transmission can overcome multiple donor and target cell barriers imposed on cell-free HIV. PloS one. 2013;8(1):e53138.

239. Ivetac A, Swift SE, Boyer PL, Diaz A, Naughton J, Young JA, Hughes SH, McCammon JA. Discovery of novel inhibitors of HIV-1 reverse transcriptase through virtual screening of experimental and theoretical ensembles. Chemical biology & drug design. 2014;83(5):521-531.

240. Adriaens E, Remon JP. Mucosal irritation potential of personal lubricants relates to product osmolality as detected by the slug mucosal irritation assay. Sexually transmitted diseases. 2008;35(5):512-516.

241. Fuchs EJ, Lee LA, Torbenson MS, Parsons TL, Bakshi RP, Guidos AM, Wahl RL, Hendrix CW. Hyperosmolar sexual lubricant causes epithelial damage in the distal

colon: potential implication for HIV transmission. The Journal of infectious diseases. 2007;195(5):703-710.

242. Owen DH, Katz DF. A review of the physical and chemical properties of human semen and the formulation of a semen simulant. J Androl. 2005;26(4):459-469.

243. Introini A, Vanpouille C, Lisco A, Grivel JC, Margolis L. Interleukin-7 facilitates HIV-1 transmission to cervico-vaginal tissue ex vivo. PLoS Pathog. 2013;9(2):e1003148.

244. Vandergeeten C, Fromentin R, DaFonseca S, Lawani MB, Sereti I, Lederman MM, Ramgopal M, Routy JP, Sekaly RP, Chomont N. Interleukin-7 promotes HIV persistence during antiretroviral therapy. Blood. 2013;121(21):4321-4329.

245. das Neves J, Araujo F, Andrade F, Amiji M, Bahia MF, Sarmento B. Biodistribution and pharmacokinetics of dapivirine-loaded nanoparticles after vaginal delivery in mice. Pharm Res. 2014;31(7):1834-1845.

246. Blakney AK, Krogstad EA, Jiang YH, Woodrow KA. Delivery of multipurpose prevention drug combinations from electrospun nanofibers using composite microarchitectures. International journal of nanomedicine. 2014;9:2967-2978.

247. Mamo T, Moseman EA, Kolishetti N, Salvador-Morales C, Shi J, Kuritzkes DR, Langer R, von Andrian U, Farokhzad OC. Emerging nanotechnology approaches for HIV/AIDS treatment and prevention. Nanomedicine. 2010;5(2):269-285.

248. Rejman J, Oberle V, Zuhorn IS, Hoekstra D. Size-dependent internalization of particles via the pathways of clathrin- and caveolae-mediated endocytosis. The Biochemical journal. 2004;377(Pt 1):159-169.

VITA

Vivek Agrahari received his Master of Pharmacy in 2008 with specialization in Medicinal & Pharmaceutical Chemistry from Shri G. S. Institute of Tech. and Science, Indore, India. He has received his bachelor's degrees in Pharmacy in 2005. After his masters' education, Mr. Agrahari has joined the Ph.D. program in pharmaceutical Sciences and Chemistry as a co-discipline at UMKC School of Pharmacy. In his Ph.D. projects, he worked on NIH funded research projects aimed at developing bio-responsive formulation development for the prevention and treatment of HIV/AIDS infections. He has published several peer reviewed research papers, received several research awards and got opportunities to present his work at various international conferences. He has received the AAPS-Graduate Student Research Award in APQ Section-2015, Controlled Release Society-Nicholas A. Peppas Young Student Scientist Award, 2015, UMKC-School of Graduate Studies Research Award, 2014, and the Community of Scholars-UMKC-Best Paper Presentation Award, 2014. He is a member of several professional organizations such as the American Association of Pharmaceutical Scientists (AAPS), Controlled Release Society (CRS), and European Society for Nanomedicine (ESNAM).